

UNIVERSITY OF SOUTHAMPTON

**FACULTY OF ENGINEERING, SCIENCE AND MATHEMATICS
SCHOOL OF ENGINEERING SCIENCES**

**Evaluation and Characterisation of the Tribological Properties of
Polymeric Coatings for Downhole Application**

By

Jelili Olakunle Bello

Thesis submitted for the degree of Doctor of Philosophy

December 2003

UNIVERSITY OF SOUTHAMPTON

ABSTRACT

FACULTY OF ENGINEERING, SCIENCE AND MATHEMATICS
SCHOOL OF ENGINEERING SCIENCES

Doctor of Philosophy

EVALUATION AND CHARACTERISATION OF THE TRIBOLOGICAL
PROPERTIES OF POLYMERIC COATINGS FOR DOWNHOLE
APPLICATIONS

By Jelili Olakunle Bello

It is common practice within the oil industry to coat the internal surfaces of downhole water injection tubulars to reduce the total life costs. These coatings, plus primers, are typically polymeric and allow the tubulars to be manufactured from carbon steel instead of monolithic tubulars of expensive high Cr alloys. These coating/primer systems have to be corrosion resistant to protect the substrate from the service conditions of re-injected produced water and seawater. However, periodic inspection and testing of the tubulars by wireline tools results in coating damage from tool impacts and wireline abrasion. Thus, these coatings must have high abrasion and impact resistance in addition to corrosion barrier properties. Hence, this thesis details the current investigation undertaken to evaluate and characterise the tribological properties of filled and unfilled, commercial and experimental polymeric coatings for downhole application. The focus of the study was on the microstructure property interaction of the matrix and fillers as it relates to wear resistance optimisation of the coatings.

A novel evaluation of the adhesive properties of the thermoplastic and thermoset polymeric coatings to their substrates has been performed using a truncated ASTM G8-98 standard. The test, which utilises the cathodic disbondment method, has shown that disbondment of coatings occurs at coating/primer and/or primer/substrate interfaces and the results compared with the interface indentation test adhesion method. The crack path and thus, the resistance of coating to disbondment is influenced by the shot blasted surface of the carbon steel substrate.

The wireline wear rig was used primarily to rank and characterise the wireline wear performance of the polymeric coatings currently used downhole. The results show a superior performance by the thermoplastic polyamide 11 (PA11) coating, in terms of wear rate, over the rest of the coatings studied. In addition, micro-ploughing was identified as the dominant wear mechanism for thermoplastic coatings, while evidence of fatigue failure was seen for thermoset coatings. Poor bonding between filler and matrix was identified as the main cause of coating failure in the filled coatings.

Further studies were carried out on the PA11 coating using the more repeatable micro abrasion test method. Although more aggressive than the wireline, the micro-abrasion test was used to reproduce the type of wear mechanism (2-body abrasion) found in the wireline wear test. Also, the test method allowed comparative analysis to be carried out between the wireline and micro abrasion test method. Experimental coatings were also designed with suitable fillers incorporated in the matrix of PA11 coatings and studied using the micro-abrasion test method. Results showed that TiO₂ fillers are generally detrimental to the mechanical properties of the coatings. However, incorporation of secondary filler, dolomite, was seen to offer approximately 20 % more wear resistance compared to TiO₂. Nevertheless, the unfilled coatings exhibited a superior wear resistance compared with the filled coatings, with approximately 30 % abrasion resistance. The inverse of the coating property ($\sigma_b \epsilon_b$) was identified as the controlling parameter for the wear of PA11 matrix in the micro-abrasion test, showing the wear mechanism is controlled by tensile rupture. The effect of the mode of cooling after coating deposition was also investigated and results showed that water-cool mode enhanced the abrasion resistance of PA11 coatings compared to air-cool mode.

Abstract	
List of Content.....	I
Acknowledgement.....	VII
List of Figures	VIII
List of Tables	XVI

Chapter One

1.0 Introduction.....	1 - 5
1.1 Research overview.....	1
1.2 Scope of research work.....	3
1.3 Thesis structure.....	3
<i>References.....</i>	<i>5</i>

Chapter Two

2.0 Literature review.....	6 - 67
2.1 Polymers.....	6
2.1.1 Structure of polymers	6
2.1.1.1 <i>Classification of polymers.....</i>	<i>7</i>
2.1.1.2 <i>Polyamide 11.....</i>	<i>8</i>
2.2 Wear.....	10
2.2.1 Topography of contacting surfaces.....	10
2.2.2 Sliding wear of polymers.....	12
2.2.3 Abrasive wear of polymers.....	14
2.2.3.1 <i>Classification of abrasive wear..</i>	<i>16</i>
2.2.4 Corrosive wear.....	17
2.3 Wear test methods.....	18
2.3.1 Autoclave test.....	22
2.3.2 Rocker arm test.....	22
2.3.3 Acid resistance test..	23
2.3.4 Wireline abrasion test.....	23
2.3.5 Experimental methods for sliding and abrasive wear tests.....	24
2.3.5.1 <i>Micro-scale abrasive wear test.....</i>	<i>25</i>
2.3.6 Factors affecting wear rate.....	26

2.3.6.1	<i>Effect of temperature</i>	30
2.3.6.2	<i>Effect of sliding speed</i>	31
2.3.7	Analytical methods to assess wear damage.....	32
2.4	Friction.....	33
2.4.1	Sliding friction.....	34
2.4.1.1	<i>Adhesion component of friction</i>	34
2.4.1.2	<i>Ploughing component of friction</i>	34
2.4.2	Sliding friction of polymers.....	35
2.4.2.1	Effect of load on the friction of polymers.....	35
2.5	Corrosion.....	36
2.5.1	Forms of corrosion.....	36
2.5.1.1	<i>Crevice corrosion</i>	36
2.5.2	Cathodic disbondment.....	37
2.6	Coatings used for protection of injector tubulars.....	39
2.6.1	Polymeric coatings.....	39
2.6.1.1	<i>Thermoplastic coatings</i>	39
2.6.1.2	<i>Thermosetting coatings</i>	40
2.6.1.3	<i>Adhesive wear of polymeric coatings</i>	41
2.6.1.4	<i>Abrasive wear of polymeric coating</i>	43
2.6.1.5	<i>Mechanism of action of fillers</i>	44
2.6.2	Friction of polymeric coatings.....	44
2.6.3	Factors affecting wear and friction of polymeric coating.....	45
2.6.3.1	<i>Effect of particle size and spacing</i>	45
2.6.3.2	<i>Effect of temperature</i>	48
2.7	Modelling of wear rate.....	49
2.7.1	Matrix (W_M).....	49
2.7.2	Fillers (W_F).....	52
2.7.3	Filler pullout (ϕ_F).....	54
2.7.4	Filler fracture (η_F).....	56
2.7.5	Friction modifier (W_{FM}).....	53
2.8	Summary.....	58
	<i>References</i>	60

Chapter Three

3.0 Material characterisation.....	68 - 94
3.1 Introduction.....	68
3.2 Experimental.....	68
3.2.1 Surface roughness measurement.....	68
3.2.2 Analysis of coating details using the scanning electron microscopy.....	69
3.2.3 Energy dispersive X-ray (EDX) analysis... ..	69
3.2.4 Filler size measurement and quantification.	70
3.3 Characterisation of polymeric coatings.....	72
3.3.1 Thermoplastic TP-9	72
3.3.2 Thermosetting coatings.....	74
3.3.3 Fluoropolymer, PVDF and dual layer coatings.....	79
3.3.4 Coatings investigated in the second study.....	86
<i>References</i>	94

Chapter Four

4.0 Overview of previous and initial wear testing thermoplastic and thermosetting coatings.....	95 – 112
4.1 Introduction.....	95
4.2 Overview of previous works.....	97
4.2.1 Experimental methods.....	100
4.2.2 The wear rate.....	100
4.2.3 Wear mechanism.....	101
4.3 Preliminary investigation.....	102
4.3.1 Experimental.....	102
4.3.1.1 Methodology.....	102
4.3.2 Results and discussion.....	103
4.3.2.1 Summary	110
4.3.3 Conclusions.....	111
<i>References</i>	112

Chapter Five

5.0 Evaluation of the adhesive properties of polymeric coatings by cathodic disbondment.....	113 - 141
5.1 Introduction.....	113
5.2 Experimental details.....	114
5.2.1 The CD test cell.....	114
5.2.2 The IIT test set-up.....	115
5.2.3 The CD test electrolyte.....	116
5.2.4 Test sample preparation.....	116
5.2.5 Methodology.....	117
5.3 Results and discussion.....	118
5.3.1 Cathodic disbondment (CD) test....	118
5.3.2 Interface indentation test (IIT).....	129
5.3.3 PA11 coating A.....	132
5.3.4 Summary.....	137
5.4 Conclusions	140
<i>References.....</i>	<i>141</i>

Chapter Six

6.0 Wireline wear of commercially available polymeric coatings.....	142 - 169
6.1 Introduction	142
6.2 Experimental details.....	143
6.2.1 Methodology.....	143
6.2.2 Evaluation of wear rate	145
6.3 Results and discussion.....	146
6.3.1 Wear rate ranking... ..	146
6.3.2 Wear mechanisms.....	147
6.3.2.1 <i>Wear mechanism of coating matrix.....</i>	<i>147</i>
6.3.2.2 <i>Functions of fillers in coating during wear.....</i>	<i>155</i>
6.3.3 Modelling the POW wear rate.....	160
6.3.4 Summary.....	166
6.4 Conclusions.....	168
<i>References.....</i>	<i>169</i>

Chapter Seven

7.0 Micro-abrasion performance of PA11 coating.....	170 - 195
7.1 Introduction	170
7.2 Experimental details.....	170
7.2.1 Preparation of test materials.....	170
7.2.2 Methodology.....	172
7.3 Results and discussion.....	175
7.3.1 Wear rates... ..	175
7.3.2 Effect of load on wear rate.....	179
7.3.3 Effect of sliding distance on wear rate.....	182
7.3.4 Comparing SiC and GB abrasives tests.....	186
7.3.5 Effect of sliding speed on wear rate	189
7.3.6 Control test.....	191
7.3.7 Summary.....	192
7.3.8 Other abrasives.....	193
7.4 Conclusions.....	194
<i>References.....</i>	<i>195</i>

Chapter Eight

8.0 Micro-abrasion performance of filled and unfilled PA11 coatings: Influence of fillers and coatings properties on wear rate and wear mechanism.....	196 - 214
8.1 Introduction.....	196
8.2 Experimental details.....	197
8.2.1 Tensile test method.....	197
8.2.2 Methodology.....	199
8.3 Results and discussion.....	199
8.3.1 Effect of load on wear rate.....	199
8.3.2 Effect of sliding distance on wear rate.....	206
8.3.3 Effect of fillers on wear resistance of coatings.....	209
8.3.4 Correlation between wear rate and mechanical properties.....	210
8.4 Conclusions.....	213
<i>References.....</i>	<i>214</i>

Chapter Nine

9.0 Summary and Future work.....	215 - 220
9.1 Summary.....	215
9.2 Future work	219
<i>Appendix 1</i>...	221
<i>Appendix 2</i>.....	222
<i>Appendix 3</i>.....	226
<i>Appendix 4</i>.....	228

ACKNOWLEDGEMENTS

I will like to thank God Almighty for giving me the strength, grace and ability to complete this thesis in one piece. His guidance over me is unquestionable and cannot be quantified.

My unreserved gratitude goes to my supervisor, Dr R. J. K. Wood, whose patience, perseverance, encouragement has helped and motivated me immensely towards the successful completion of this research work; thank you for ever ready to listen and advice.

Thanks to Dr Julian Wharton for proofreading every chapter of this thesis. My acknowledgement also goes to the sponsors of this research, BP Amoco Exploration and the School of Engineering Sciences, for providing the financial support. I also wish to recognise the moral support from my colleagues in the school, especially Y. M Xu and K. Bose whose encouragement by virtue of sharing the same office has helped.

Acknowledgements are due to the staff of the School of Engineering Sciences, especially those of the Department of Mechanical Engineering, Engineering Materials, EDMC and Bioengineering Research Group, to whose support I am very grateful.

To my family; your all round support cannot be rivalled. To all members of Christ Foundation Missions, many thanks.

Last but not in any case the least, to miss Judith Ebitu, words are not enough to describe my appreciation. Thanks for being ever supportive and for caring so much; I love you.

Chapter 1

- Figure 1.1: *Schematic diagram of a water injector tubular showing typical wear and impact damage. The Tool typically weighs about 200 kg and it is lowered at a speed of about 2.2 m/s* 2
- Figure 1.2: *Flow chart representation of the thesis structure* 4

Chapter 2

- Figure 2.1: *Schematic of the triclinic α phase form of the PA11^[2.6]* 9
- Figure 2.2: *Nature of contacting bodies showing the areas of true contact^[2.18]* 11
- Figure 2.3: *Common relation found between the wear of brittle and ductile polymers^[2.24]* 13
- Figure 2.4: *Repeated ploughing showing the weakened zone of material^[2.22]* 14
- Figure 2.5: *Cutting action of the abrasives during abrasive wear^[2.24]* 15
- Figure 2.6: *Relationship between the volumes of material displaced and the base angle of a conical indenter^[2.28]* 16
- Figure 2.7: *Schematic showing a two-body abrasive wear^[2.17]* 16
- Figure 2.8: *Schematic showing the three-body abrasive wear^[2.17]* 17
- Figure 2.9: *Schematics showing various wear testing configurations^[2.17]* 20
- Figure 2.10: *The schematic showing the apparatus used for comparing the resistance of internal coatings to wireline damage.* 24
- Figure 2.11: *Schematic diagram of the ball-cratering micro-abrasion tester^[2.53]* 25
- Figure 2.12: *Schematic diagram showing the evolution of a single contact patch as two asperities move over each other^{2.17}* 27
- Figure 2.13: *Effect of load on the wear rate of polymers for dry sliding^[2.28]* 30
- Figure 2.14: *Variation of wear rate with temperature for some polymers sliding against a steel counterface. A, polystyrene; B, polymethylmethacrylate; C, polyacetal; D, polypropylene; F, PA 66^[2.64]* 31
- Figure 2.15: *Variation of wear rate with sliding speed for nylon 66 and other polymers sliding (dry) against mild steel^[2.65]* 32
- Figure 2.16: *Effect of load on friction of different polymers^[2.27]* 35
- Figure 2.17: *Schematic of metal dissolution, liberating into solution a metal ion M^{2+} and electron, e^- , which are consumed by reduction of H^+ to form*

H_2 ^[2.77]	38
Figure 2.18: <i>Effect of fibre volume content in polymer composite on the wear rate</i> ^[2.86]	42
Figure 2.19: <i>Variation in wear and specific wear rate with sliding distance for a candidate polymeric composite</i> ^[2.88]	43
Figure 2.20: <i>Geometry of contact between an idealized conical abrasive particle and a surface, a) in elevation; b) in plan view</i> ^[2.17]	46
Figure 2.21: <i>Illustration of the importance of the relative size of the particle contact zone and the hard phase regions in the abrasive wear of a two-phase (or composite) material. In a) material responds in an homogeneous manner while in b) material responds in an heterogeneous manner</i> ^[2.17]	47
Figure 2.22: <i>Contours of principal shear stress beneath a sliding spherical point contact over a flat surface where the coefficient of friction is 0.3</i> ^[2.97] .	51
Figure 2.23: <i>Schematic of the different types of filler shape</i>	53
Figure 2.24: <i>Pullout test and the resulting stress-strain curve showing the difference in magnitude of energies of debonding</i> ^[2.102]	55
Figure 2.25: <i>Model of filler pullout compared between two different filler shapes</i>	55
Figure 2.26: <i>Model of filler deforming elastically and fracturing under load and wear</i>	56

Chapter 3

Figure 3.1: <i>An example of a profile trace of a coating surface</i>	69
Figure 3.2: <i>An Example of the EDX analysis performed on the chemical composition of the fillers in the filled coatings</i>	70
Figure 3.3: <i>SEM image showing the measurement of the filler size in thermosetting coating</i>	71
Figure 3.4: <i>SEM image showing the measurement of the filler percentage in a thermosetting coating.</i>	72
Figure 3.5: <i>SEM image of the transverse section of coating TP-9</i>	73
Figure 3.6: <i>SEM image of the transverse section of coating TS-5</i>	75
Figure 3.7: <i>SEM image of the transverse section of coating TS-7</i>	76
Figure 3.8: <i>SEM of a more detailed transverse section of TS-7</i>	76
Figure 3.9: <i>SEM image of the transverse section of coating TSX-4</i>	78

Figure 3.10: <i>SEM of a more detailed transverse section of coating TSX-4</i>	79
Figure 3.11: <i>SEM image of the transverse section of coating F-4001</i>	80
Figure 3.12: <i>SEM image of the transverse section of the PVDF coating. Note the poor bond between coating and substrate</i>	82
Figure 3.13: <i>SEM image of the transverse section of the dual layer coating</i>	83
Figure 3.14: <i>SEM image of the transverse section of the dual layer coating. Note the poor bond between the two layers</i>	83
Figure 3.15: <i>SEM of the transverse section of coating A</i>	87
Figure 3.16: <i>SEM of the transverse section of coating B</i>	88
Figure 3.17: <i>SEM of the transverse section of coating C</i>	89
Figure 3.18: <i>SEM of a more detailed transverse section of coating C</i>	90
Figure 3.19: <i>SEM of the transverse section of coating D</i>	92
Figure 3.20: <i>SEM of the transverse section of a more detailed view of coating D</i>	92

Chapter 4

Figure 4.1: <i>Summary of some of the coatings investigated by MECS for BPX and Statoil under reciprocating wireline abrasion conditions</i>	96
Figure 4.2: <i>Overview of the studies carried out on TP-9 single and dual layer coatings under water lubricated conditions. Note RWL means reciprocating wireline, POW means pin-on-wire. Tests were carried out under different loads using ϕ 3.2 mm wireline, an average sliding speed of 0.46 m/s for POW and 0.85 m/s for RWL. JB means Jelili Bello and NS means Nicola Symonds</i>	98
Figure 4.3: <i>Picture of the laboratory pin-on wire test rig</i>	99
Figure 4.4: <i>Schematic of the reciprocating wireline wear rig</i>	99
Figure 4.5: <i>Specific wear rate of TP-9 as a function of the sliding distance</i>	103
Figure 4.6: <i>SEM of the worn surface of TP-9 after sliding for 2000m</i>	104
Figure 4.7: <i>SEM of worn surface of TP-9 showing repeatedly rubbed wear debris</i>	104
Figure 4.8: <i>Specific wear rate of the dual layer (TP-9 on TS-5) as a function of the sliding distance.</i>	105
Figure 4.9: <i>Optical image of the worn sample of the dual layer coating showing the weak interface between the topcoat and the bottom coat</i>	106
Figure 4.10: <i>Specific wear rate of TS-5 as a function of the sliding distance</i>	107

Figure 4.11: SEM micrograph of the worn surface of TS-5 at 1100 m sliding distance	108
Figure 4.12: Coefficient of friction as a function of sliding distance for TP-9	108
Figure 4.13: Coefficient of friction as a function of sliding distance for TS-5	109
Figure 4.14: Coefficient of friction as a function of sliding distance for dual layer	109

Chapter 5

Figure 5.1: Performance of coatings at low angle impact energy	113
Figure 5.2: Schematic of the CD test set-up with the electrical connections.	115
Figure 5.3: Schematic of the interfacial indentation test set-up	116
Figure 5.4: Schematic of (a) impact damage and (b) simulated damage caused by a typical downhole tool	117
Figure 5.5: Results of the CD test showing the curve of TP-9	120
Figure 5.6: Results of the CD test showing the curve of TS-5	121
Figure 5.7: Results of the CD test showing the curve of TS-7	121
Figure 5.8: Schematic showing the transverse section of a typical coating system (a) TS coatings, (b) TP coatings	122
Figure 5.9: SEM images of the cathodic disbondment test samples for TP-9 (a) and (b) are the thin coatings while (c) and (d) are the thick coatings	124
Figure 5.10: SEM images of the cathodic disbondment test samples for TS-5 (a) and (b) are the thin coatings while (c) and (d) are the thick coatings	125
Figure 5.11: SEM images of the cathodic disbondment test samples for TS-7 (a) and (b) are the thin coatings while (c) and (d) are the thick coatings	125
Figure 5.12: Graph showing correlation between charge and radius of disbondment for TP coatings. The difference between the average disbondment radius and the holiday radius represents how much a coating has delaminated from its substrate	126
Figure 5.13: Graph showing correlation between charge and radius of disbondment for TS Coatings	127
Figure 5.14: A model showing the interfacial bond between coating and its substrate ^[5,9] . W represents atomic interaction of bonds	127
Figure 5.15: Schematic models showing mechanical action of debonding caused by trapped hydrogen gas. (1) Delamination occurring at coating/primer interface; (2) Delamination occurring at primer substrate interface	128
Figure 5.16: SEM images of the mechanical delamination test samples for TP-9 (a) and (b)	

<i>are the thick coatings while (c) and (d) are the thin coating</i>	130
Figure 5.17: <i>SEM images of the interfacial indentation test samples for TS-5 (a) and (b) are the thick coatings while (c) and (d) are the thin coatings</i>	130
Figure 5.18: <i>SEM images of the interfacial indentation test samples for TS-7 (a) and (b) are the thick coatings while (c) and (d) are the thin coatings</i>	131
Figure 5.19: <i>Cathodic disbondment test for coating A with primer</i>	133
Figure 5.20: <i>Cathodic disbondment test for coating A without primer</i>	133
Figure 5.21: <i>SEM micrographs of the transverse section of the tested CD samples; (a) is with primer and (b) is without primer</i>	135
Figure 5.22: <i>SEM micrographs of the transverse section of the tested IIT samples; (a) is with primer and (b) is without primer</i>	136
Figure 5.23: <i>Correlation between the IIT and CD test methods</i>	137
 Chapter 6	
Figure 6.1: <i>A photograph of the laboratory pin-on-wire arrangement</i>	144
Figure 6.2: <i>A 2-D Talysurf taken across the wear scar in a coating. Horizontal and vertical scales are 500 and 50 μm per division respectively</i>	145
Figure 6.3: <i>Specific wear rate for the six coatings tested under wireline wear. The sliding distance was 150 m and applied load was 150 N</i>	146
Figure 6.4: <i>SEM of the worn surface of TP-9 showing plastic deformation around the edge of the wear track</i>	147
Figure 6.5: <i>SEM of the centre of the wear scar. Note the tiny grooves and deposit of minute wear debris</i>	149
Figure 6.6: <i>SEM of the worn surface of TS-5. Note the tiny grooves across the $\text{CaCO}_3/\text{SiO}_2$ fillers and matrix as well as the cracks on the fillers</i>	149
Figure 6.7: <i>SEM of TS-7. Note the fatigue wear mechanism found in the matrix</i>	150
Figure 6.8: <i>SEM image of TSX-4 showing the cracks all over the matrix and around the Al_2O_3 fillers</i>	151
Figure 6.9: <i>SEM image of F-4001 coating showing tendrils at the edge of the wear track</i>	152
Figure 6.10: <i>SEM image of F-4001 coating showing grooves on the wear scar</i>	152
Figure 6.11: <i>Surface profile of a wireline used to lower tools into the tubulars downhole. The</i>	

<i>asperities were found to have an average of 5μm height and 12μm base width and approximately 20 μm peak-to-peak asperity spacing</i>	153
Figure 6.12: <i>SEM image of F-4001 coating at a higher magnification showing cavities within the coating matrix</i>	153
Figure 6.13: <i>SEM image of the PVDF coating showing the edge of the wear track</i>	154
Figure 6.14: <i>SEM image of the PVDF coating showing the centre of the wear scar</i>	155
Figure 6.15: <i>SEM of TS-5 showing the compression and cracking of the CaCO₃/SiO₂ fillers</i>	156
Figure 6.16: <i>SEM of TS-5 showing possible initiation of the CaCO₃/SiO₂ filler pullout</i>	156
Figure 6.17: <i>SEM micrograph of TSX-4. Note the fillers being pulled out</i>	157
Figure 6.18: <i>SEM of TSX-4. Note the cracks in the Al₂O₃ filler and the matrix</i>	157
Figure 6.19: <i>SEM of the worn surface of TS-7. Note the filler preventing wear of the matrix as indicated by the arrow</i>	158
Figure 6.20: <i>Schematic showing how the fillers prevent abrasion in coatings during wear</i>	158
Figure 6.21: <i>SEM image of the worn surface of TS-7. Note the wear of fillers</i>	159
Figure 6.22: <i>Schematic of an elastic line contact between two bodies</i>	161
Figure 6.23: <i>Schematic of tribo-contact pair of wire and PA11 sample</i>	162
Figure 6.24: <i>Talysurf trace across a wireline showing the size of an asperity</i>	162
Figure 6.25: <i>SEM of the wear scar of PA11 coating. Note the highlighted groove width</i>	163
Figure 6.26: <i>Talysurf trace of individual groove width on PA11 TP-9 at 150 N and 1000m sliding distance</i>	163
Figure 6.27: <i>Schematic of an elastic point contact between two bodies</i>	164
Figure 6.28: <i>Schematic showing the total number of asperities in contact during wear</i>	164
Figure 6.29: <i>Schematic showing the depth of material removed by an asperity</i>	165
Figure 6.30: <i>Relationship between the volumes of material displaced and the base angle of a conical indenter</i>	166

Chapter 7

Figure 7.1: <i>SEM of the silicon carbide (SiC) abrasives. Note the angular nature and sharp edges of the abrasives</i>	171
Figure 7.2: <i>SEM of the glass beads abrasives. Note the spherical nature of the abrasives and the size range</i>	171

Figure 7.3: Schematic of the micro-scale abrasive wear-testing machine ^[7.1]	172
Figure 7.4: 3-D surface profile of the pitted ball used for the micro-abrasion tests	173
Figure 7.5: Typical image of a crater produced by CASA	175
Figure 7.6: Talysurf trace showing the abrasive nature of the surface of the wireline. The asperities were found to have an average dimension of 5 μm height and 12 μm base width	177
Figure 7.7: Micro-abrasion of the SiC test showing the behaviour of the volume loss per sliding distance against load at a sliding speed and distance of 0.1 m/s and 157 m respectively	180
Figure 7.8: SEM images of the polyamide 11 coating at (a) at 4 N normal load and (b) at 10 N normal load (SiC)	181
Figure 7.9: Wear mode map as a function of severity of contact and hardness ratio between ball and specimen ^[7.9]	181
Figure 7.10: SEM of the bottom of the wear scar on the tested sample for the pin-on wire	182
Figure 7.11: Results of the SiC test showing the behaviour of the volume loss per unit normal load at a sliding speed and load of 0.1 m/s and 6 N respectively. Note the two regions of wear rate	183
Figure 7.12: Comparison between experimental (O) and theoretical data (continuous line) for the craters at a sliding speed and load of 0.1 m/s and 6 N respectively	184
Figure 7.13: Sphere fit analysis of a typical crater, 40 m sliding distance and 6 N load (SiC)	185
Figure 7.14: SEM images of the worn sample (a) at 20 m sliding distance and 6 N load (SiC) and (b) at 40 m sliding distance and 6 N load (SiC)	186
Figure 7.15: Result of the glass bead abrasive tests at 6 N load and sliding speed of 0.1 m/s	187
Figure 7.16: Schematic of the ball-on-coating contact for the cases where SiC and glass beads were used as abrasives	188
Figure 7.17: SEM images of the worn samples for the GB abrasive tests (a) at 120 m SD, 6 N load and, 0.1 m/s (b) at 140 m sliding distance 6 N load and 0.1 m/s	189
Figure 7.18: Result of the wear rate plotted against the sliding speed. The load was 6 N and sliding distance was 100 m using GB abrasives	189
Figure 7.19: SEM images of the worn samples for the GB tests, sliding distance of 100 m at	

(a) at 0.12 m/s sliding speed and load of 6 N, (b) at 0.13 m/s sliding speed and load of 6N, (c) at 0.15 m/s sliding speed and load of 6N	191
Figure 7.20: Comparison between the results of the coating and monolithic tests at 0.1 m/s and 6 N normal load (SiC)	192
Figure 7.21: Graph comparing wear rate of TP-9 and other thermosets using glass abrasives (2-10 μm), or natural diamond (4-8 μm) sizes	193

Chapter 8

Figure 8.1: Graph showing the SWR of all the coatings for variable loading	201
Figure 8.2: Volume loss per sliding distance (V/D) versus load (L), at a sliding speed of 0.1 m/s and sliding distance of 154 m for coating B	201
Figure 8.3: SWR (m^3/Nm) of the coatings versus load (L), at a sliding speed of 0.1 m/s and sliding distance of 154 m	202
Figure 8.4: SWR (m^3/Nm) versus load (L), at a sliding speed of 0.1 m/s and sliding distance of 154 m for air and water-cooled sample compared with Coating E and the monolithic PA11	203
Figure 8.5: SEM of worn surface of (a) water-cooled and (b) air-cooled both at 154 m and 2N respectively, (c) water-cooled and (d) air-cooled both at 20 m and 6 N respectively	204
Figure 8.6: SEM of worn surface of (a) Coating A, (b) Coating B, (c) Coating C and (d) Coating D all at 10 N and sliding speed of 0.1 m/s	205
Figure 8.7: Plot of the wear volume per unit load (V/L) against sliding distance (m) for Coating B	206
Figure 8.8: Comparison between the $\text{SWR}_{(\text{load})}$ for the variable load and the variable sliding distance	207
Figure 8.9: SWR (m^3/Nm) of the coatings versus sliding distance (m), at a sliding speed of 0.1 m/s and normal load of 6 N	208
Figure 8.10: Comparing trends found between mechanical properties and SWR in this study with those of other authors	211

Chapter 2

Table 2.1: <i>Comparison of three polymer categories</i> ^[2.1]	7
Table 2.2a: <i>Various test configurations as compiled by ASLE</i> ^[2.34]	18
Table 2.2b: <i>Continuation of table 2.2</i>	19
Table 2.3: <i>Mechanical and physical properties of some common thermoplastics</i>	50
Table 2.4: <i>Mechanical and physical properties of common thermosetting polymers</i> ^[2.99]	50
Table 2.5: <i>Mechanical and physical properties of some ceramic fillers</i>	54

Chapter 3

Table 3.1: <i>Details of the physical properties of TP-9</i>	73
Table 3.2: <i>Details of the physical properties of coating TS-5</i>	74
Table 3.3: <i>Details of the known properties of coating TS-7</i>	75
Table 3.4: <i>Details of the known properties of coating TSX-4</i>	77
Table 3.5: <i>Details of the known properties of coating F-4001</i>	80
Table 3.6: <i>Details of the known properties of the Fluorinated (PVDF) coating</i>	81
Table 3.7: <i>Summary of the first set of coatings studied. Note: the dual layer combines the details Coating TP-9 and TS-5</i>	85
Table 3.8: <i>Details of the polyamide coating A</i>	87
Table 3.9: <i>Details of the polyamide coating B</i>	88
Table 3.10: <i>Details of the polyamide coating C</i>	89
Table 3.11: <i>Details of the polyamide coating D</i>	91
Table 3.12: <i>Summary of the coatings investigated in the second study</i>	93

Chapter 4

Table 4.1: <i>Summary/overview of the test conditions adopted for the pin-on-wire and the reciprocating wireline wear tests</i>	100
Table 4.2: <i>The experimental conditions employed for the preliminary investigation test</i>	103

Chapter 5

Table 5.1: <i>Details of the experimental conditions for the cathodic disbondment tests</i>	118
Table 5.2: <i>Details of the experimental conditions for the IIT tests</i>	118
Table 5.3: <i>The total charge produced during disbondment test (mean value of two tests)</i>	123

Table 5.4: <i>The radius and approximate area of the disbonded region</i> <i>(mean value of two tests)</i>	126
Table 5.5: <i>Measured extent of delamination (mean value) for the interfacial indentation test</i>	131
Table 5.6: <i>Measured data (mean value of two tests) for the charge produced from the test on coating A</i>	134
Table 5.7: <i>Measured extent of delamination for the interfacial indentation test</i>	136
Table 5.8: <i>Summary of the coatings studied with the results. CP=Coating Primer; PS=Primer Substrate and CS=Coating Substrate. TPWP means Thermoplastic with primer and TPWOP means Thermoplastic without primer (coating A)</i>	138
Table 5.9: <i>Summary of ranking for the coatings studied</i>	139

Chapter 6

Table 6.1: <i>Experimental conditions employed during the study of wireline wear of polymeric Coatings</i>	144
Table 6.2: <i>Summary of the coating rankings in terms of wear rate and mechanism</i>	167

Chapter 7

Table 7.1: <i>The experimental conditions employed for the three SiC experiments</i>	174
Table 7.2: <i>The experimental conditions employed for the SG abrasive experiments</i>	174
Table 7.3: <i>Comparison of the wear rates from pin-on-wire and reciprocating rig tests with the micro-abrasion test</i>	176
Table 7.4: <i>Comparison of wear rates found in the literature with this work</i>	178
Table 7.5: <i>Comparison between the pin-on-wire test and the micro-abrasion test</i>	179

Chapter 8

Table 8.1: <i>Details of the coatings studied. The bulk sample is included for comparison purpose. Note the inclusion of Coating E (TP-9) is for comparison</i>	198
Table 8.2: <i>Details of the test conditions employed in this study</i>	199
Table 8.3: <i>Specific wear rates ($SWR_{(load)}$) from variable loading (2 – 10 N) and correlation coefficients (R^2) for 154 m sliding distance</i>	200

Table 8.4: <i>Specific wear rates ($SWR_{(SD)}$) from variable sliding distance (20 – 140 m) and correlation coefficients (R^2) from volume loss at 6 N</i>	207
Table 8.5: <i>Hardness and density details for the filler particulates and abrasive used</i>	209
Table 8.6: <i>Ultimate tensile stress (UTS) and Young's modulus (E) values for coatings from this study compared with the wear rates</i>	211

1.0 Introduction

This chapter will summarise the problems currently faced during oil production, which have given rise to this research work. The reasons for undertaking the work and the scope of the research work are also discussed.

1.1 Research overview

In the oil industry, the extraction of crude oil (Petroleum) from an oil well often creates a fluid potential gradient (drop in the depth/height of fluid) towards the well. This is accompanied by a drop in the pressure of the reservoir around the well. According to Groves ^[1.1], the pressure and temperature of a well are typically 34.5 bar (3.5 MPa) and between 55 °C and 180 °C.

In some instances, water surrounding the reservoir will permeate through pores in the rock to fill the space created by the extracted oil, but the rate of flow of the water into the reservoir is very much less than the flow rate of the oil out through the production lines. Consequently, water and sometimes gas are re-injected back into the well through the injector tubulars, to stabilise the reservoir pressure. Injector tubulars are typically 140 mm in diameter, made from carbon steel and handle flow velocities of between 0.7- 7 m/s. Due to the corrosivity of the re-injected water, which is usually a combination of sea and produced water, (sea water contains species such as O₂, CO₂, chloride ions), the water injector tubulars are internally coated with polymeric coatings primarily for corrosion resistance.

However, in service it has been found that the polymeric coatings can be damaged by tools used during work-overs and/or inspection of the oil well, which are lowered by wireline at high speed, typically 2.2 m/s ^[1.1], down the well. Usually, the damage on the coatings is in two form: (1) wear from abrasion by the wireline (2) impact damage from high-energy tool impact on the internal surface of the tubular, see Figure 1.1.

Two coating types have been used in the past, thermoplastic and thermosett coatings ^[1.1, 1.2]. These coatings are thermally deposited hot spraying the atomised polymer

powder using a spray gun onto the bore of the tubular (substrate) after a thin layer of primer has been applied.

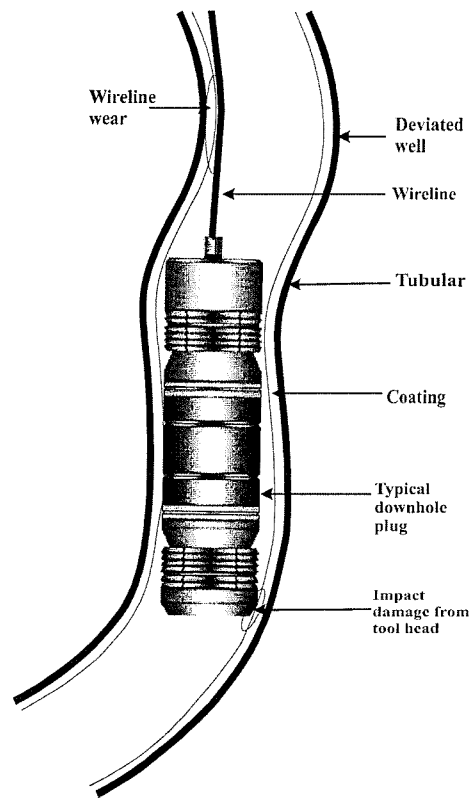


Figure 1.1: Schematic diagram of a water injector tubular showing typical wear and impact damage sites. The tool typically weighs about 200 kg and it is lowered at a speed of about 2.2 m/s.

Normally, the coatings contain fillers, but in some instances, fillers are not used depending on the application. The fillers are mostly manufactured from low cost materials and come in different shapes (angular, flakes) and sizes (3-40 μm). They are added to reduce the overall cost and enhance the strength of the coating. It has been found that the wear resistance performance of this type of coating system has not been optimised in regard to its matrix (type and thickness), filler (proportion, size and surface properties) and primer (type and thickness) ^[1,3]. Studies have also shown that the impact damage often leads to delamination of the coatings from their substrate, ultimately leading to coating failure ^[1,3]. The delamination of the coating is a consequence of the product of cathodic reactions taking place at the unexposed areas of the coating surrounding impact sites which have exposed the substrate. These

unexposed areas act cathodically to the rest of the substrate with the exposed area (steel tubulars) acting anodically with respect to the rest of the substrate.

1.2 Scope of the research work

This investigation will attempt to address the problem of coating optimisation through a detailed study of the microstructure interactions of the basic constituents of the coating vis-à-vis the matrix, filler and primer. This will ultimately lead to an improvement in the understanding of the wear mechanisms of these coatings using different wear testing methods such as pin-on-disc and micro-abrasion. In particular, effort will be made to reproduce the wear mechanisms found in the wireline test using the micro-abrasion test method. The adhesion of the coatings to the carbon steel substrate tubulars will be evaluated by a cathodic disbondment method. Overall, the aim of this research work is to establish a coating system that will resist corrosion and wear for application to downhole water injector tubulars.

1.3 Thesis structure

The first chapter of this thesis gives a general background to the research work. The setting for the current work is provided by previous work reported in the published literature, which has been examined in chapter 2. The key words employed for the journal search were: Polymer, polymeric coatings, filler, wear, corrosion and cathodic disbondment. Research at the University of Southampton began with the development of screening test to measure the erosion, abrasion and impact performance of polymer coatings conducted by the Mechanical Engineering Consultancy Service in 1995. An overview of this work and the different techniques used, together with the typical wear rates obtained are presented in chapter 4.

The current investigation will be reported under three different headings: adhesion properties of polymeric coatings, wireline wear of polymeric coatings, and micro-abrasion of polymeric coatings. For clarity, each of these has been presented in three different chapters of 5, 6, and 7 respectively with methodology, results and discussion, after a detail characterization of the materials studied in chapter 3. Chapter 8 presents the results of an investigation of the effect of fillers on the tribological properties of selected polymeric coatings based on the results from chapter 7. Chapter 9 gives a

general summary of the work conducted so far and further work. Figure 1.2 is a flow chart of the thesis structure.

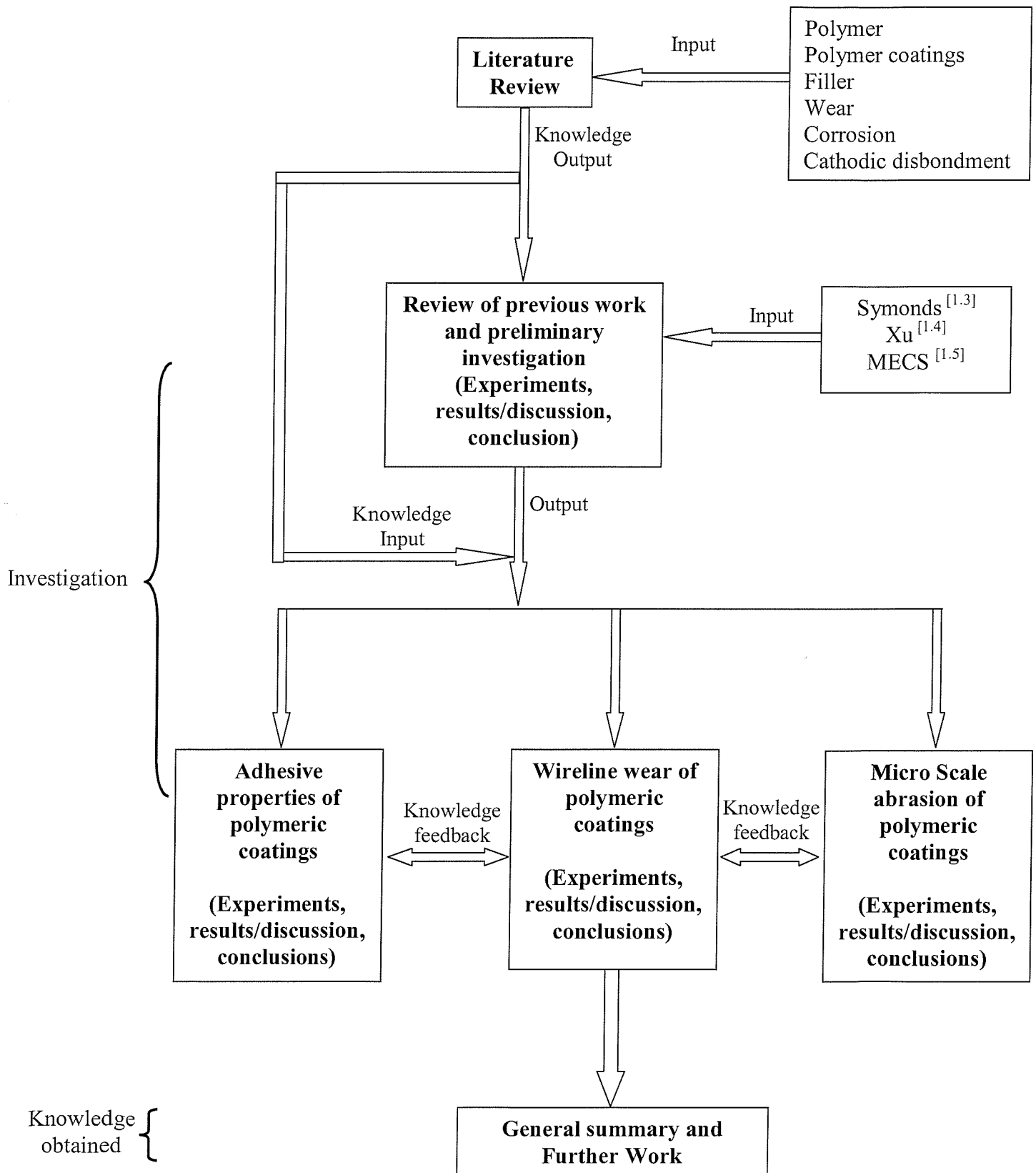


Figure 1.2: Flow chart representation of the thesis structure.

References

- 1.1 Groves, S., Technical Meeting, BP Research Centre, Sunbury (March 2000).
- 1.2 Symonds, N and Mellor, B. G., Polymeric Coatings for Impact and Wear resistance. *Wear*, 225-229 (1999) 111-118.
- 1.3 Symonds, N., Wear and Impact of Polymeric Coatings, PhD thesis, University of Southampton, (2000).
- 1.4 Xu, Y. Wear and Impact of polymeric Coatings, PhD Thesis, School of Engineering Science, University of Southampton, (2003).
- 1.5 Wood, R. J. K. and Symonds, N. Wear testing of internal coatings for downhole tubulars. Mechanical Engineering Consultancy Services, University of Southampton. Report number 96/EC191, (1996).

2.0 Literature review

This chapter reviews the past and present work relevant to the wear, corrosion and friction of candidate downhole polymeric coatings. It is intended to provide background knowledge to the present studies by reviewing literature of related subjects.

2.1 Polymers

A group of materials normally obtained by joining organic molecules into giant molecular chains or networks are known as polymers^[2.1]. They are characterized by low strength; low melting temperatures, and poor electrical conductivity. An alternative name for this category of engineering materials is plastics, which describe the extensive formability of many polymers during fabrication^[2.2]; hence, they find wide usage in composites, both as fibres and as a matrix.

2.1.1 Structure of polymers

To study the engineering applications of polymers or polymer-based coatings, it is essential to understand their structure. Often, the structure of a material plays a key role in controlling its tribological applications. For example, an elastomer will have a different wear mechanism compared to either a thermoplastic or a thermosetting polymer.

Unlike solid metals, polymers, in their synthetic state, are generally known to be partly crystalline and partly amorphous. In fact, any polymer referred to as crystalline is indeed semi-crystalline^[2.3]. When a polymer melt is cooled below its melting temperature, crystallization is initiated at nuclei (minute specks of impurities) at different points in the melt. The crystallization proceeds by the growth of the spherulites (spherulites are globe-like structures of freshly nucleated polymer particles within the melt), which at this stage are usually spherical, each spherulite having a nucleus at its centre. The spherulites expand at a constant rate if the temperature is held constant^[2.3, 2.4]. As the growth front advances into the melt, amorphous polymer is left trapped between the crystals. In some polymers, linear polyethylene or polytetrafluoroethylene (PTFE) for example, the trapped macromolecules are identical to those which have crystallized. The trapped (amorphous) macromolecules can crystallize in a secondary crystallization process after the cessation of primary crystallization. It is believed that the more the secondary crystallization proceeds the more the solid polymer approaches

that of a crystal ^[2.3]. The end solid is a disordered structure with a relatively high modulus at room temperature ^[2.4]. The resulting structure after cooling explains the ductile nature of polymers in general. Examples of the different polymer structures are given in Table 2.1.

Polymer crystals are known to be extremely anisotropic in nature. Along the molecules the bonds are covalent. In the two transverse directions, molecular packing is generated by much weaker secondary forces (van der Waals, dipole and hydrogen bonds, depending on the chemical structure of the molecule) ^[2.3]. The most important consequence of this for mechanical properties is that the elastic modulus of the crystalline structure depends critically on direction. For instance, in the direction of the molecule, the modulus of polyethylene is of the order of 200 GPa. In both transverse directions, the modulus is approximately 100 times lower ^[2.3].

2.1.1.1 Classification of polymers

Polymers are classified in several ways: by how the molecules are synthesized, by their molecular structure, or by their chemical family ^[2.1]. However, the most commonly used classification method is to describe polymers in terms of their mechanical and thermal behaviour, see Table 2.1.

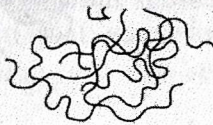
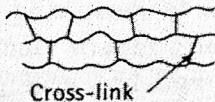
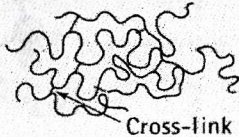
Behaviour	General Structure	Diagram
Thermoplastic	Flexible linear chains	
Thermosetting	Rigid three-dimensional network	
Elastomers	Linear cross-linked chains	

Table 2.1: Comparison of three polymer categories ^[2.1].

Thermoplastic polymers are composed of long chains produced by joining small molecules, or *monomers together*; they typically behave in a plastic flexible manner. Because of their soft nature, they can be formed by viscous flow when heated to

elevated temperatures, and they can also be recycled ^[2.1]. Examples include: polyethylene (PE), PTFE, polyvinylidene fluoride (PVDF), and polyamide 11 (PA11). Thermosetting polymers are the opposite of thermoplastics. They become hard and rigid upon heating. Unlike thermoplastic polymers, this phenomenon is not lost upon cooling. These are characteristic of network molecular structures formed by the step growth mechanism. The chemical reaction “steps” are enhanced by higher temperatures and are irreversible; that is, the polymerisation (the process by which small organic molecules are joined into giant molecules, or polymers) remains upon cooling. Examples include: phenolics (phenol formaldehyde, Bakelite), and amino resins (urea formaldehyde). Elastomers have not been mentioned because they do not have much relevance to the current research. The reader is referred to ^[2.1] for more information on elastomers.

2.1.1.2 Polyamide 11

Thermoplastic polyamide 11 (PA11) has been used extensively in this study. Hence, the need to understand the structure of this type of thermoplastic polymer. The review of PA11 is necessary because the understanding of the structure will aid the detail characterisation of its tribological properties.

PA11 $[-(\text{CH}_2)_{10}\text{CONH}-]$, a semi crystalline polymer (degree of crystallinity is about 35 %) ^[2.5], is a linear aliphatic chain polyamide consisting of an even number of methylene (CH_2) groups and one amide group ($\text{O}=\text{C}-\text{N}-\text{H}$) in its structural unit ^[2.6]. The polarity of the amide group induces hydrogen bonding between neighbouring chains. These hydrogen bonds are crucial to the crystalline structure. At room temperature, about 95 % of the hydrogen bonds are formed and even in the melt (above $T_M = 190^\circ\text{C}$) a large number of the hydrogen bonds are still present ^[2.7].

The crystalline part of PA11 cooled from the melt is generally composed of two phases at room temperature: the stable triclinic α -phase and the metastable, smectic pseudo-hexagonal δ' -phase ^[2.8, 2.9]. Many cell structures have been proposed for the triclinic α -phase. The most probable structure consists of antiparallel chains linked by hydrogen – bonds in the (010) planes, which gives a layer-like structure ^[2.8] (see Figure 2.1). Between 60 and 100°C , the triclinic α -phase changes progressively and reversibly into the hexagonal δ -phase, a process known as the Brill transition ^[2.10]. According to Chocinski-Arnault et al. ^[2.5], the stable crystalline form of PA11 is the triclinic α -phase

at room temperature whereas the δ -phase is usually formed at temperatures above 100°C. It was also noted that the characteristic α -phase can be reached only when the melt is slow cooled. A quench leads to the smectic δ' -structure where the chains do not respect the antiparallel distribution, so that this δ' -phase cannot change into the α -phase at room temperature.

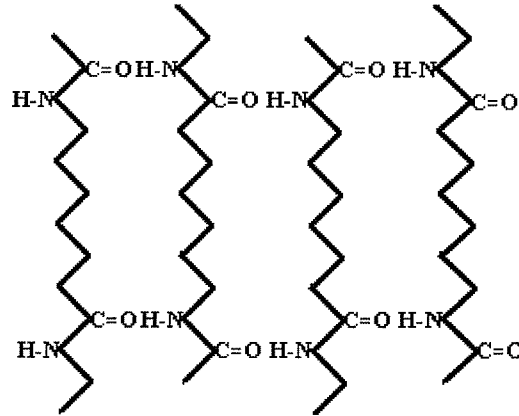


Figure 2.1: Schematic of the triclinic α -phase form of the PA11 ^[2.6]

During forming from the melt, the polymers are sheared which induces local chain alignments. In polyamide 6, for example, Khanna ^[2.11 – 2.14] has shown that processes such as melt shearing introduce local zones of orientation leading to an ordered environment stabilized by hydrogen bonds. The persistent alignments act as crystalline phase nuclei during the cooling. They have an essential role on the crystallization: a high concentration of the nuclei is known to increase the crystallization temperature. The alignments enhance the density of the crystallites and modify the structure and thus the properties of the polymer. Anik et al. ^[2.15] in calculating the Young's modulus of the different α polyamides has shown that the structure of the polymer, which is defined by the orientation of the molecules, will indeed influence this property of the polyamide. Belec et al. ^[2.16] has studied the creep of polyamide 11 at different temperatures and shown that the structure of PA11 affects its creep properties.

2.2 Wear

The movement of one solid over another is fundamental to the performance of many kinds of mechanism, both artificial (engineering devices) and natural (human joints) ^[2.17]. When these solids undergo slip or sliding, wear is inevitable ^[2.18]. This leads to the question, “what is wear”?

Several authors have given different definitions to wear in terms of many factors. A simple definition states that, “wear is the loss of material from a surface caused by interaction with another surface or material” ^[2.19]. The main interactions are load and motion producing adhesion, abrasion or fatigue, all of which can lead to the loss of wear fragments ^[2.20, 2.21]. The different types of wear processes are fully discussed in sections 2.2.2 to 2.2.4.

Sarkar ^[2.21] has defined wear as the rupturing of “hills and valleys” on mating surfaces which are areas of molecular contact; they are generally much smaller than the geometrical area of the mating surfaces. Other authors ^[2.18, 2.22, 2.23] have referred to these hills and valleys as asperities. Hence, in order to fully understand the process of wear, the concept of surface topography of engineering materials moving against one another must be understood.

2.2.1 Topography of contacting surfaces

When two nominally plane and parallel surfaces are brought gently together, contact will initially occur at only a few points ^[2.19]. These individual point (asperity) contacts sum up to make up what is referred to as the true area of contact. As the normal load is increased, contact between the surfaces also increases with asperities coming into contact thereby increasing the true area of contact. According to Kragelski ^[2.18], it is possible to distinguish between several areas of contact, see Figure 2.2:

1. The apparent (geometrical) contact area, Aa , which is the geometrical locus of all possible real contact areas; outlined by the dimensions of the contacting solids, it is independent of load.
2. The contour area, Ac , which is the area constituted by the deformation of the surface undulations. The real contact areas are situated within the contour

area; the latter depends both on the geometrical outline of the surface and on the load.

3. The real (physical) area of contact, A_r , which is the sum of all the small areas over which the asperities touch. This is a function of both the load on individual asperities and their geometrical contour. Kragelski ^[2.18] also noted that the most important characteristic of the real area of contact is the contact density, which is the number of asperities of area, n_o , per unit area for a stationary contact, Figure 2.2.

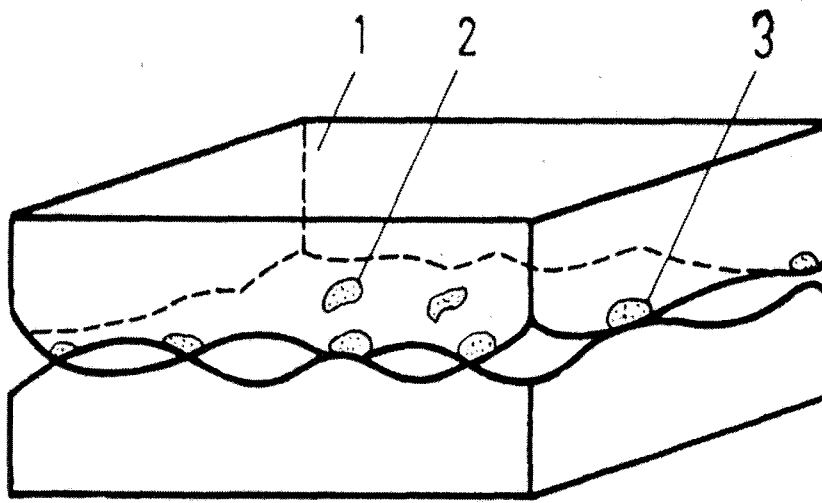


Figure 2.2: Nature of contacting bodies showing the areas of true contact ^[2.18]. (1) is the apparent contact area, (2) is the contour area and (3) is the real area of contact.

It is widely accepted that asperity interactions between two metallic surfaces in relative motion consists of two principal components namely, adhesion and deformation. The former mostly results from the cold-welding of the asperities over the area of real contact and the resulting 'junction' formed requires shearing during sliding. The latter, which is sometimes referred to as ploughing, results from the inter-penetration of asperities on the surfaces, thereby causing removal of materials during sliding. When any two surfaces are brought into solid-state contact and thereafter separated, the nature of one or both surfaces frequently changes because of the contact. The application of an external load could even increase the severity of the changes on the surfaces. Polymeric materials are not different from other solids in this respect. The surface and sub-surface

changes that occur in polymers may, however, be more difficult to characterize. In part, this is because of the difficulty in the identification of these materials ^[2.24].

2.2.2 Sliding wear of polymers

The term *adhesive wear* is sometimes used to describe sliding wear, but its use can be misleading. Although adhesion plays an important role in sliding wear, it is only one of several physical and chemical processes that may be involved ^[2.17]. Therefore, the general term 'sliding wear' is used in preference.

In contrast to metals and ceramics, polymers exhibit lower coefficient of friction, which is defined as

$$\mu = \frac{F}{N} \dots\dots\dots 2.1$$

(where μ is the coefficient of friction, F is the frictional force and N is the applied normal load), with values typically between 0.1 and 0.5, whether the polymers slide upon themselves or against other materials ^[2.17]. However, when certain polymers slide over clean and smooth surfaces the adhesive forces between the polymer and counterpart are sufficient to inhibit sliding ^[2.24], resulting in wear from adhesion between the surfaces, and involving deformation in the surface layer of the polymer only. According to Rabinowicz ^[2.24], a small patch on one of the surfaces comes into contact with a similar patch on the other surface during sliding, and there is a probability, small but finite, that when this contact is broken the break will occur not at the original interface but within one of the materials, most probably in the softer of the two. On the other hand, if the counter face is rough, then its asperities will cause deformation in the polymer to a significant depth. Wear then results either from abrasion associated with plastic deformation of the polymer, or from fatigue crack growth in the deformed region. These two types of wear mechanisms, involving surface deformation have been termed interfacial and cohesive wear processes ^[2.17] respectively.

Adhesive wear occurs mostly when the counterface is smooth, and involves the transfer of a polymer layer to the harder counterface and its subsequent removal as wear debris ^[2.17]. However, when the transferred layer is not removed from the counter face, a continuous build up occurs at the sliding interface and the nature of this transferred film

has a profound influence on the tribological behaviour of the mating parts. A durable transferred film would be expected to reduce the polymer volume loss. Often, this relation is dependent on the roughness of the transferred layer ^[2,24]. Wear debris formed by soft polymers usually fills the spaces between asperities of the harder surface, eventually leading to a smooth, composite, surface layer. When the steady-state condition is reached, the wear rate is often directly proportional to the load over quite a large range.

On the other hand, not all polymers show adhesive wear of this nature. Thermosets, for example, which are less ductile, do not form transfer films easily, but wear instead by fatigue processes or abrasion from cracks generated at the surface parallel to the sliding direction. Figure 2.3 shows the typical relationship between a soft (ductile) and a hard (brittle) polymer.

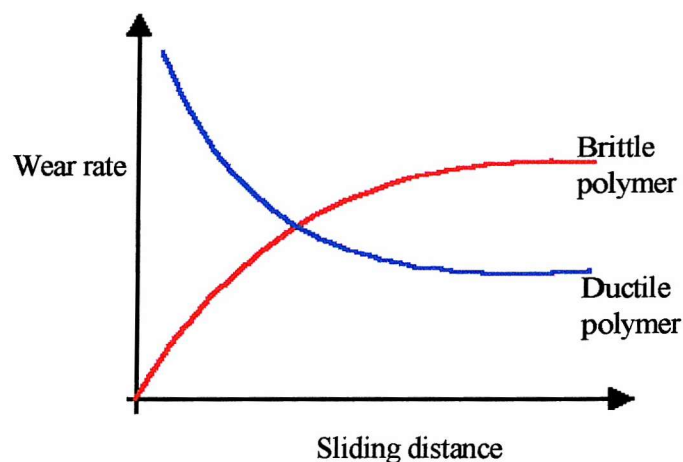


Figure 2.3: Common relation found between the wear of brittle and ductile polymers ^[2,24]

In the past, the adhesion properties of several polymers have been studied. Hutchings ^[2,17] in his review of some of these polymers, for example, PTFE, high density polyethylene (HDPE) and ultra-high molecular weight polyethylene (UHMWPE), noted that they form transfer layers of a rather different type under certain conditions which are associated with low friction and wear rates. For smooth counter faces or at low sliding speeds typically 0.01ms^{-1} , a very thin transfer layer is laid down, perhaps 5 to 10 nm thick whereas a return to 'normal' transfer occurs with rougher counter faces or higher sliding velocities.

Other authors have comprehensively reviewed the mechanism of adhesion [2.21, 2.23, 2.26, 2.27]. This has led to the suggestion of a number of possible theories, which take place during the process of adhesion:

- Mechanical theory
- Absorption theory
- Diffusion theory
- Chemical theory
- Molecular-Kinetic theory

In practice, the theory or combination of theories which best describe each situation largely depends on how well the theory is interpreted.

2.2.3 Abrasive wear of polymer

The removal of material from a surface by harder material impinging on or moving along the surface under load is termed abrasive wear [2.19]. The hard material indents the surface and depending on the properties of the materials and the type of motion or loading, may remove material by various mechanisms, e.g. cutting, ploughing, chipping or fatigue cracking [2.19]. During ploughing, material is displaced sideways, normal to sliding direction, Figure 2.4, and ahead of the abrading particle [2.24].



Figure 2.4: *Repeated ploughing showing the weakened zone of material* [2.22].

Likewise, in the case of abrasive cutting, material loss is equal to the volume of the wear groove produced by the abrasive particle acting like a cutting tool, Figure 2.5.

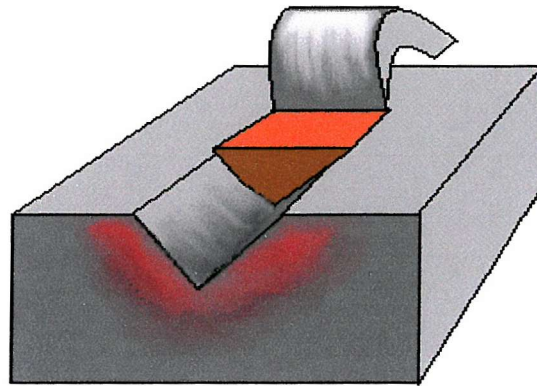


Figure 2.5: *Cutting action of the abrasives during abrasive wear* ^[2.24].

This has also been illustrated by a model experiment involving conical indenters of various angles sliding over smooth, softer surfaces, Figure 2.6 ^[2.28]. The figure shows how the volume of the groove produced per unit sliding distance varies with the base angle of the indenter for poly methyl methacrylate (PMMA) and a soft metal (tin). It is obvious that plastic deformation occurs at all angles for soft metals while for polymers, a linear relationship between volume and $\tan \theta$ only occur when θ exceeds about 30° . Evans and Lancaster ^[2.26] also noted from Figure 2.6 that plastic deformation and cutting of polymers are likely to occur only during sliding against surfaces with a R_a of the order of $12 \mu\text{m}$.

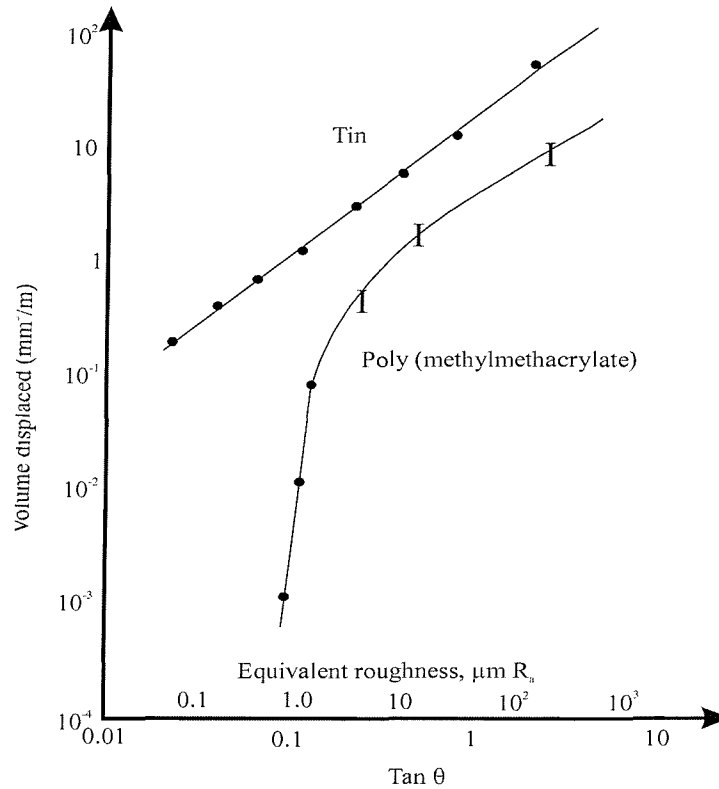


Figure 2.6: Relationship between the volumes of material displaced and the base angle of a conical indenter ^[2.28].

2.2.3.1 Classification of abrasive wear

In the study of abrasive wear mechanisms, a distinction is often made between two-body abrasive wear, Figure 2.7, and three-body abrasive wear Figure 2.8. The former is caused by hard asperities penetrating into the counterface, while in the latter case, free particles are trapped in-between the sliding surfaces and can roll, slide or even abrade each other.

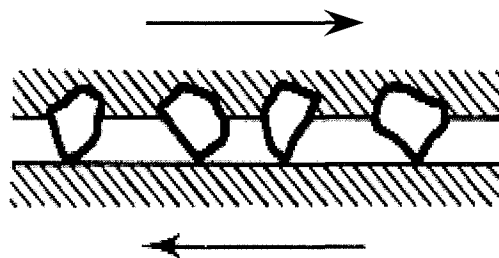


Figure 2.7: Schematic showing a two-body abrasive wear ^[2.17].

Three-body abrasive wear is generally less severe than two-body because the abrasive particles are free to roll, slide, and vary their approach angles between the sliding

surfaces. Other terms have been used to describe abrasive wear ^[2.19]. When abrasive material slides over a surface at relatively small loads without significant impact, the wear produced by the ploughing or cutting action is termed low-stress abrasion.

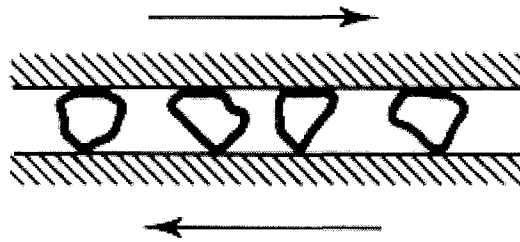


Figure 2.8: Schematic showing a three-body abrasive wear ^[2.17].

On the other hand, when a hard asperity or particle slides over a surface at high load such that wear is characterised by high stresses, and results in macro-deformation ^[2.29] or causes a significant impact on the mating surfaces, the term used is high-stress abrasion. In the latter case the particles may be broken due to the high stress developed.

2.2.4 Corrosive wear

Due to a large number of environmental factors that are responsible for corrosion, it is somewhat difficult to describe a single definition for corrosion and corrosive wear. Faced with this problem, individual authors seem to define it with respect to the environmental condition acting on the component at a particular time. For example, Arthur and co-workers ^[2.19] have defined corrosive wear as a process which is at least partly chemical and in which the chemical effect is not beneficial. Elsewhere ^[2.30], corrosive wear has been explained in terms of the dynamic interactions between environment and mating material surfaces. According to Fischer ^[2.31] and Quinn ^[2.32], the interaction gives rise to a cyclic stepwise process:

- In the first step, the contacting surfaces react with the environment, and reaction products are formed on the surface.
- In the second step, attrition of the reaction products occurs because of crack formation and/or abrasion in the contact.

This process results in increased reactivity of the asperities because of the changes in their mechanical properties and/or temperature change. It has been noted by Fischer ^[2.31] that where corrosion is a major cause of wear, there is usually complex interactions between various mechanisms. In most cases, wear of surface films could be due to

either adhesion or abrasion. Since many commonly occurring films, notably iron oxides, are abrasive, both corrosion and abrasion will combine. High contact stresses have also been noted to enhance corrosion locally, leading to pitting ^[2.33].

2.3 Wear test methods

There are several laboratory wear testing methods; American Society of Lubrication Engineers (ASLE) ^[2.34] lists some 270 types of friction and wear testing devices. A limited number of these test methods are commonly used in the laboratories. Details of some of the ASLE test devices are given in Table 2.2.

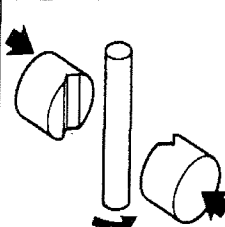
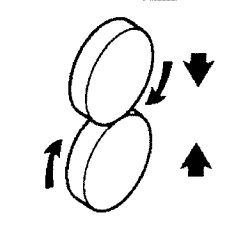
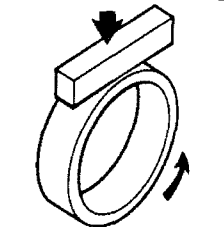
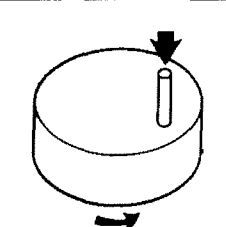
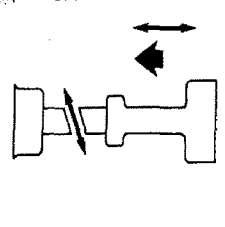
	(a)	(b)	(c)	(d)	(e)
TEST CONFIGURATION					
TEST PURPOSE	Determination of the wear rate, load carrying capacity and friction coefficient for sliding contacts.	Determination of the sliding wear rate of test materials, treatments or coatings.	Determination of the adhesive wear rate of materials against an SAE 4620 steel ring.	Determination of sliding wear rate	Determination of cohesion and adhesion qualities of coatings and also their wear characteristics under arduous vibrating conditions.
SPECIMENS	A 5.35 mm diameter cylindrical journal is rotated within two loaded stationary V-blocks to give a 4-line contact.	Normally two discs 40 mm diameter and 10 mm thick. Alternatively the discs may be made 30 and 50 mm diameter.	The steel ring is rotated with a stationary block of the test material (which may be a coating) in loaded contact.	A pin rubbing on a rotating circular plate.	Obliquely cut specimens of 23 mm ² contact area.
TEST CONDITIONS	Journal speed 290 rev/min Sliding velocity 0.1 m/s Load (constant or increasing) 89-20,000 N Hertz stress 242-3450 MN/m ² Specimens can be immersed in oil or other fluid.	Lower disc speed 400 rev/min Upper disc speed 440 rev/min Load 196 N. May be run dry or lubricated	Ring speed (max) 197 rev/min. Load (typical) =340 N Load (max) 2800 N Duration 20,000 cycles.	Specific to type of test.	Combined impact and sliding Sliding distance: 0.76 mm Impact frequency: 60-70 Hz Impact load: 60-223 N Temperature: 600°C Duration: 6-10 hr
MEASUREMENTS	Journal driving torque Progressing wear depth Wear life. Seizure failure load Final specimen weights	Individual disc weight loss. Total disc weight loss.	Test block weight loss. Scar width. Ring weight loss.	Weight loss of disc. Height loss of pin.	Volume loss Fretting resistance =1/volume loss
WEAR TYPES	Mild and severe adhesive wear Scuffing	Mild and severe adhesive wear. Machining wear.	Mild and severe adhesive wear	Mild and severe adhesive wear	Adhesive wear Fatigue Fretting

Table 2.2a: Various test configurations as compiled by ASLE ^[2.34]: (a) is Falex, (b) is Amsler, (c) is LFW-1, (d) is pin-on-disc and (e) is Hammer.

WEAR TYPES	MEASUREMENTS	TEST CONDITIONS	SPECIMENS	TEST PURPOSE	TEST CONFIGURATION
Adhesive wear. Fretting.	Volume loss.	Sliding amplitude: 0.254 mm Sliding frequency: 25 Hz Load: 5.57 N Temperature: 20-800°C Duration 10 ⁵ cycles.	Spherical buttons against a flat pad.	To evaluate over a broad temperature range, materials used in gas turbines.	(f)
Low stress abrasion.	Weight loss Taber Wear Index = weight loss/1000 revs (mg)	Load 9.81 N Wheels cleaned with abrasive paper every 1000 revolutions Test is run without lubricant	Flat face of the disc abraded by two CS-10 rubber bonded abrasive wheels.	Determination of the abrasive wear rate and the Taber wear index of material surfaces.	(g)
High stress grinding abrasion Low stress abrasion Machining wear	Volume loss.	Load per pad 112 N Runs in bath of abrasive slurry	Two specimen pads loaded against a rotating circular plate.	Determination of the abrasive wear rate and the abrasion resistance of materials and treatments.	(h)
Contact fatigue (pitting).	Cycles to first fatigue pit. Endurance limit = stress to produce pitting in 10 ⁷ cycles.	Speed 1050 to 1500 rev/min Load variable Lubrication by spray fed gear oil	Roller of 102 mm diameter in the test material loaded against and driven by a 25 or 51 mm diameter carburised shaft.	Determination of the rolling contact fatigue life of materials and treatments used for gears.	(i)
Scuffing.	Load to produce scuffing.	Gear tooth 15/16 (16/24) Pinion speed 2000 (2170) rev/min Load increased in equal steps (log. steps) Temperature 60°C (90°C) Lubrication by oil spray (oil bath)	Gears made from test material.	Determination of the load to cause scuffing of test gear material/lubricant combinations.	(j)

Table 2.2b: Continuation of table 2.2: (f) is Dry rubbing wear, (g) is Taber abrasion, (h) is Wet slurry abrasion, (i) is Roller contact fatigue and (j) is Gear scuffing.

Laboratory investigations of wear are usually carried out either to examine the mechanisms by which wear occurs, or to simulate practical applications and provide useful design data on wear rates and coefficients of friction^[2.17]. In either case, control and measurement of influencing variables on wear are very important. Wear rate and friction are critically dependent on sliding conditions; therefore, minor changes in the test conditions could lead to enormous changes in the dominant wear mechanism associated with the wear rate^[2.17].

There are two main classifications of laboratory test configurations: symmetric and asymmetric, see Figure 2.9, A-F. Symmetric geometries, Figure 2.9, (A) and (B),

expect the wear rates of the two contacting surfaces with identical material to be the same. The asymmetric geometries, which are more commonly used, do not require the two sliding bodies to produce the same wear rate. Though they are made of the same material the surfaces experience different wear rates, Figure 2.9, (C) – (F). Hutchings^[2.17] has given reasons for the difference in the two types of testing configurations.

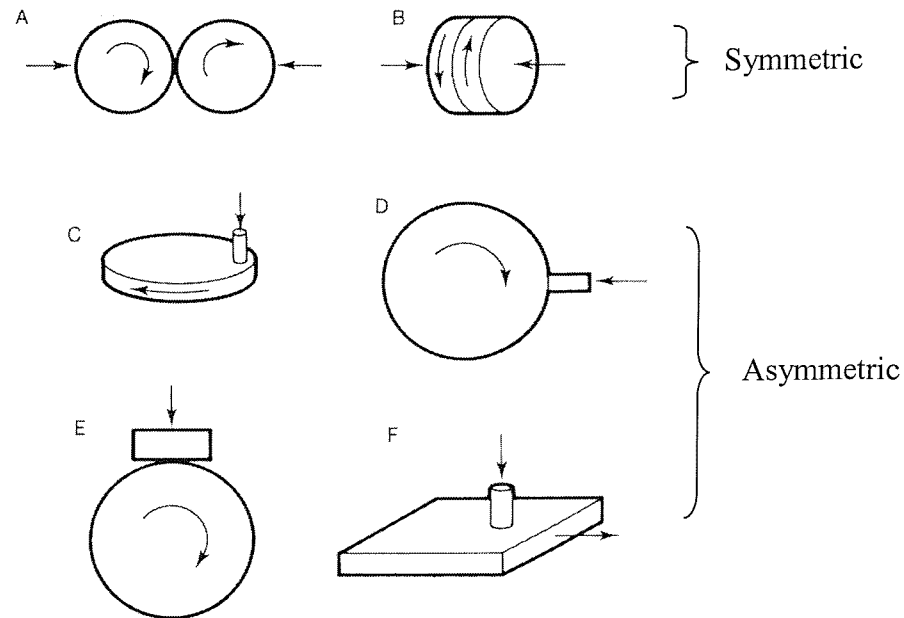


Figure 2.9: Schematics showing various wear testing configurations^[2.17].

Several sliding wear test methods have been the subject of national standards. Examples include the block-on-ring (ASTM G77), Crossed cylinder (ASTM G83), Pin-on-disc (DIN 50324) and rotating pin-on-flat (ASTM G98) geometries^[2.17]. This has led to a considerable research effort into the study and measurement of the wear of a range of polymer-based materials. Alliston-Greiner^[2.35] noted the framework offered by Hogmark and Jacobson^[2.36] for the selection of test machines and conditions. They have suggested the following possible classes of test:

1. Complete tribocouple- using the actual components
2. Semi tribocouple- one true component and one model
3. Model test- using two model surfaces

The model test offers simplicity, a high degree of control and accessibility, while complete tribocouples give the most reliable results.

Apart from the normal variables of load, contact area, sliding speed and time, several other factors must also be considered and monitored in wear testing. For example,

Hutchings^[2.17] has noted the influence of temperature on the mechanical properties of materials and on thermally activated chemical processes, although these may often be dominated by a frictionally generated temperature rise. Thus, the list of influences mentioned earlier may suggest that it is not possible to produce a valid laboratory simulation of a practical application, and that the only valid wear test is a service trial. Sviridyenok and Kirpichenko have noted that standardization of test methods is quite difficult for most metals^[2.37]. As for polymeric materials, the situation is not always the same, but it is important to be aware of the possible consequence of departing too far from actual test conditions^[2.17].

Over the years, a number of relatively simple laboratory wear testing machines have been developed and used to assess the wear behaviour of polymers. A common and widely accepted technique is to slide a polymer, which is usually made the pin, over the surface of a rotating disc. This technique, as much as possible, tries to simulate the practical conditions. The different types of configurations for the techniques have been explained earlier, Figure 2.9 (C) and (D). Some of the problems encountered by previous researchers with this type of rig system have been noted and discussed elsewhere^[2.24].

However, it is interesting to note that despite the few problems associated with the pin-on-disc machine and similar rigs, they are still widely accepted as the most reliable rig for the laboratory wear test. The reason being that it is simple to design, easy to modify and adapted to suit individual research needs and the ability to manipulate variables with an appreciable degree of accuracy. A major problem of the pin-on-disc, though, is rigidity. It has been noted that edge loading, which arises from low stiffness of the whole pin-on-disc structure, give rise to a higher contact pressure at the edge of the rotating pin^[2.24]. This eventually leads to uneven wearing of the pin and complicates the post-test analysis of worn pins. Attempts have been made in the past to rotate the pin, but this tends to make it more difficult as the wear mechanisms post-test features would have been disrupted. For example, the wear direction on the pin would be difficult to identify. Also, the fact that displacement transducers and force transducers are both used to measure the smallest changes that take place on the pin, and the frictional forces respectively indicate that the rigidity of the machine has to be considered. Especially from the design stage, as any small compromise in this factor will have considerable

effect on the accuracy of the overall test result. Greenwood et al. ^[2.38] have used a dial indicator gauge to level the sample pin on the rotating disc. Although some degree of success was achieved, this does not apply to all test rigs. For instance, in a true tribocouple wireline wear test, this corrective method may not be effective because the slickline wire is not a flat surface

However, there are standard industrial tests, which every coating is expected to pass before it can be certified for use downhole by NACE (National Association of Corrosion Engineers). Lewis and Barbin ^[2.39, 2.40] have listed the four types of experiments as: Autoclave test, Rocker Arm test, Acid Resistance test, and Wireline Abrasion test.

2.3.1 Autoclave test

This is used to measure a coating's ability to withstand CO₂ blistering, which may occur during a rapid decrease in the production pressure of the well ^[2.41]. Carbon dioxide, which diffuses into the coating during production, is not able to escape quickly from some of the coating during a rapid pressure decrease. This can cause coating failure by severe blistering or, in the worst case, partial or complete coating disbondment. This test simulates possible extreme field conditions. A typical autoclave consists of distilled water, a mixture of hydrocarbon phase and carbon dioxide gas. Although the test conditions are considered extreme, its selection largely depends on the experimentalist. For example, the authors in ^[2.39] have used a pressure of 68.95 MPa, test temperature of 177 °C and period of 18 hours. According to the authors, the conditions used are a good representation of most oil wells.

2.3.2 Rocker arm Test

This is also used for checking for blistering or disbondment of the coating as the autoclave test except that it uses lower pressures and temperatures than the autoclave test ^[2.42]. The fluid content also may vary in the case of rocker arm test. For example, a tubular test section is 2/3 filled with fluid containing 80 % de-ionised water, 10 % depolarised kerosene, and 10 % toluene ^[2.39]. The remaining 1/3 volume is filled with 20 % carbon dioxide and 80 % methane gas mixture. The test is maintained at 149 °C and a pressure of 13.8 MPa and the tubing was gently rocked about 30 degrees from a horizontal position, to expose the internal coatings to the test fluid.

2.3.3 Acid resistance test

This method is used to test for the resistance of the coatings to acid degradation. Acid degradation is reported to be cumulative and is hastened by higher temperatures ^[2.43]. Mineral acids are used for this purpose. The test section is a cut internally coated tubular capped at both ends with acid resistant plugs. The tubular is filled to about 2/3 levels with uninhibited acid and then capped at both ends and set vertically in a water bath maintained at 85 °C. The sample is drained periodically and visually examined for evidence of blistering and coating disbondment. The duration of the acid resistance test depends largely on when evidence of degradation and disbondment is noticed after which the test is terminated. Depending on the resistance offered by any coating, the test period ranges between 72 hours and 96 hours ^[2.39].

2.3.4 Wireline abrasion test

Wireline damage to internally coated tubing has been a major concern since nearly all oil well are subjected to periodic wireline work. NACE international report RP0291-91 ^[2.44] outlines procedures for minimizing wireline damage to internally coated tubing. No industrial guidelines have been developed for evaluating internally coated tubing for wireline abrasion resistance, although some commercial laboratories and coating applicators have used the modified version of the ASTM tests for rating coatings for resistance to abrasion from sand and a reciprocating, rigid looped-wire under load ^[2.45]. However, Lewis and Barbin ^[2.39], have adopted a similar method to that used previously by Wolfe et al. ^[2.46]. The resistance of coatings to wireline damage was measured with a device that consists of a reel and idler pulleys plus the necessary counters and motors, see Figure 2.10. The diameter of the idler is 203.2 mm and it rotates at a linear velocity of 0.25 m/s - 1.5 m/s. The device reverses the wireline direction every 30.5 m. A lever arrangement is used to force the internal coatings against the wireline as it passes under the 203.2 mm diameter idler pulley. The test device has been designed in such a way that, when an electrical contact is created, when the wireline wears through the coating and the steel pipe substrate is contacted, the test is stopped automatically.

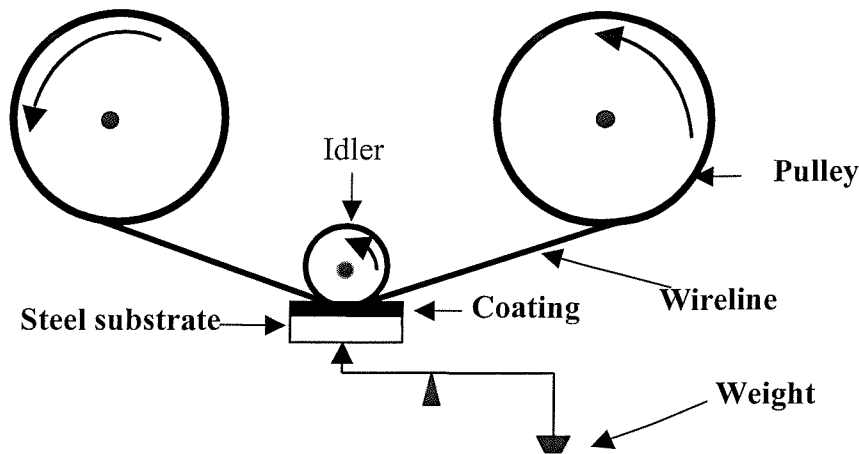


Figure 2.10: Schematic showing the apparatus used for comparing the resistance of internal coatings to wireline damage.

2.3.5 Experimental methods for sliding and abrasive wear tests

Several authors have used different experimental methods to study the sliding and abrasive wear of engineering materials ^[2.29]. Most of the test configurations have been previously tabulated by Symonds ^[2.24], together with the different types of experimental methods that have been used to study the abrasive and adhesive wear of engineering materials. According to Symonds, each method is not sample dependent. For example, a pin-on-disc rig can not only be used to test samples of polymers but also metals, and with different pin configurations, e.g. square, rectangular and circular ends. The motion of the pin on the disc is of importance as this could have a significant influence on the wear result at the end of the experiment. The common ones are listed below:

- Reciprocating
- Linear
- Rotational
- Helical
- Spiral

The most common test rigs adopt the reciprocating and continuous rotational counterface motion. The pin-on-disc test rig, one of the methods used in this study, adopts the continuous rotational counterface motion. Many authors have used this method to study the sliding wear of engineering materials ^[2.47 – 2.50]. It consists of a rotating disc and a sample pin, where the pin is normally loaded against the disc Figure 2.9 (C). Despite the wide acceptability of this experimental test method, it is characterised by a number of problems, which has been discussed earlier. Based on the associated problems of the pin-on-disc, a new method of studying the abrasive wear

behaviour of engineering materials has evolved; the ball-cratering micro-scale abrasive test.

2.3.5.1 Micro-scale abrasive wear

The micro-scale abrasive wear test method has been identified as a reliable means of evaluating, quantitatively, the wear of engineering materials compared to other experimental methods ^[2.51 - 2.56]. The reliability of this experimental method lies in its reproducibility, and the fact that it can be used to estimate wear at the micro-scale; thus its use for testing thin coatings. Micro-abrasion was employed in this study, as an alternative method, due to the problems identified with the pin-on-disc.

The ball-crater micro-scale abrasive wear test ^[2.51 - 2.54] is an example of a test method, which produces an imposed wear scar geometry. In this method, a hard steel sphere of radius R is rotated against a sample in the presence of slurry of fine abrasive particles, usually silicon carbide or diamond. The geometry of the wear scar is assumed to reproduce the spherical geometry of the ball, and the wear volume may then be calculated by measurement of either the crater diameter or its depth ^[2.56]. A typical micro-scale abrasive tester is shown in Figure 2.11.

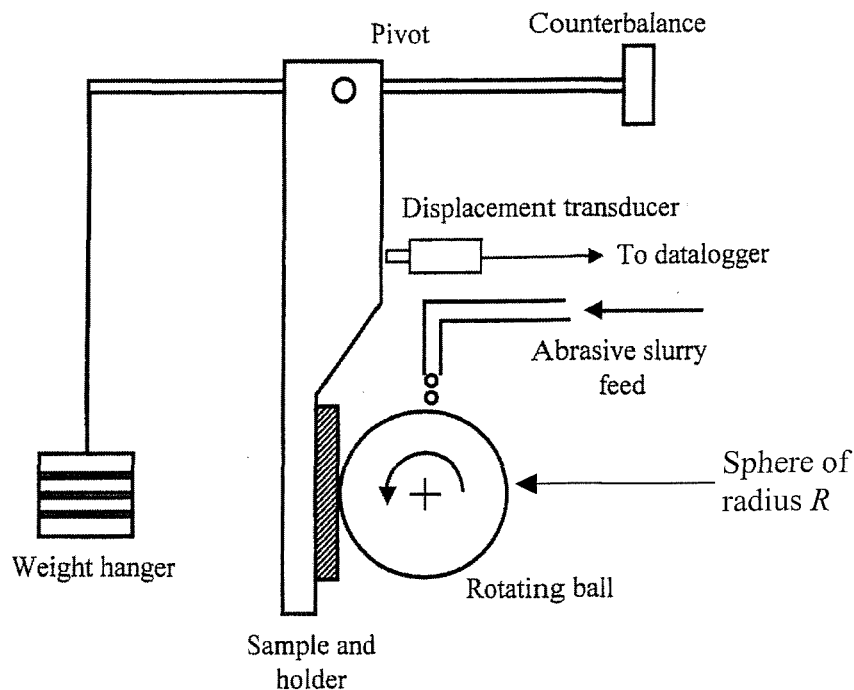


Figure 2.11: Schematic diagram of the ball-cratering micro-abrasion tester ^[2.53].

Many authors have used this method to study not only the tribology of engineering materials, but also the different conditions and factors which may influence the outcome of the result. For example, Allsopp et al. ^[2.56] have used it to study the effects of the ball surface condition in the micro-scale abrasive wear test. Their results show that variation in the ball surface condition strongly influences the wear processes and wear coefficients. It was found that the use of a new, well-polished ball in the test could result in a delayed onset of wear compared to using a finely pitted ball, which gives a higher magnitude of wear rate. It was noted that the effect of using a new ball was more pronounced in a relatively soft material. Other authors ^[2.57 - 2.62] have adopted the micro-abrasion test method to study various engineering materials, which includes polymeric materials such as paint films and soda-lime glass, under different conditions.

2.3.6 Factors affecting wear rate

Strict proportionality between wear rate and the normal load is not often found ^[2.17].

Until Archard ^{2.17} proposed the generally accepted calculation of wear volume, V , in 1953, the estimation of wear rate was based on three basic laws of adhesive wear. These are:

1. the amount of wear is generally directly proportional to the load, W
2. the amount of wear is generally proportional to the distance slid, say, S
3. the amount of wear is generally inversely proportional to the hardness H of the surface being worn away

which can be represented mathematically as;

$$V = \frac{CWS}{H} \quad (2.2)$$

Where C is a dimensionless constant dependent on the materials in contact and their exact degree of cleanliness. According to Rabinowicz ^{2.21}, many investigators have found that the above equation is not always perfectly obeyed, but in almost all cases it represents the experimental data.

Archard ^{2.17} in 1953 proposed a model of the sliding process, which enables equation (2.2) to be obtained in a simpler way and also offering a definite meaning to the constant C in equation (2.2). Figure 2.12 presents, diagrammatically, the Archard model in which two asperities slide over one another.

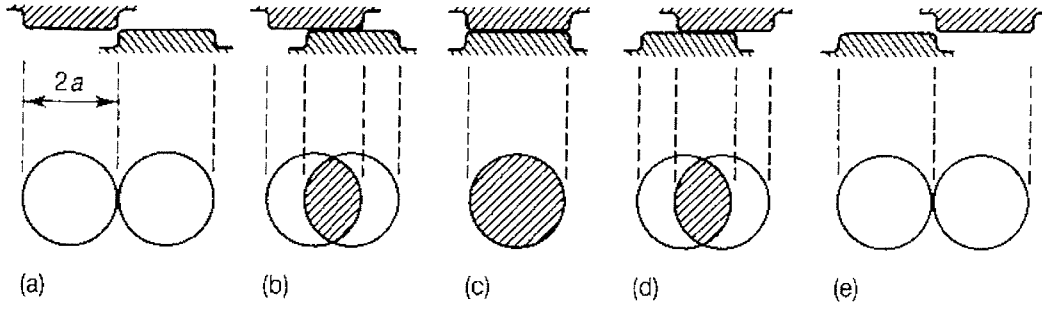


Figure 2.12: Schematic diagram showing the evolution of a single contact patch as two asperities move over each other ^{2.17}.

Observing the movement of these asperities from the plan view, he assumed that they are circular with radius a at various stages of evolution during sliding ^{2.17}. At position (c), Figure 2.12, the normal load supported by it δW , will be given by

$$\delta W = PA \quad 2.3$$

$$\text{But } A = \pi a^2 \quad 2.4$$

$$\text{Therefore } \delta W = P\pi a^2 \quad 2.5$$

P is the yield pressure for the plastically deformed asperity and this is assumed to be close to its indentation hardness, H . Equation (2.3) is based on the fact that contact between two asperities will occur where asperities touch, and that the true area of contact will be equal to the sum of the individual asperity contact area. This area will be closely proportional to the normal load, and it can be assumed that under most conditions, for metals at least, the local deformation of the asperities will be plastic. As sliding progresses, displacement of asperities occur as shown in Figure 2.12, and there is transfer of loads originally borne by the previous asperity junction to another which is in the process of forming elsewhere on the surfaces. In the process, asperity contact is formed and destroyed and knowing that wear is associated with the detachment of fragments of material from the asperities. It is assumed that the volume of material removed by wear, say, δV , will be proportional to the cube of the contact dimension a , which implies that the shape of the wear particle should be independent of its size. Assuming the shape of the wear particle to be an hemisphere with radius a , then

$$\delta V = \frac{2}{3}(\pi a^3) \quad 2.6$$

If we represent the sliding distance, $2a$, of one asperity by S , then the volume loss per unit sliding distance will be

$$\frac{\delta V}{S} = \frac{2}{6a}(\pi a^3) = \frac{\pi a^2}{3} \quad 2.7$$

By summing the volume over the entire set of asperities,

$$\sum \frac{\delta V}{S} = \sum \frac{(\pi a^2)}{3}$$

$$\frac{1}{S} \int \delta V = \frac{1}{3} \int \pi a^2 \quad 2.8$$

from equation (2.5) that

$$\delta W = P \pi a^2$$

Integrating,

$$\Rightarrow \int \delta W = P \int \pi a^2$$

$$\text{Or} \quad \frac{W}{P} = \int \pi a^2 \quad 2.9$$

Putting equation (2.9) in (2.8),

$$\frac{V}{S} = \frac{1}{3} \frac{W}{P} \quad 2.10$$

We know, of course, that not all the asperities make contact that gives rise to wear at the same time. So if we assume that q number of asperities make contact that gives rise to wear, then equation (2.10) can be re-written as,

$$\frac{V}{S} = \frac{q}{3} \frac{W}{P} \quad 2.11$$

The dimensionless parameter, q , is referred to as the coefficient of wear and by replacing $\frac{q}{3}$ with k , and the quantity P which is close to the hardness of the abraded surface by H . Equation (2.11) becomes the well referenced Archard wear equation

$$\frac{V}{S} = k \frac{W}{H} \quad 2.12$$

The conclusion from Archard's work was that wear volume is directly proportional to load and sliding distance for a given material couple, i.e.

$$V = kWS \quad 2.13$$

However, as noted earlier, strict proportionality is not always found between wear volume and load or sliding distance. This is because the Archard model is based on two sliding metals and plastic deformation, and does not take into account contacts between materials of different properties. It has also been found that Archard law does not hold where transitions occur between wear mechanisms in the contact. It is also important to point out that Archard's model was based on a single asperity, which was integrated (summed) over the true area of contact. Again the model does not recognise that all the asperities do not normally have the same height. The consequence is that as wear progresses, and new contacts are formed, the load distribution over the contact area is not uniform because the contact pressure is changing, hence, Equation (2.13) is less likely to be obeyed. There are other issues, such as; hydrodynamic (lubrication) and velocity and temperature effects, which are not incorporated. Hence, it is not surprising that Archard's law is often found not to hold. For instance, experimental evidence shows that direct proportionality between wear rate and load is not often found.

Archard and Hirst^[2.63] further show that, for the effect of load on engineering materials for many systems, the wear rate varies directly with load over limited ranges; abrupt transitions from low to high wear rate, and sometimes back to low wear rate, are often

seen with increasing load, see Figure 2.13. However, it has been noted that proportionality will be observed only when changes in load does not induce changes in any other variable affecting wear, such as temperature or the topography of the polymer and its counterface ^[2.28].

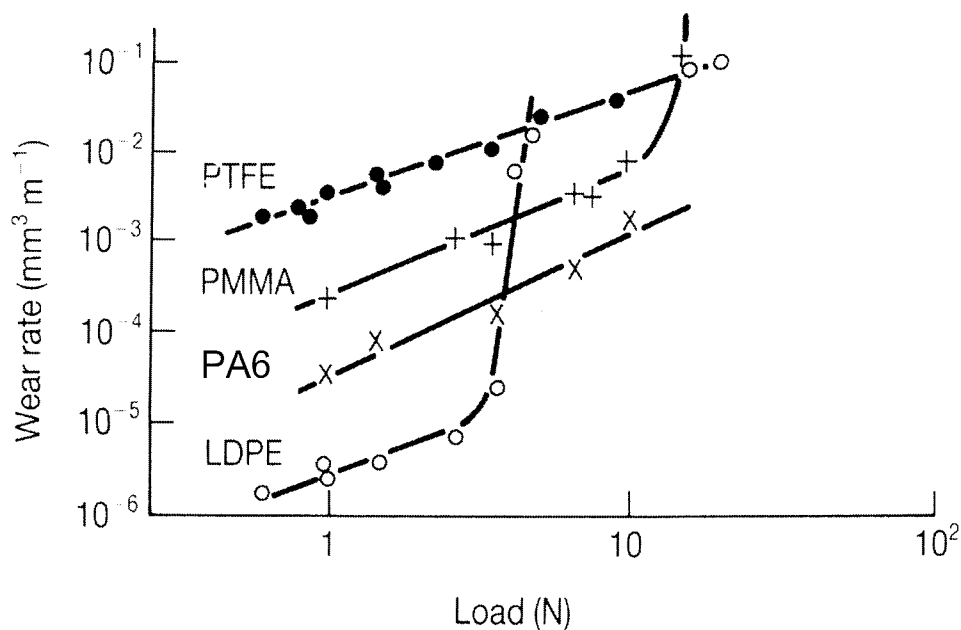


Figure 2.13: Effect of load on the wear rate of polymers for dry sliding ^[2.28].

2.3.6.1 Effect of temperature

Polymers are known to have poor thermal properties except for a few such as PVDF. Figure 2.14 shows results ^[2.64] from a pin-on-disc machine with a spiral track with variation of the ambient temperature on the wear rate. It can be seen for some polymers that as the temperature is increased, wear rate falls initially.

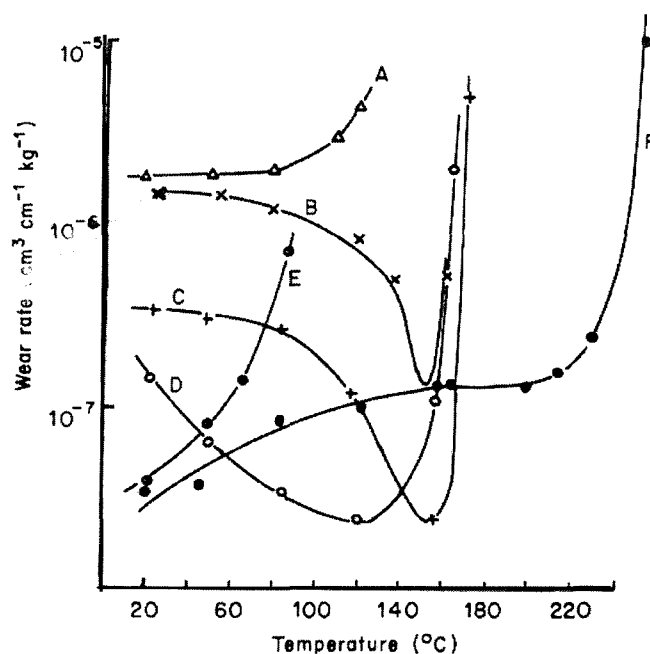


Figure 2.14: Variation of wear rate with temperature for dry sliding of some polymers against a steel counterface. A, polystyrene; B, polymethylmethacrylate; C, polyacetal; D, polypropylene; E, polypropylene; F, PA 66 ^[2.64].

It was suggested that there is probably a decrease in the modulus of elasticity with a rise in temperature. It was further thought that if the mode of wear is by fatigue, this means that the number of cycles to initiate fatigue increases and wear is low because the sliding time is kept constant ^[2.18]. At a characteristic temperature, however, thermal softening results in a rapid rise in the wear rate. Hutchings ^[2.17] has reported the behaviour of a number of polymeric materials as they respond to interfacial temperature during sliding. It was concluded that the rapid increase in the wear rate of low-density polyethylene (LDPE) and polymethylmethacrylate (PMMA) at higher loads resulted from thermal softening. This transition occurs when the flash temperature at the interface reaches the softening point (glass transition temperature, GTT's) of the polymer, see Appendix 1 for GTT's.

2.3.6.2 Effect of sliding speed

Lancaster and Evans ^[2.65] have studied the effect of sliding speed on the wear rate of some polymers, see Figure 2.15. The effect of thermal softening due to flash temperatures when the critical speed is reached, as indicated by the arrows is thought to be responsible for the behaviour of polymers, which is consistent with the observations of Hutchings ^[2.17] and Sarkar ^[2.21]. Sarkar ^[2.21], however, noted in the further work of

Lancaster that although the effect of the flash temperature should be to increase the wear rate by facilitating transfer of polymer to the counter face, not all the polymers show this behaviour with increasing speed, in fact, PTFE shows a decrease in the wear rate because of its self lubricating properties, Figure 2.15.

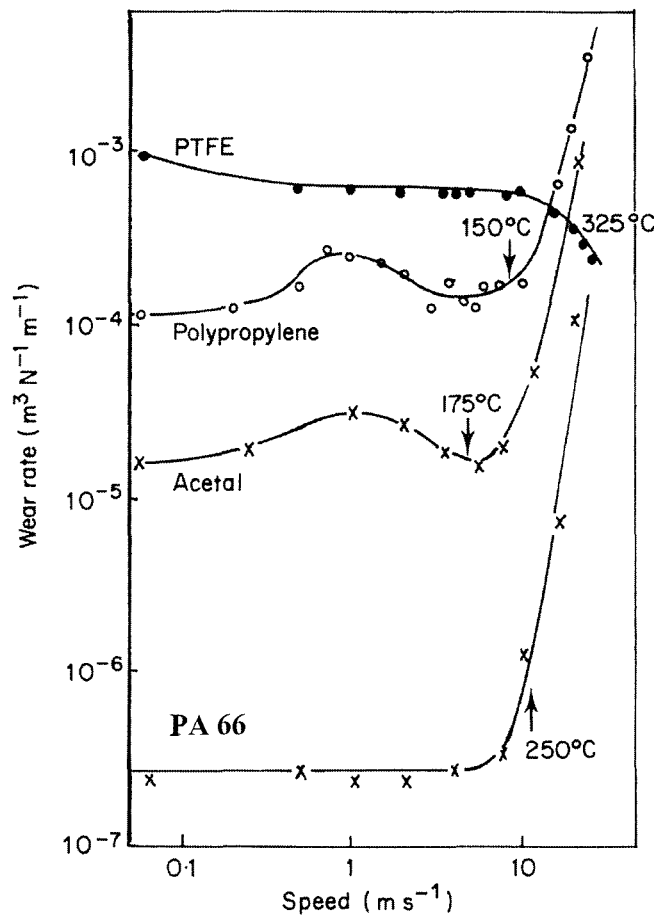


Figure 2.15: Variation of wear rate with sliding speed for PA 66 and other polymers sliding (dry) against mild steel^[2.65].

2.3.7 Analytical techniques to assess wear damage

In tribology, it is not enough just to test a material in the laboratory, but the damage caused by surface interactions needs to be analysed so that the mechanisms responsible for the wear damage may be understood.

Several studies have used different analytical techniques such as field ion microscopy^[2.66] and atom probes to analyse the surface of the tested sample in the laboratory. Since material transfer could be at the atomic scale, these analytical tools are widely employed to study the chemical and structural aspect of material transfer, especially for polymers.

They can also be used to obtain information on the adhesive strength of the polymer to metal bonds, the amount of material transfer and surface energy^[2.24].

However, in most cases, the detail offered by these instruments are not always required, as such, less powerful and more conventional ones are used to characterize the worn surface and the transferred material. The most commonly used of these instruments includes the scanning electron microscope (SEM)^[2.67, 2.68], the optical microscope, the surface profilometer and the energy diffraction x-ray analysis (EDX). All of these were employed throughout this research work.

2.4 Friction

Friction is the resistance to motion which exists when a solid object moves tangentially with respect to the surface of another which it comes in contact with, or when an attempt is made to produce such motion^[2.25].

The work expended against friction is often redundant, that is, it makes no useful contribution to the overall operation of the device of which the bodies are apart, and ultimately must be dissipated as waste heat^[2.69]. Consequently, in most tribological designs, the aim is to keep these frictional forces as low as possible. Although, there are exceptions to this general rule; occasions when sufficient friction is essential to continued progress and there are many practical devices which rely on the frictional transmission of power: automobile tires on the roadway, vehicle break and clutches, as well as several of the variable speed transmission systems.

Usually, friction is classified into two components, based on the nature of the motion experienced by the contacting surfaces. The friction experienced during sliding condition is known as sliding friction, and friction experienced during rolling condition is known as rolling friction^[2.30]. This review will focus on sliding friction as this applies mostly to the work conducted in this research.

A considerable amount of work has been devoted to the study of friction since the early investigations of Leonardo da Vinci, Amontons, Coulomb, Euler and Parents^[2.22]. Despite this fact, there is no simple model to predict or calculate the coefficient of friction of a given pair of materials. It is evident from the results of various studies^{[2.18,}

2.21, 2.22, 2.25 - 2.27] that friction originates from complicated molecular-mechanical interactions between contacting bodies and that these interactions differ from one application to another.

2.4.1 Sliding friction

The friction between two sliding surfaces is due to the various combined effects of adhesion between the flat surfaces, ploughing by wear particles and hard surface asperities, and asperity deformation ^[2.30]. The relative contribution of these components depends on the specific material used, the surface topography, conditions of sliding interface, and the environment.

2.4.1.1 Adhesion component of friction

According to Bowden and Tabor ^[2.22], the adhesion component of friction results from the deformation and rupture of interfacial bonds. These bonds are the result of interfacial inter-atomic forces that depend on the degree of interpenetration of asperities and the surface composition. Williams ^[2.69] noted that, the pressure at the asperity contact (true contact) is correspondingly higher than the nominal value. This implies that the outermost atoms of one surface can be in very close proximity to those of the counter face and that this is especially true if the surfaces are relatively clean and uncontaminated by extraneous surface layers. For sliding to take place, the friction force is needed to shear the weakest tangential planes at the areas of real contact ^[2.30].

2.4.1.2 Ploughing component of friction

If one of the surfaces is harder than the other, the asperities of the harder surface may penetrate and plough into the softer surface ^[2.30]. Ploughing into the softer surface may also occur as a result of impacted wear particles.

Rabinowicz ^[2.25] has shown that the slope of an asperity, especially for a conical one, is an important factor contributing to the coefficient of friction. A typical surface asperity seldom has an effective slope exceeding 5 or 6° and from the mathematical relation between coefficient of friction and angle of slope ^[2.25], therefore, the contribution to coefficient of friction is of the order of 0.05. Other possible contributions to friction have also been discussed ^[2.25, 2.30]

2.4.2 Sliding friction of polymers

In contrast to metallic materials, which are essentially incompressible in the plastic state, many polymers have relatively low bulk moduli and increase their density by a significant factor under the action of hydrostatic pressure. Williams^[2.69] has suggested that changes in intermolecular spacing can lead to two tribologically significant effects in considering a single heavily loaded asperity contact. The first of this arises from the fact that the material shear stress becomes a function of the local normal pressure. The second effect, that this change in density can have, is to make the contact area a non-linear function of the load, which ultimately affect the application of these materials for tribological purposes.

2.4.2.1 Effect of load on the friction of polymers

The result of Bowden and Tabor^[2.27] has shown that the coefficient of friction of polymers decreases with increasing load, see Figure 2.16. This has been attributed to the deformation processes taking place at the asperity contact. The asperities are believed to behave in an elastic manner during deformation and because the true area of contact increases proportionately with load, the overall effect this has on the friction coefficient is to decrease it as the load increases, assuming the shear stress is constant. The result of Hutchings^[2.17] work on polymethylmethacrylate (PMMA) was consistent with this behaviour for polymers.

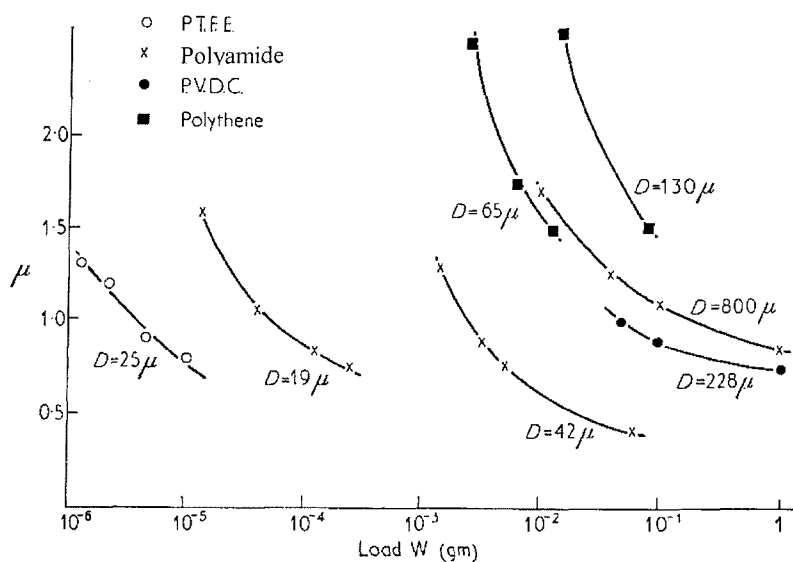


Figure 2.16: Effect of load on friction of different polymers^[2.27].

2.5 Corrosion

Corrosion is defined as “the destruction of a substance (usually a metal) or its properties because of reaction with its environment”. This definition does not make use of the terms *chemical* and *electrochemical* because such terms would define corrosion only as related to metals and would not allow its application to many other materials which disintegrate due to environmental exposure ^[2.70].

For many years, corrosion has been a problem in the oil industry. This has led to a considerable amount of research work on this subject. As explained earlier (section 1.1), water injector tubulars are used to increase the pressure drive of the oil well. The re-injected fluid (seawater, produced water and gas) is corrosive to the carbon steel pipes, and thus necessitates the need to protect the internal surface of the tubulars with barrier coatings. The substitute option, i.e. the replacement of carbon steel tubulars with 13% Cr steel pipes is not cost effective ^[2.71]. Although, the coatings protect the tubulars, manufacturing defects and damage, which results from the inspection tool impact, often leave the substrate exposed; thus the steel pipes corrode.

2.5.1 Forms of Corrosion

It has been observed that engineering materials corrode by different mechanisms ^[2.72]. Among such mechanisms are: galvanic, pitting and crevice. Crevice corrosion is the most prevalent of these downhole.

2.5.1.1 Crevice corrosion

Differential aeration has been identified as the initial cause of crevice corrosion ^[2.73]. The composition of the liquid within the crevices will become different from that prevailing outside, not only through the exhaustion of oxygen but also through changes in pH value. Ulick ^[2.73], while explaining the work of Rosenfel'd and Marshakow noted that for mild steel, the local attack on the metal within the crevice renders the liquid less acidic and this also renders the interior anodic with respect to the outside. Other factors have also been observed ^[2.73] to be responsible for crevice corrosion. The author noted that when only part of metallic surface is coated with paraffin and the whole immersed in an oxygen-free acid environment, corrosion develops along and below the edge of the paraffin. This is analogous to the situation downhole. Scratches and defects may allow

passage of corrosive fluid through the coatings and thus crevice forms underneath the coatings; hence, delamination/disbonding of the coating from its substrate is initiated.

The delamination of coatings from their substrate has been the subject of concern to the coating manufactures and the users alike for some time. Although, crevices constitute one of the causes of delamination, experiments ^[2.23] have shown that coatings are poorly adhered to their substrates after impact from an inspection tool. Many studies have used different methods such as: pullout tests, acoustic emission, and the punch test to study the adhesive properties of coatings on steel. This has led to various standards being established. For example, the ASTM D 4541 outlined the standard test methods for evaluating the adhesion of coatings to their substrate using the pull-off technique ^[2.73]. Other standards such as ASTM C 633, ASTM D 3359 and AWWA C203 have been listed as adhesion test methods ^[2.75]. Most of these standards have been explored in this study but were found not to be reliable enough to assess the adhesion of the coatings. Hence, the cathodic disbondment test method was adopted for evaluating the adhesion of coatings to their substrate.

2.5.2 Cathodic disbondment

Cathodic disbondment is the resulting delamination of coatings from their substrate due to loss of adhesion resulting from cathodic polarization of the steel surface. The guideline for this test is stated in the ASTM G8 – 98 ^[2.76]. Ordinarily, when metals are exposed to an electrolyte, see Figure 2.17, they dissolve by the following reaction,



liberating electrons into the bulk of the metal which migrate to the adjoining surface, where they react with the H^{+} in solution to form H_2 by the following reaction,



According to Denny ^[2.77], when excess electrons are supplied to the metal i.e. cathodically polarizing the exposed surface, the rate of corrosion, expressed by the anodic reaction (Equation 2.14), is always reduced, while the rate of hydrogen evolution reaction (Equation 2.15) is increased. The author also noticed that all corrosion reactions in solution involve an anodic reaction such as in Equation 2.14. It was observed that application of a negative potential, with attendant excess electrons, always

decreases the corrosion rate. This is the basis of cathodic protection for the mitigation of corrosion of pipelines, offshore oil drilling structures, and steel hot water tanks, ships, etc.

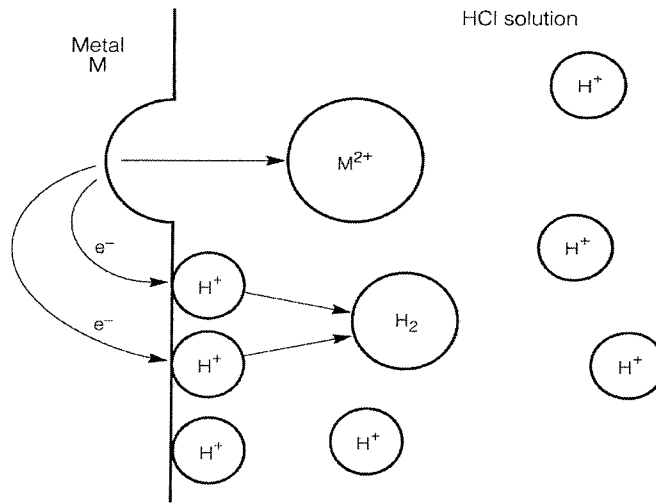
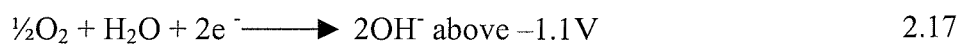
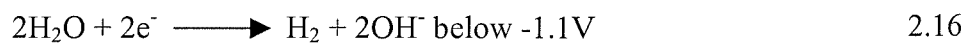


Figure 2.17: Schematic of metal dissolution, liberating into solution a metal ion M^{2+} and electron, e^- , which are consumed by reduction of H^+ to form H_2 [2.77].

The fast rate of disbondment of organic polymers by cathodic disbondment experiments has been reported [2.78–2.81]. It is believed that the accelerated disbonding may be due to a chemical attack of the coating by the intermediates, especially peroxides, or its decomposition products, hydroxyl ions (OH^-) formed during the reduction of oxygen on the cathodically polarized steel surface. For example, Chang and Asein [2.78] in their work reported that at coating holidays (defects or intentional holes drilled through coating to act as defects), the following chemical reactions occur due to negative polarization of more than $-1.05V$ using a $Cu/CuSO_4$ reference electrode.



The hydroxyl ions are believed to be detrimental to the coating. However, according to the authors, it is still not very clear whether the disbondment of the coatings is through the intermediate products of hydroxyl ions or the formation of hydrogen gas.

Coulson and Temple ^[2.79] suggested that it is the accumulation of hydrogen between the coating and the pipe surface, resulting in the delamination of coatings. However, although hydrogen produced at the coating/substrate interface aggravating delamination, chemical attack of the interfacial bond, at the holiday (perforation of coatings) by OH⁻, usually initiates the delamination ^[2.80].

Kamalanand et al. ^[2.81] have used different electrolytes to simulate different environments such as acidic, neutral, alkaline and oxygenated environments in order to ascertain which of the cathodic reduction products are responsible for debonding. Their results were consistent with the work of Leidheiser ^[2.80] that OH⁻ ions are largely responsible for the disbondment of organic coatings and that the rate of disbondment is proportional to the concentration of OH⁻ ions produced. Although a high rate of hydrogen gas evolution was observed in the acidic environment, according to Equation 2.15, post-test examination showed that there was no disbondment around the intentional holiday. They also reported that the oxygen concentration in the environment enhances the cathodic disbondment process but it was not the main cause of disbondment.

2.6 Coatings used for protection of injector tubulars

The type of coatings used for protecting the internal surface of injector tubulars downhole has been discussed briefly in Section 1.1. However, the chemistry and other processes, which have a significant influence on the performances of the coatings were not discussed in-depth.

2.6.1 Polymeric coatings

A coating is a complex material made from a series of interacting constituent/constituents such as resins, plasticizers, pigments, extenders, catalysts, fungicides, and solvents and sometimes reinforcing agents (fillers). When the matrix (the main constituent of the coating, usually makes up the largest volume) of the coating is made of polymer, it is called a polymeric coating. There are two commonly used polymeric coatings: thermoplastic and thermosetting coatings.

2.6.1.1 Thermoplastic coatings

This type of coating, which dries solely by the evaporation (thermal process) of the solvent (the resin is already in its final form), with no chemical or physical change in the nonvolatile portion of the coating that forms the film ^[2.70]. In this case, the film-forming process is merely the evaporation of the solvents from the liquid leaving the thermoplastic resins on the surface of the continuous film. Examples of this type of coating system include polyamide, polyetheretheroketone (PEEK), PTFE.

2.6.1.2 Thermosetting coatings

Thermoset coatings usually involve catalytic conversion or cross-linking at ambient temperatures ^[2.70]. For these coatings, of which epoxy coatings are an example, the resin is mixed with an amine just prior to application. The drying process consists of solvent evaporation followed by a chemical reaction of the amine and the resin in such a way that cross-linkage (joining of two or more molecules of the resin through a chemical bond with the amine) takes place. In this case, the amine actually becomes part of the reaction and is an integral part of the new polymer coating.

Fillers in coating

Polymers are known to have poor thermal and mechanical properties (toughness, hardness, elastic modulus), which can be limiting when the materials are being considered for engineering applications ^[2.21]. Inadequate mechanical properties has the consequence that even at loads considered safe for metals the polymer may deform plastically or even fracture under tensile loads. For these reasons, solid particles are incorporated in the polymers to improve their properties. Sarkar ^[2.21] noted that apart from enhanced strength, addition of asbestos and glass fibres to certain polymers has the beneficial effect of improving the heat resistance of moulded components. Likewise, rubber particles have been used to toughen brittle polymers and achieved considerable results in wear resistance ^[2.82]. Thus, coatings with the addition of solid particles are termed *filled coatings or polymer composites*, while those without solid particles are referred to as *unfilled coatings*.

The solid particles used to reinforce the polymers are widely referred to as “fillers”. Some common fillers used include; china clay, calcium carbonate, talc, barium sulphate, silica, aluminum oxide and glass fibers. They often come in different shapes depending

on tribological requirements ^[2.17]. Some of these filler materials could make up the entire matrix depending on the test design. Aside from the listed fillers above, some polymers require the addition of solid lubricants ^[2.81] in order to reduce friction ^[2.17, 2.24]. Kovacevic et al. ^[2.84] have studied the influence of filler surface pre-treatment on the mechanical properties of composites. In their findings, they noted that pre-treating the fillers with a suitable acid gave rise to good chemical interactions which exerts a dominant influence on filler dispersion in polymers and that the mechanical properties vary with the acid-based forces acting at matrix/filler interface, especially the ultimate tensile property. Fei et al. ^[2.85], adopted a similar mode used by Kovacevic and co-workers ^[2.84] when they studied the effect of masking a graphite filler, with copper, on friction and wear of PTFE. The coated filler in PTFE matrix was considered to give a better coefficient of friction compared to copper filled PTFE.

2.6.1.3 Adhesive wear of polymeric composites

For polymers, material removal results from processes occurring close to or at the surface of the polymer. The most important of such processes is wear by adhesion ^[2.17]. Adhesive forces generated at the interface give rise to deformation ^[2.22] and subsequent transfer of material to the harder surface and its removal as wear debris.

Most unfilled polymers wear readily, a good example being PTFE. In its neat (virgin) state, PTFE wears easily due to its ductile nature, but like other fluorocarbons it exhibits low wear rates if suitable fillers are incorporated ^[2.21]. Lu and Friedrich ^[2.86] in their investigation of the effect of short carbon fibres on the friction and wear of PEEK were able to show that carbon fibres incorporated in the PEEK matrix improve their wear resistance by more than one order of magnitude see Figure 2.18.

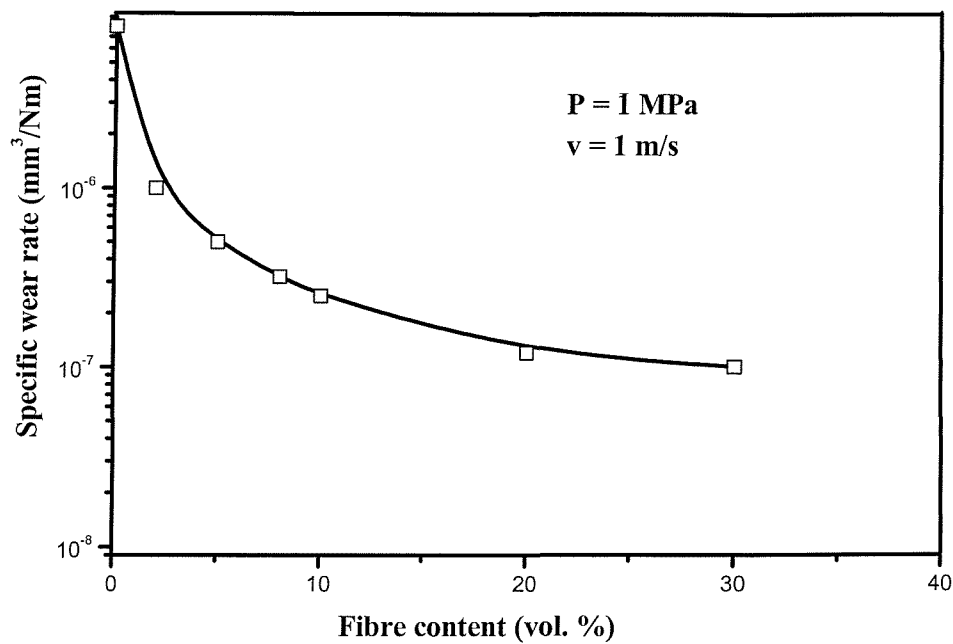


Figure 2.18: *Effect of fibre volume content in polymer composite on the wear rate* [2.86]

Sarkar^[2.21] suggested that the reasons for the behaviour of this material may be due to improved compressive strength and thermal conductivity of the composite. It was further suggested that, at the initiation of sliding, the PEEK portion of the composite begins to transfer to the counter face, but this is interrupted as soon as the carbon fibre fillers made contact with the rubbing surface. The PEEK films protected the counter face and the composite wears at a low rate because the loss of material is now governed by the wear rate of the fillers. Generally, it might be expected that all polymeric composites except for composites with a thermoset matrix would have the same wear behaviour. Due to their brittle nature, they do not wear by adhesion, but mostly they wear by fatigue processes or abrasion^[2.87]. However, the result of Bijwe and Tewari^[2.88] seems to disagree with Lu and Friedrich^[2.86] where a continuous increase in the wear rate was observed, Figure 2.19, as the sliding distance increases.

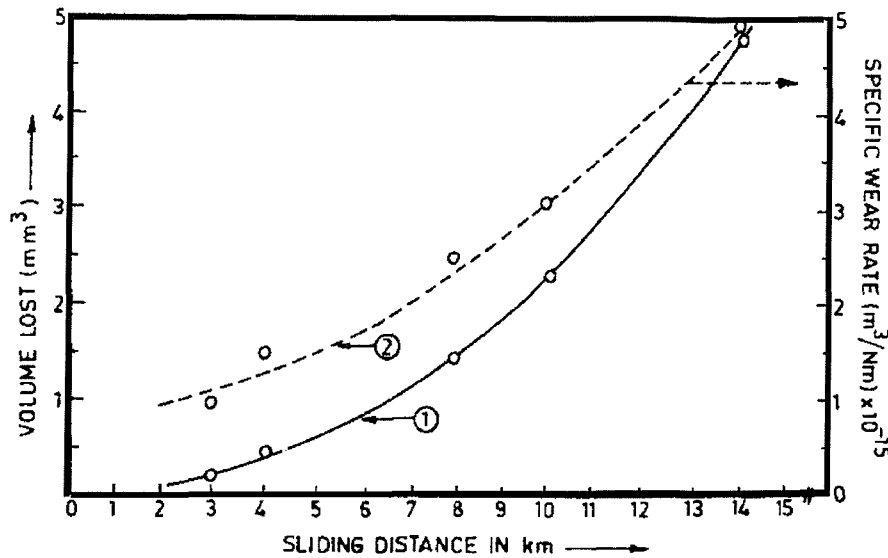


Figure 2.19: Variation in wear and specific wear rate with sliding distance for a candidate polymeric composite ^[2.88].

It was suggested that this might be attributed to the effect of the glass fiber, which was used as the filler. The filler was thought to produce hot spots as it makes contact with the counter face, which causes thermal degradation of the polyetherimide (PEI) matrix subsequently leading to a continuous wear rate. It is not surprising that there is some disagreement in the adhesive wear rate of polymer composite ^[2.89, 2.90]. This can be attributed to differences in experimental test conditions, matrices of coatings and particulate fillers in coatings. For these reasons, it is expected that there will be appreciable variations in results; for example glass fibres do not have good wear resistance properties though they may have other tribological applications.

2.6.1.4 Abrasive wear of polymeric composites

In line with other definitions, Rabinowicz ^[2.25] put the definition of abrasive wear as the loss of material from a surface when a hard, rough surface slides over a softer one, digs into it, and plough a series of grooves. The removal of materials in the grooves is in the form of loose fragments.

Well-bonded fillers to a matrix are expected to act as a load-bearing element for the composite. Sim and Freti ^[2.91], noted that load and abrasive size on an abrasive paper act in the same way. Increasing the abrasive size diminishes the grain density on the paper, so for the same loading condition, the load on each individual particle increases

allowing deeper penetration of the abrasive. The following phenomena have been suggested^[2.25] to be responsible for the abrading inefficiency of the counter face;

1. Fracture, or pull out of the abrasive grains due to hard fibres such as glass in successive runs.
2. The transfers of wear debris of polymer and solid lubricants or film transfer to the counterface. This wear debris collects in the crevices and depressions in the counter face or abrasive paper leading to a clogging effect. Thus, after a certain number of traversals, abrasion of the material eventually stops or occurs at a very low rate due to the system reaching a state of equilibrium.

2.6.1.5 Mechanisms of action of fillers

In the study of the tribology of polymeric composites, it has been found that fillers play an important role. Briscoe et al.^[2.92] have identified a marked reduction in the wear of specific polymers, under suitable conditions, by adding a combination of CuO and Pb₃O₄ to the polymer matrix. The fillers are believed to produce some specific chemical interactions with the steel counterface at the temperatures generated by the sliding process. Arkles et al.^[2.93] suggest that the filler particles used to reinforce PTFE reduce wear by preventing the drawing out of long thin filaments characteristic of the wear of unfilled polymer. Evans and Lancaster^[2.28] have reported that the inclusion of solid lubricant fillers such as graphite, MoS₂ (molybdenum sulphide) and PTFE appear to transfer preferentially to the counterface, reducing both friction and wear. They also suggested that for fibre-reinforced polymers, the fibres support the load preferentially, but this is only likely to occur when the fibres are relatively long and oriented perpendicular to the sliding surface.

2.6.2 Friction of polymeric composites

In the past, there have been numerous investigations into the friction behaviour of polymeric coatings. Odi-wei and Schipper^[2.94] have studied the tribological behaviour of polyoxymethylene composites and show that polymeric composites exhibit good frictional properties especially when solid lubricants are incorporated. Fillers such as graphite and MoS₂ have been found to be reliable solid lubricants in polymeric composites, although there are cases where graphite does not always reduce friction and/or wear^[2.88]. This indicates that in composites the effect of fillers or reinforcing agents are not always predictable and their effect have to be evaluated in true tribo-

couple. Another good solid lubricant is PTFE. A number of successes have been achieved using PTFE as a solid lubricant in polymer composites because of its good friction reducing properties. Contrary to most fillers, glass fibres exhibit poor friction properties when incorporated into a polymer matrix.

2.6.3 Factors affecting wear and friction of polymeric composites

2.6.3.1 Effect of particle size and spacing

Most polymeric materials selected to resist abrasive wear contain hard phases within a softer matrix ^[2.17]. Such microstructures are mostly developed during the production stage of the composite. The response of these materials depends on the size of the hard phase regions compared with the scale of the deformation caused by individual abrasive particles. This scale of deformation can be described either by the width, a , or depth, x , Figure 2.20, of the indentation formed by each particle. If this dimension is substantially greater than the size of the particles (or fibres in a fibre-reinforced composite) and their separation, then the material will behave very much like a homogeneous solid. This situation is illustrated schematically in Figure 2.21a. According to Hutchings ^[2.17], there is a correlation between volume fraction and resistance to abrasive wear; for a given volume fraction of filler, the wear resistance of a material; is improved by finer filler distribution, leading to a shorter inter particle spacing.

Lu and Friedrich ^[2.86], Figure 2.18, confirm the earlier finding of Hutchings that reducing the inter particle spacing by increasing the amount of filler actually reduces the wear of the composites. They, however, noted that there is an optimal filler volume of between 15% and 25% of the total volume content of the coating after which there is no significant decrease in the wear rate. Hutchings ^[2.17] considered that although a high volume of the second hard phase particles is desirable for abrasion resistance, this is not, however, universally true.

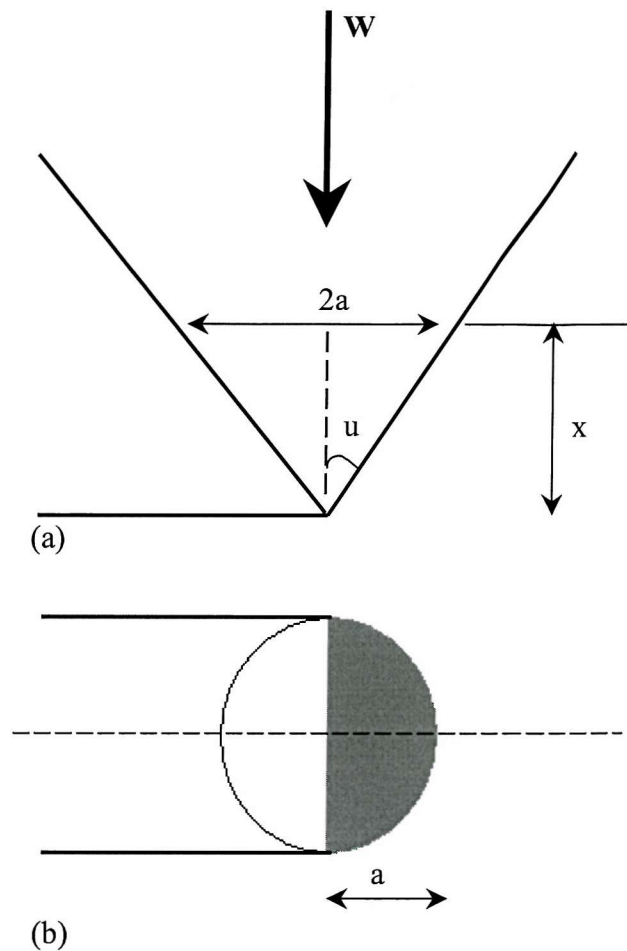


Figure 2.20: Geometry of contact between an idealized conical abrasive particle and a surface, a) in elevation; b) in plan view^[2.17].

The matrix must also possess adequate toughness and good bonding with the filler particles. In fact, some authors^[2.84, 2.85] have suggested that pre-treating the fillers with suitable acid can improve the interfacial bonding between the fillers and the matrix, consequently improving the free surface energy and the wettability of the fillers within the matrix. Hutchings^[2.17] further noted that if the bond between fillers and matrix is weak and the matrix itself is brittle, cracks could initiate at the interface and propagate through the matrix. In addition, if the size of the fillers is comparable or even larger than the scale of the abrading particle, the coating is thought to respond heterogeneously Figure 2.21b.

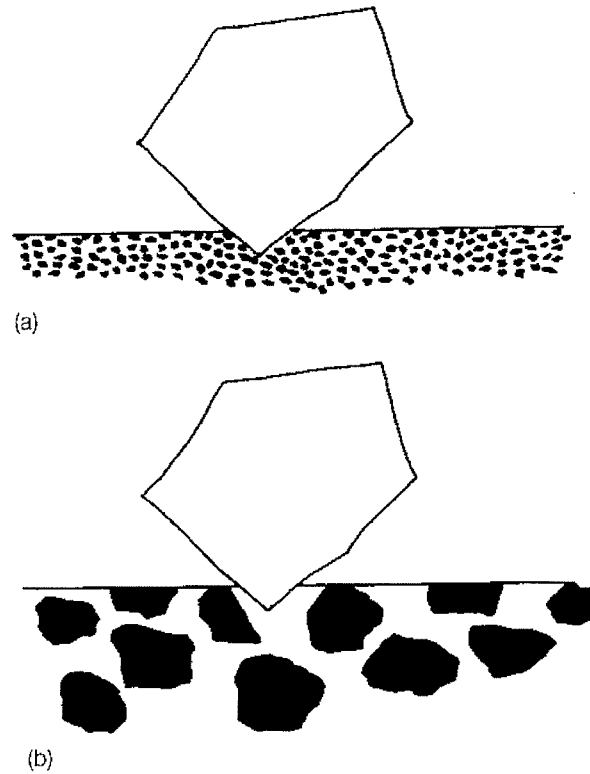


Figure 2.21: Illustration of the importance of the relative size of the particle contact zone and the hard phase regions in the abrasive wear of a two-phase (or composite) material. In a) material responds in an homogeneous manner while in b) material responds in an heterogeneous manner^[2.17].

However, it has been found, through surface profilometry, that the types of wireline in use downhole have abrasive asperities. These asperities have been observed^[2.24] to gouge or plough the fillers out during wireline wear. Symonds^[2.24] suggested that this might be due to the weak bonding between the fillers and the matrix. It was also thought that the size of the fillers play a major role in this regard. If the size of the fillers could be set relative to the size of the abrasive (asperities) and are closely packed such that the transition between moving one asperity (abrasive) over one filler and the next adjacent filler is small, then the wear rate may be reduced. Care must be taken not to exceed the optimum filler content (about 15-25% volume of the coating) to avoid the onset of brittle failures. This is also consistent with the observations from Hutchings^[2.17].

Generally, it appears that the amount of filler that a composite can accommodate is not the only defining factor for optimum wear resistance. The wear resistance also depends on many other factors among which are the chemical and mechanical properties of the

matrix and filler (such as toughness, hardness, elastic modulus). Also important is the bonding strength or the strength of the interface between the filler and matrix. However, Rabinowicz ^[2.25] offers an explanation from the point of view of the abrasive particle size using an abrasive paper counterface as the abradant. It was suggested that when the abrasive particle size on the paper is small compared to the fillers, though clogging of the system (abrasive paper) by abraded debris occurs, the formation of large particles, which prevent the abrasive from contacting the coating surface seems to be the cause of wear reduction. It was suggested that large particles arise from the adhesive wear process which takes place at the same time as abrasive action is occurring.

2.6.3.2 Effect of temperature

The role of the filler (additives) in polymers is to first improve their mechanical and thermal properties; though some act as solid lubricants ^[2.21]. The effect of temperature on polymeric materials has not received as much attention as other influencing factors.

Hanchi and Eiss ^[2.95] have studied the tribological behaviour of carbon fibre-reinforced PEEK composites at elevated temperatures. At temperatures below T_g (glassy temperature), in spite of a wear performance comparable to that of its unreinforced counterpart, PEEK composites exhibited higher friction coefficients than unfilled PEEK. A further inspection of the recovery parameter data revealed that below T_g , visco-elastic ploughing and removal of material in the case of PEEK composite and visco-elastic plastic ploughing in the case of unfilled PEEK were the main dissipative processes giving rise to friction and wear during sliding. It was noted that at the glass transition, thermal softening brought about noticeable deterioration of wear performance in both filled and unfilled PEEK. Friedrich et al. ^[2.96] have observed similar behaviour for PEEK composites, but have focused on reducing the wear rate and the coefficient of friction at elevated ambient temperature by incorporating solid lubricants such as PTFE and graphite.

2.7 Modelling of Wear rate

Based on previous work ^[2.24] on the wear and friction of polymeric composites, the following equation has been suggested by the author of this thesis for the modelling of wear rate of composite surface,

$$W_T = W_M + W_F + \phi_F + \eta_F + W_{FM} \quad \dots\dots\dots 2.18$$

Where W_T is the total wear rate of the composite

W_M is the wear rate of the matrix

W_F is the wear rate of the filler

ϕ_F is the rate of filler pull-out

η_F is the rate of filler fracture

W_{FM} is the contribution friction modifiers make to wear

The contribution of each component to wear rate of polymeric coatings is directly linked to their mechanical and physical properties, and in some cases, chemical properties that are discussed below.

2.7.1 Matrix (W_M)

The polymer matrix is typically the largest volume in a polymeric composite. The two commonly used matrices are thermoplastic and thermosetting polymers, as mentioned earlier. Wear rates, mechanical and physical properties for a number of commonly used thermoplastics and thermosetting polymers can be seen in Table 2.3 and 2.4.

Properties	Ref	PA11	LDPE	HDPE	PEEK	PTFE
Tensile Strength (MN/m ²)	[2.1]	80	20	37	68	47
% Elongation	[2.1]	300	800	130	150	400
Elastic Modulus (MN/m ²)	[2.1]	3330	270	1200	3660	540
Density (kg/m ³)	[2.1]	1.14	0.92	0.96	1.31	2.17
Izod Impact (J/m ¹)	[2.1]	112	480	214	85	160
Water Absorption 24hr/23°C (%)	[2.70]	1.0 – 2.8	<0.01	>0.01	0.5	<0.01
Compressive strength (MN/m ²)	[2.70]	8.8–10.5	—	2.0 – 2.5	12.03	1.2
Hardness, Rockwell		R120	R10	R65	R126	D50-65
Typical wear rate (abrasive)	[2.70]	—	—	—	—	Poor
(adhesive) (mm ³ /Nm)	[2.70]	6.58 E-6	—	—	—	
Abrasion Resistance (mg/1000 cycles)	[2.70] [2.98]	—	10 -15	2.0 – 5.0	Good	—

Table 2.3: Mechanical and physical properties of some common thermoplastics.

Properties	Ref	Phenolics	Epoxies	Urethane	Polyesters
Tensile strength (MN/m ²)	[2.99]	60	100	67	87
% Elongation	[2.99]	2	6	6	3
Elastic Modulus (MN/m ²)	[2.1]	9	3		4
Density (kg/m ³)	[2.1]	1.27	1.25	1.30	1.28
Typical Wear Rate		NA	NA	NA	NA

Table 2.4: Mechanical and physical properties of common thermosetting polymers ^[2.99].

During wear, the combination of normal load and tangential motion often creates shear stresses around the point of contact between the mating surfaces. This is a consequence of the resulting frictional forces and pressure. Figure 2.22 shows contours of principal shear stress distribution beneath two bodies sliding relative to one another with the location of maximum shear stress at the surface for a coefficient of friction greater than 0.3 ^[2.97].

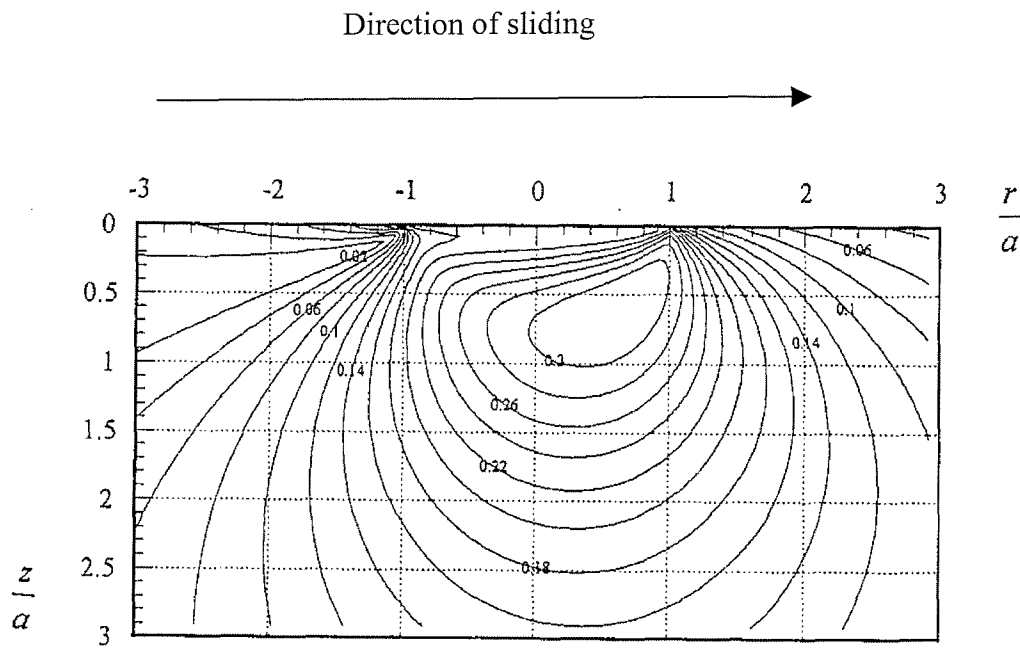


Figure 2.22: Contours of principal shear stress beneath a sliding spherical point contact over a flat surface where the coefficient of friction is 0.3^[2.97].

The ability of a polymer matrix to resist the shear stress created by the asperities of the abrading counterface lies in its tensile strength, hardness, elastic modulus and inherent friction modifiers. Most of the properties exhibited by polymers are because of the chemical manipulation of the microstructure, which is imparted in the manufacturing stages. For example, the soft nature of fluoro-polymers, such as PTFE, is due to the presence of fluorine atoms in the chemical structure.

It has been suggested that polymers with good stiffness exhibit a good wear resistance^[2.58]. The wear performance of Polyetheretheroketone (PEEK) seems to confirm this suggestion (see Table 2.3). The excellent mechanical properties of PEEK such as stiffness, tensile strength and hardness are believed to be responsible for its good abrasion resistance. The same analogy can be drawn from the abrasion resistance of both high and low-density polyethylene (HDPE and LDPE).

The difference in the abrasive wear resistance of the two polyethylene polymers (HDPE and LDPE) is an indication of the difference in their stiffness. For example, from Table 2.3, it can be seen that both the abrasion resistance and the elastic modulus (stiffness) of HDPE are five times those of LPDE. Although it was difficult to obtain data for the

abrasion resistance of a virgin polyamide (PA), the adhesive wear resistance indicate that it might have a good abrasion resistance, and moreover since PA has mechanical properties similar to that of PEEK it suggests that it might have a similar abrasion resistance. The labelling of PTFE as a poor wear resistance polymer is not surprising. Like LDPE its elongation is relatively high and the elastic modulus is small. Thus, these materials are relatively soft and the effect is shown in the poor wear resistance. From Table 2.3, PTFE has the highest density and one would expect it to have good mechanical and physical properties. This is not so due to the presence of fluorine atoms in the chemical structure of PTFE. This confirms the earlier suggestion that the chemical and molecular structure of the polymers determine most of the mechanical and physical properties. However, PTFE has its own tribological advantages especially in its application as a solid lubricant because of the good inherent transfer and friction properties, which is evident in their low shear resistance, resulting from the weak van der Waals forces that exist between the molecules.

There is very little tribological data available for “virgin” thermosetting polymers. Most are produced with some sort of reinforcement and this makes it difficult to comprehensively review the tribological behaviour with respect to the mechanical and physical properties in the un-reinforced state.

From Table 2.4, it is evident that thermosetting polymers are generally brittle because of their very low elastic modulus and percentage elongation. Consequently, their application is limited to specific areas where stiffness does not play an important role. This suggests wear may occur by fatigue processes and failure by micro-cracking. They also have poor toughness and as such are not immediate options as impact resistance materials. The results of experiments ^[2.24] suggest that most thermosetting polymers do not exhibit good wear properties because of their failure mode.

2.7.2 Fillers (W_F)

The role of fillers in polymeric composites is to increase the strength of the matrix, which is soft and has low resistance to wear. Fillers by virtue of their strength and hardness restrict the chain mobility in the polymer microstructure. They often come in different shapes, which have a considerable influence on the wear rate of the coatings.

Among the common shapes are: short fibre, continuous fibre, flakes and spherical, as shown schematically in Figure 2.23 (a-d).

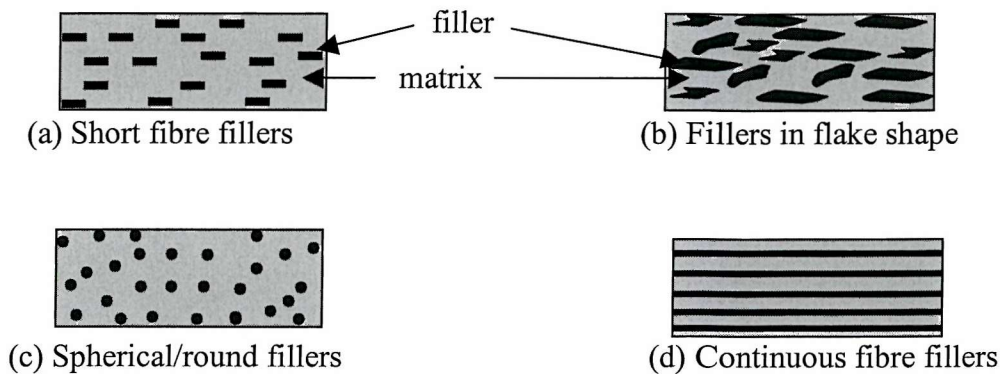


Figure 2.23: Schematic of the different types of filler shape.

Fillers act as load bearing materials for the matrix as well as enhance the tribological performance. The mechanical and physical properties of some common reinforcing fillers are shown in Table 2.5.

Properties	Alumina Al_2O_3	Silicon Carbide SiC	Silicon Nitride Si_3N_4	Ref
Elastic Modulus (GPa)	~390	480	210	[2.69]
HV Vickers hardness (GPa)	~22	~28	18	[2.69]
Fracture Toughness (MPa)	~5	~3	~5	[2.69]
Density (g/cm^3)	4.0	3.2	3.2	[2.100]
Tensile strength (GN/m^2)	0.2-0.7	9.5	5-7.7	[2.100]
Typical wear rate. $\times 10^{-5}$ (mm^3/Nm)	0.117	4.90	6.50	[2.101]
Typical friction coefficient	0.98	0.84	0.68	[2.101]

Table 2.5: Mechanical and physical properties of some ceramic fillers.

As indicated by the data shown in Table 2.5 most fillers are brittle in nature. They have poor tensile strength and fracture toughness, even though they often act as load bearing

elements in composites, and as such will not normally deform either plastically or elastically to an appreciable extent. Typical wear rates obtained for these materials suggest that their wear resistance is low. Due to the hardness of filler materials, the volume proportion when they are used as reinforcing materials in polymer should be controlled. The work of Kato ^[2.101] confirms the assumption that ceramics have low resistance to wear at room temperature.

2.7.3 Filler Pullout (ϕ_F)

It has been observed that filler pullout is one of the causes of failure in polymeric coatings ^[2.24] and in most cases, can be attributed to the poor adhesion between the filler and matrix. A prime requirement for a good composite is an excellent adhesion between fibre and matrix, a condition that depends on features such as the chemical bonding and surface cleanliness in addition to the mechanical factors. The free surface energy of the fillers, which is a consequence of the wettability, has to be excellent ^[2.84, 2.85] to give a good adhesion between the fillers and matrix.

In a composite experiencing surface shear stress during wear, new interfaces are created which involve the expenditure of energy. Ward and Hadley ^[2.102], have modelled the process of debonding/fibre pullout by considering a single fibre embedded in a block of matrix. At a depth x , the debonding energy is maximum when x is equal to half the critical length, l_0 , of the fibre, see Figure 2.24. If the embedded length is less than $l_0/2$, the fibre will pull out of the matrix rather than fracturing, so involving the expenditure of further energy. The stress-strain curve derived from the tensile load-extension experiment, Figure 2.24, shows that area OAB represents the energy of debonding while the usually large pullout energy is associated with the area OBCD ^[2.102].

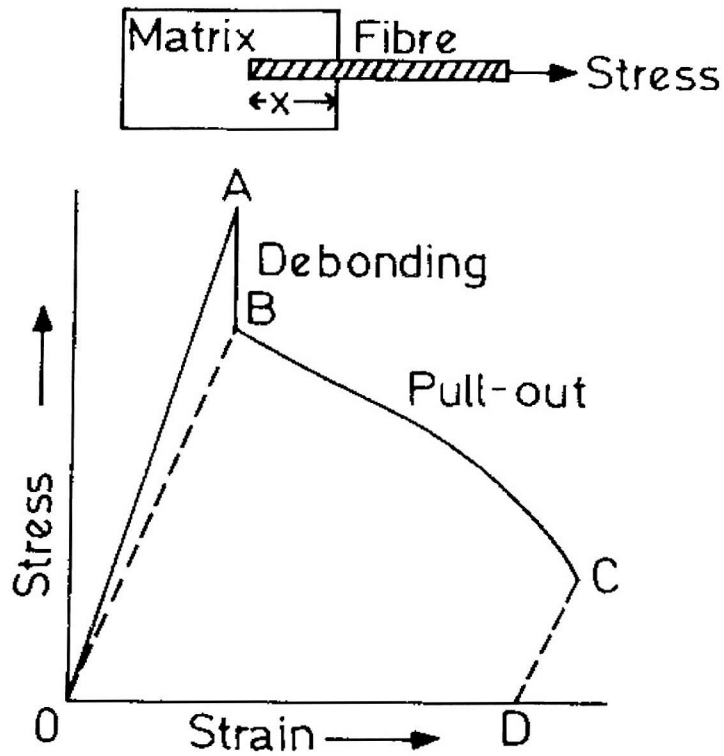


Figure 2.24: Pullout test and the resulting stress-strain curve showing the difference in magnitude of energies of debonding ^[2.102].

However, it is believed that the shapes of the fillers play an important role in filler pullout. For example, an asperity has a high tendency to abrade spherical fillers rather than pull out as the case may be for rectangular filler, if the approach angle is very small, and the fillers are close to the surface as shown in Figure 2.25 (a) and (b).

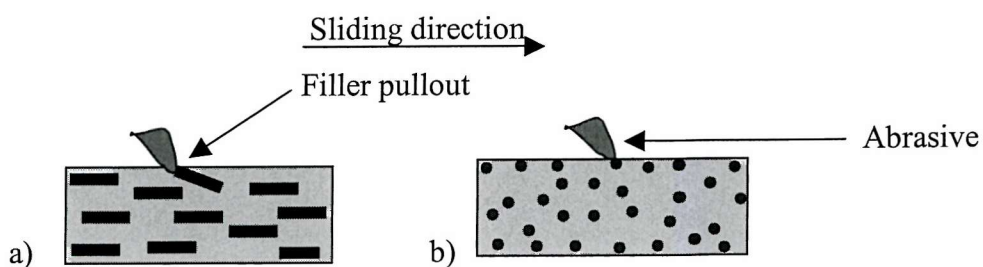


Figure 2.25: Model of filler pullout compared between two different filler shapes.

2.7.4 Filler fracture (η_F)

As explained previously, fillers must act as the load-bearing element for polymeric composites. The hardness of the fillers need not be too high and as such must be able to withstand elastic deformation to a reasonable extent. The absence of this property could lead to filler fracture, as shown in Figure 2.26 (a) and (b).

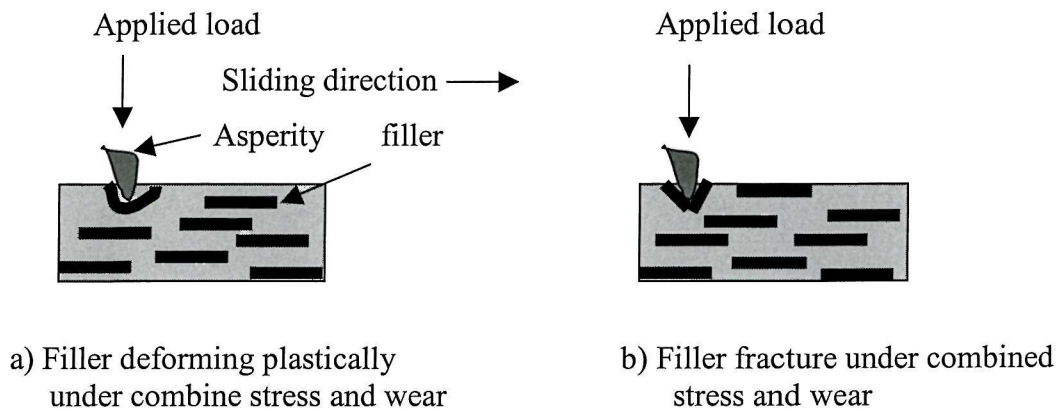


Figure 2.26: Model of filler deforming elastically and fracturing under load and wear.

Variations in critical length of the filler (short fibres) and energy of debonding from the matrix have been observed to be one of the factors responsible for filler fracture in some cases ^[2.80].

2.7.5 Friction modifier (W_{FM})

Low friction materials can be incorporated in polymeric composites to reduce the wear rate as they have good transfer properties (low shear strength) and as such, reduce friction. Typical friction modifiers include PTFE and graphite.

The process of friction involves two mechanisms taking place at the same time during wear. These are adhesion and deformation, and can be modelled by the following equation.

$$F_{\text{friction}} = F_{\text{adhesion}} + F_{\text{deformation}} \quad \dots\dots\dots 2.19$$

The adhesion component of friction results from the cold welding of asperities even at low loads in the case of metals sliding over metals. In polymeric composites sliding over a metal, adhesion has been linked to the forces of attraction between the outermost

electrons of the asperities in the contact. Deformation, on the other hand, results from the ploughing of asperities of the harder surface into the softer one during sliding.

In its simplest form, the adhesion theory of friction supposes that because the real contact is made only at the tips of the asperities then, even at relatively low loads, true contact pressures are sufficiently high to bring about local plastic deformation. The load can be related to the true area of contact (A) by the material property which represents the yield pressure of the softer surface. Numerically, it will be very close in value to the indentation hardness, H , thus,

$$W = A \times H \quad 2.20$$

Because of the severe, although localized, plastic deformation, strong adhesive junctions are formed and if there is to be a tangential motion of mating surfaces, these junctions must be sheared ^[2.69]. The total friction force is then made up of the product of the area (A) and the specific shear strength of the softer solid. If we designate the shear strength by τ , it thus follows that

$$F = A \times \tau \quad 2.21$$

$$\begin{aligned} \mu &= F/A \\ &= \tau/H \end{aligned} \quad 2.22$$

Where F is the frictional force. The above expression shows that friction is independent of load, nominal or apparent area of contact. It also shows that the coefficient of friction, μ , is the ratio of two strength properties of the softer solid, which may vary among materials ^[2.69].

Polymers are known to have relatively low bulk moduli and increase their density by a significant factor under the action of hydrostatic pressure. This change in intermolecular spacing can lead to two tribological effects in considering a single heavily loaded asperity contact. First the material shear stress, τ , becomes a function of the normal

pressure P . Experimental evidence suggests that to a satisfactory degree of modelling, τ and P are related by the equation,

$$\tau = \tau_o + \alpha P \quad 2.23$$

where τ_o (intrinsic or limiting shear stress at the interface) and α (pressure or attraction coefficient) are material constants ^[2,69].

Secondly, the contact area is dependent on a non-linear function of the load; empirically they are related in the following way,

$$A \propto W^{2/n} \quad \text{where } 2 < n < 3$$

Since friction, F , is equal to $\tau \times A$, it follows that

$$\mu = F/W = \tau_o W^{(2-n)/n} + \alpha \quad 2.24$$

If $n > 2$, then μ is decreased as the load is increased and vice versa.

2.8 Summary

The use of pin-on-disc and the micro-abrasive machine to investigate the tribological performance of polymeric coatings have been reviewed. Several mechanisms have been suggested for material removal, one of which is the shearing of material due to *adhesion* processes occurring during asperities interaction. It has also been established that some thermosetting coatings wear by fatigue processes leading to failure by micro cracking. Likewise, wear by micro-ploughing has been reported for some thermoplastic coatings. This has been attributed to deformation from inter-penetration of asperities.

The inclusion of fillers in the matrix of polymers has been found to reduce wear rate of filled coatings considerably. The mechanism of action of these fillers has been proposed. Optimum filler content has also been suggested to be between 20-30% of the total coating volume. Addition of solid lubricants (friction modifier) such as PTFE and graphite has also been claimed to encourage material transfer as this helps lower wear

rate substantially. The cause and the consequence of corrosion, which compromises the protection offered by the coatings to the tubulars, have been elucidated.

To the knowledge of the author, a coating, which resists corrosion and mechanical damages such as wear and impact, all at the same time, is yet to be established. Thus, the detailed understanding of the microstructure property interaction of such coatings, which is a function of the overall performance, has not been established. Consequently, a model has been proposed for the wear rate of polymeric coatings. This will be considered when designing a candidate polymeric coating, which will resist corrosion and wear of injector tubulars as required downhole.

References

- 2.1 Donald, R. A, Science and Engineering of Materials 3rd (ed), Stanley Thornes Publisher (1998).
- 2.2 Shakelford, J. F., "Introduction to Materials Science for Engineers". 2nd (ed), Macmillan publisher, (1988), (9).
- 2.3 Ward, I. M. Introduction to the Mechanical Properties of Solid Polymers, John Wiley Publishers, Chichester, (1993).
- 2.4 Kaufman, H. S and Falcetta, J. J. Introduction to Polymer Science and Technology, John Wiley Publishers, Rochester, (1977).
- 2.5 Chocinski-Arnult, L., Gaudefroy, V., Gacougnolle, J. L and Riviere, A., J. Memory effect and crystalline structure in polyamide 11, *Macromolecular Science*, Part B – Physics, B41, 4 – 6 (2002), (777 –785).
- 2.6 Rhee, S and White, J. L., Crystalline structure and morphology of biaxially oriented polyamide 11 film, *Journal of Polymer Science: Part B: Polymer Physics*, 40, (2002) 2624 – 2640.
- 2.7 Scrovanek, D. J., Painter, R. C and Coleman, M. M. Hydrogen bonding in polymers (2), infrared temperature studies of PA11, *Macromolecules*, 19 (1998) 699 – 705.
- 2.8 Autran, J. P. Structure, Deformation, Behaviour and Properties in Polyundecanamide (PA11) and High – Density polyethylene (HDPE) subjected to Planar (Equibiaxial) Deformation by Forging. PhD Thesis, University of Massachusetts, United States, (1990).
- 2.9 Jolly, L. Analyse de la Micro-diffusion du Polyamide 11 par Diffusion des Rayons X: Application a une Deformation Uniaxiale. Ph.D. Thesis, Universite de Metz, France (1995).
- 2.10 Kim, K. G., Newman, B. A and Sheinbeim, J. I. Temperature dependence of the crystal structures of PA11, *Journal of Polymer Science: Part B: Polymer Physics*, 23 (1985), 2477 – 2482.
- 2.11 Khanna, Y. P and Reimschuessel, A. C. Memory effects in polymers (I). Orientational memory in the molten state: Its relationship to polymer structure and influence on recrystallization rate and morphology, *Journal applied Polymer Science*, 35 (1988), 2259 – 2268.
- 2.12 Khanna, Y. P., Reimschuessel, A. C, Banerjee, A and Altman, C. Memory effects in polymers (II). Processing history vs. Crystallization rate of PA6 – Observation

- of phenomenon and product behaviour, *Polymer Engineering Science*, 28, (1988) 1600 – 1606.
- 2.13 Khanna, Y. P., Kumar, R and Reimschuessel, A. C. Memory effects in polymers (III). Processing history vs. Crystallization rate of PA6 – Comments on the origin of memory effect, *Polymer Engineering Science*, 28, (1988) 1607 – 1611.
- 2.14 Khanna, Y. P., Kumar, R and Reimschuessel, A. C. Memory effects in polymers (IV). Processing history vs. Crystallization rate – Effect of polymer structure, *Polymer Engineering Science*, 28, (1998) 1612 – 1615.
- 2.15 Peeters, A. Van Alsenoy, C. Bartha, F. Bogar, F. Zhang, M. L and Van Doren, V. E. Ab Initio calculation of the Young's modulus of α - polyamide, *Journal of Quantum Chemistry*, 87, (2002) 303 – 310.
- 2.16 Belec, L., Dang, P and Gacougnolle, J. L., 1st International Conference on Mechanics of Time Dependent Materials, Ljubljana, 1995.
- 2.17 Hutchings, I. M. 'Tribology- Friction and wear of engineering of materials' Arnold publisher. 2nd (ed.) (1992).
- 2.18 Kragelski, I. 'Friction and Wear', Butterworth publishers. 1st (ed.) (1965).
- 2.19 Arthur, G 'Wear resistance surfaces in Engineering'. International Research and Development Co Ltd 1st (ed.) (1985).
- 2.20 Keller, D. V. Adhesion between solid metals, *Wear*, 6, (1963) 353-365.
- 2.21 Sarkar, A. D. 'Friction and Wear', Academy press, 2nd (ed.) (1980).
- 2.22 Bowden, F. P and Tabor, D. 'The friction and lubrication of solids' (I). Oxford university press, 1st (ed.) (1950).
- 2.23 Fundamentals of friction and wear of materials- Papers presented at the ASM materials, Pittsburgh, Pennsylvania, (1980).
- 2.24 Symonds, N., Wear and Impact of Polymeric Coatings, PhD thesis University of Southampton, Southampton, UK, (2000).
- 2.25 Rabinowicz, E; 'Friction and wear of materials' John Wiley. 1st (ed.) (1965).
- 2.26 Bowden, F. P and Tabor, D. 'Friction and lubrication'. Methuen & Co., 2nd (ed) (1962).
- 2.27 Bowden, F. P and Tabor, D. 'The friction and lubrication of solids' (II) Oxford university press 1st (ed.) (1964).
- 2.28 Evans, D. C. and Lancaster. J. K., The Wear of Polymers. Treatise on Materials Science and Technology Volume 13, Ministry of Defence, Procurement Executive

- Materials Department, Royal Aircraft Establishment, Hants, England, Academy Press, (1979).
- 2.29 Moor, D. F., Principles and Applications of Tribology. Robert Maxwell, M. C. Publishers, (1976).
- 2.30 Bhushan, B., Handbook of Tribology, McGraw-Hill Publishers (1991).
- 2.31 Fischer, T. E “Tribiochemistry”, *Ann Rev Material science* 18 (1988), 303-323.
- 2.32 Quin, T. F. J., *J. Appl. Physics*, 13 (1962), 33-37.
- 2.33 Hallings, J., Principles of Tribology. Macmillan Publishers (1975).
- 2.34 ASLE Lubrication Fundamentals Committee. Catalogue of Friction and Wear devices, ASLE, Illinois, (1973).
- 2.35 Alliston-Greiner, A, “Guidelines for laboratory wear Testing” The Donald Julius Green Prize Lecture, (1996).
- 2.36 Hogmark, S and Jacobson, S., Hint and Guidelines for Tribotesting and Evaluation. *Lubrication Engineering*, 48 (1992) 401 – 409.
- 2.37 Sviridzenok, A. I and Kirpichenko, Y. E, in ref. LEE, L. H, “Standardization of Laboratory methods to evaluate friction behaviour of polymer based Materials”, 22 (1984) 332-387.
- 2.38 Greenwood, O. D. Moulzolf, S. C. Blau, P. J. and Lad, R. J. The influence of microstructure on tribological properties of WO₃ thin films, *Wear*, 232 (1999) 84-90.
- 2.39 Lewis, R. E, Barbin, D. K. “Selecting Internal Coatings for Gas well tubulars, NACE Annual Conference, 70 (1997).
- 2.40 Lewis, R. E, Barbin, D. K, “Selecting Internal Coatings for Sweet Oil Well tubing Service, NACE Annual Conference, 15 (1999).
- 2.41 NACE Standard Test Method TM0185-93. “Evaluation of internal Plastic Coatings for Corrosion Control of Tubular Goods by Autoclave Testing.” NACE International, Houston, Texas, (1993).
- 2.42 Ruschau, G. “Realistic Performance Testing of Internal Coatings for Oilfield Production” *Proc. Of the Am. Chem. Soc. Nat. Mtg.*, Div. of Polymeric Materials, New Orleans, LA, (1996).
- 2.43 ASTM D5178-91. “Standard Test Method for Mar Resistance of Organic Coatings” ASTM, Philadelphia, PA, 1991.

- 2.44 NACE Standard RP0291-91. “Care, Handling, and Installation of internally plastic-coated oilfield Tubular Goods and accessories”, NACE International, Houston, TX. 7 (1991).
- 2.45 ASTM D968-81 (Re-approved 1991). “Standard Test Method for Abrasion Resistance of Organic Coatings by Falling Abrasion”, ASTM, Philadelphia, P. A (1991).
- 2.46 Wolfe, L. H, Burnette, C. C, Fisher, K. P and Joosten, M. W. “Laboratory Testing of In-service Performance Parameters of Internal Pipe Coatings”. Corrosion/92 NACE International, Houston, TX 333 (1992).
- 2.47 Reinicke, R. Friedrich, K. Beier, W. and Liebald, R. Tribological Properties of SiC and C-fibre reinforced Glass Matrix Composite, *Wear* 225 - 229 (1999) 1315 – 1321.
- 2.48 Palabiyik, M and Bahadur, S., Tribological study of polyamide 6 and HDPE blends filled with PTFE and copper oxide and reinforced with short glass fibres, *Wear* 253 (2002) 369 – 376.
- 2.49 Khedkar, J. Negulescu, I. And Meletis, E. Sliding wear behaviour of PTFE composites, *Wear* 252 (2002) 361 – 369.
- 2.50 Feng, X., Lu, Z and Zhang, R.. Analysis of electron spectroscopy for chemical analysis of the transferred film formed during sliding wear for carbon fibre reinforced polyetheretherketone and its composites, *Journal of Materials Science* 34 (1999) 3513 – 3524.
- 2.51 Rutherford, K. L. and Hutchings I. M., A micro-abrasive wear test, with particular application to coated system, *Surface and Coatings Technology* 79 (1996) 231-239.
- 2.52 Rutherford, K. L. and Hutchings I. M. Theory and application of a micro-scale abrasive wear test, *JTEVA* 25 (2) (1997), 250-260.
- 2.53 Shipway, P. H and Ngao, N. K. Micro-scale Abrasive wear of polymeric materials, *Wear* 255 (2003) 742 – 750.
- 2.54 Trezona, R. I and Hutchings, I. M., Three-body abrasive wear testing of soft materials, *Wear* 233 – 235 (1999) 209 – 221.
- 2.55 Stachowiak, G. B and Stachowiak, G. W., The effect of particle characteristics on three-body abrasive wear, *Wear* 249 (2001) 201 – 207.

- 2.56 Allsopp, D. N., Trezona, R. I., Hutchings, I. M. The effect of ball surface condition in the micro-scale abrasive wear test, *Tribology Letters* 5 (1998) 259-264.
- 2.57 Gahlin, R., Larsson, M., Hedenqvist, P., Jacobson, S., Hogmark, S. The crater grinder method as a means of coating wear evaluation – an update, *Surface and Coatings Technology*, 90 (1997) 107-114.
- 2.58 Nothnagel, G. Wear resistance determination of coatings from cross-sectional measurements of the ball ground crater, *Surface and Coatings Technology*, 57 (1993) 151-154
- 2.59 Rutherford, K. L., Trezona, R. I., Ramamurthy, A. C., Hutchings, I. M. The abrasive and erosive wear of polymeric paint films, *Wear* 203-204 (1997) 325-334.
- 2.60 Trezona, R. I., Allsopp, D. N., Hutchings, I. M., Transitions between two-body and three-body abrasive wear: Influence of TEST conditions in the micro-scale abrasive wear test, *Wear*, 225-229 (1999) 205-214.
- 2.61 Shipway, P. H., The role of test conditions on the micro-abrasive wear behaviour of soda-lime glass, *Wear*, 233-235 (1999) 191-199.
- 2.62 Shipway, P. H. and Hodge, C. J. B., Micro-Abrasion of Glass - the Critical Role of Ridge Formation, *Wear*, 237 (2000) 90-97.
- 2.63 Archard, J. F and Hirst, W. *Proc. Roy. Soc.* 236A (1956) 397-410.
- 2.64 Lancaster, J. K *Proc. Inst. Mech. Eng.* 183 (1968), (3P), 98.
- 2.65 Evans, D. C and Lancaster, J. K, in Scott, D (ed) *Wear*, 13 (1979) 85-139.
- 2.66 Bahadur, S. Gong, D and Anderegg, W. J. Studies of the worn surfaces and the transfer film formed in sliding by CuS-filled and carbon fibre reinforced nylon against a steel surface, *Wear* 181 – 183 (1995) 227 – 235.
- 2.67 Kishore, P. Sampathkumaran, S. Seetharamu, S. Vynatheya, A. and Kumar, R. K, SEM observation of the effect of velocity and load on the sliding wear characteristic of glass fabric-epoxy composites with different fillers, *Wear*, 237 (2000) 20 – 27.
- 2.68 Kukureka, N. Hooke, C. J. Liao, P and Chen, Y. K. The wear mechanism of acetal in unlubricated rolling-sliding contact, *Wear*, 185 (1995) 1 – 8.
- 2.69 Williams, J. A. 'Engineering Tribology' John Wiley publishers, (1991).
- 2.70 Charles, G. M., Corrosion Prevention by Protective coatings. NACE Publication, 1440 South Creek Drive, Houston, Texas. (1984).

- 2.71 Groves, S., Technical Meeting, BP Research Centre, Sunbury (2000).
- 2.72 Schweitzer, P. A; Mechanical and corrosion Resistant Properties of Plastics and Elastomers. Mercel Dekker Publisher (2000).
- 2.73 Evans, U. R., The Corrosion and Oxidation of Metals. Edward Arnold Publishers (1968).
- 2.74 ASTM D4541, "Standard Test Method for Pull-Off Strength of Coatings, Using Portable Adhesion Testers," ASTM Annual Book of Standards, West Conshohocken, PA: ASTM: (1995).
- 2.75 Cunningham, T and Steele, J., Measuring Adhesion of Coatings to Concrete and Steel. Paper presented at NACE CORROSION/2000, Orlando Florida, USA 614 (2000).
- 2.76 ASTM G8-98, "Standard Test Method for Pull-Off Strength of Coatings, Using an Electrochemical Test Cell." ASTM Annual Book of Standards West Conshohocken, PA: ASTM: (1998).
- 2.77 Denny, A. J; "Principles and prevention of corrosion" Prentice-Hall publishers, 2nd (ed) (1996).
- 2.78 Chang, J. C., and Asein, C. C., The proceedings of the 6th Asian Passific Corrosion conference, Hong Kong, (1991).
- 2.79 Coulson, K. E. W and Temple, D. G. 5th International Conference on Internal and External Protection of Pipes, Insbruck, Austria, 25-27 (1983), 21 -49.
- 2.80 Leidheiser, H., Issues in cathodic disbondment of organic coatings, *Industrial Engineering Chemical Product Development* 20 (1981) 547
- 2.81 Kamalanand, N. Gopalakrishnan, G. Ponnambalam, S. G. Mathiyarasu, J. Natarajan, R. N. Submramaniam, P. Palaniswamy, N and Rengaswamy, N. S. Role of hydrogen and hydroxyl ion in cathodic disbondment. *Anti Corrosion Methods and Materials*, 45 (4) (1998) 243 – 247.
- 2.82 Raymond, A. P., Sue, H. J and Yee, A. F., Toughening of Plastics, Oxford University Press (2000).
- 2.83 Uchiyama, Y; Iwai, T and Ueno, Y., Proceedings of the International Tribology Conference, Yokohama, Japan, (1996).
- 2.84 Kovacevic, V; Lucic, S and Cerovecki, Z. Influence of filler surface pre -treatment on the mechanical properties of composites, *International Journal of Adhesion and Adhesives* 17 (1997) 239-245.

- 2.85 Fei, L. Feng-yuan, Y. Lai-gui, Y and Wei-min, L. The tribological behaviour of copper-coated graphite filled PTFE composites, *Wear*, 237 (2000) 33-38.
- 2.86 Lu, Z. P and Friedrich, K. On sliding friction and wear of PEEK and its composites, *Wear*, 181-183 (1995) 624-631.
- 2.87 Lancaster, J. K Fatigue wear in polymers. *Plastics and Polymers*, 41 (1973), 297.
- 2.88 Bijwe, J and Tewani, U. S., Friction and wear study of polyethramine composites, *Wear*, 138 (1990) 61-76.
- 2.89 Yelle, H, Benebdallah, H and Richards, H., Friction and Wear of Polyethylene-Nylon Blends, *Wear*, 149 (1991) 341 – 352.
- 2.90 Schwartz, C. J and Bahadur, S., The role of filler deformability, filler-polymer bonding and counterface material on the tribological behaviour of polyphenylene sulphide (PPS), *Wear*, 251 (2001) 1532 - 1540.
- 2.91 Simm, W. and Freti, S, Abrasive wear of multiphase materials, *Wear*, 129 (1989) 105.
- 2.92 Briscoe, B. J, Pogolian A. K and Tabor. D., The Friction and Wear of High Density Polyethylene: The Action of Lead Oxide and Copper Oxide Fillers. *Physics and Chemistry of Solid*. Cavendish Laboratory, Madingley Road, Cambridge. (1973).
- 2.93 Arkles, B., Gerakaris, S., and Goodhue, R., “Wear Characteristics of Fluoropolymer Composites”, in *Advances in Polymer Friction and wear*, Polymer Science and Technology, Lee edition, 5b, Plenum, New York. (1974).
- 2.94 Odi-owei, S and Schipper, D. J, Tribological behaviour of unfilled and composites polyoxymethylene, *Wear*, 148 (1991) 363-376.
- 2.95 Hanchi, J and Eiss, N. S. Dry sliding friction and wear of short carbon-fibre reinforced polyetheretherketone (PEEK) at elevated temperatures, *Wear*, 203-204 (1997) 380-386.
- 2.96 Friedrich, K. Karger-Kocsis, J and Lu, Z. Effect of steel counterface roughness and temperature on the friction and wear of PEEK composites under dry sliding conditions, *Wear*, 148 (1991) 235-247.
- 2.97 Dwyer-Joyce. R. S; “Tribological Design Data (Part 3)” 1st (ed) Institute of Mechanical Engineers Tribology Group. (1997).
- 2.98 Brandrup, J and Immergut, E. H; *Polymer Handbook*. 2nd (ed), John Wiley Publishers, (1975).

- 2.99 Kostetskii, B. I. 'Conference on Friction and Wear in Machine', London, (1951) (201).
- 2.100 Richardson, M. O. W. Polymer Engineering Composites. Applied Science Publishers, (1977).
- 2.101 Kato. K. Tribology of Ceramics, *Wear*, 136 (1990) 117-133.
- 2.102 Ward, I. M and Hadley, D. W., Introduction to the Mechanical Properties of Solid Polymers, John Wiley publisher, Chichester, (1993).

3.0 Material Characterisation

3.1 Introduction

Detailed examination of the materials used in this study will be presented in this chapter. In total, eleven (11) different polymeric coatings were investigated, which were supplied by two coating manufacturers. The coatings can be categorised into two main groups, thermoplastics and thermosets, based on the matrix type. Usually, a primer was initially applied on to the shot blasted carbon steel substrate before the polymeric coating. The shot blasting of the carbon steel facilitates adhesion between the primer and the substrate.

Since the microstructure of a coating, which is a result of the overall composition, will influence the performance of the coating {Section 2.6}, it is important to characterise the coating with regards to its compositional properties. These properties may or may not change during a laboratory test, depending on the nature of the test. As a result, before detailed discussion of the test results and possible changes within the coatings can be made, it is necessary to understand the interaction among the constituents of the coating in their as-received commercial state.

The material characterisation has been aided by data supplied by the coating manufacturers and independent laboratory investigations. Laboratory equipment such as a JEOL JSM T300 and Field Electron Gun (FEG) scanning electron microscopes, Taylor Hobson Form Talysurf 120L for surface analysis and MHT-1 NT 600 micro hardness testing equipment were used.

3.2 Experimental

3.2.1 Surface roughness measurement

The coating surface roughness was determined by drawing a 2 μm radius diamond tipped stylus of the 'Form' Talysurf across the surface of the as-received coating at 90 degrees to the plane of the surface. The detailed surface profile is then printed out after analysis through a software package. Figure 3.1 is an example of a surface profile.

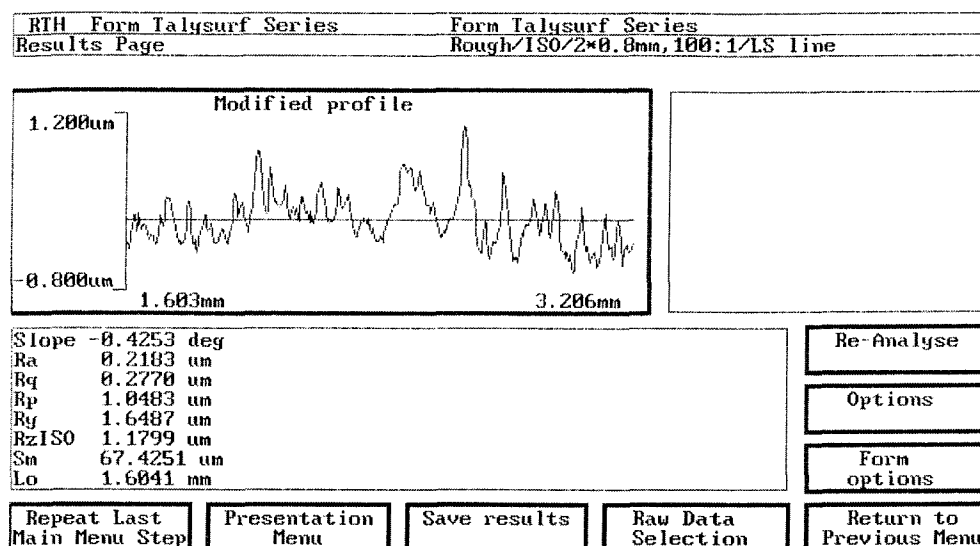


Figure 3.1: An example of a profile trace of a coating surface.

3.2.2 Analysis of coating details using the Scanning Electron Microscopy (SEM)

Detailed microstructural analysis of coatings used scanning electron microscopy (SEM). The sample size was 10×10 mm. For examination of the plan view of each coating, the sample was gold coated to prevent charging and observed directly in the SEM. However, for transverse sectional examination, the sample was initially cold mounted in a resin and a series of standard grinding stages performed using graded silicon abrasive papers from 120 to 2500 grades followed by polishing using 5 and 1 μm size diamond abrasives respectively. The polished sample was then gold-coated before being examined in the SEM.

3.2.3 Energy dispersive X-ray (EDX) analysis

Some of the coatings studied contain filler particles which have been previously specified, in terms of composition and quantity, by the coating manufacturers. However, in order to validate the manufacturers claims, EDX analysis was performed on the filled coatings. The EDX is an integral part of the SEM, which allows the dispersive energy of the individual element in the periodic table of elements to be measured with respect to the X-ray energy in the SEM. The package then predicts the compositional elements with respect to the energy level of each compositional element, which allow the type of filler(s) within a coating to be

identified. An example of the EDX for one of the coatings is shown in Figure 3.2. This procedure was adopted for all the filled coatings and as required throughout the study.

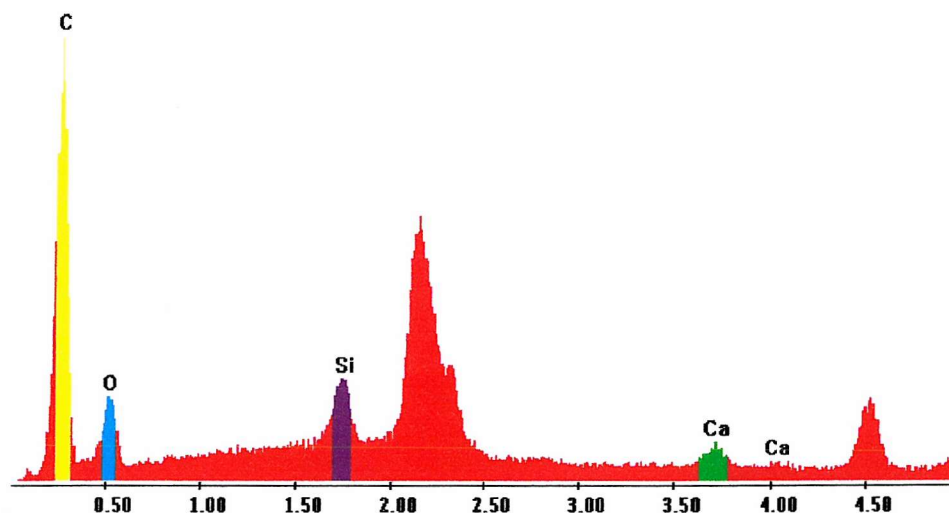


Figure 3.2: An example of the EDX analysis performed on the chemical composition of the CaCO_3 and SiO_2 fillers in a filled thermosetting coating.

3.2.4 Filler size measurement and quantification

a) Filler size measurement

The computer software package of the SEM utilises a function that allows the size of any particle to be measured directly from the SEM image during analysis. The function provides a facility to draw lines across the filler in any direction and automatically estimates the size of the filler. The same procedure is also used for measuring the filler mean free part (MFP). The MFP is the average distance between adjacent fillers, which defines how closely packed the fillers are within the matrix. Figure 3.3 is an example of a coating where the filler size has been measured ^[3.1].

b) Quantification of Fillers

The fillers were quantified in terms of the percentage volume occupied by the fillers of the total volume of the coating. The procedure for measuring the size of the fillers described above provides the starting point. After the size of the fillers is estimated, a line is drawn across successive number of fillers (usually between 10 and 15 fillers). The length of the line is calculated and the total size of the fillers that falls within the line is estimated. The length of the line then divides the total size of the filler multiplied by 100 to give an

approximate percentage of filler within that region. This procedure is repeated at least 20 times over the transverse section of the coating and the average filler percentage is obtained [3.1].

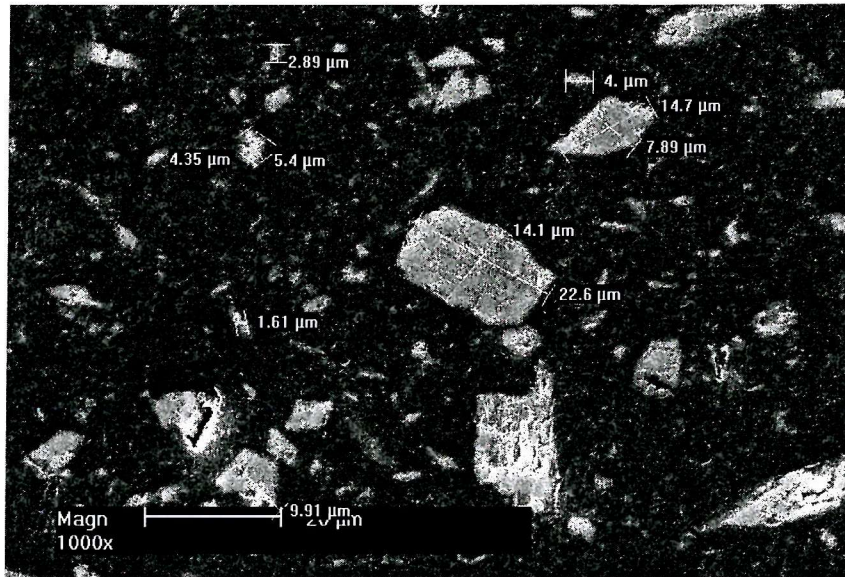


Figure 3.3: SEM image showing the measurement of the filler size in a thermosetting coating.

Figure 3.4 is an image of a coating for which the percentage of the fillers has been estimated. The estimated percentage by volume of filler content of the coatings is consistent with the manufacturers specifications with about 2% deviation i.e. the percentage of fillers obtained using this method is about 2 % more or less than that value supplied by the manufacturer.

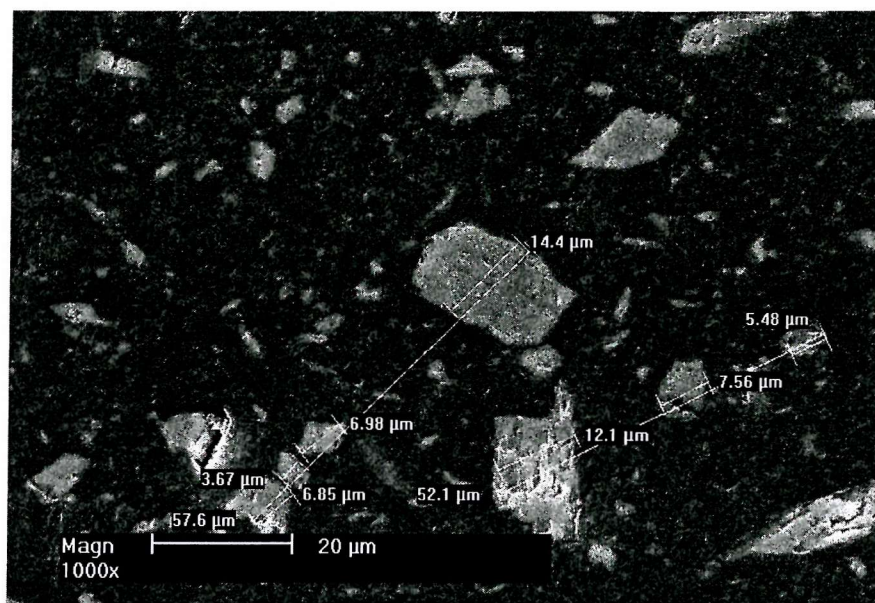


Figure 3.4: SEM image showing the measurement of the filler percentage in a thermosetting coating.

3.3 Characterisation of polymeric coatings

This section presents the results of the microstructural and compositional study of the as-received thermoplastic and thermoset coatings. The basic difference between a thermoplastic (denoted by TP) and a thermosetting (denoted by TS) coating has been discussed in Section 2.1.1. The first set of coatings studied: TP-9, TS-5, TS-7, TSX-4 and the dual layer TP-9 on TS-5 are discussed in Section 3.3.1 through to 3.3.3, while the coatings investigated in the second study with annotations A, B, C and D are discussed in Section 3.3.4.

3.3.1 Thermoplastic TP-9

Details of the thermoplastic, PA11 based coating TP-9 are presented in Table 3.1 below. According to the coating manufacturers, TP-9 is a highly flexible, thick film coating that is designated for general protection against aggressive corrosive environments. It is formulated with a thermoplastic PA11 resin and can withstand substrate deformation and impact damage ^[3.2].

Designation	TP-9
Polymer base	Thermoplastic
Resin type	PA11 (powder)
Filler type	None
Colour	Black (contains carbon black)
Filler percentage	N/A
Filler size (μm)	N/A
Filler shape	N/A
Coating thickness (μm)	535 – 550
Primer type	Phenolic
Primer thickness (μm)	25 – 30
Surface roughness (R_a , μm)	11.0 \pm 0.2

Table 3.1: Details of the physical properties of TP-9.

The transverse section, see Figure 3.5, together with the information provided by the coating manufacturer confirm that TP-9 is unfilled. The transverse section shows that a thin layer of phenolic primer, 25-30 μm thick, was applied to the roughened carbon steel substrate before the PA11 coating. The coating shows good adhesion with the primer and does not show any obvious manufacturing defects.

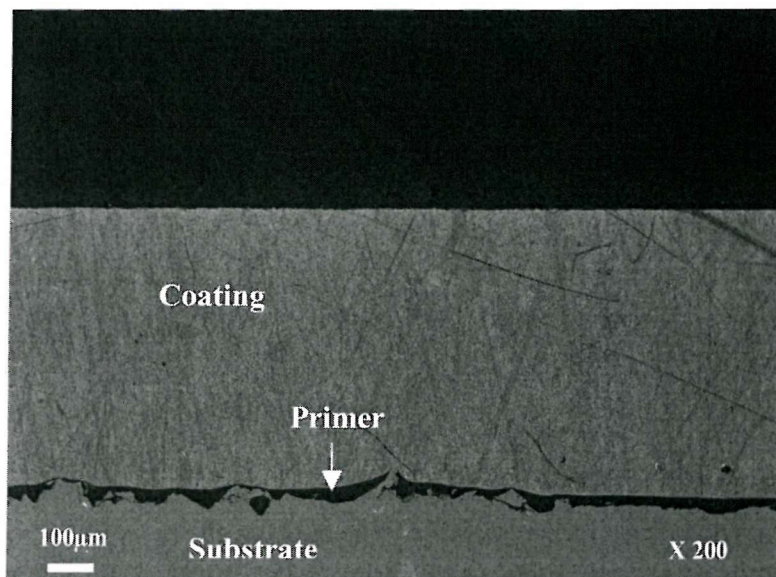


Figure 3.5: SEM image of the transverse section of coating TP-9.

3.3.2 Thermosetting coatings

Three of the coatings studied fall under this category: TS-5, TS-7 and TSX-4, their characterisation is discussed below.

(a) TS-5

Details of the coating are presented in Table 3.2. TS-5 is a modified Novolac coating system formulated for critical oilfield environments containing high water cuts including CO₂ up to 148 °C, where improved mechanical properties would be advantageous. The resin system utilised in TS-5 produces a material with significantly improved flexibility and impact resistance without sacrificing chemical resistance^[3.2].

Designation	TS-5
Generic name	Thermoset
Resin type	Modified novolac (powder)
Filler type	CaCO ₃ /SiO ₂
Filler percentage	~9%
Filler size (µm)	10 – 30
Filler shape	Angular and flake
Matrix thickness (µm)	250 – 270
Primer type	Phenolic
Primer thickness (µm)	15 – 30
Surface roughness (Ra, µm)	6.0±0.4

Table 3.2: Details of the physical properties of coating TS-5.

The transverse sections of TS-5 show that the coating is 250 to 270 µm thick. The matrix is filled with filler particles of varying sizes between 10 to 30 µm. The energy diffraction X-ray analysis of the coating agrees with the coating suppliers that the fillers, which are generally angular and flake-like in shape, are CaCO₃ and SiO₂. The fillers were found to be approximately 9 % of the total volume of the coating. The phenolic primer was measured to be 15-30 µm thick. The coating transverse section, Figure 3.6, shows that the fillers are evenly distributed within the matrix.

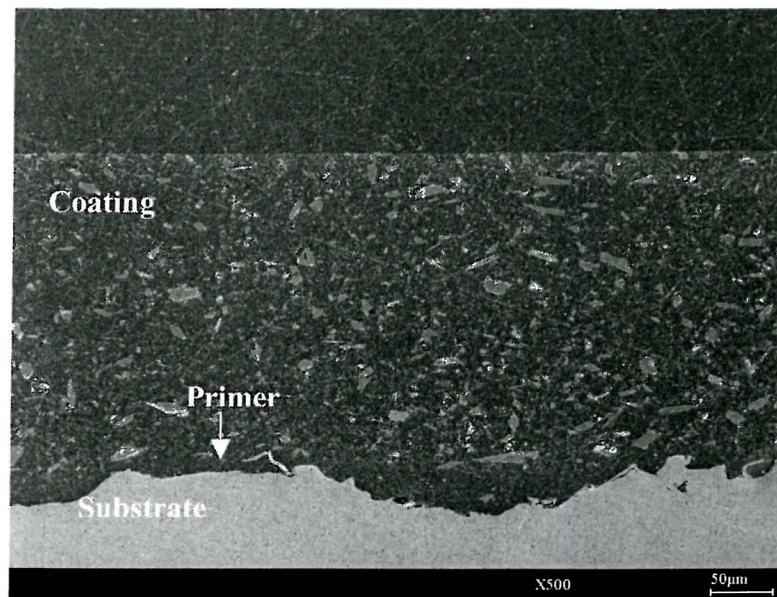


Figure 3.6: SEM image of the transverse section of coating TS-5.

(b) TS-7

According to the coating manufacturer, this is an epoxy (powder) resin with a high level of corrosion resistance and has good flexibility and durability. These properties should resist most mechanical damage normally identified in the field ^[3,2]. Details of the coating are shown in Table 3.3.

Designation	TS-7
Generic name	Thermoset
Resin type	Epoxy (powder)
Filler type	Glass
Filler percentage	~15%
Filler size (µm)	5 – 40
Filler shape	Angular
Matrix thickness (µm)	260 – 280
Primer type	Phenolic
Primer thickness (µm)	15 – 40
Surface roughness (Ra, µm)	9.0±0.2

Table 3.3: Details of the known properties of coating TS-7.

The transverse section of TS-7 suggests that the filler particles in the matrix are angular in shape, see Figure 3.7. The filler volume was found to be approximately 15 % of the total coating volume. The EDX procedure performed on the coating confirms that the fillers are

mainly glass. The fillers were found to range in size from 5 to 40 μm . Overall, the matrix thickness is 260-280 μm and the phenolic primer is 15-40 μm thick.

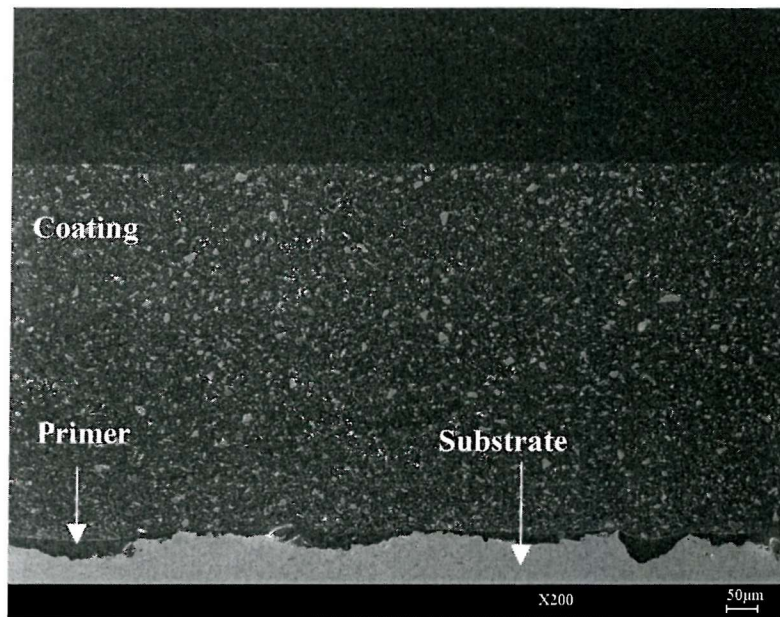


Figure 3.7: SEM image of the transverse section of coating TS-7.

Higher resolution images of the coating show poor bonding between fillers and matrix, see Figure 3.8. This effect tends to reduce the strength of the coating. The score marks found on the surface are the effect of different stages of polishing.



Figure 3.8: SEM of a more detailed transverse section of TS-7.

c) TSX-4

TSX-4 is a modified epoxy-phenolic (liquid) with a good abrasion resistance and specifically formulated to provide improved wear resistance in drilling environments. The coating is durable and has a good resistance to temperature, chemical and impact from wireline tools ^[3.2]. Details of the coating are presented in Table 3.4.

Designation	TSX-4
Generic name	Thermoset
Resin type	Modified epoxy-phenolic (liquid)
Filler type (in matrix)	Al ₂ O ₃
Filler percentage (in matrix)	~20%
Filler size (in matrix) (μm)	5 – 20
Filler shape (in matrix)	Angular
Matrix thickness (μm)	135 – 145
Primer type	Phenolic
Primer thickness (μm)	50 – 100
Filler type (in primer)	CaSiO ₃
Filler percentage (in primer)	~40%
Filler size (in primer) (μm)	5 – 30
Filler shape (in primer)	Angular/flake/oblong
Surface roughness (Ra, μm)	3.0±0.1

Table 3.4: Details of the known properties of coating TSX-4.

The SEM of the transverse section of coating TSX-4, Figure 3.9, shows that the matrix is about 135-145 μm thick and the phenolic primer contains filler particles. EDX analysis on the coating confirms that the matrix and the primer are filled with Al₂O₃ and CaSiO₃ respectively, which is consistent with the information supplied by the coating manufacturer. It appears that the fillers in the coating are mainly angular while the fillers in the primer have different shapes, varying between angular, flakes and oblong.

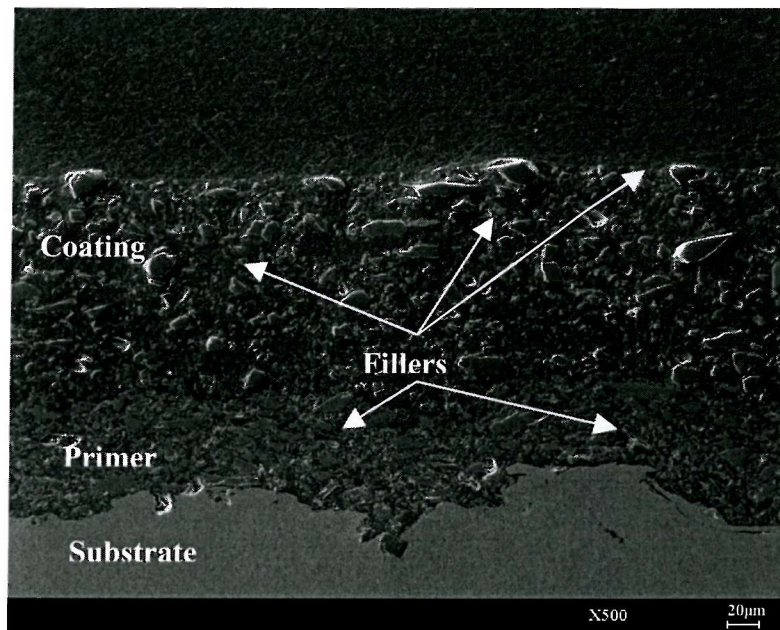


Figure 3.9: SEM image of the transverse section of coating TSX-4.

The quantitative study performed on the coating shows that the fillers in the matrix and primer occupy approximately 20 and 40 % by volume of the total coating thickness respectively. The size of the fillers in the matrix ranges from 5 to 20 μm while that in the primer is between 5 to 30 μm . The primer thickness, 50-100 μm , is thick compared to other coatings. The microstructural composition of coating TSX-4, by virtue of the closely packed fillers, suggests that coating embrittlement may characterise TSX-4, which is evident in the high filler content both in the matrix and primer, and also in its physical appearance. Figure 3.10 is of TSX-4 at a higher magnification. Although the fillers appear to be well bonded to the matrix, the effectiveness of the bonding appears to be questionable. This is evident in the voids found in the coating after polishing, presumably, where fillers have fallen out.

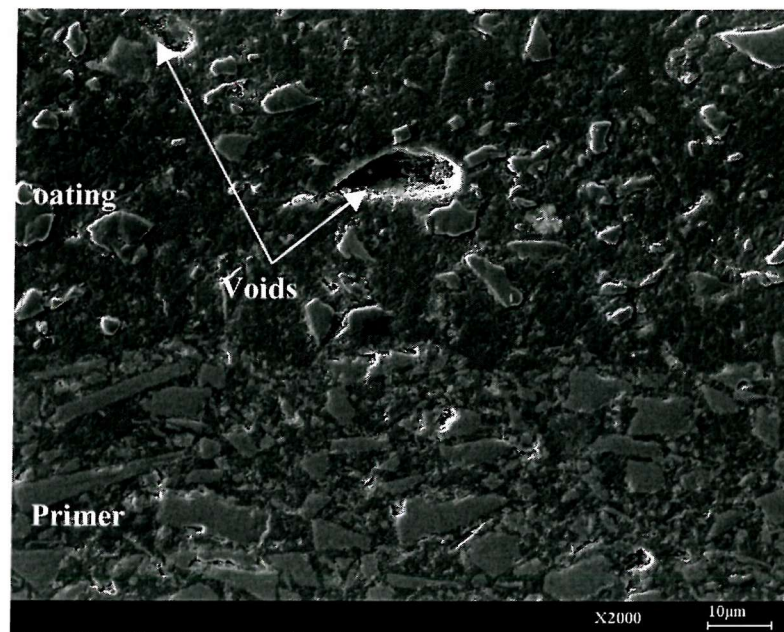


Figure 3.10: SEM of a more detailed transverse section of coating TSX-4.

3.3.3 Fluoropolymer, PVDF and dual layer coatings

Two fluorinated coatings and one dual layer of thermoplastic on top of a thermoset are characterised in this section. Two different manufacturers supplied the two fluorinated coatings.

a) Thermoplastic Fluoropolymer F-4001

Information relating to the F-4001 coating specification is shown in Table 3.5. The coating is formulated from a thermoplastic polymer. According to the coating manufacturers it offers a good protection to downhole tubulars, able to withstand temperatures between -100 and 160 °C compared with other available polymeric system ^[3.3]. The coating was supplied in three different thickness of 500, 1000 and 1500 μm.

Designation	F-4001
Colour	Black
Polymer base	Thermoplastic
Resin type	Fluoropolymer (powder)
Filler type (in matrix)	CaF ₂
Filler percentage (in matrix)	3%
Filler size (in matrix) (μm)	20 – 40
Filler shape (in matrix)	Rounded

Matrix thickness (μm)	500, 100, 1500
Primer type	Not supplied
Primer thickness (μm)	80 – 200
Fill type (in primer)	SiC
Fill percentage (in primer)	12%
Filler size (in primer) (μm)	5 – 10
Filler shape	Angular
Surface roughness (R_a , μm)	0.30 ± 0.04

Table 3.5: Details of the known properties of coating F-4001.

The SEM of the transverse section of coating F-4001 is shown in Figure 3.11. Like TSX-4, both the matrix and the primer contain fillers with approximate volume fraction of 3 and 12 % of total coating volume respectively.

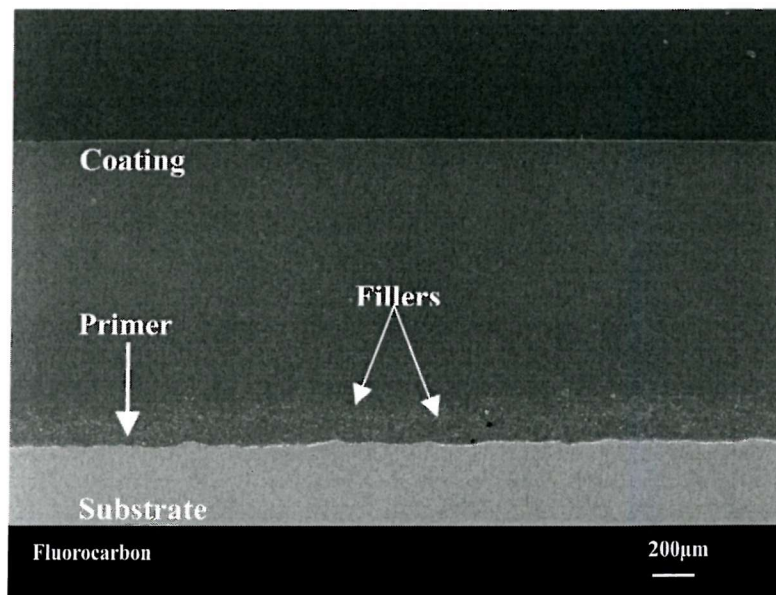


Figure 3.11: SEM image of the transverse section of coating F-4001.

From Figure 3.11 it can be seen that the interface between the coating and the primer is not distinguishable, which is an indication of good bonding between the two layers. The fillers in the primer are not evenly distributed, which is a consequence of the manufacturing process.

b) Polyvinylidene fluoride (PVDF)

This coating was manufactured by electrostatic spraying. It serves as a replacement for metallic coatings and widely used plastics, which suffer deterioration and deformation when exposed to corrosive environments ^[3,4]. The coating is a semi-crystalline thermoplastic PVDF powder coating, free from any additive. Table 3.6 details the specifications of the coating.

Designation	PVDF
Colour	Yellow
Polymer base	Thermoplastic
Resin type	Fluorinated semi-crystalline thermoplastic PVDF
Filler type	None
Coating thickness (μm)	600 – 650
Primer type	None
Surface roughness (R_a , μm)	2 ± 0.70
Micro hardness Hv (25g load)	13.0 ± 0.6

Table 3.6: Details of the known properties of the Fluorinated (PVDF) coating.

The SEM of the coating transverse section, Figure 3.12, shows that the bonding between the coating and the substrate is very poor. This is due to the unmelted particles found at the interface between the coating and the substrate, which may have been caused by bad substrate preparation before the coating was applied and/or the cooling process after the coating was applied to the substrate. Whichever is the case this will reduce the adhesion between the coating and the substrate.

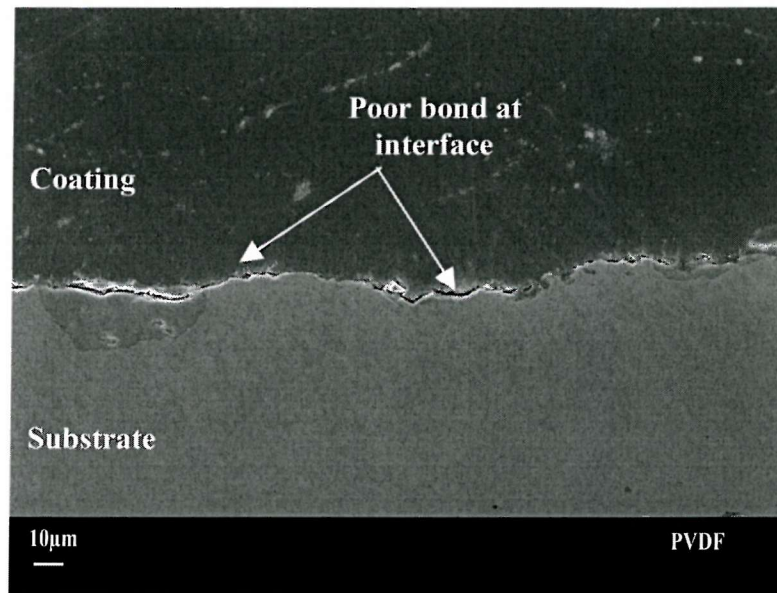


Figure 3.12: SEM image of the transverse section of the PVDF coating. Note the poor bond between coating and substrate.

c) Dual layer coating of TP-9 on TS-5

The dual layer coating was manufactured by depositing the TP-9 on top of TS-5. To date, there is no service history of this special coating, which was specifically formulated to improve impact resistance in a working environment. The properties of the individual layers of the dual layer coating have similar characteristics to those previously described in Sections 3.3.2 (a) and (b). Figures 3.13 and 3.14 show the transverse section of the coating with a total thickness of approximately 500 μm.

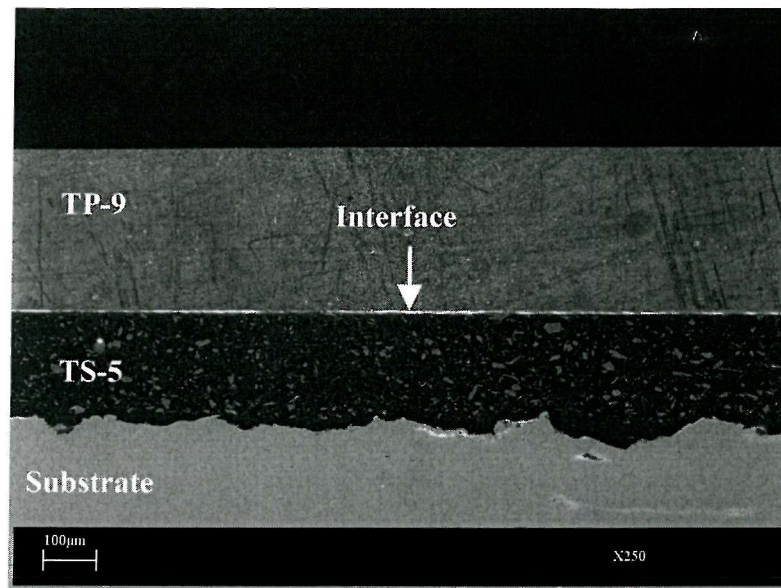


Figure 3.13: SEM image of the transverse section of the dual layer coating.

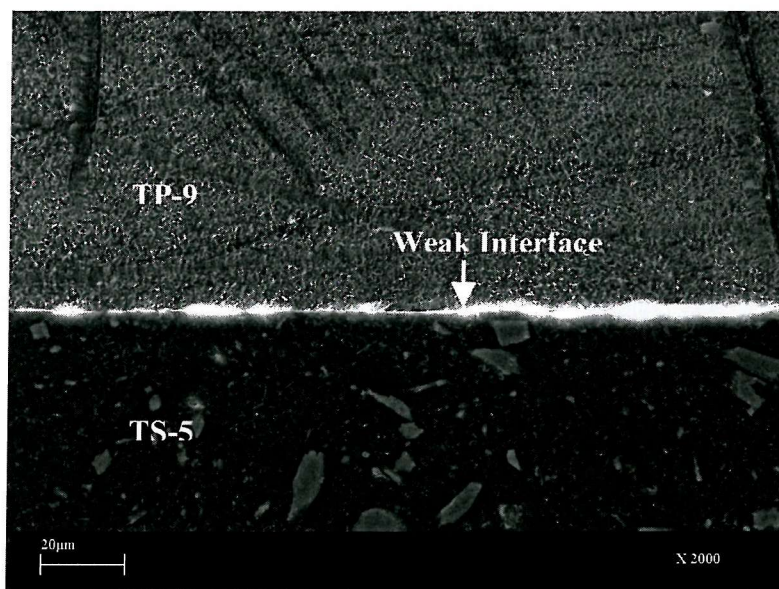


Figure 3.14: SEM image of the transverse section of the dual layer coating. Note the poor bond between the two layers.

From Figure 3.14, it is apparent that the bond between the two layers is poor, suggesting a weak interface. This is believed to be due to manufacturing inconsistencies. Since the matrix of the two coatings differs considerably in chemical structure, inhomogeneous post-deposition cooling results after coating is applied. This produces compressive stresses at the

interface, which will tend to force the coatings apart, leading to the observed weak interface.

Designation	TS-5	TSX-4	TS-7	TP-9	Fluorocarbon	PVDF	Dual Layer (TP-9/TS-5)	HH205	IPC 800
Generic name	Thermoset	Thermoset	Thermoset	Thermoplastic	Thermoplastic	Thermoplastic	Thermoplastic / Thermoset	Thermoset	Thermoset
Resin type	Modified Novalac (Powder)	Modified Epoxy phenolic	Epoxy (Powder)	PA 11 (Powder)	Fluoropolymer	Fluorinated semi-crystalline	PA11/ Modified Novalac	Epoxy Phenolic	Modified Epoxy powder
Filler type (In the matrix)	CaCO ₃ /SiO ₂	Al ₂ O ₃	Glass	None	CaF ₂	None	None/ CaCO ₃ /SiO ₂	SiO ₂	SiO ₂
Filler %	~ 9	~ 20	~ 15	N/A	~ 3	N/A	None/~9	10	16
Filler size (µm)	10 - 30	5 - 20	5 - 40	N/A	20 - 40	N/A	None/10-30	10 - 15	10 - 25
Filler shape (In matrix)	Angular and Flakes	Angular	Angular	N/A	Rounded	N/A	None/Angular and Flakes	Angular	Angular
Coating thickness (µm)	250 - 270	135 - 145	260 - 280	535 - 550	500	600 - 650	~500	500	203 -330
Primer type	Phenolic	Phenolic	Phenolic	Phenolic	Unknown	None	Phenolic	Phenolic	Phenolic
Primer thickness	15 - 30	50 - 100	15 - 40	24 - 30	80 - 200	N/A	20 - 30	15 - 20	10 - 15
Filler in primer	None	CaSiO ₃	None	None	SiC	N/A	None	None	None
Filler % in primer	N/A	~ 40	N/A	N/A	12	N/A	N/A	N/A	N/A
Filler size in primer	N/A	5-30	N/A	N/A	5 - 10	N/A	N/A	N/A	N/A
Filler shape in primer	N/A	Angular/flak e/oblong	N/A	N/A	Angular	N/A	N/A	N/A	N/A
Surface roughness (Ra)	6.0±0.4	3.0 ± 0.1	9.0±0.2	11.0 ± 0.2	0.30 ± 0.04	2.0 ± 0.7	8.0 ± 0.4	4.0±0.5	5.0±0.8

Table 3.7: Summary of the first set of coatings studied. Note: the dual layer combines the details Coating TP-9 and TS-5.

3.3.4 Coatings investigated in the second study

The following coatings were formulated and deposited based on the results of the studies performed on the seven coatings discussed previously. The coatings were manufactured and supplied by a different manufacturer using a different manufacturing process. Unlike the initial seven coatings that were hot-sprayed from the powdery state through an air gun, both the thermoplastics and the thermosets, the new coatings were produced through a hot-dipped process via a fluidised bed.

Hot-dipped process

Hot dipping is a simple but effective process of depositing coatings. Prior to the application of the coating, surface treatment such as degreasing and shot blasting is applied to the substrate. A controlled process is then used to deposit a thin layer of primer on the substrate; usually water based primers are used ^[3,5]. The primer-coated substrate is then heated to 400 °C in an oven and held for a few minutes to allow temperature equilibrium within the substrate. Upon satisfactory conditions, the substrate is swiftly transferred into a fluidised bed of the powdered coating, while being constantly shaken for a period of about four minutes. The coated carbon steel is then cured close to 400 °C for few minutes in the oven to allow any possible unmelted particles to melt properly and redistribution of the coating on the substrate to be achieved. The four coatings, as-received from the manufacturer, are characterised below. For the purpose of confidentiality, the coatings have been designated: A, B, C and D respectively.

a) Coating A

Details of the coating are shown in Table 3.8. Coating A is an unfilled natural grade PA11 coating, which contains no additive ^[3,6]. Independent laboratory tests performed on the coating are consistent with the information supplied by the manufacturers. The EDX does not reveal any chemical composition other than that of the matrix. Figure 3.15 shows the coating transverse section. It can be seen that the coating does not contain fillers. The score marks are due to polishing.

Designation	Coating A
Generic name	Thermoplastic
Resin type	PA11 (powder)
Filler type	None
Filler percentage	N/A
Filler size (μm)	N/A
Filler shape	N/A
Matrix thickness (μm)	350 – 400
Primer type	Phenolic
Primer thickness (μm)	10 – 15
Surface roughness (R_a , μm)	0.60 ± 0.01

Table 3.8: Details of the polyamide coating A.

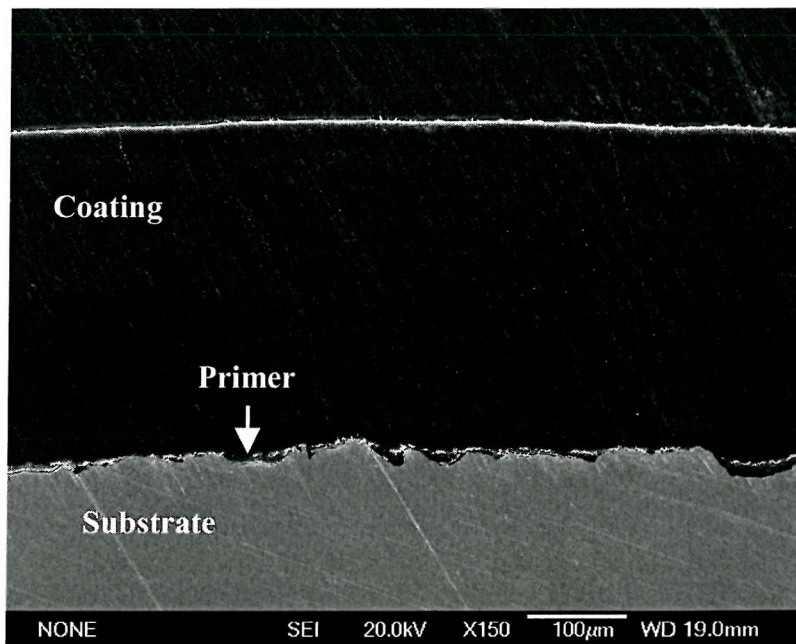


Figure 3.15: SEM of the transverse section of coating A.

b) Coating B

Details of the coating are shown in Table 3.9. Unlike Coating A, coating B contains 2 % carbon black, which has been added as a colouring pigment ^[3,6]. In addition to the colouring pigment, a negligible amount of anti-oxidant and surface smoothening agents were added to coating B.

Designation	Coating B
Polymer base	Thermoplastic
Resin type	PA11 (powder)
Filler type	None
Colour	Black (contains 2 % carbon black)
Filler percentage	N/A
Filler size (μm)	N/A
Filler shape	N/A
Coating thickness (μm)	350- 400
Primer type	Phenolic
Primer thickness (μm)	10 - 15
Surface roughness (R_a , μm)	0.40 ± 0.03

Table 3.9: Details of the polyamide coating B.

The surface smoothening agent was added to improve the surface finish of the coating. This explains the slight difference in the surface roughness observed between coating A and coating B. The SEM of the transverse section is shown in Figure 3.16.

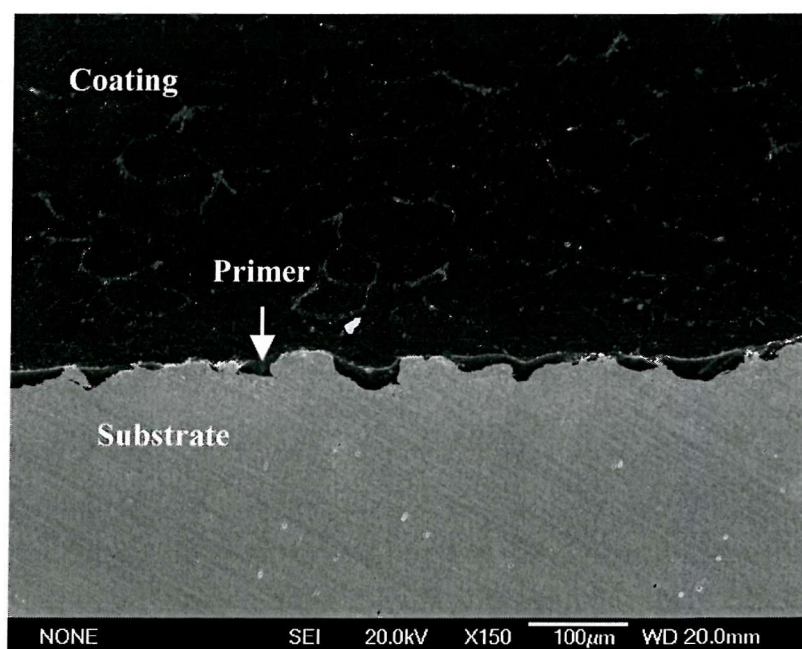


Figure 3.16: SEM of the transverse section of coating B.

c) Coating C

The two coatings, A and B, discussed above are categorised as unfilled, except for the colouring pigment added to coating B. The remaining two coatings investigated are

filled with fillers to a different proportion. Table 3.10 details the compositional characterisation of coating C.

Designation	Coating C
Polymer base	Thermoplastic
Resin type	PA11 (powder)
Filler type	TiO ₂
Colour	Blue (contains blue pigment and carbon black)
Filler percentage	14 %
Filler size (µm)	1-2
Filler shape	Polygonal
Coating thickness (µm)	350- 400
Primer type	Phenolic
Primer thickness (µm)	10 - 15
Surface roughness (Ra, µm)	0.20 ± 0.06

Table 3.10: Details of the polyamide coating C.

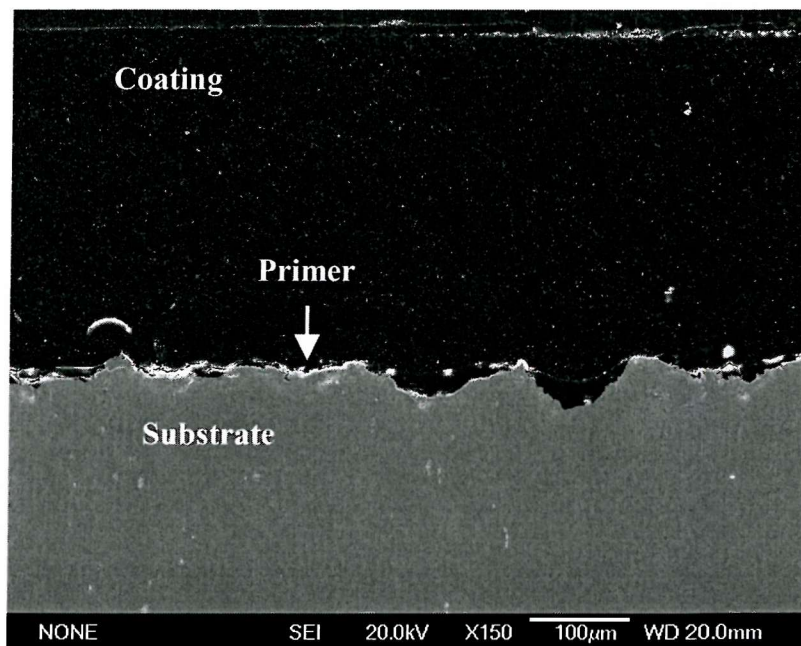


Figure 3.17: SEM of the transverse section of coating C.

Table 3.10 shows that coating C is filled to approximately 14 % with titanium oxide. Unlike coating B, two pigments, blue and carbon black, were added to coating C. The

blue pigment was used as a colorant. The fillers were found to be between 1 and 2 μm in size. Although the coating manufacturers did not give the details for the small filler size, it is thought that the choice of a small filler size may be to facilitate a good adhesion between filler and matrix and to reduce the inter filler spacing. This has the tendency to enhance mechanical property such as toughness and hardness. The fillers are well distributed within the matrix as evident in the SEM image, Figure 3.17. A more detailed SEM image of the coating confirmed good bonding between the well-interspaced fillers and matrix, see Figure 3.18.

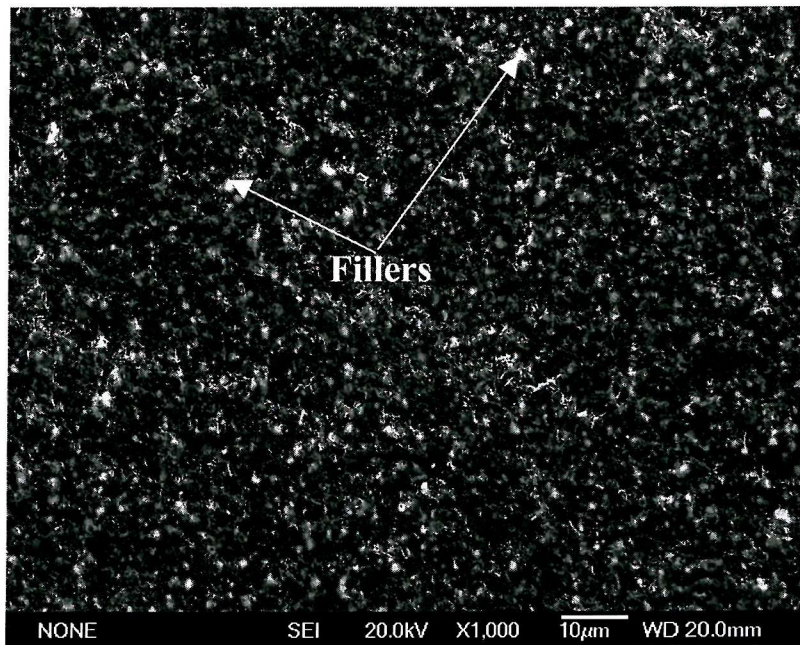


Figure 3.18: SEM of a more detailed transverse section of coating C.

d) Coating D

Coating D is filled with titanium oxide and Dolomite (calcium and magnesium carbonate), 9 and 7.5 % respectively ^[3.6]. Details of the coating are shown in Table 3.11.

Designation	Coating D
Polymer base	Thermoplastic
Resin type	PA11 (powder)
Filler type	TiO ₂ and Dolomite
Colour	Blue (contains blue pigment and carbon black)
Filler percentage	16.5 %
Filler size (μm)	1-6
Filler shape	Polygonal
Coating thickness (μm)	350- 400
Primer type	Phenolic
Primer thickness (μm)	10 - 15
Surface roughness (Ra, μm)	0.30 ± 0.07

Table 3.11: *Details of the polyamide coating D.*

The EDX analysis performed on coating D confirms the presence of both TiO₂ and Dolomite fillers. Figures 3.19 and 3.20 are transverse sections of the coating at low and high magnifications respectively. The wider range in filler size can be seen in Figure 3.20 compares with the narrower range for coating C. Like coating C, the fillers are well interspaced within the matrix and the coatings contains equal amount of negligible colouring pigments. The fractured fillers are thought to be due to the polishing effect. Table 3.12 is a summary of the coatings investigated in the second study.

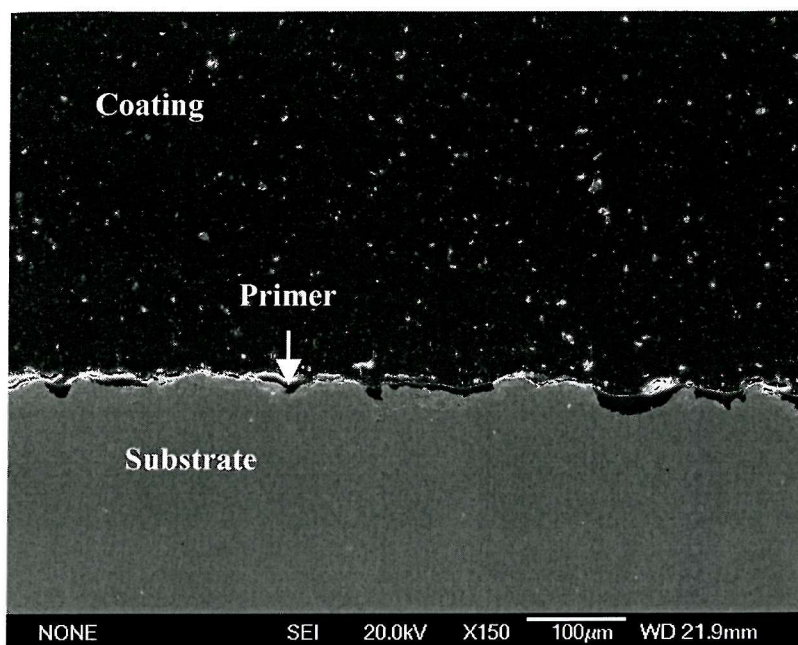


Figure 3.19: SEM of the transverse section of coating D.

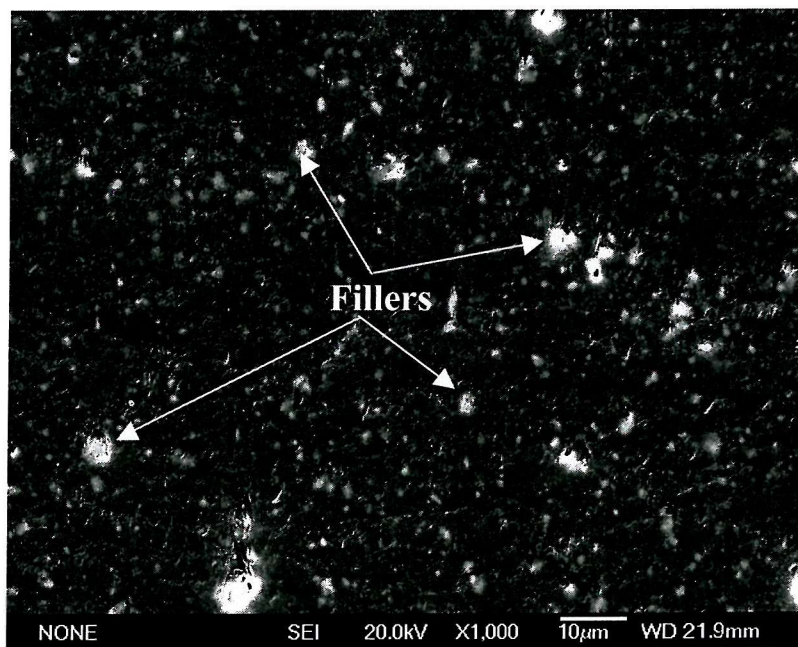


Figure 3.20: SEM of the transverse section of a more detailed view of coating D.

Designation	A	B	C	D
Resin type	PA11 (powder)	PA11 (powder)	PA11 (powder)	PA11 (powder)
Filler type	None	None	TiO ₂	TiO ₂ and Dolomite
Colour	Colourless	Black (contains 2 % carbon black)	Blue (contains blue pigment and carbon black)	Blue (contains blue pigment and carbon black)
Filler percentage	NA	N/A	14 %	16.5 %
Filler size (µm)	NA	N/A	1-2	1-5
Filler shape	NA	N/A	Cuboids	Cuboids
Matrix thickness (µm)	350 – 400	350- 400	350- 400	350- 400
Primer type	Phenolic	Phenolic	Phenolic	Phenolic
Primer thickness (µm)	10 – 15	10 - 15	10 - 15	10 - 15
Surface roughness (Ra, µm)	0.60 ± 0.01	0.40 ± 0.03	0.20 ± 0.06	0.30 ± 0.07

Table 3.12: *Summary of the coatings investigated in the second study.*

References

- 3.1.Symonds N, Wireline Wear of Polymeric Coatings, PhD Thesis, School of Engineering Sciences, University of Southampton, 2000.
- 3.2.Information Manual Brochure, Tuboscope Vetco International.
- 3.3.Information of Fluorocarbon Coating, Fluorocarbon Company, 1998.
- 3.4.N. Maquet, Translated by E. R. Dilley, The Use of SOLEF PVDF as Anti-corrosion Coatings and Linings, Engineering Polymer SOLVAY, 2000.
- 3.5.Michael Werth, Report of the Technical Meeting with the representatives of the Surface Engineering Group, Southampton University, at ATOFINA Technical Polymers, CERDATO, France, 2002.
- 3.6.Information Manual Brochure prepared and supplied by ATOFINA Technical Polymers, CERDATO, France, 2000.

4.0 Overview of previous and initial wear testing of thermoplastic and thermosetting coatings

4.1 Introduction

Over the last few years there has been considerable industrial activity based on material options for the protection of downhole tubing used in water injection wells ^[4.1]. Numerous laboratory tests, as well as field experience, have demonstrated that tubular coatings that are currently available do not have sufficient mechanical robustness to survive downhole tool impact and abrasion from slickline wire operations. Current coating options are damaged by tool impact and wireline cutting during well intervention operations. It would appear that several orders of magnitude improvement in coating performance, particularly under impact, are required to give the mechanical robustness needed to allow confident long term use of the coatings downhole as truly “corrosion resistant” options.

In view of this problem, glass filled epoxy resin composite lined tubing (such as Duoline 20) was considered as an alternative to coated tubulars for some water injection wells, as a mechanically robust, corrosion resistant option to increase the life of the field. These liners are cemented as whole cylinders onto the bore of the tubulars.

In 1995, with common interest in coatings for protection of downhole tubing, BP Exploration and Statoil embarked on a joint development programme to extend the capability of protection system for downhole tubing, in particular to investigate the capability of current and novel coatings ^[4.1]. Between 1996 and 1999, work carried out at Southampton University, has defined a set of screening tests that can be used to characterise the performance of composite liners and coatings for use in downhole tubing. Presented in Figure 4.1 is a summary of some of the coatings investigated. The work forms the basis of this BP Exploration sponsored PhD studentship to examine and improve coating performance.

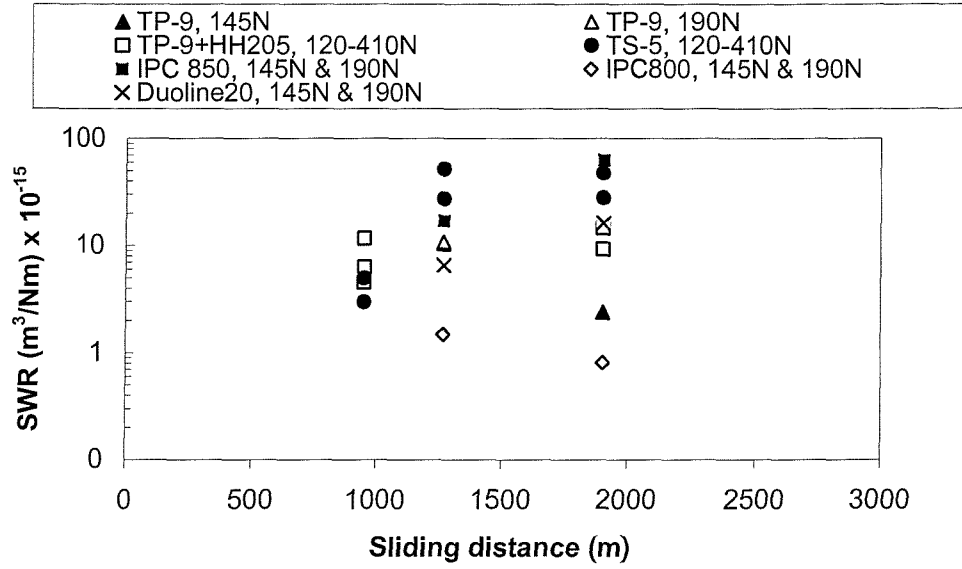


Figure 4.1: Summary of some of the coatings investigated by MECS for BPX and Statoil under reciprocating wireline abrasion conditions.

The general conclusion from this study is that under wireline wear conditions a wide coating performance range was seen, as shown in Figure 4.1. In terms of the coating chemistry, IPC 800 (a thermoset coating) appears to be the best. Coating IPC 850 being the worst coating. The hybrid coating TP-9+HH205 shows a wear rate that is comparable with the Duoline 20 liners. The TP-9+HH205 is a hybrid of two different coatings. The TP-9 was applied onto the HH205. The “Duoline 20” liners are a rival technology to coatings and generally exhibit a superior wear performance over coatings except for IPC 800. From these results, it can be shown that the life of a coating is directly proportional to the coating thickness and inversely proportional to the wear rate, i.e.

$$CL = f\left(\frac{t}{SWR}\right) \quad \text{-----} 4.1$$

Where CL is coating life, t is the coating thickness and SWR the specific wear rate. It then implies that

$$\frac{CL_{Coating}}{CL_{liner}} = \frac{f_1(t_C SWR_C^{-1})}{f_2(t_L SWR_L^{-1})} \quad \text{-----} 4.2$$

where subscripts C and L represent coating and liner respectively.

From Equation 4.2, it means that

$$\frac{t_c}{t_L} \times SWR_L = SWR_C \quad \text{-----} 4.3$$

However, the coating and liner thickness are known to be approximately 300 and 2600 μm respectively. Thus

$$\frac{t_c}{t_L} = \frac{300}{2600} = 0.12$$

Hence,

$$0.12SWR_L = SWR_C \quad \text{-----} 4.4$$

This implies that for any coating system to be a preferred option, it must show a wear rate that is always less than 0.12 times that of a liner. In the case of Duoline 20 the coatings have to have a SWR_C better than $1 \times 10^{-15} \text{ m}^3/\text{Nm}$.

Thus, this chapter will review the methods that have been used to investigate the tribology of polymeric coatings and the typical wear rates obtained from work conducted by previous researchers within the University of Southampton. The results of some initial studies undertaken for the present investigation will also be presented.

4.2 Overview of previous works

Research at the University of Southampton began with the development of screening tests to measure the erosion, abrasion and impact performance of polymer coatings conducted by the Mechanical Engineering Consultancy Service (MECS) in 1995. Symonds was actively involved in this screening test development. The MECS work primarily focused on the two main polymer coatings: thermoplastics and thermosets ^[4.2, 4.3].

The performance of these coatings eventually led to a further study and consequent submission of a PhD thesis by Symonds on the wear and impact resistance of polymeric coatings. Symonds ^[4.3] primarily studied thermosetting coatings, though some thermoplastics such as PA11 were also reported in her work. Figure 4.2 is an overview,

which includes work from MECS ^[4.2], Symonds ^[4.3] and the preliminary investigation currently undertaken (detailed in the later section).

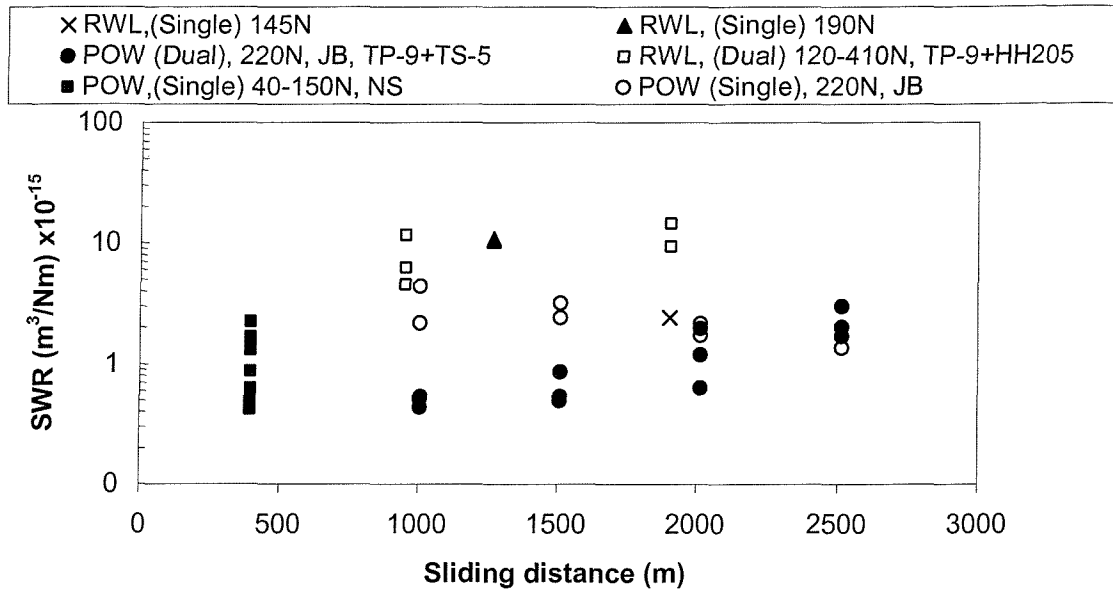


Figure 4.2: Overview of the studies carried out on TP-9 single and dual layer coatings under water lubricated conditions. Note RWL means reciprocating wireline, POW means pin-on-wire. Tests were carried out under different loads using ϕ 3.2 mm wireline, an average sliding speed of 0.46 m/s for POW and 0.85 m/s for RWL. JB means Jelili Bello and NS means Nicola Symonds.

The following can be deduced from Figure 4.2. For clarity, the deductions have been classified under three headings: experimental methods, the wear rate and the governing wear mechanism(s). Figure 4.3 and Figure 4.4 are the laboratory picture of the POW rig and schematic of the RWL rig, while Table 4.1 summarises the test conditions used for both tests.

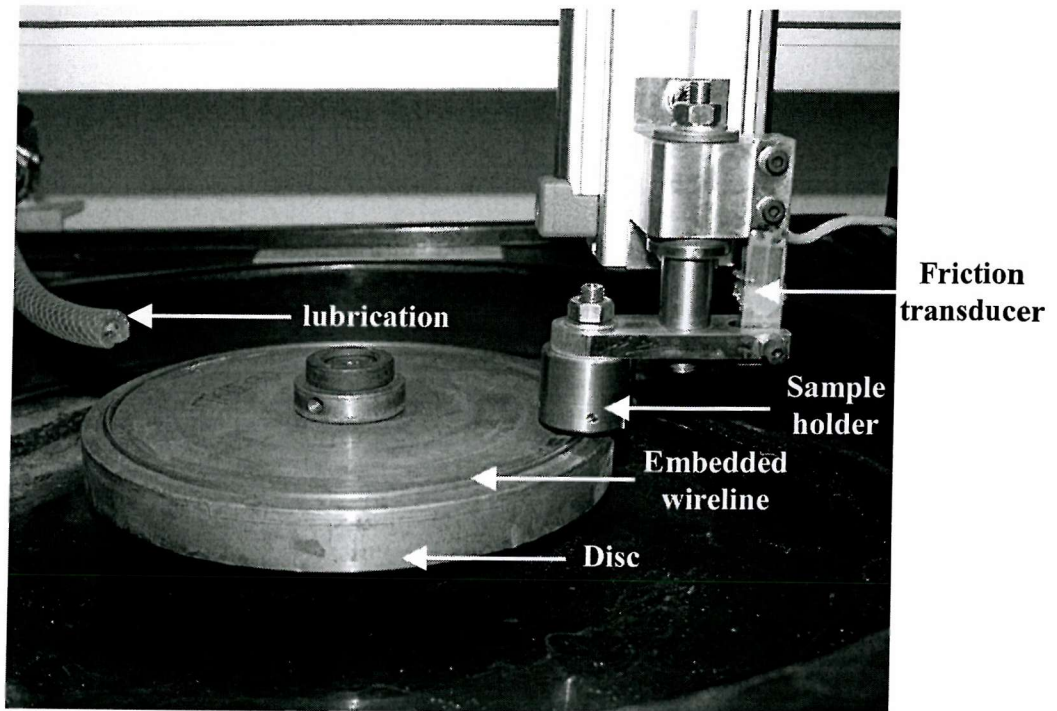


Figure 4.3: *Picture of the laboratory pin-on wire test rig.*

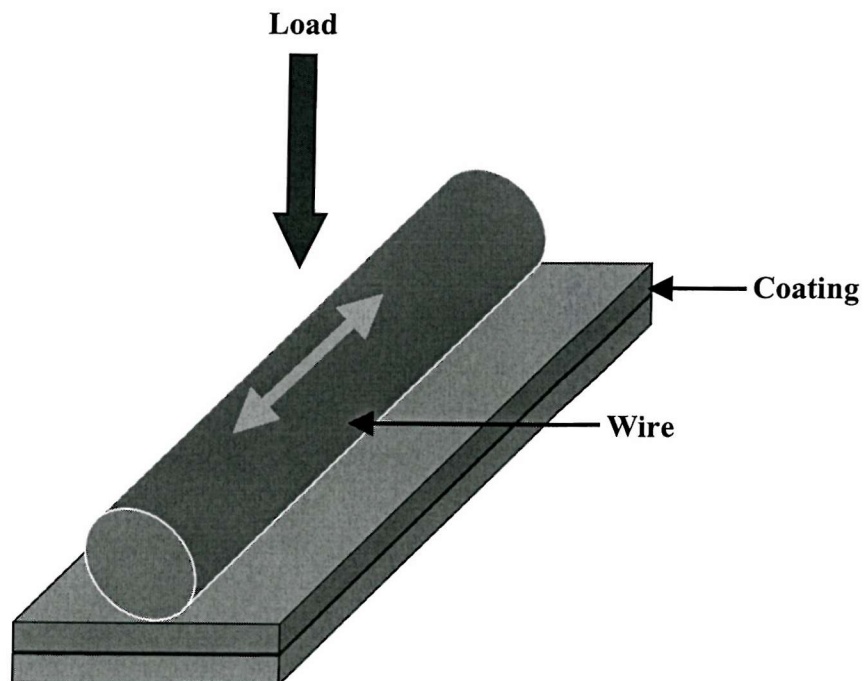


Figure 4.4: *Schematic of the reciprocating wireline wear rig.*

	Reciprocating Wireline (RWL)	Pin-on-Wire (POW)
Diameter of wire (mm)	3.2 (slick)	3.2 (slick)
Line contact (mm)	100	10
Load (N)	190 - 410	40 - 220
Sliding speed (m/s)	0.85	0.46
Test duration (min)	40 - 60	3 - 50

Table 4.1: Summary/overview of the test conditions adopted for the pin-on-wire and the reciprocating wireline wear tests.

4.2.1 Experimental Methods

Figure 4.2 shows that the two test methods, pin-on-wire (POW) and reciprocating wireline (RWL), generate different wear rates. The RWL method generates wear rates that are about 1.5 times higher in magnitude than that produced by the POW. The main difference between the methods is that RWL has bi-directional sliding motion and the POW uni-directional, although the RWL was operated at an average sliding speed of 0.46 m/s while the POW tests were carried out at a sliding speed of 0.84 m/s. Both methods used the same type of slickline wire with a diameter of 3.2 mm.

4.2.2 The wear rate

Previous work by Symonds^[4.3] focused on the wear mechanisms of the coatings; however, a number of wear rates were reported and are shown in Figure 4.1. The typical wear rate reported by Symonds, MECS and the present investigation are: $2.25 \times 10^{-15} \text{ m}^3/\text{Nm}$ (400 m, 150 N), $1.45 \times 10^{-14} \text{ m}^3/\text{Nm}$ (1900 m, 410 N), and $4.30 \times 10^{-15} \text{ m}^3/\text{Nm}$ (1000 m, 220 N) respectively for the PA11 based TP-9 coating. From these wear rates and the associated test conditions, it appears that there is no logical continuity in the test conditions adopted so far.

The differing wear rates may also be due to the effectiveness of the testing rigs used. Symonds reported a lack of rigidity in the POW rig used^[4.3]. During the preliminary investigation carried out in the current work, similar problems were observed in the rigidity of that the pin-on-wire rig. Symonds also reported extensive edge loading, which has also been observed in this preliminary investigation. The edge loading is primarily due to the design of the sample pin holder, which lacks adequate stiffness and rigidity. In addition, it

was observed that the loading system may have a significant influence on the wear rate produced. For example, the wear rates measured during the preliminary investigations by the author using a more rigid system are approximately twice that obtained by Symonds. In this work, the direct loading system was adopted, while Symonds used a cantilever loading system, which encourages edge loading.

Symonds^[4.3] also employed gravimetric methods as a means for evaluating the SWR. The method has a disadvantage, as it requires measurement of the coating density (which is a composite) for volume loss to be evaluated. In addition, if the change in mass, in the coating before and after test, is very small then the accuracy of the measured value is questionable because the measured mass difference is sometimes less than the error margin of the weighing balance. For these reasons, the present investigation has adopted the volume loss method. This involves tracing the wear scar profile using a Talysurf 120L Profilometry, scanning the resulting image into a computer software package, which can more accurately estimate the volume of the wear scar.

4.2.3 Wear mechanism

Micro-ploughing characterised by large tendril formation was observed by Symonds, using the pin-on-wire test rig, for most of the coatings. However, during this current investigation, fewer tendrils were observed. Again, it is thought that the lack of rigidity of the test rig combined with edge loading may have favoured the large tendrils observed by Symonds. This is not conclusive and it will be investigated further. Micro-ploughing characterised by grooves was also observed in this work as the dominant wear mechanism.

In summary, the overview suggests that various factors will have a significant influence on the results of wear tests performed on polymeric coatings depending on the level of control over the test procedure. Such factors include: the type of rig, the condition and nature of the rig used, selection of the appropriate test conditions. Based on these emerging facts, it was considered necessary to redesign the wear rig and set a unified test conditions for the current work. The reciprocating rig will not be considered in the current work because most of the damage to coatings are caused by unidirectional motion of the wireline. Although, sometimes during wireline operations, reciprocating motion comes into play, it is less

frequent. Hence, a preliminary investigation was conducted on three coating samples that were inherited from Symonds. The results of the study are presented below, which have also been included in the overview above (Figure 4.2).

4.3 Preliminary investigation

The preliminary investigations were carried out with major modifications to the loading system and the wire end joints on the pin-on-wire rig used by previous researchers at Southampton University.

4.3.1 Experimental

4.3.1.1 Methodology

The apparatus was a pin-on-disc rig modified for the purpose of pin-on-wire tests. It utilises a true tribo-couple consisting of a “slickline” wire used downhole embedded in an aluminium alloy disc to form a complete circular loop with a radius of 80 mm radius, see Figure 4.3. The sample pin was cut from coated tubulars.

The sample pin was loaded against the rotating wire. A pump supplies tap water lubrication at the rate of $17\text{cm}^3/\text{s}$. Profilometry was used to estimate the volume of the material loss. Since the dual layer comprised two polymers with different densities, mass loss measurements could not be employed. The wear rate was estimated by dividing the wear volume by the applied load and the total sliding distance. The friction force was measured using a force transducer connected to an HP Vee computer controlled programme. The experimental conditions used in the test are shown in Table 4.2. The wear scars were investigated by SEM. This study was conducted at $25\text{ }^\circ\text{C}$ but future work will look at higher temperatures.

Applied Load (N)	220
Disc rotational speed (rev/min)	100
Radius wire from centre of disc (m)	0.08
Test times for dual layer and TP-9 (min)	20, 30, 40, 50
Test times for TS-5 (min)	5, 10, 15, 20
Temperature	Room, 25 °C
Lubrication	Tap water
Lubrication rate (ml/min)	1000

Table 4.2: *The experimental conditions employed for the preliminary investigation test.*

4.3.2 Results and Discussion

Figure 4.5 presents the specific wear rate of TP-9 as a function of the sliding distance in m^3/Nm ., the result shows that the wear rate decreases with increasing sliding distance.

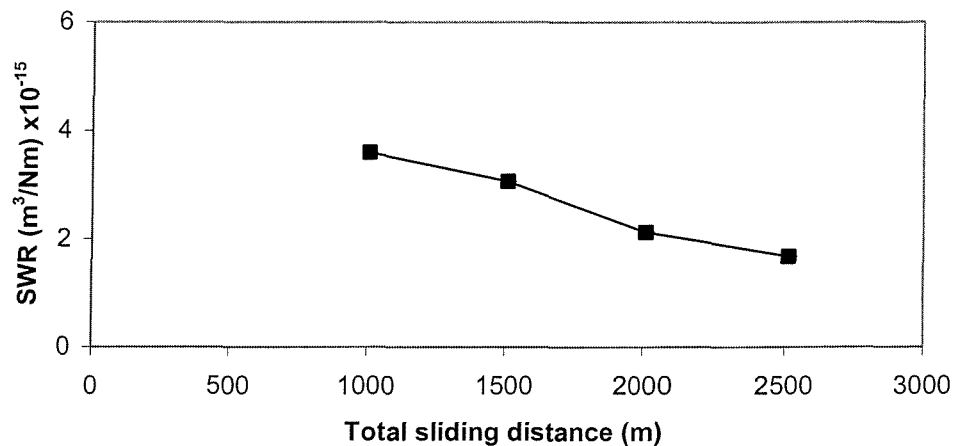


Figure 4.5: *Specific wear rate of TP-9 as a function of the sliding distance.*

It has been established in the literature that polymers have the ability to transfer material to their rubbing counterface during sliding {see section 2.2.2}. It has been observed that when polymers rub against harder materials, steel for example, adhesive forces at the asperity contact are sufficient to cause local welding ^[4.4]. The shearing of these adhesive forces often gives rise to deformation in the softer material, in this case, the polymer. The resulting effect is a transfer of material to the harder surface, which acts as a friction modifier at the interface to assist in reducing wear of the coating. Sometimes, these transferred films detach from the counterface and are either re-attached to the polymer itself or swept away by the lubricant, see Figures 4.6 and 4.7. In addition, the change in initial

contact area with sliding, causing a drop in the load per asperity distance, could be an additional factor for the trend shown in Figure 4.5

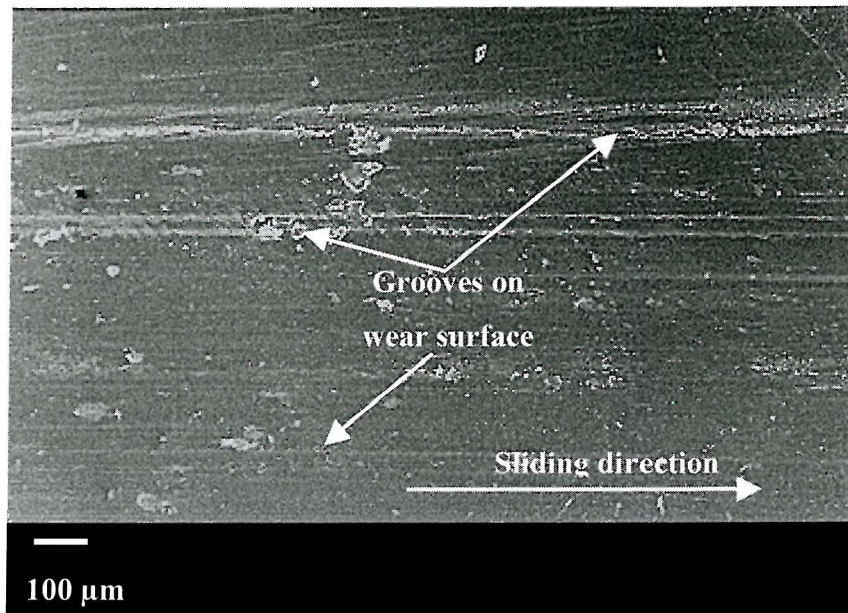


Figure 4.6: SEM of the worn surface of TP-9 after sliding for 2000m.

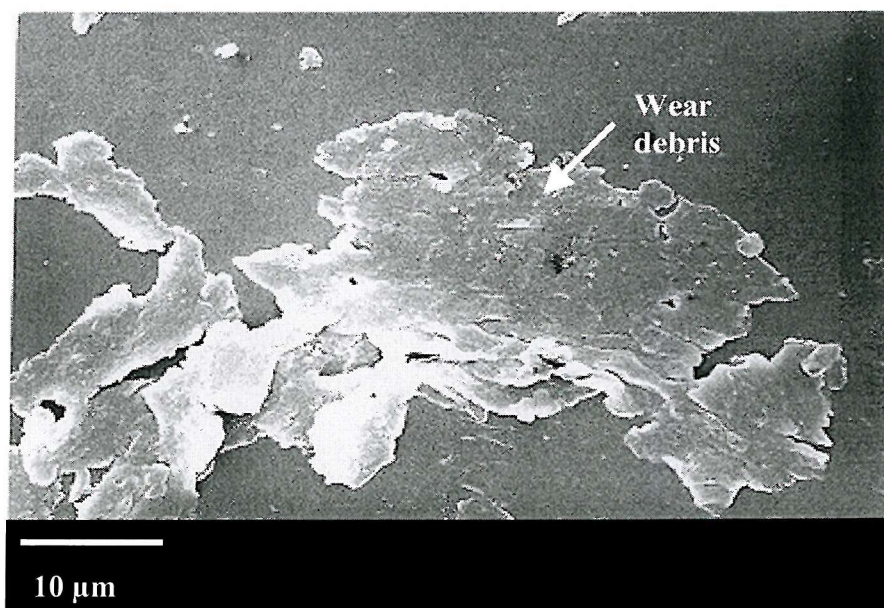


Figure 4.7: SEM of worn surface of TP-9 showing repeatedly rubbed wear debris.

Figure 4.5 suggests that more material is transferred as sliding distance increases lowering the wear rate. It must be emphasised that no film of coating was seen on the wireline after the test.

The wear rate of the dual layer as function of the sliding distance is shown in Figure 4.8. The specific wear rate initially appears to decrease over a distance of about 1500m. However, between 1500 and 2500 m, the SWR increases. It was observed that the wireline did not wear through the top layer, TP-9, of the dual layer coating. Hence, it may be reasonable to expect a similar behaviour for TP-9 single layer in Figure 4.5.

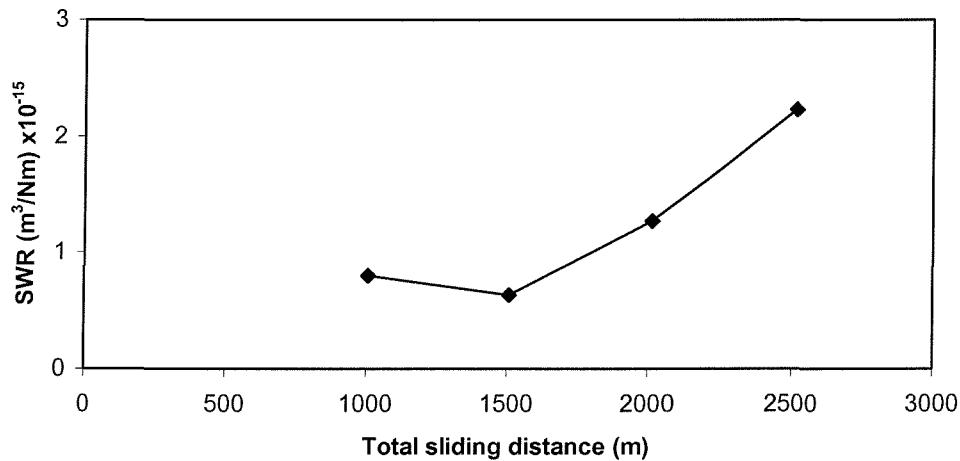


Figure 4.8: *Specific wear rate of the dual layer (TP-9 on TS-5) as a function of the sliding distance.*

The trend shown in Figure 4.8 is thought to be associated with mechanistic change within the top coat close to the interface which may have been induced by defects/unmelted PA11 powder, in the form of weak interlayer, incurred during coating manufacture, see Figure 4.9. The depth of the wear scar is about 150 μm .

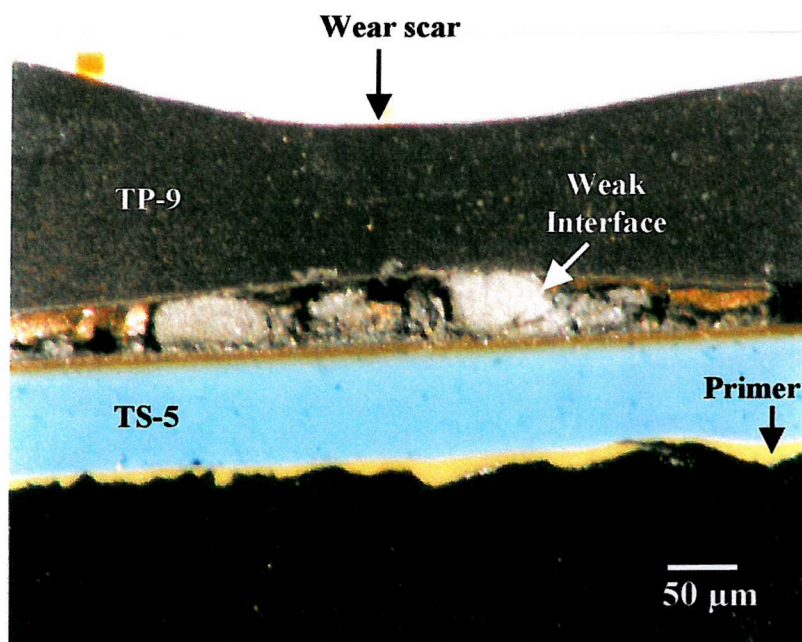


Figure 4.9: Optical image of the worn sample of the dual layer coating showing the weak interface between the topcoat and the bottom coat.

The weak interface is thought to have a significant influence on the changes that occur in the physicochemical properties, such as molecular chain redistribution, resulting in a possible change in toughness and hardness, as a function of depth, which in turn affects the wear rate of the coating and the top coat in particular. The consequence, of course, is a possible mechanistic change in the coating with depth. However, no conclusive evidence was found to suggest this is the case.

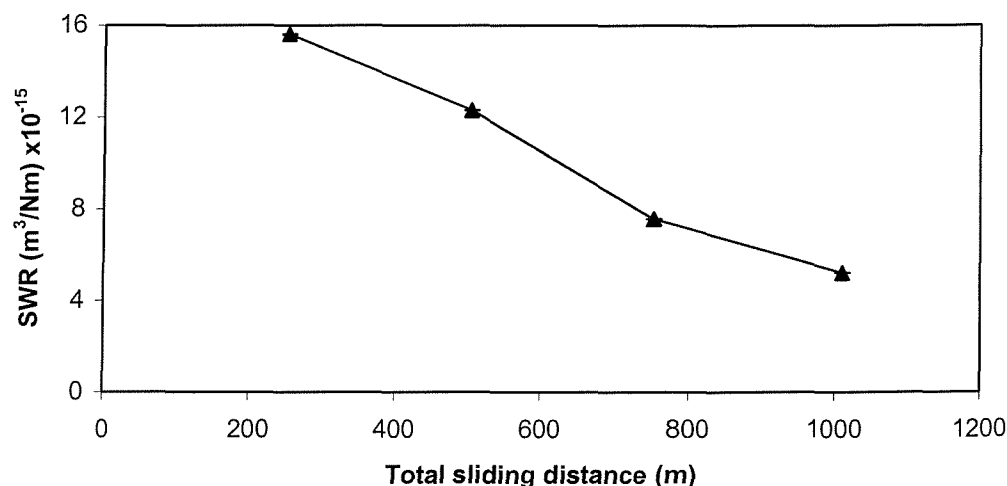


Figure 4.10: Specific wear rate of TS-5 as a function of the sliding distance.

The last coating studied in this preliminary investigation is the TS-5, a thermoset. Figure 4.10 shows the specific wear rate of TS-5 as a function of the sliding distance. A continuous decrease in specific wear rate with increasing sliding distance is seen. This is probably due to the presence of filler in the matrix. Fillers have been found to reduce the wear rate of polymers to a certain extent when incorporated in the polymer matrix ^[4.3], by reducing the rate of material removal by the asperities of the mating surface. It is important to note that TS-5 could not be slid for more than 1100 m as attempts to go beyond this distance saw the wire wearing through the coating. An SEM examination of the worn surface of the sample after 1100 m of sliding, revealed large cracks at the edges of the fillers, see Figure 4.11. Unlike the thermoplastic coatings, no material transfer was observed on the worn sample and the wire.

This suggests that prior to 1100 m sliding distance, the fillers support the load and help to reduce the wear rate but are pulled out at distance above 1100m and may either act as further abrasives within the contact and/or are swept away by the lubricant. Continuous removal of the fillers weakens the matrix which could lead to increases in wear rate. It can also be seen that TS-5 produced a wear rate higher than TP-9. For example TS-5 is 2 and 6 times higher than TP-9 and Dual layer coatings respectively.

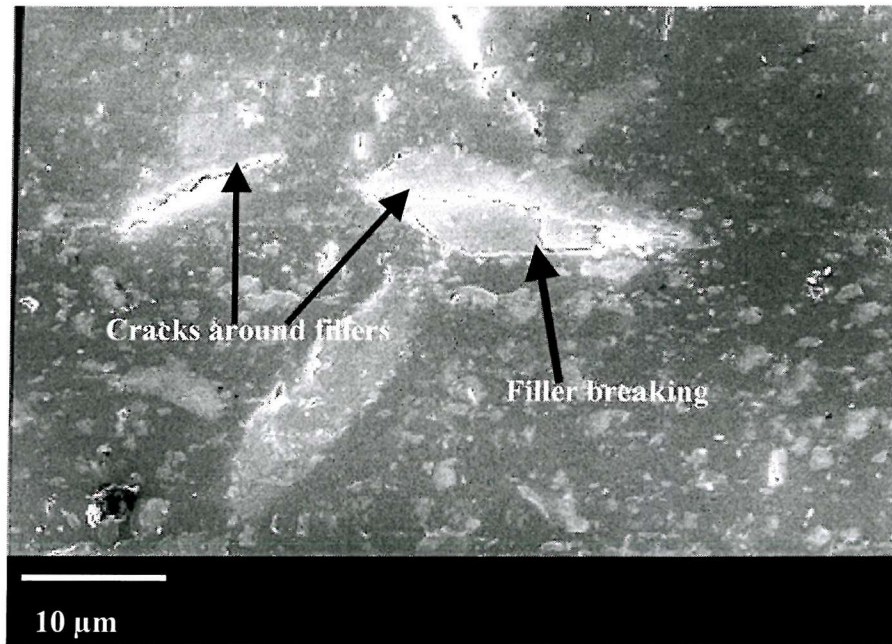


Figure 4.11: SEM micrograph of the worn surface of TS-5 at 1100 m sliding distance.

The friction coefficients exhibited by the coatings during sliding wear were also measured. Figures 4.12, 4.13 and 4.14 are the coefficient of friction plots for TP-9, TS-5 and the dual layer coatings respectively.

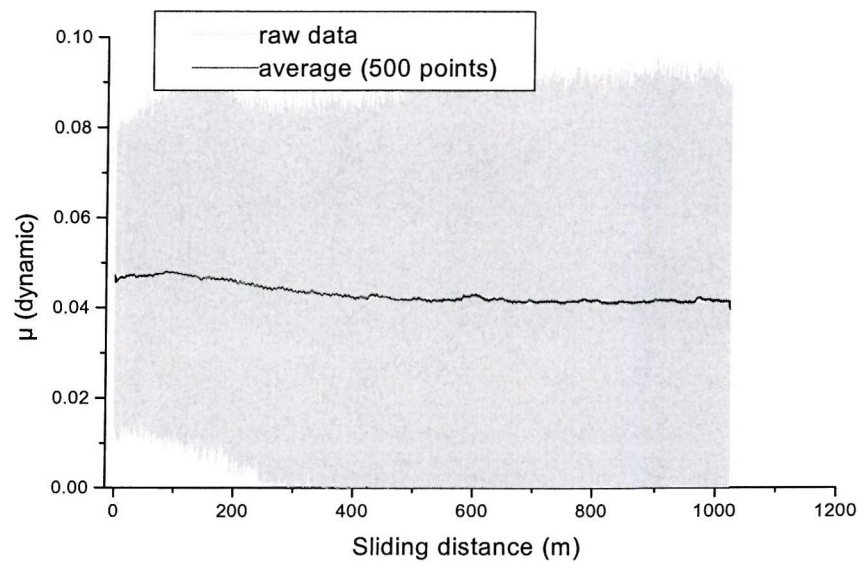


Figure 4.12: Coefficient of friction as a function of sliding distance for TP-9.

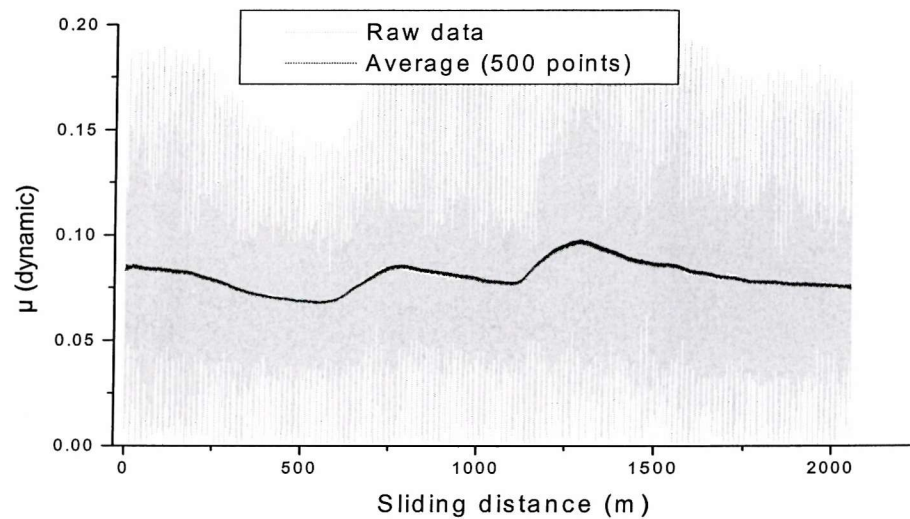


Figure 4.13: Coefficient of friction as a function of sliding distance for TS-5.

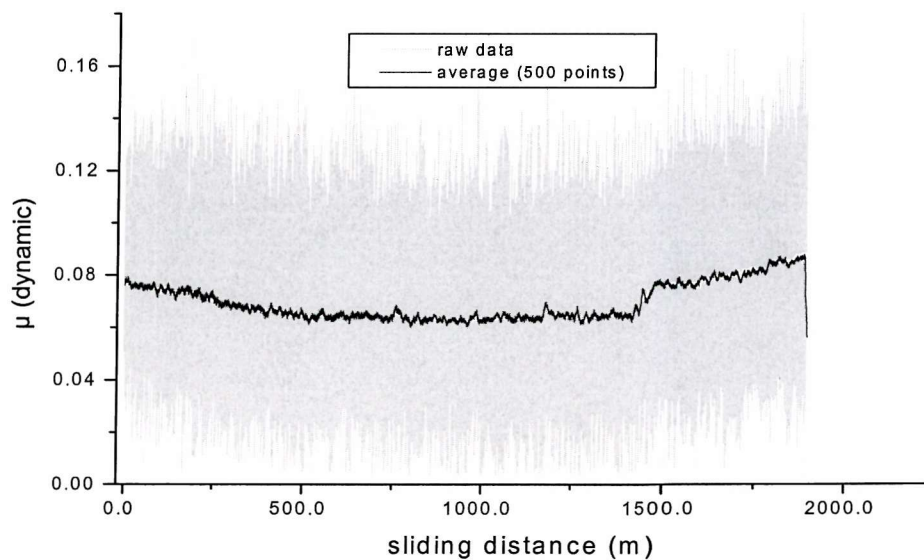


Figure 4.14: Coefficient of friction as a function of sliding distance for dual layer.

The coefficient of friction of TP-9 initially increases over a very short distance and later drops to a near-constant level. This is consistent with the self-lubricating property of thermoplastics as shown in Figure 4.7. The fluctuation and high friction exhibited by TS-5

could be attributed to the silica fillers in the matrix. The fillers have higher friction compared to the matrix; therefore, the movement of the counterface asperities between the matrix and the adjacent fillers could be responsible for the high fluctuation. Figure 4.14 is the friction curve of the dual layer and a rapid increase in friction can be seen to coincide with a corresponding increase in wear rate at about 1500m. This confirms an earlier assumption that there may be a mechanistic change with depth in the coating. However, it is not clear if there is a direct link between the sudden increase in wear and friction at 1500 m but it appears that there is some indirect agreement between the two parameters at this sliding distance. The SEM observation of the worn surface does not reveal any unusual features; rather it shows a smooth surface with patches of wear debris. The mean friction curves were obtained by smoothing 500-points per data plot. The mean friction coefficient for the coatings TP-9, TS-5 and Dual layer were: 0.045, 0.08 and 0.07 respectively.

4.3.2.1 Summary

The preliminary investigation has led to some basic understanding of the wear behaviour of the coatings. Particularly, how fillers are likely to influence the wear performance of the coatings. The performance of the test rig was found to be unsatisfactory, even with the minor modification, as edge loading was still prevalent. Thus, it is concluded that further modification in the rig design was required to optimise the rig (pin-on-wire). The knowledge gained and the result from the performance of the coatings forms the platform for the selection of experimental conditions for further studies in chapters 6-8. However, prior to the next stage of wear study, the investigation of the adhesion of the coatings to their substrate is necessary. The findings in this preliminary study have shown that coatings are poorly adhered to their substrate ^[4.3], which will have significant influence on the overall tribological performance of the coatings.

4.3.3 Conclusions

1. Substantial improvement was achieved in the pin-on-wire rig due to modification of the loading system and improved stiffness of frame.
2. The reciprocating wireline wear test method was found to be more aggressive than the pin-on-wire wear test method.
3. The dual layer coating produced a wear rate that is about 3.5 times lower than TP-9 and 6 times lower than TS-5 but the wear rate tends to increase with sliding distance.
4. The presence of fillers influences the friction and wear rate of TS-5. The fillers wear by micro-cracking initiated during sliding and acted as abrasive within the sliding contact.
5. The presence of a weak interface between the TP-9 and TS-5 coatings of the dual layer has an adverse effect on the wear resistance.
6. Thermoplastic coatings show a better wear resistance than the thermosetting coatings.
7. The relatively low coefficient of friction produced by the three coatings tested: TP-9, dual layer and TS-5 can be ordered such that $TS-5 > \text{dual layer} > TP-9$.



References

- 4.1. Symonds. N, Wood R. J. K., Mechanical Engineering Consultancy Services report number 96/EC179 and 96/EC180 (1996).
- 4.2. Wood, R. J. K., Symonds, N, and Wheeler. D. W, Erosion, Wireline, Abrasion and Impact resistance of coatings for downhole tubulars, Mechanical Engineering Consultancy Services Report number 98/EC211 (1998).
- 4.3. Symonds, N., Wireline wear and Impact of Polymeric Coatings for Downhole Application, PhD thesis, School of Engineering Sciences, University of Southampton, (2000).
- 4.4. Rabinowicz, E. 'Friction and wear of materials' John Wiley. 1st (ed.) (1965).

5.0 Evaluation of the adhesive properties of polymeric coatings by cathodic disbondment

5.1 Introduction

The adhesive properties of coatings to their substrates are important when considering the control of damage by high-energy impacts, particularly for thermoset (TS) coatings and/or by cathodic reactions associated with corrosion of impact damaged polymer-coated tubulars. Preliminary investigations and previous work have shown that commercial polymeric coatings are poorly adhered to their substrate. High-energy impact tests on TS coatings (1-100 J) at low angle (30°) using a falling tup impact rig at Southampton University have revealed that coating rupture occurs due to poor adhesion at the coating/substrate interface ^[5.1], at low impact energy, see Figure 5.1. Thermoplastic (TP) coatings generally performed better and failed by localised plastic deformation rather than by delamination/crack propagation. Coatings IP-5 and TS-6 are both thermosets filled with particulates and have been studied elsewhere ^[5.1]. The two coatings are not part of this programme; their inclusion in Figure 5.1 is for comparison purpose only. Thus, to improve impact resistance the adhesive properties of these coatings must be better understood allowing improvements to be made.

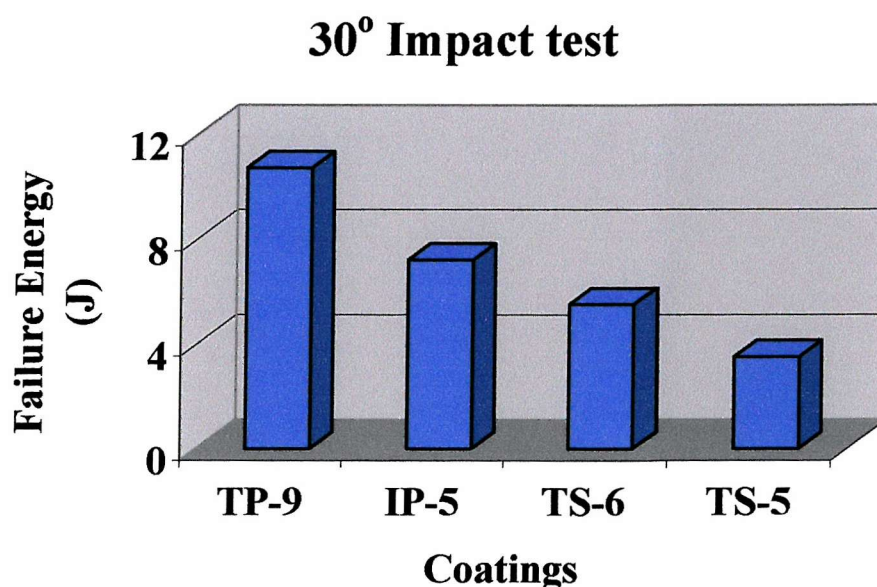


Figure 5.1: *Performance of coatings at low angle impact energy.*

To provide better understanding of the adhesive properties, commercially available polymeric coatings have been investigated, supplied by two coating manufacturers. The

initial studies were performed on coatings TP-9, TS-5 and TS-7, see chapter 3. Based on the performance of these samples, a new coating system designated coating A, was designed with improvements to the mode of deposition and substrate preparation. All the coatings are polyamide 11 based.

Two independent, experimental techniques, cathodic disbondment (CD) and interfacial indentation tests (IIT), were employed to investigate the adhesive properties of the coatings. The various standards used to investigate the adhesion of coatings have been reviewed in the literature, see section 2.6. The pull off test has been explored without success while others were found not to be practicable in the relation to the aims of this study. The CD test is based on the ASTM standard G8-98 ^[5.2] which uses OH^- and H_2 pressure to chemically attack bonds or apply tensile stresses at the coating/primer/substrate interfaces. While the IIT is a relatively new test methodology, it has been used to investigate the adhesion of commercial coatings ^[5.3 – 5.6]. The method applies a stress field surrounding a mechanical indent at the interface.

The ultimate aim of this study is to establish an understanding of coating disbondment from their substrate. Factors such as substrate preparation and residual stresses in the coating, which are often responsible for the disbondment will be studied. It is anticipated that the failure mode will be adhesive; however, any possibility of a cohesive failure will be investigated. Overall, the tests will allow the coatings to be ranked based on their resistance to disbondment.

5.2 Experimental details

5.2.1 The CD test cell

The test cell used for the CD tests is similar to the ones used by other authors ^[5.3]. A schematic of the test cell is shown in Figure 5.2. It consists of two cylindrical concentric electrolyte chambers. The inner chamber of approximately 50 ml capacity is in contact with the coated test panel and the intentional holiday in the coating. The outer chamber of approximately 100 ml capacity holds the platinum counter electrode. The two chambers are connected by two small bridging holes.

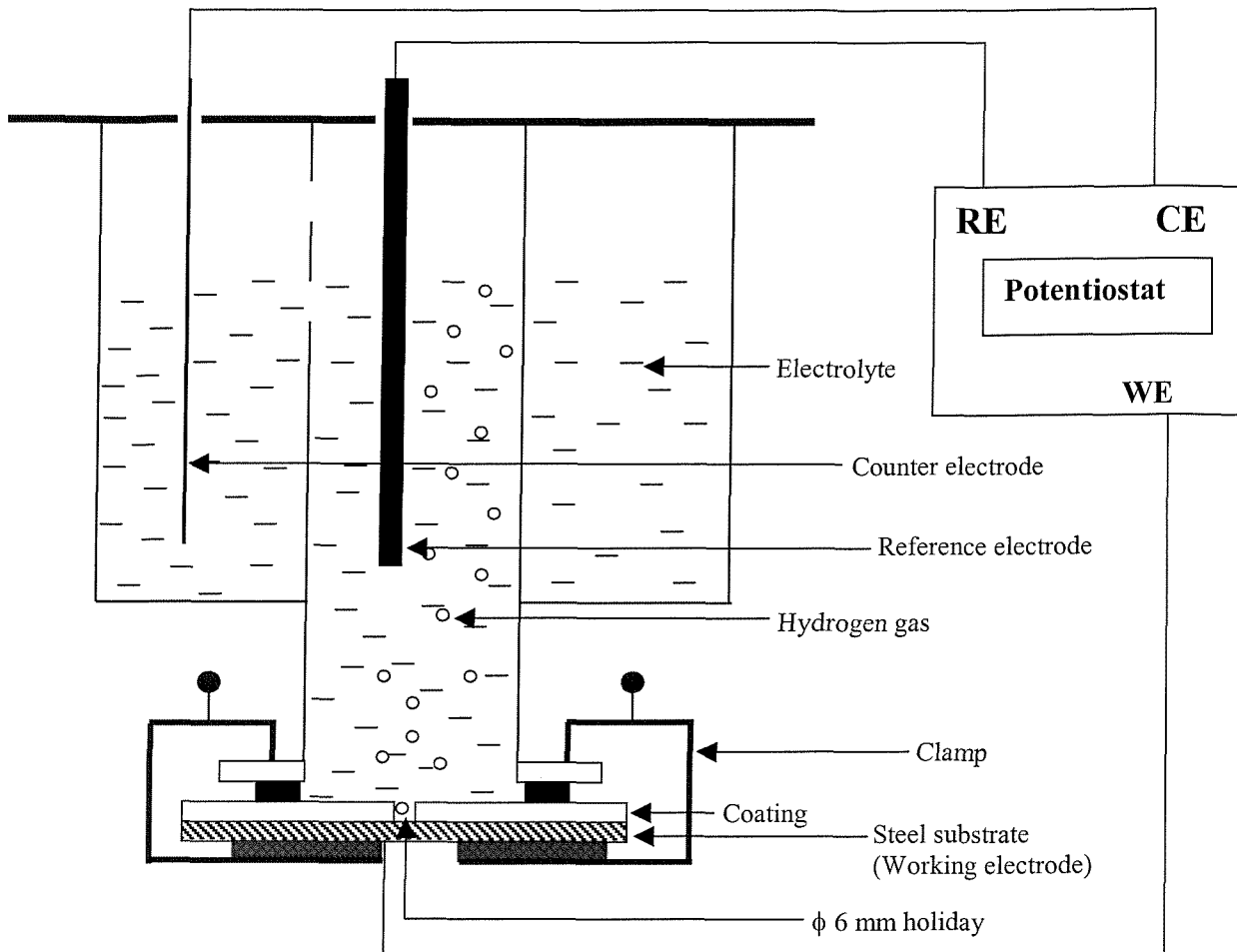


Figure 5.2: Schematic of the CD test set-up with the electrical connections.

Separating the cathode and the anode was deemed necessary because during an initial study, before the chambers were separated, it was observed that the hydrogen gas produced at the cathodic site clung to the surface of the counter electrode (the anode) thereby masking it, interfering with the current measurement.

5.2.2 The IIT test set-up

The IIT made use of the conventional Vickers' hardness indenter. The samples were held within the jaws of a clamp holder with its transverse section firmly supported by the base of the clamp. The interface to be indented is located before indentation using the microscope on the Vickers' hardness indenter. A detail of the method is described in section 5.2.4. The schematic of the test set-up is shown in Figure 5.3.

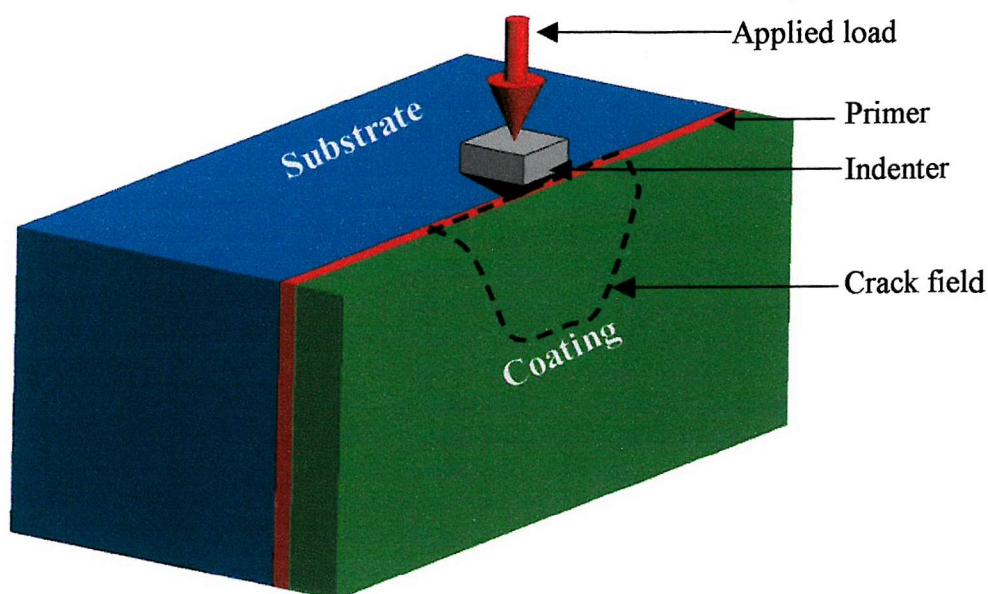
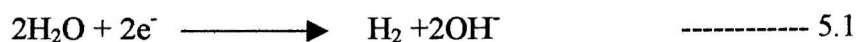


Figure 5.3: Schematic of the interfacial indentation test set-up.

5.2.3 The CD test electrolyte

It has been established in the literature {section 2.5.2} that delamination of a coating from its substrate is mostly caused by the chemical attack of hydroxide ions on the interfacial bonds, Equations 5.1 and 5.2, and partly by the pressure built up by trapped hydrogen gas ^[5.2, 5.9], which is evolved. Hence, the electrolyte employed for this study was prepared to favour the production of hydroxide ions, using the ASTM standard G8-98 ^[5.2] as a guide, and was made with 30 g NaCl, 17 g KOH, 2 g NaOH in 1 dm³ of distilled water. The pH of the final solution was measured to be 12.5 ± 0.2.



5.2.4 Test sample preparation

The coatings studied in this chapter, TP-9, TS-5, TS-7 and coating A (Coating A was supplied in two types – one with primer and one without primer) have been characterised in sections 3.3.1, 3.3.2 and 3.3.4 respectively. The test samples were cut into 35 × 35 mm pieces and in accordance with the ASTM standard G8-98. An intentional holiday of 6 mm diameter was drilled in the centre of the test samples through the coating just exposing the substrate. Usually, the holiday simulates a defect in coating; however, for the purpose of this study it represents the impact damage inflicted by inspection tools, see Figure 5.4.

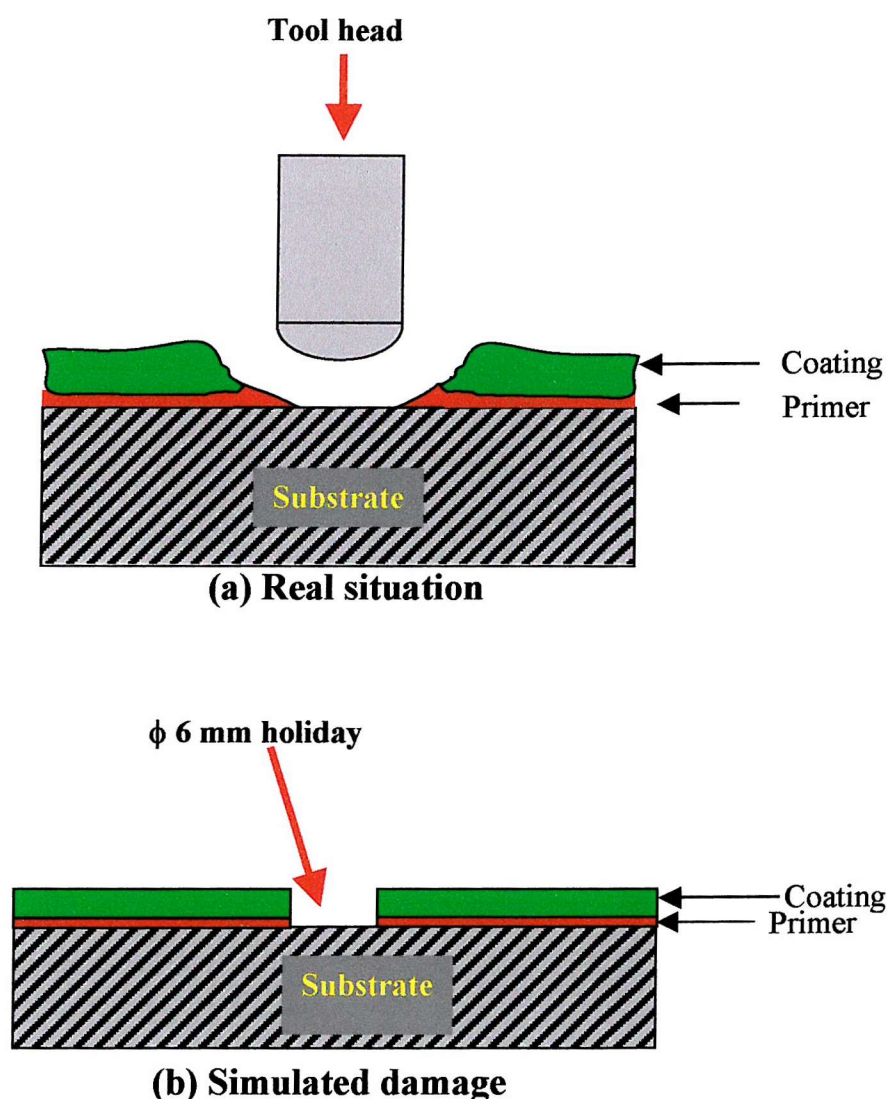


Figure 5.4: Schematic of (a) impact damage and (b) simulated damage caused by a typical downhole tool.

Before testing, the samples were cleaned with a degreasing agent (usually acetone) to remove any surface contamination. Flexible wires of about 20 cm length were solder-welded to the underside of the test panels, which provides electrical connection between the test piece and the potentiostat.

5.2.5 Methodology

The test assembly for the CD test was filled with the alkaline electrolyte, and the test panel polarized to -1.5 V (ASTM recommended) by a three-electrode cell arrangement. The current generated due to cathodic polarization was sampled every second (1 Hz) between the test sample and a platinum counter electrode via a computer controlled potentiostat (Gamry PC4/750). The duration of each test was four days (96 hours),

which is truncated (ASTM recommends 30 – 90 days). The experiment was monitored every five hours for the possibility of changes in environmental factors such as temperature and humidity. The experimental conditions used for the CD tests are detailed in Table 5.1.

Test duration (hrs)	96
Applied polarization voltage (V)	-1.50
Acquisition frequency (Hz)	1
Temperature (°C)	Room
Electrolyte	KOH + NaOH + NaCl
Electrolyte (pH)	12.5 ± 0.2

Table 5.1: Details of the experimental conditions for the cathodic disbondment tests.

The test set-up adopted for the interfacial indentation tests is similar to the one adopted for previous investigations ^[5.5 - 5.7] and a schematic is shown in Figure 5.3. The samples were cut into squares of 15 mm and the transverse section to be indented is cleaned polished before each test. Tests were carried out on the transverse section of the coatings near the coating/primer/substrate interface using a standard pyramidal Vickers indenter, at a normal load of 40 N. The indenter tip was loaded onto the interface, and held for approximately 10 seconds, inducing a lateral crack at either the coating/primer and/or primer/substrate interface(s). The load was held constant for all the samples tested to allow comparisons to be made. The samples were examined in the SEM and the extent of delamination was measured. The procedure was repeated for the two coating thicknesses at least three times. The experimental conditions used for the IIT tests are detailed in Table 5.2.

Duration of hold for each indent (s)	~ 10
Applied load (N)	40
Temperature (°C)	Room, 23 °C
Shape of indenter	Pyramidal

Table 5.2: Details of the experimental conditions for the IIT tests.

5.3 Results and Discussion

5.3.1 Cathodic disbondment (CD) test

The ASTM standard ^[5.2], used as a guideline in this study, recommends a visual examination of disbonded regions, and also the current at the beginning and the end of

each test should be measured. However, in this study the duration of the test was truncated to 4 days and the current was sampled continuously throughout the test duration. This provided an understanding of how early the coatings lose their adhesion. Measurable disbondment was observed after 4 days.

Figure 5.5 shows the results of the cathodic disbondment test in the form of current-time ($I-t$) curves for the two thicknesses of coating TP-9. The current-time trace is a measure of the rate of cathodic reaction occurring at the metallic interface. Thus, it follows that as disbondment increases, more metallic surface is exposed causing an increase in the rate of cathodic reaction, i.e. an increase in exposed metallic surface area leads to increase in the current generated at the cathodic sites. It should be emphasised, however, that the relative positions of the two coatings on the $I-t$ graph (Figure 5.5) do not necessarily represent which is a better coating. The slope of the $I-t$ curves (dI/dt) is thought to relate in part to the rate of disbondment and in part to the changes in localised pH or changes in hydrogen evolution processes. Therefore, it can be implied for the two coating thicknesses that disbondment of the thicker coating (1572 μm) occurs at a higher rate compared to the thinner coating (657 μm). This suggests that the thinner coating is better adhered than the thicker one.

However, the total charge produced should be proportional to the area of disbonded region, since surface conduction is necessary for charge production. Hence, the charge was estimated in accordance with Equation 5.3.

$$Q = I \times t \dots\dots\dots 5.3$$

Where Q , I and t are charge, current and time respectively. The result of the charge density is tabulated in Table 5.3.

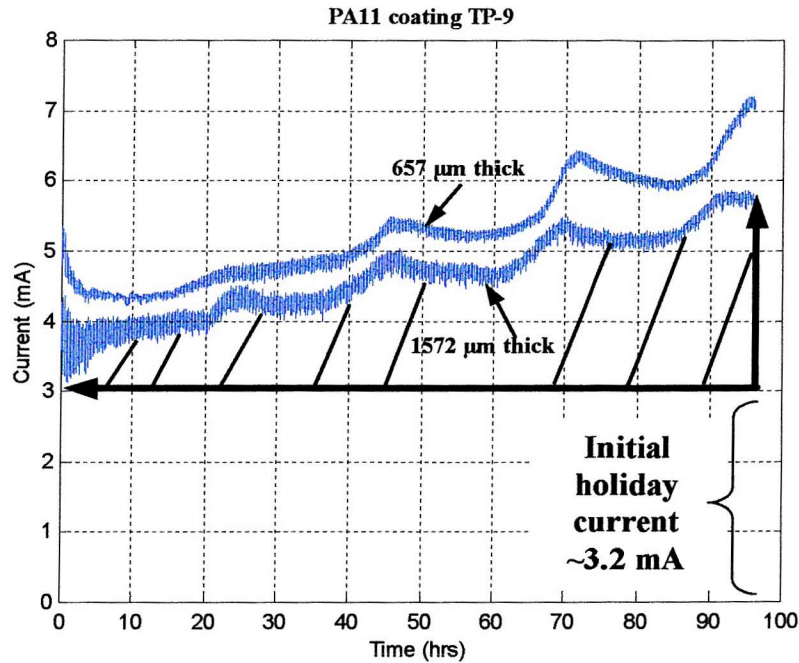


Figure 5.5: Results of the CD test showing the curve of TP-9. The initial holiday current indicated is for 1572 thick coating only and differs for other coatings.

Figures 5.6 and 5.7 are the results of the CD tests for the epoxy coatings, TS-5 and TS-7. Like the TP-9, the thinner coatings generally out-performed the thicker coatings in terms of the current produced due to cathodic reactions. The reason for this is thought to be due to the time it takes for thicker coatings to cool after manufacture. Consequently, some of the heat required to effect adhesion is lost to the atmosphere, resulting in a possible weaker adhesion to the metallic substrate or the primer. In addition, it is thought that residual stresses trapped within the coatings, in particular, the thick coatings, may be another cause of weak adhesion at the interface. This appears to be more pronounced for the TS coatings.

From Figure 5.5 it can be seen that there is a higher degree of standard deviation (noise) in the sampling of the current produced by TP-9 coatings compared to TS-5 and TS-7, see Figures 5.6 and 5.7. Initially, it would appear that this phenomenon could be associated with the coating material possibly due to differences in coating/substrate bond adhesive properties due to the two different coating matrices.

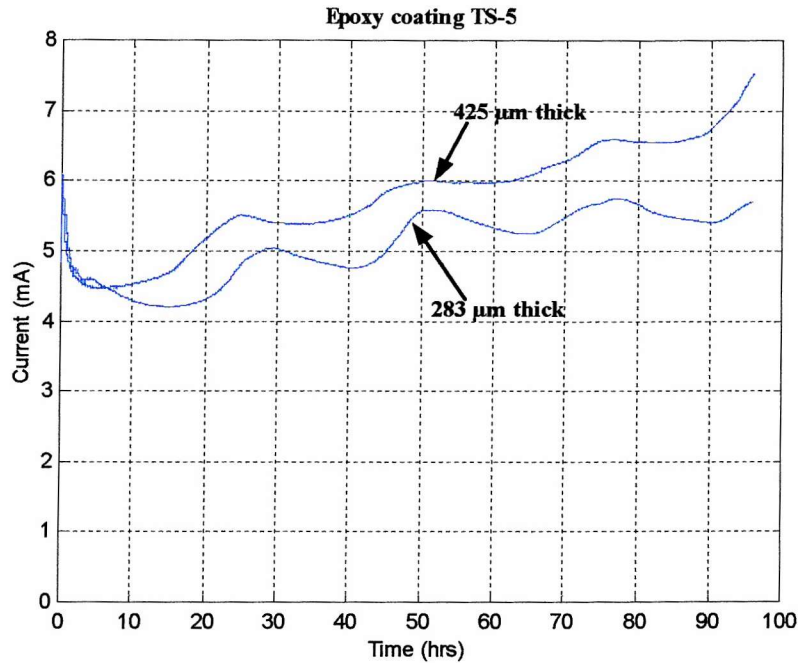


Figure 5.6: Results of the CD test showing the curve of TS-5.

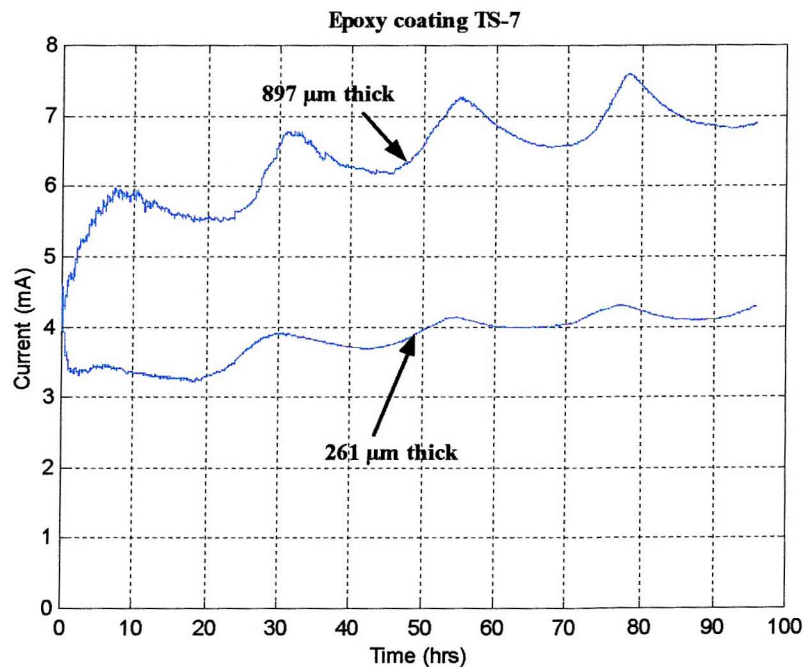


Figure 5.7: Results of the CD test showing the curve of TS-7.

Figure 5.8 is a schematic showing a typical coating transverse section. If the primer is of insufficient thickness to completely cover the substrate asperities, once CD initiates, this may lead to instabilities in disbondment growth rate. Thus, possibly resulting in rapid current fluctuations, due to the random exposure of the asperity tips causing non-linear increase in the exposed metallic area. Delamination could also lead to complexity in the

current measurement, depending whether delamination occurs along the substrate/primer, substrate/coating or the coating/primer interface, or even a combination of the three interfaces.

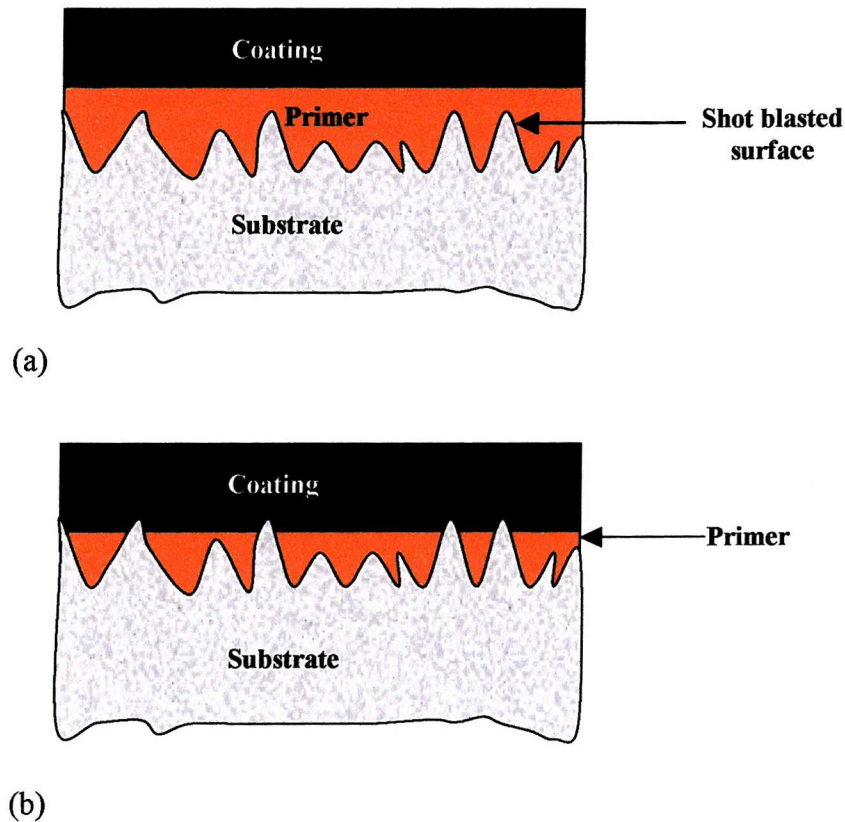


Figure 5.8: Schematic showing the transverse section of a typical coating system (a) TS coatings, (b) TP coatings.

Also apparent from Figures 5.5 – 5.7 are oscillating features on the curves, which appear to be systematically occurring at about 24 hrs intervals. These oscillations were not caused by changes in temperature and/or humidity as these two parameters were constantly monitored throughout the tests and did not change significantly. An initial observation suggests that these oscillations can be linked to vibrations induced by daytime laboratory activities. These vibrations are thought to disturb the hydrogen gas bubbles that clung to the holiday, which influences current magnitudes.

It can be seen from the $I-t$ curves of all coatings, Figures 5.5 – 5.7, that between 0 and 10 hrs, a stabilisation period exists due to surface conditioning. This period is thought to be before delamination initiates and may differ between different coating systems due to

the difficulty in reproducing a uniform holiday size for all the test samples. Some authors^[5,7] have observed a similar phenomenon in their studies.

To quantify the extent of delamination, the charge was estimated by integrating the $I-t$ response after the charge associated with the holiday was removed; this procedure is indicated in Figure 5.5 with the hatched region representing the charge associated with blister growth. It is believed that the total charge relates in part to the extent of disbondment and in part to the change in localised pH or changes in the hydrogen evolution processes. It was observed that both the thick and thin coatings follow the same ranking order in terms of the charge produced, see Table 5.3. The two thicknesses can be ordered, in terms of resistance to disbondment, such that TP-9 > TS-5 > TS-7.

	TP-9 (Thick)	TP-9 (Thin)	TS-5 (Thick)	TS-5 (Thin)	TS-7 (Thick)	TS-7 (Thin)
Charge (Coulomb)	406	266	457	277	515	311

Table 5.3: *The total charge produced during disbondment test (mean value of two tests).*

For direct comparison the extent of delamination was also measured from the SEM micrographs of the transverse sections, see Figures 5.9 - 5.11. For all TS coatings delamination primarily occurred at the primer/substrate interface, while for the TP, delamination occurred at both the coating/primer and primer/substrate interfaces. From Figure 5.9 bifurcation of the delamination is seen for TP, which was not so apparent for the TS coatings, Figures 5.10 and 5.11. Table 5.4 shows the measured delamination length (taken to equal the blister radius). It is apparent that the measured radius for the thicker coatings is higher than that of the thinner coatings and this is consistent with the charge measurement for the three coating systems, see Table 5.3.

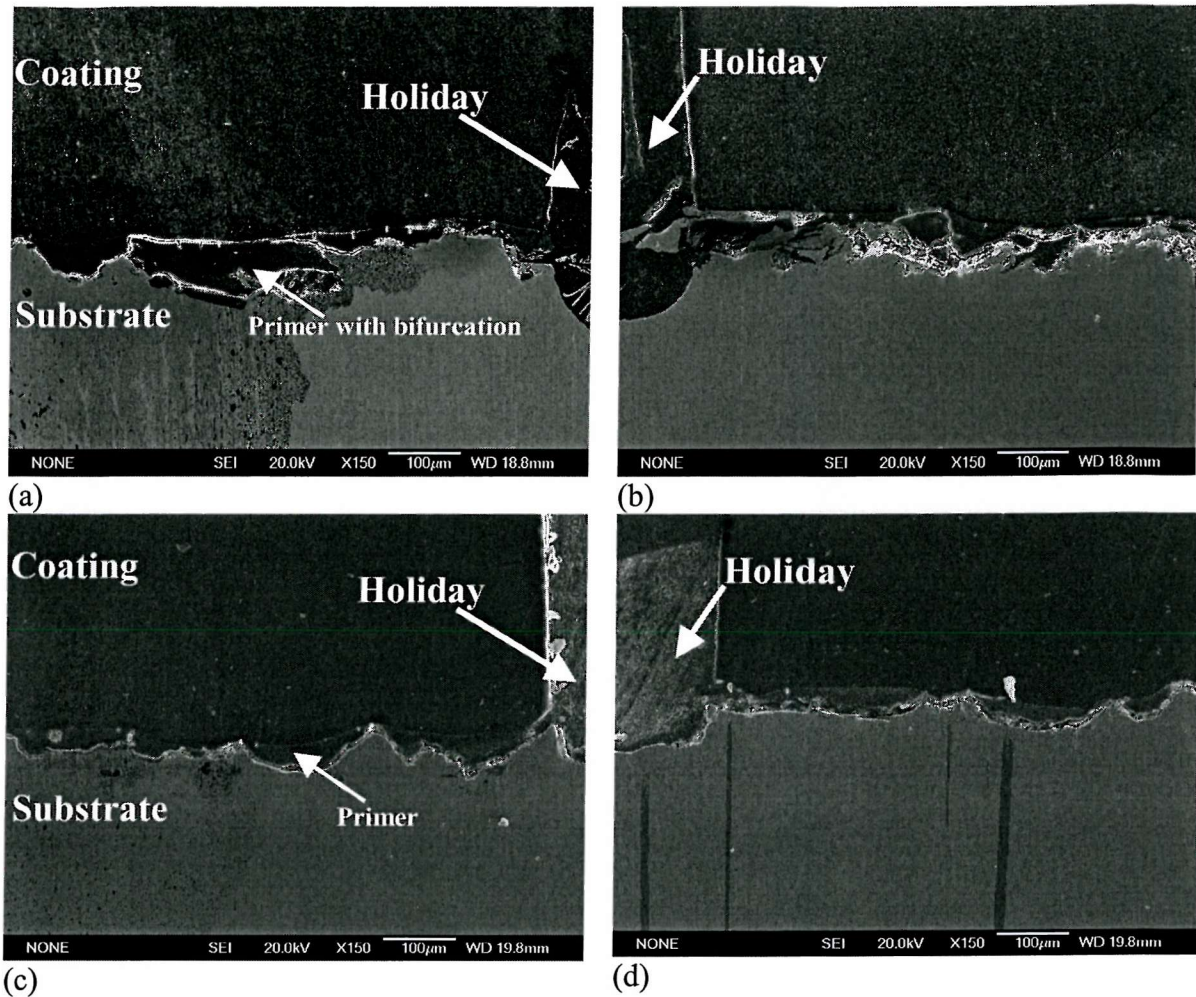
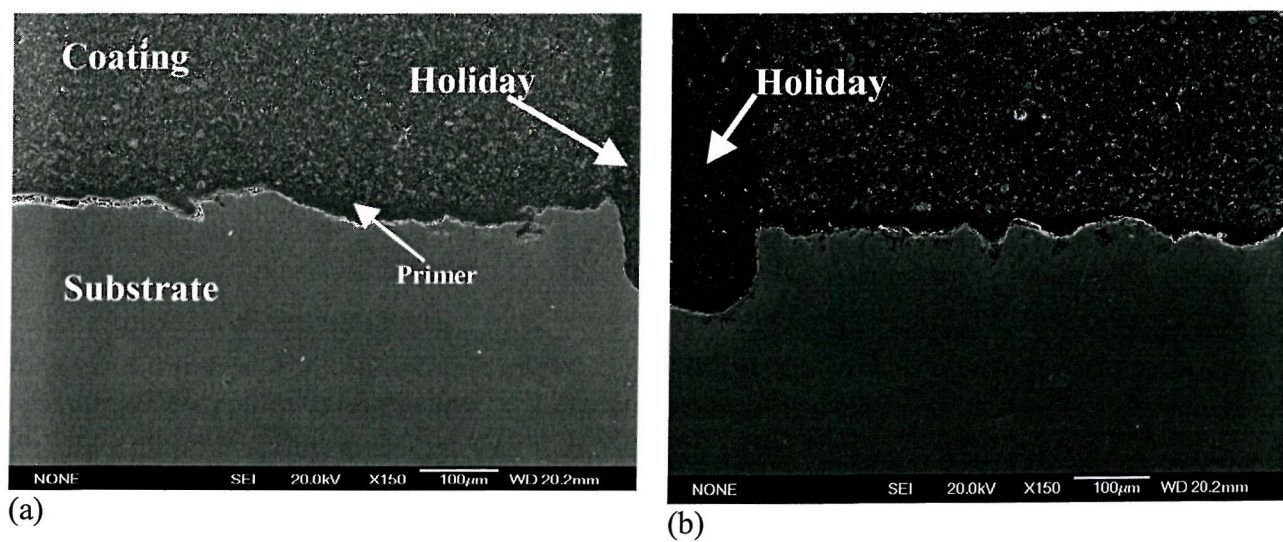


Figure 5.9: SEM images of the cathodic disbondment test samples for TP-9 (a) and (b) are the thin coatings while (c) and (d) are the thick coatings.



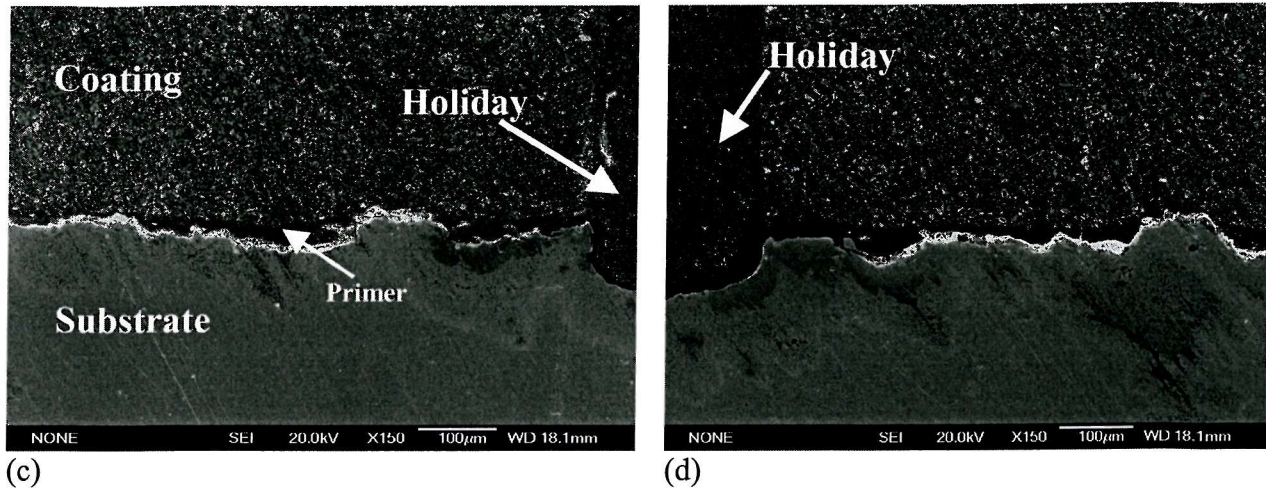


Figure 5.10: SEM images of the cathodic disbondment test samples for TS-5 (a) and (b) are the thin coatings while (c) and (d) are the thick coatings.

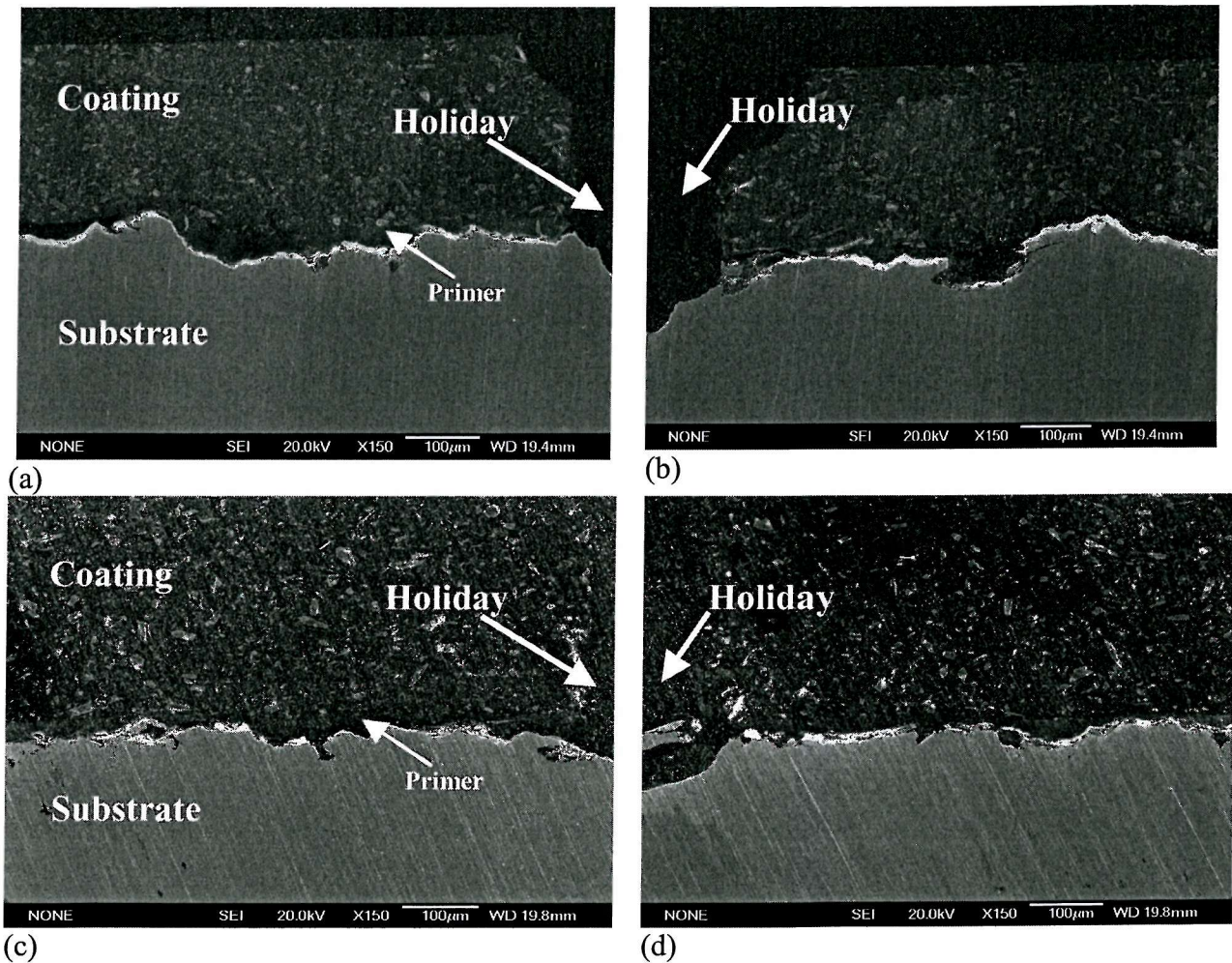


Figure 5.11: SEM images of the cathodic disbondment test samples for TS-7 (a) and (b) are the thin coatings while (c) and (d) are the thick coatings.

	TP-9 (Thick)	TP-9 (Thin)	TS-5 (Thick)	TS-5 (Thin)	TS-7 (Thick)	TS-7 (Thin)
Radius (μm)	1327	1034	1687	1082	1823	1530
Approximate Area (mm^2)	5.53	3.36	8.95	3.68	10.44	7.36

Table 5.4: The radius and approximate area of the disbonded region (mean value of two tests).

In addition, it can be seen from Table 5.4 that the two coating thicknesses agrees with the same ranking order as the charge produced, i.e. TP-9 > TS-5 > TS-7 in terms of resistance to disbondment, see Table 5.3. Figures 5.12 and 5.13 further support this correlation, where the charge is plotted against the radius of delamination for the two coating systems: thermoplastics and thermosets. Comparing the two figures shows that TS form larger blisters and have a different slope.

TP Coatings

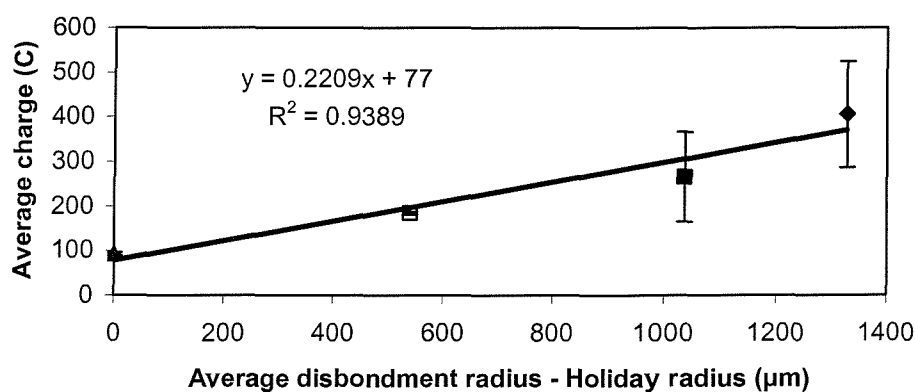


Figure 5.12: Graph showing correlation between charge and radius of disbondment for TP coatings. The difference between the average disbondment radius and the holiday radius represents how much a coating has delaminated from its substrate.

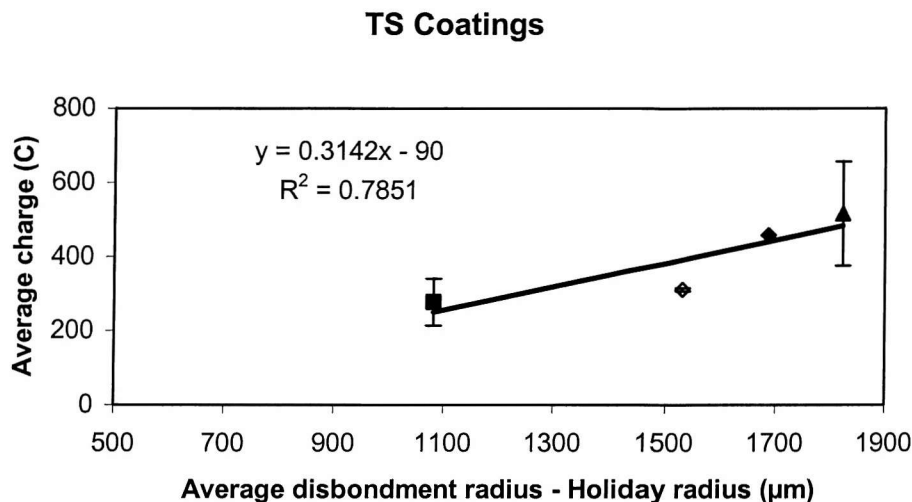


Figure 5.13: Graph showing correlation between charge and radius of disbondment for TS coatings.

Generally, cathodic disbondment has been modelled by two mechanisms:

1. Chemical attack. ^[5.8]

When coatings are deposited onto their substrate and subsequently cured, atomic scale chemical and physical bonds are established between the coating and the steel substrate via a thin layer of metallic oxide on the surface of the steel. The ingress of the hydroxyl ions then initiates chemical attack of the interfacial bonds ^[5.8], which can be modelled like a spring ^[5.9] as shown in Figure 5.14. Chemical attack ruptures the bonds and causes the eventual delamination of the coating from the substrate.

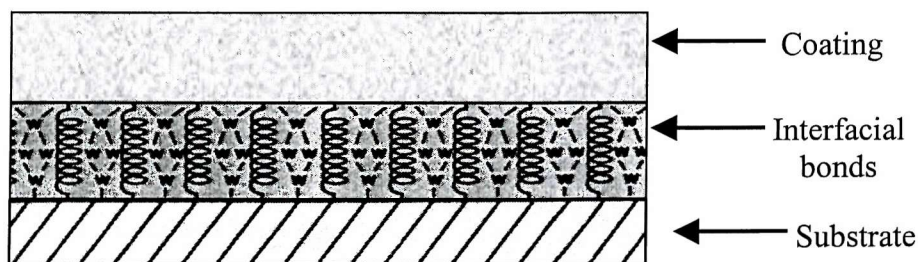


Figure 5.14: A model showing the interfacial bond between coating and its substrate ^[5.9]. W represents atomic interaction of bonds.

2. Mechanical processes.

A mechanical action due to the trapped hydrogen gas at or near the interface. The process of cathodic disbondment is characterised by the production of large volumes of hydrogen gas, see Equation. 5.1. Some of the gas escapes to the atmosphere while some remains trapped at the interface within the disbondment. Over time, the

accumulation of the hydrogen gas builds up pressure at the interface(s) leading to mechanical debonding, see Figure 5.15.

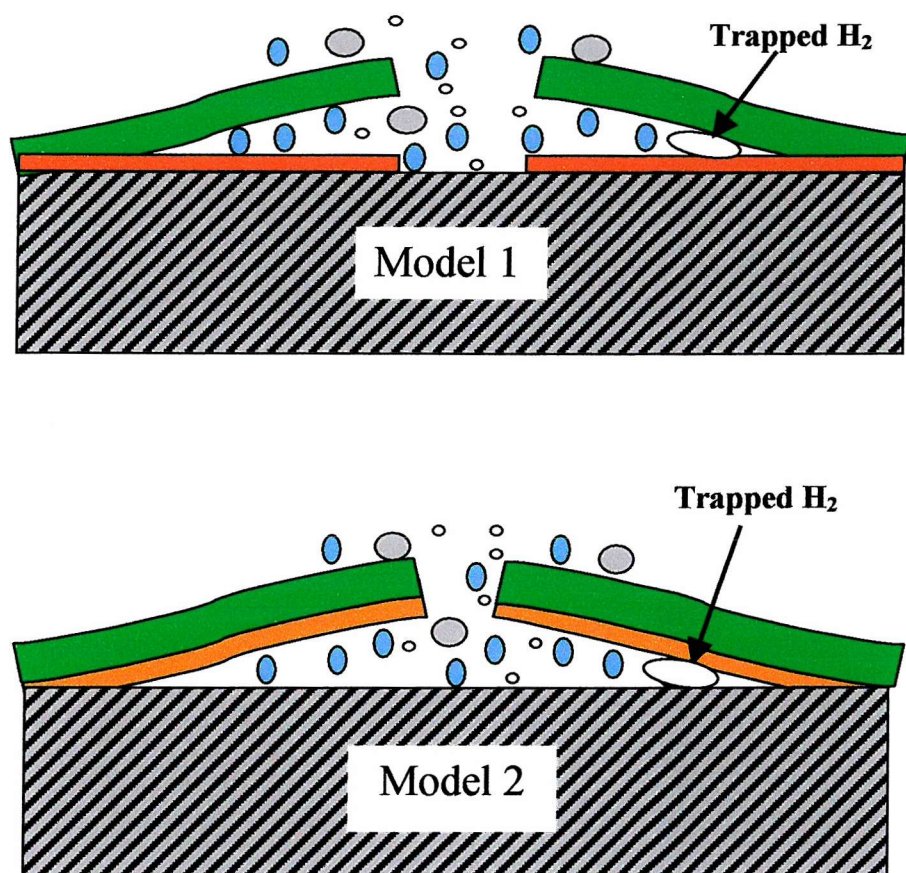





Figure 5.15: Schematic models showing mechanical action of debonding caused by trapped hydrogen gas. (1) Delamination occurring at coating/primer interface; (2) Delamination occurring at primer/substrate interface.

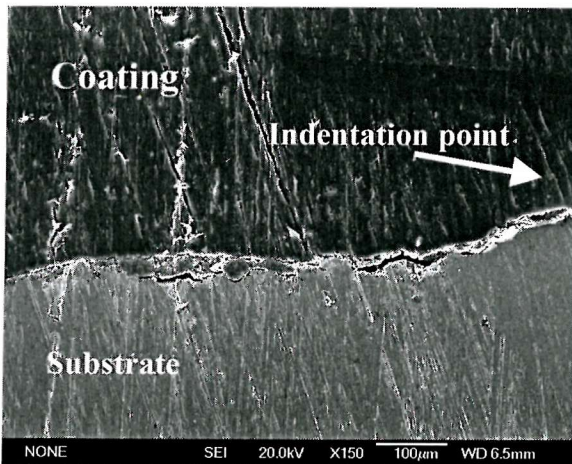
Key

-  Hydrogen gas
-  Hydroxyl ion
-  Water molecule

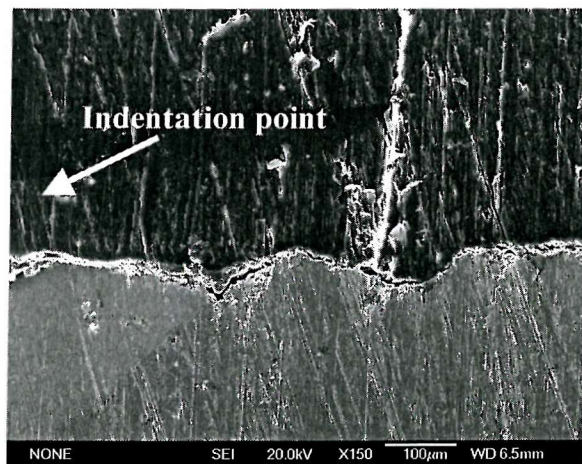
5.3.2 Interface indentation test (IIT)

Usually, the IIT provides a relationship between the applied load and the length of crack created at the interface between the coating and the primer and/or the primer and the substrate. In analysing the results of an IIT [5.3 – 5.6] the load that initiates the crack is usually estimated. However, in this work, since the primary aim is to investigate the mechanism of delamination in order to draw a comparison in the performance of the coatings between the CD test and IIT, the load was kept constant at 40 N.

Figures 5.1 to 5.18 show the transverse sections of the coatings samples after the IIT. Usually, delamination results from the inability of the coating/primer and/or primer/substrate interface(s) to successfully accommodate the tension induced by the indenter geometry. When the indenter is loaded onto the interface, a certain amount of energy is transferred to the interfacial bonds by the load. When this energy exceeds the strength of the bonds or the force of molecular attraction at the interface, the bonds rupture and delamination occurs; this is seen for all the coatings tested in this study. Table 5.5 shows the measured extent of delamination for all the coating systems.



(a)



(b)

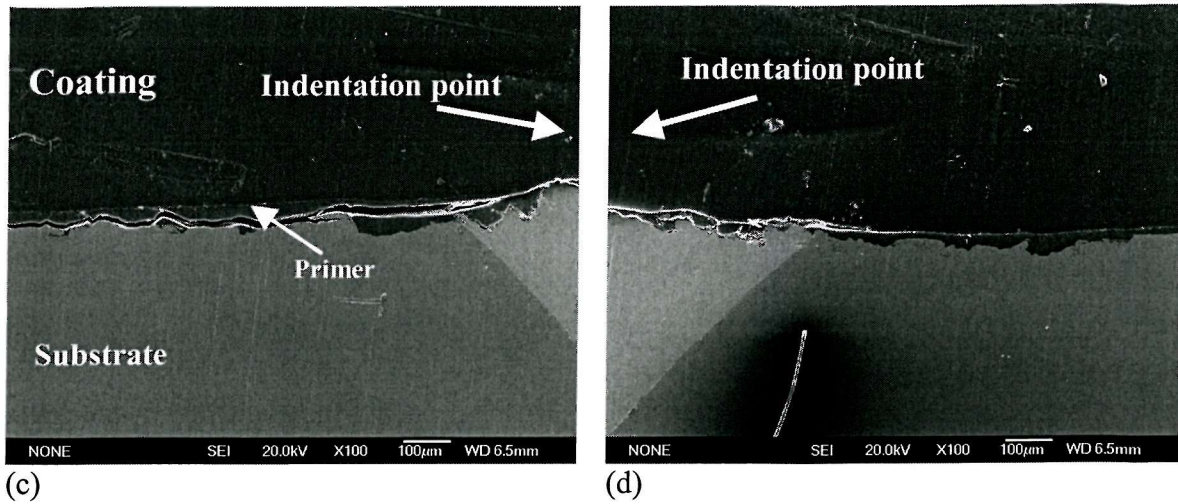


Figure 5.16: SEM images of the mechanical delamination test samples for TP-9 (a) and (b) are the thick coatings while (c) and (d) are the thin coatings.

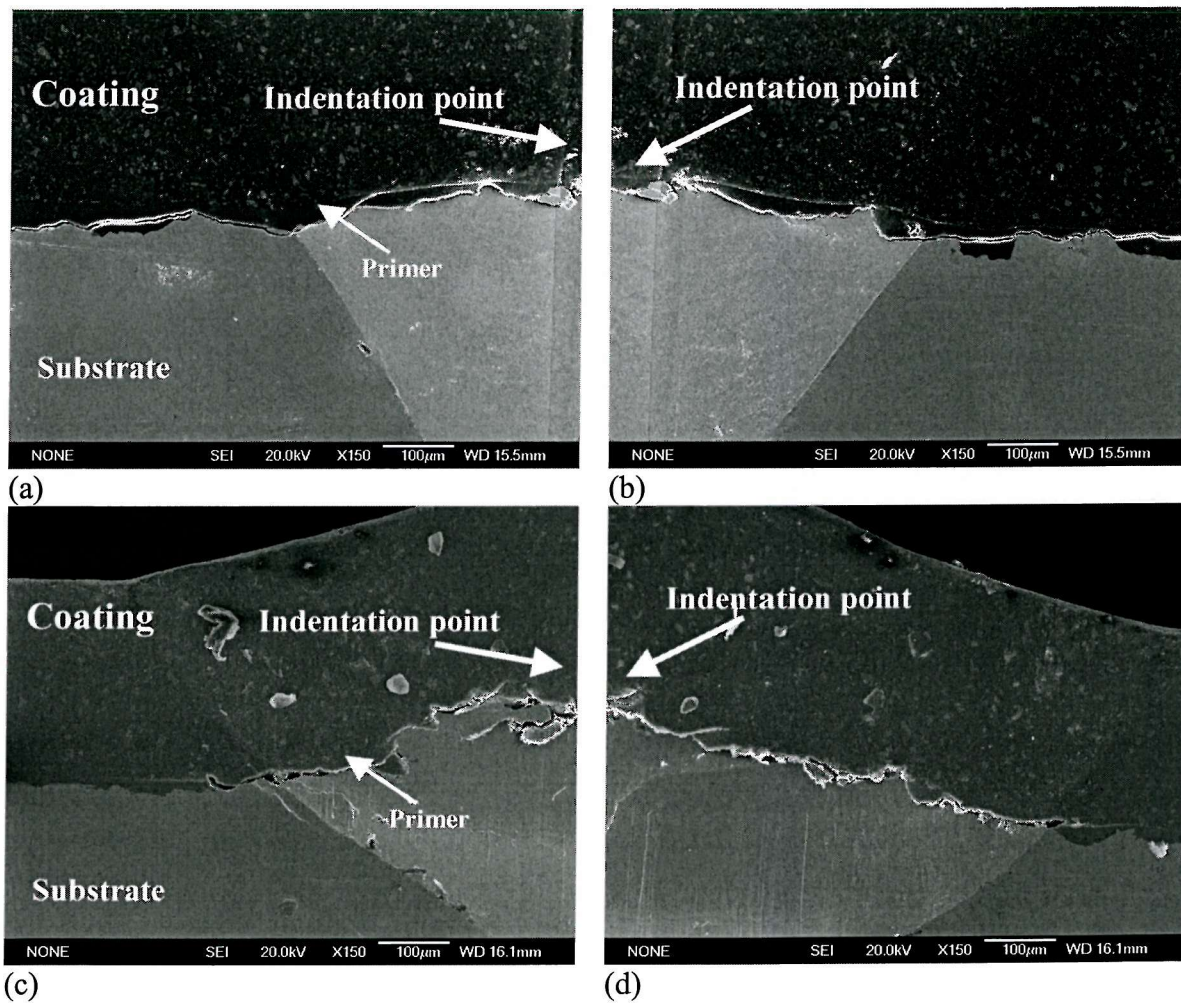


Figure 5.17: SEM images of the interfacial indentation test samples for TS-5 (a) and (b) are the thick coatings while (c) and (d) are the thin coatings.

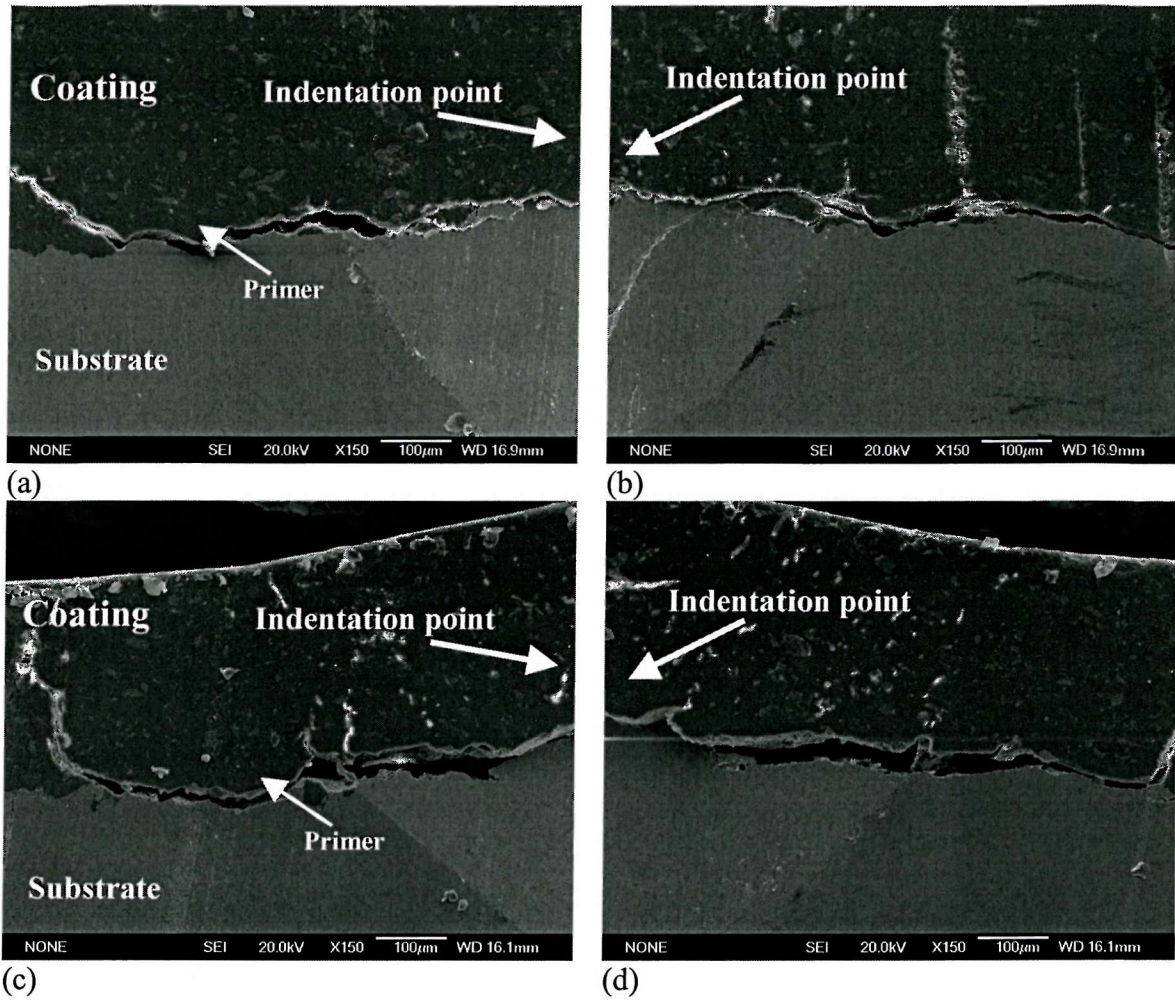


Figure 5.18: SEM images of the interfacial indentation test samples for TS-7 (a) and (b) are the thick coatings while (c) and (d) are the thin coatings.

	TP-9 (Thick)	TP-9 (Thin)	TS-5 (Thick)	TS-5 (Thin)	TS-7 (Thick)	TS-7 (Thin)
IIT length of delamination (μm)	2309	2502	2399	1928	2293	2146

Table 5.5: Measured extent of delamination (mean value) for the interfacial indentation test.

The results suggest that TS-5 has the lowest adhesion strength among the thicker coatings with TS-7 having the highest. This is in agreement with the CD resistance ranking in Table 5.3, i.e. TS-7 > TP-9 > TS-5. Likewise, from Table 5.3 and 5.4, TP-9 and TS-5 appear to be the worst and the best of the thin coating systems respectively, and can be ordered, in terms of resistance to delamination, such that TS-5 > TS-7 > TP-

9. For all coating systems studied under the IIT delamination predominantly occurred at the primer/substrate interface.

It was observed during the indentation tests that the surface roughness of the carbon steel substrate appears to have significant effect on the delamination path of the coatings, similar to that found in the CD tests. Inadequate control of the surface roughness during coating application seems to leave the shot-blasted surface with sharp uneven asperity peaks, which act as stress raisers and crack initiators. The sharp peaks cause the delamination path to deviate through the primer, see Figures 5.16 to 5.18. Tricard ^[5,10] has observed that sub-surface residual stresses induced by grit blasting of substrate are compressive in nature and could be detrimental to the adhesion of a coating to its substrate. The tendency is for the compressive stress to cause 'buckling' near or within the sub-surface layer, thus encouraging coating delamination.

In general, the surface preparation applied to the carbon steel substrates has made the analysis of the results of TP-9, TS-5 and TS-7 more complicated and this has to be better controlled. Consequently, a new coating, designated coating A, was developed with more careful control of the substrate surface roughness. The results of the CD test and the IIT performed on coating A are discussed below.

5.3.3 PA11 Coating A

The deposition process and coating details have been described in section 3.3.4. Two variants of the coating: with primer and without primer were deposited, in order to investigate the role of primer in the adhesion of polymeric coatings. As with TP-9, TS-5 and TS-7 coatings, cathodic disbondment and interface indentation tests were conducted using the same methodology as outlined in section 5.2.4.

Figures 5.19 and 5.20 show the CD data for coating A, with and without primer, respectively. The role of the primer in the adhesion of the coating can be seen in the difference between the two figures. No significant disbondment was observed for the coating with primer while the coating without primer show a reasonable amount of delamination; the slope of the curve for the coating with primer did not change, Figure 5.19, while the slope of the coating without primer show appreciable change with time, Figure 5.20. In contrast to TP-9, TS-5 and TS-7, the tests show a good repeatability with

fewer systematic oscillations, which suggest that the oscillations may also be coating dependent.

Table 5.6 details the amount of charge produced and the approximated area of disbondment from the two tests. It can be seen that the coating with primer produced no measurable radius of disbondment, which confirm that no significant disbondment occurred. In contrast to the coating with primer, a measured radius of disbondment for the coating without primer matches the change in slope. This confirms that a layer of primer is essential to facilitate the adhesion of coatings to their substrates.

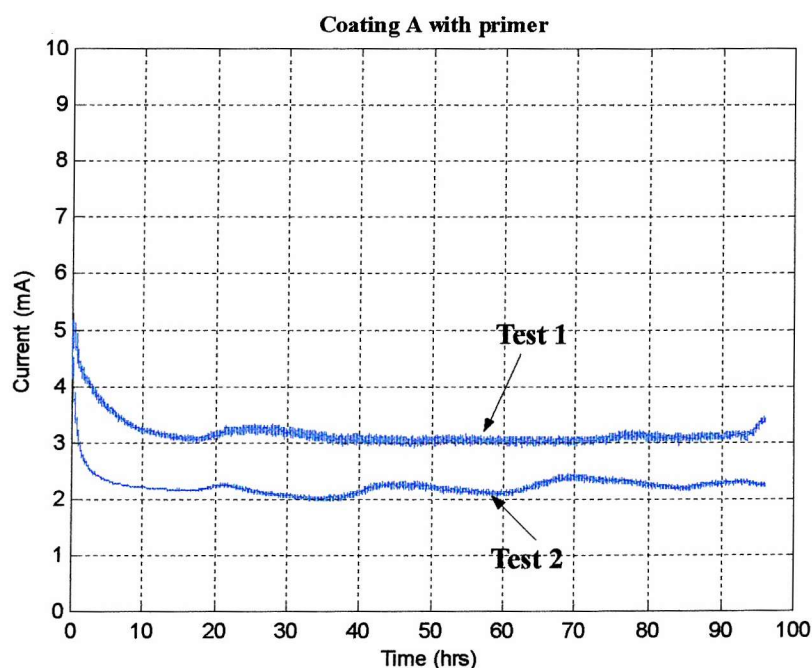


Figure 5.19: Cathodic disbondment test for coating A with primer.

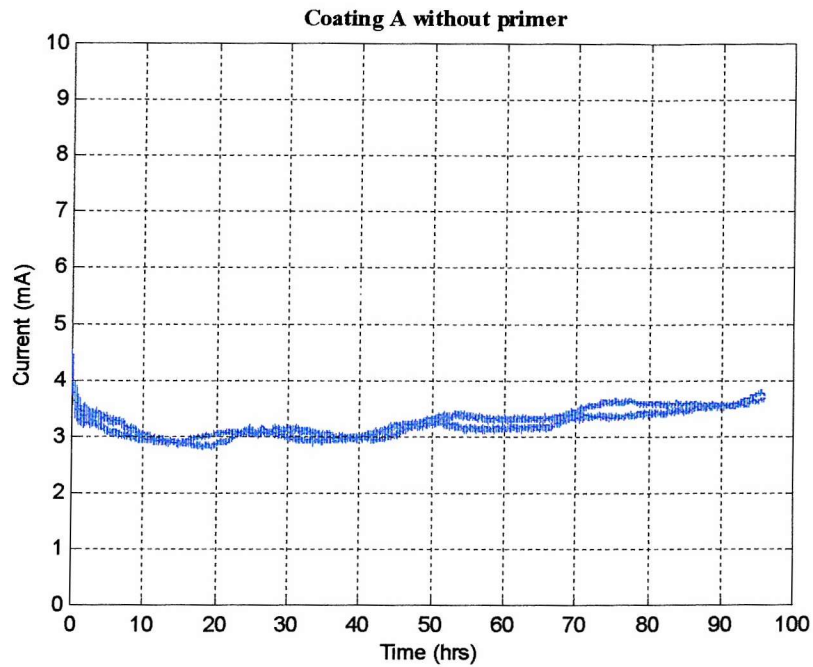


Figure 5.20: Cathodic disbondment test for coating A without primer.

	Coating A With primer (1)	Coating A With primer (2)	Coating A Without primer (1)	Coating A Without primer (2)
Charge (Coulomb)	96	90	187	182
Radius (μm)	0	0	539	541
Approximate Area (mm^2)	0	0	0.91	0.91

Table 5.6: Measured data (mean value of two tests) for the charge produced from the test on coating A.

The SEM of the transverse section of the tested samples is shown in Figure 5.21. There is no evidence of disbondment at either the coating/primer or the primer/substrate interfaces for the sample with primer, Figure 5.21 (a), which is consistent with Figure 5.19.

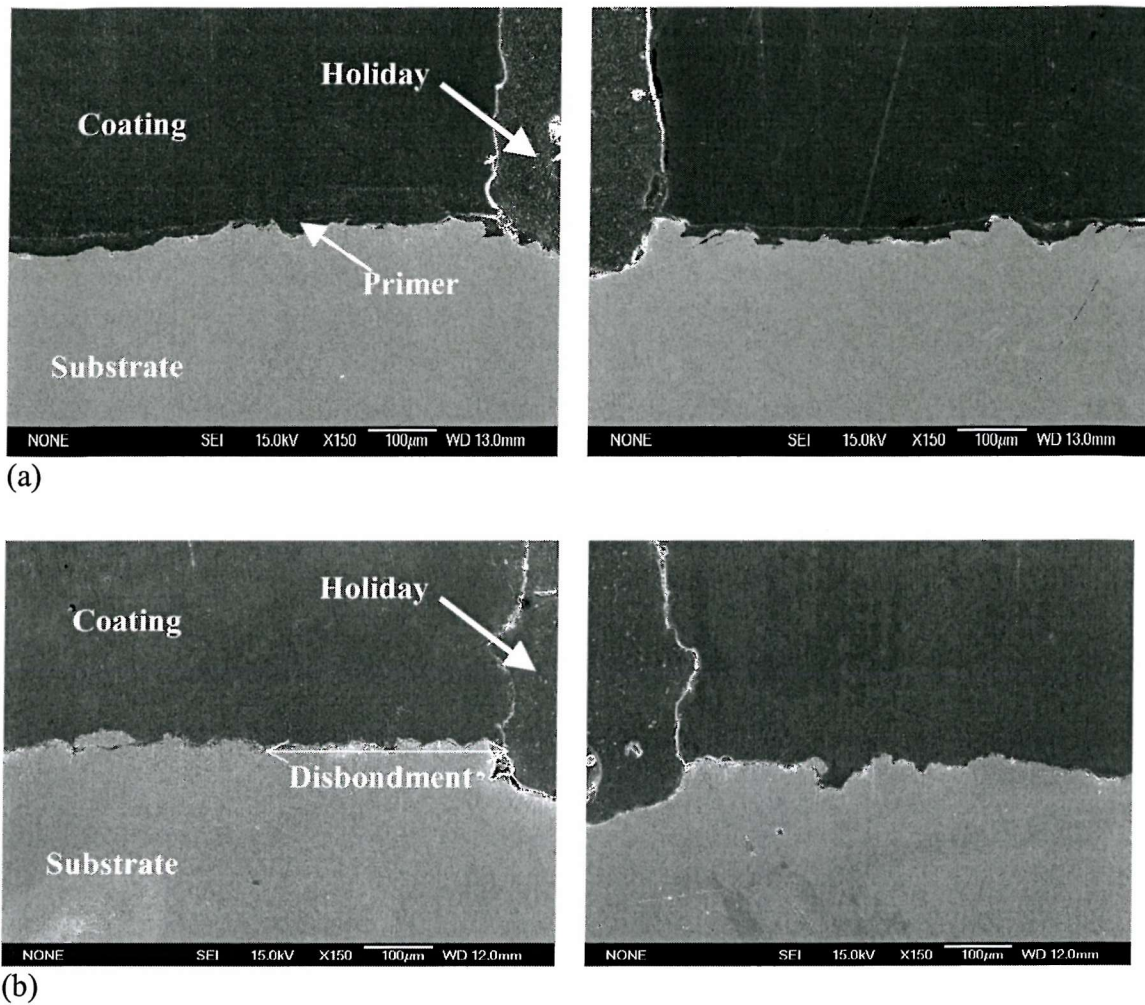


Figure 5.21: SEM micrographs of the transverse section of the tested CD samples; (a) is with primer and (b) is without primer.

One of the reasons for the better result shown by coating A over TP-9, TS-5 and TS-7 can be linked to the deposition process. Significantly, the substrate preparation i.e. the shot blasting appears to have improved as evident in Figure 5.21. The primer, Figure 5.21 (a), covers the substrate evenly with less asperity peaks from the shot blasting protruding above the primer. This is probably the reason why coating A demonstrated a better performance compared to TP-9.

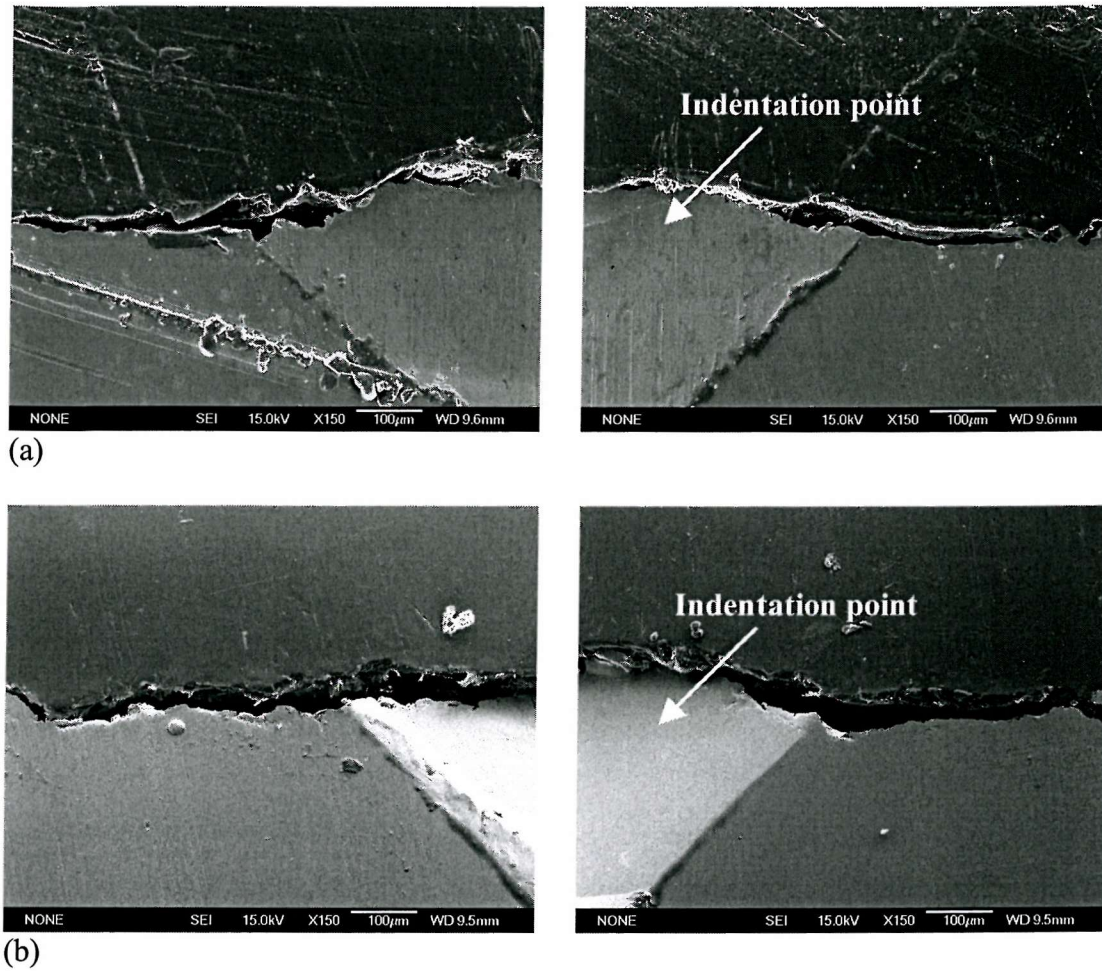


Figure 5.22: SEM micrographs of the transverse section of the tested IIT samples; (a) is with primer and (b) is without primer.

Figure 5.22 show that the delamination for the coating with the primer occurs at the primer/substrate interface for the IIT performed on coating A. The size of the delaminated area is smaller for the coating A with primer compared with that of coating A without primer, see Table 5.7. An appreciable agreement can also be seen between the CD and the IIT data in Tables 5.6 and 5.7 respectively.

	Coating A With Primer (1)	Coating A With Primer (2)	Coating A Without primer (1)	Coating A Without primer (2)
IIT length of delamination (μm)	1855	1905	2027	2195

Table 5.7: Measured extent of delamination for the interfacial indentation test.

5.3.4 Summary

In all, the thermoplastic-based coatings appear to perform better than the thermoset counterparts, particularly in the cathodic disbondment test; there seems little difference between the two coating systems in the interface indentation test. Figure 5.23 is a plot of the CD radius of delamination against the IIT length of delamination. Figure 5.23 suggests that there is no direct correlation between the two data. Possible reasons for this are:

- (1) The IIT is mechanically based and the test conditions may have been too aggressive for the relatively sensitive polymer coatings. It is well known that polymers combine properties such as ductility and plasticity; hence, there may have been some relaxation when the load is removed after indentation, thereby introducing a slight complication in the outcome of the test result. Also, the IIT is normally used for studying the adhesion of metallic coatings ^[5.4 – 5.6, 5.10]. This shows that the CD is more effective in studying the adhesion of polymeric coatings, which suggests that TP coatings are more suitable for downhole application compared to other coating types.

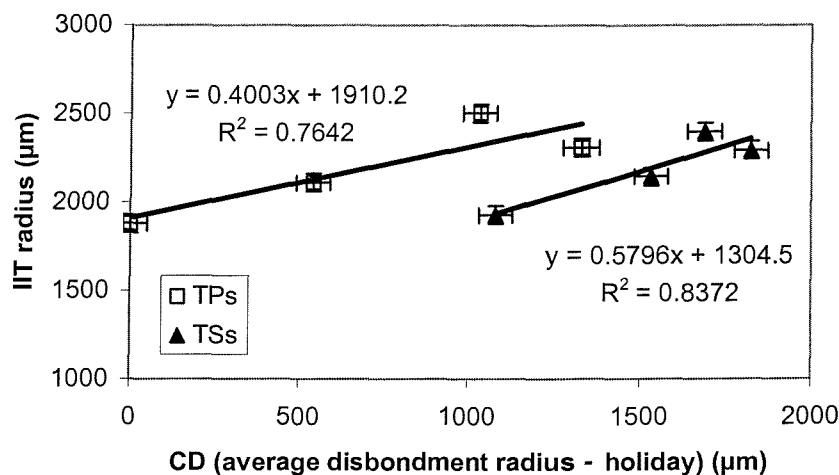


Figure 5.23: Correlation between the IIT and CD test methods.

- (2) The cathodic disbondment test combines chemical and mechanical mode of delamination, i.e. the attack of the interfacial bonds by hydroxyl ions and pressure build up at the interface by trapped hydrogen gas causing mechanical debonding.

(3) It is thought that the sensitivity of each coating system, TP or TS to inherent residual stresses will differ; hence the behaviour of the trapped stresses, in TP or TS, to chemical and mechanical attack may affect their mode of delamination.

Table 5.8 is a summary of all the coatings studied with results of each coating system. The data were derived by measuring the length of delamination that corresponds to each region i.e. coating primer (CP), primer substrate (PS) or coating substrate (CS). The relative percentage of each disbonded region was determined by dividing the length of each disbonded region by the total length of disbondment for individual coating system.

It can be seen that TP-9 thick, which has the highest thickness of all the coatings studied, is the most inconsistent regarding the delamination path in both tests. This suggests that increasing coating thickness is detrimental to its performance. For all the coatings, the failure mode was adhesive; no cohesive failure mode (failure that occur within the coating, mostly controlled by the cohesive strength of the coating) was observed for any of the coatings. A summary of ranking for the coatings is detailed in Table 5.9.

	Cathodic disbondment (CD) test			Interfacial indentation test (IIT)		
	CD radius (R-hr)	Region of Disbondment	Relative %	IIT radius	Region of Disbondment	Relative %
TP-9 thick	1327	CP/PS	38% CP	2309	CP/PS	28% CP
TP-9 thin	1034	CP/PS	15% CP	2502	PS	100% PS
TS-5 thick	1687	CP/PS	13% CP	2399	PS	100% PS
TS-5 thin	1082	PS	100% PS	1928	PS	100% PS
TS-7 thick	1823	PS	100% PS	2293	PS	100% PS
TS-7 thin	1530	PS	100% PS	2146	PS	100% PS
TPWP	0	None	N/A	1880	PS	100% PS
TPWOP	540	CS	100% CS	2111	CS	100% CS

Table 5.8: Summary of the coatings studied with the results. CP=Coating Primer; PS=Primer Substrate and CS=Coating Substrate. TPWP means Thermoplastic with primer and TPWOP means Thermoplastic without primer (coating A).

	TP-9 (Thick)	TP-9 (Thin)	TS-5 (Thick)	TS-5 (Thin)	TS-7 (Thick)	TS-7 (Thin)	TPWP	TPWOP
CD Test ranking based on charge	6	3	7	4	8	5	1	2
Indentation Test ranking	6	8	7	2	5	3	1	4
Overall ranking	6	5	8	2=	7	4	1	2=

Table 5.9: Summary of ranking for the coatings studied. 1 is given to the best performance and the least performance is assigned 6.

Xu ^[5.12] has investigated the impact failure of similar coatings using a falling tup impact energy method. Efforts were made to compare the present results with those obtained by Xu but no direct correlation was found. In particular, this work has ranked the coatings by quantifying the resistance of the coatings to disbondment but the work of Xu primarily focused on the qualitative analysis of the response of the coatings to impact; no specific ranking was assigned to the coatings. Hence, it was difficult to draw a direct comparison between the results in this work and that of Xu ^[5.12].

It must be emphasised that comparisons between the thermoplastic and thermoset coatings investigated in this study have been largely limited because of the difference in the coating systems (thermoplastic and thermoset). This is due to the limitations imposed by the lack of control over the deposition of the coatings, which are mainly commercial.

5.4 Conclusions

1. The adhesive properties under truncated cathodic disbondment tests and interface indentation tests of various commercially available polymeric coatings have been investigated. Two thermoplastic and two thermosetting coatings systems have been studied
2. The truncated version of ASTM G8-98 has been shown to be effective in evaluating the adhesive properties of polymeric coatings.
3. Under CD, the extent of disbondment for the coatings, quantified by the total charge and physical measurement, is $TP-9 > TS-5 > TS-7$ and is thought to be driven by the bond degradation due to hydroxyl ion attack.
4. The CD test and IIT for coating TP-9 resulted in disbondment at the coating/primer interface as well as the primer/substrate interface due to deviation of crack paths, induced by large asperities penetrating the primer, a consequence of poor surface pre-treatment.
5. Under IIT conditions, the coatings show good agreement with the CD tests in terms of ranking order i.e. $TP-9 > TS-5 > TS-7$.
6. Delamination under the IIT predominantly occurred at the coating/primer interface for all the coatings and at the coating/substrate for coating A without primer.
7. A combination of chemical and mechanical mode of delamination has been identified as the governing mechanism for the CD test.
8. Surface preparation of the carbon steel substrate before coating is deposited will influence the adhesive properties of polymer coatings – inadequate control of the shot blasting procedures complicated the analysis of the results.
9. It has been shown that a primer is essential to facilitate the adhesion of polymeric coating to their substrates.
10. Manufacturing residual stresses trapped within coatings may influence the adhesion of polymeric coatings to their substrates.
11. All the thermoplastic coatings out-performed the thermosets in the cathodic disbondment test due to superior resistance to chemical attack of the bonds at both coating/primer and primer/substrate interfaces.
12. The adhesions of the thick coatings are generally worse than the thin coatings.
13. The IIT test method is recommended for studying the adhesion of coatings at lower loads.

References

- 5.1 Wood R. J. K., Symonds, N, and Wheeler, D. W., Erosion, Wireline Abrasion and Impact resistance of Coatings for Downhole tubulars, Mechanical Engineering Consultancy Service Report number 98/EC211, University of Southampton, 1998.
- 5.2 Bello, J. O. Wharton, J. A. and Wood R.J.K., Evaluation of the adhesive properties of downhole corrosion resistant polymeric coatings determined by cathodic disbondment, Corrosion 2003, San Diego, NACE paper number 03604.
- 5.3 ASTM G8 – 98, Standard Test Methods for Cathodic Disbondment of Pipeline Coatings, 1998.
- 5.4 Higgins, G. L. Cable, P. J. and Parsons, L., Aspect of Cathodic Disbondment Testing at Evaluated Temperature, *Industrial Corrosion*, 5 (1987) 12.
- 5.5 Demarecaux P. Lesage, J and Chicot, D., An examination of the validity of the interfacial indentation test – application to thermal sprayed coating *Vide* 272 (1994) 524 – 527.
- 5.6 Demarecaux P, Chicot D and Lesage J., Interfacial indentation test for determination of adhesive properties of thermal sprayed coatings, *J mater Sci. Lett.* 15 (16) (1996) 1377 –1380.
- 5.7 Chicot D, Demarecaux P and Lesage J., Apparent interface toughness of substrate and coating couples from indentation tests *Thin Solid Films* 283 (1-2) (1996) 151 – 157.
- 5.8 Kamalanand, N. Gopalakrishnan, G. Ponnambalam, S. G. Mathiyarasu, J. Natarajan, R. N. Subramaniam, P. Palaniswamy, N and Rengaswamy, N. S. Role of hydrogen and hydroxyl ion in cathodic disbondment. *Anti Corrosion Methods and Materials*, 45 (4) (1998) 243 – 247.
- 5.9 Jonathan, W. Martin, Edward Embree and Wynee Tsao. Non-osmotic, Defect-Controlled Cathodic Disbondment of a coating from a steel substrate. *Journal of Coating Technology* 62 (790) (1990) 25 - 33.
- 5.10 Tricard, M., Residual Effect of Finishing Methods, in ASM Handbook, ASM International, Materials Park, Ohio, USA 1994, 145.
- 5.11 Lesage J, Demarecaux P, Bartier O. Interface indentation test to determine adhesion of coatings. *Rev. Metall-Paris* 90 (12) (1993) 1655 – 1663.
- 5.12 Xu, Y. Wear and impact of polymeric coatings for downhole application, PhD thesis, School of Engineering Science, University of Southampton, 2003.

6.0 Wireline wear of commercially available polymeric coatings

6.1 Introduction

In chapter four, it was concluded that the pin-on-disc wear rig requires further modifications. In line with the conclusions, the frame was replaced by the present author with a more rigid one. The loading system and the sample pin holder assembly were redesigned to provide a means of direct loading, and also to reduce vibration and minimise edge loading. The original electric motor was replaced with a higher torque motor to provide a wider range of disc rotating speed/load combination. In addition, the location of the slickline wire on the disc and the joining of the wire into a loop were redesigned as part of the overall improvement on the rig. The assembly drawing of the redesigned rig is presented in Appendix 2.

A pre-test study showed that the rig has improved generally. Less edge loading was observed, which is a consequence of a more rigid rig. The wear rig used has been modified for tribo-couple type wireline wear tests.

The overview and initial study presented in chapter four also show that there is need for new coatings to be designed, as the performance of the coatings inherited from N. Symonds fall short of the desired result. As a result, six new coatings were ordered from Tuboscope, SOLVAY and Fluorocarbon Company. The coatings have been characterised in chapter three. Note that the dual layer coating is not included in this study.

Hence, this chapter presents results of the wireline wear study performed on six commercial polymeric coatings: TP-9, TS-5, TS-7, TSX-4, Fluorocarbon and PVDF (see Table 3.7 for details of the coatings), undertaken in order to rank and select the coating(s) for further investigation. This chapter will focus on the wear rates, the wear mechanisms, and the relationship between the two, if any. The mechanisms of action of the fillers in the coatings will also be explored.

6.2 Experimental details

6.2.1 Methodology

The apparatus employed was a pin-on-wire (POW), which utilizes a modified pin-on-disc rig. The modification of the rig has been outline and detailed previously in section 6.1 and Appendix 1. A true tribo-couple was used consisting of “slickline” wire embedded in an aluminium disc to form a circular loop of radius 80 mm. The slickline wire was identical to that used to lower inspection tools into the downhole tubulars.

The disc-wire arrangement was mounted on a pin-on-disc machine as shown in Figure 6.1. The sample pin was secured in the holder and then loaded against the rotating wire. A water pump supplied lubrication at the rate of $16 \text{ cm}^3/\text{sec}$. The experimental conditions employed in this study are tabulated in Table 6.1. The guidelines for the selection of test conditions are based on the overview/initial study (chapter 4), the pre-test study carried out before this investigation and the in-situ downhole conditions. For example, a sliding speed of 2.2 m/s was used, as it is equivalent to the lowering speed for the downhole tools which translates into the sliding speed between the wireline and the internal coating of the injector tubulars. A sliding distance of 150 m was adopted to allow comparative analysis. A 150 N load was selected based on the overview in chapter 4. The tests were repeated three times for each coating using the same slickline wire. The pre-test study showed that there was no evidence of a transfer film to the wire, which would have necessitated the wire to be cleaned or replaced after every test. The friction force was not measured in this study because it does not form part of the selection parameters in this study.

The volume loss of the wear was estimated using surface profilometry, see chapter 4. The transverse profiles of the wear tracks were evaluated using a 2D form Talysurf profilometer see Figure 6.2. The cross-sectional area was determined by estimating the area under the wear track trace from the Talysurf. The procedure was repeated for all coatings.

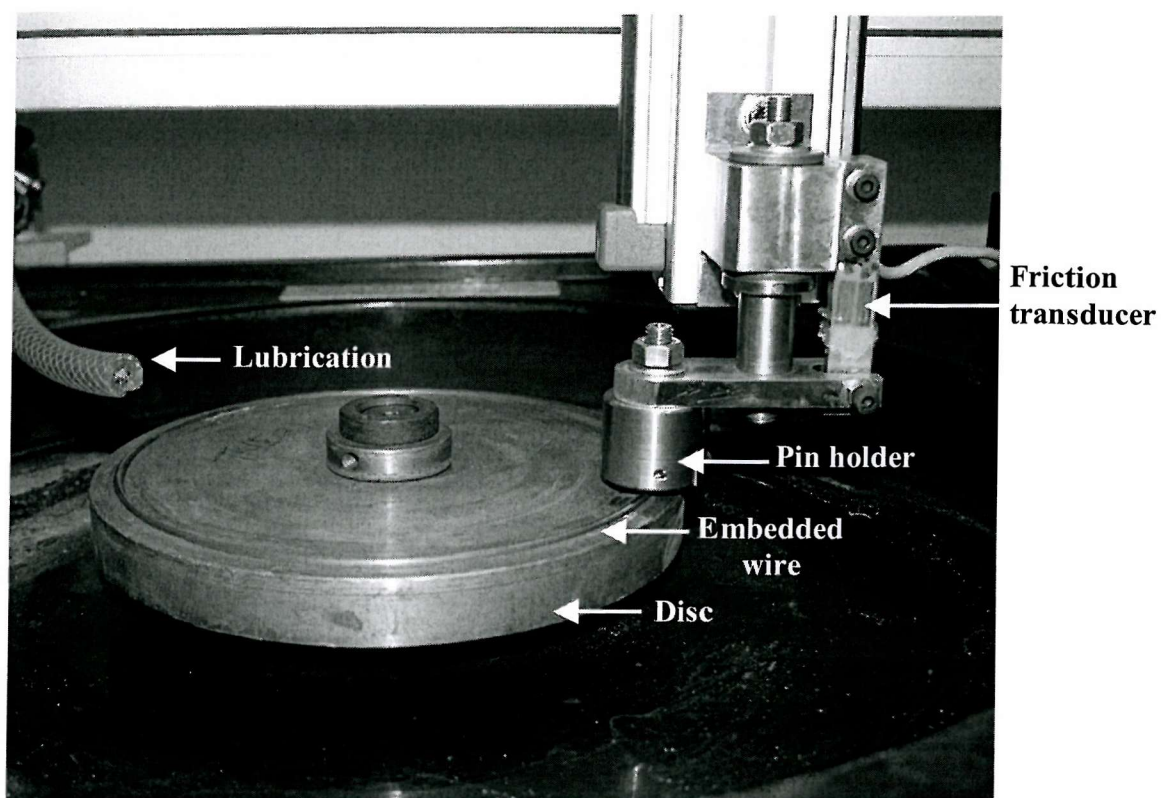


Figure 6.1: A photograph of the laboratory pin-on-wire arrangement.

Applied Load (N)	150
Disc rotational speed (m/s)	~2.2
Radius wire from centre of disc (m)	0.08
Test time (s)	480
Temperature	25°C
Lubrication	Tap water
Lubrication rate (ml/s)	16

Table 6.1: Experimental conditions employed during the study of wireline wear of polymeric coatings.

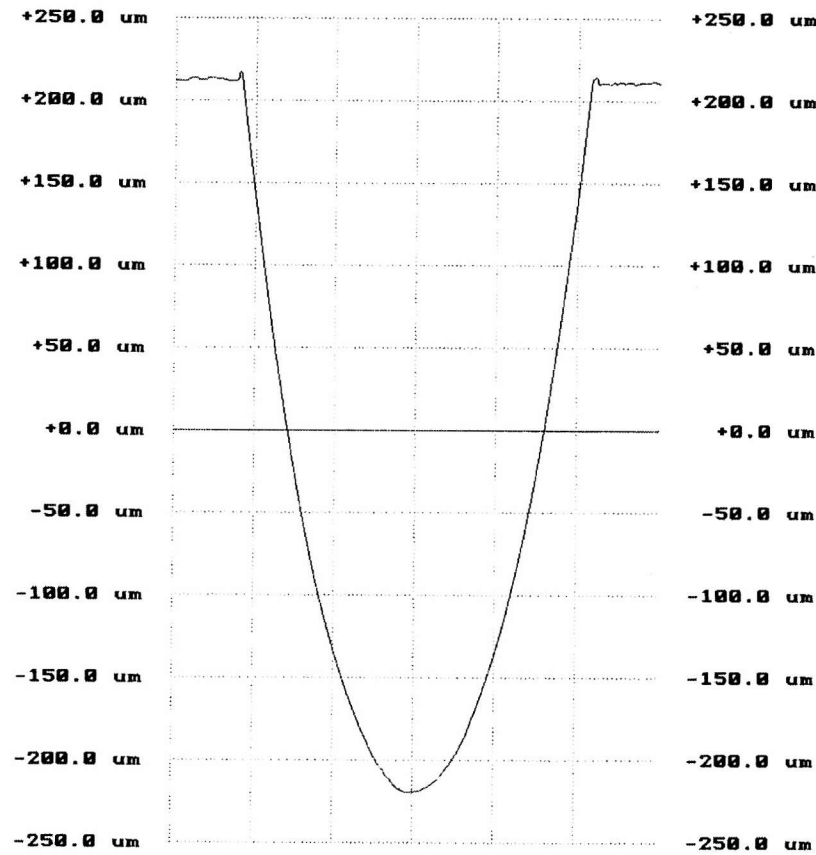


Figure 6.2: A 2-D Talysurf taken across the wear scar in a coating. Horizontal and vertical scales are 500 and 50 μm per division respectively.

6.2.2 Evaluation of wear rate

As discussed in section 6.2.1, the 2-D talysurf trace of the wear track was scanned into a computer, then the area was measured using the facilities of the CAD package Auto-sketch, which has the ability to measure accurately an area provided the perimeter is 'highlighted'. Where the perimeter was the scar trace, the upper surface was taken as an imaginary line between the top two points of the scar. Any evidence of plastic deformation was taken as negligible with respect to the wear track. The length of the wear scar was assumed the same as the length of the sample pin, 10 mm, because an estimation of the true length showed that the difference between the true and assumed lengths is 0.006 mm (0.6% error), which has been taken as negligible. The product of the estimated area, described above, and the scar length gave the volume of wear loss. Hence, k , the specific wear rate (SWR) was

estimated by dividing the volume of wear loss by the applied load (N) and total sliding distance (S) slid (m^3/Nm), see Equation 6.1.

$$k = \frac{V}{SN} \quad \dots\dots\dots 6.1$$

6.3 Results and Discussion

6.3.1 Wear rate ranking

Figure 6.3 shows the wear rates for the six coatings, with TP-9 giving the best performance with a wear rate of $9.60 \times 10^{-16} \text{ m}^3/\text{Nm}$, while PVDF appears to be the worst with a wear rate of $2.85 \times 10^{-14} \text{ m}^3/\text{Nm}$. The wear performance of the coatings can be ranked thus: TP-9 < TS-5 < TS-7 < TSX-4 < F-4001 < PVDF.

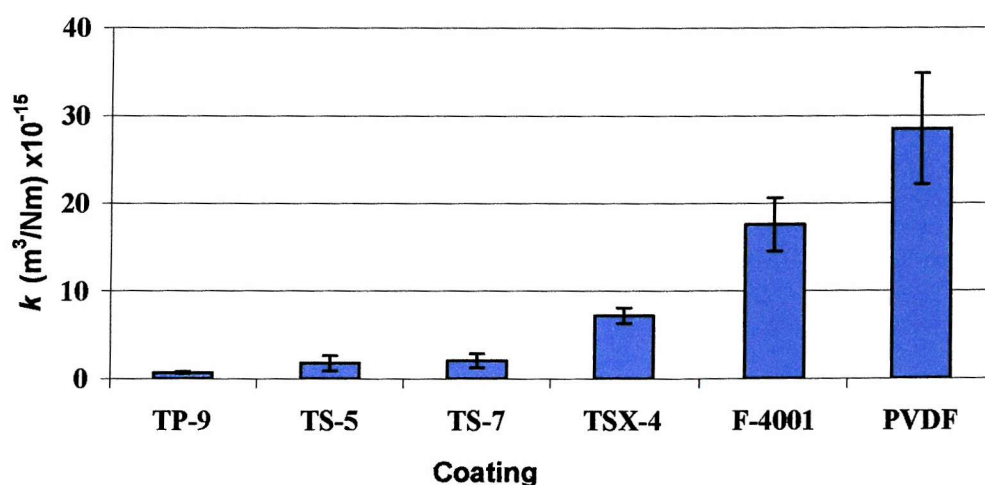


Figure 6.3: SWR, k , for the six coatings tested under wireline wear. The sliding distance was 150 m and applied load was 150 N.

The high wear rate shown by F-4001 and PVDF is consistent with what is reported in the literature {section 2.6.1.3, Table 2.3}, where most unfilled fluorinated polymers have been shown to have poor wear resistance; PTFE being an example ^[6.1]. Chemically, PVDF has a structure similar to that of PTFE; this probably explains why the wear resistance is poor. The poor wear behaviour of fluorinated polymers may be linked to the low stiffness compared to other polymers such as polyetheretherketone. The generally low hardness

value due to the presence of fluorine within the molecular structure may also contribute to poor wear resistance.

From Figure 6.3, it can be seen that thermoplastic polymer coating TP-9 out-performed the thermosets TS-5, TS-7 and TSX-4. The wear rates for TP-9 were approximately 2.5, 3.0 and 10.0 factors lower in magnitude than TS-5, TS-7 and TSX-4 respectively. In addition, TP-9 shows a lower deviation in wear rate compared to TS-5, TS-7 and TSX-4. The difference in deviation is thought to be a function of the individual coating materials because the error in wear rate is not uniform across the six coatings. Generally, early indication from Figure 6.3 suggests that thermoplastic-based polymer coatings have better wear resistance compared to the thermosets and fluoro-polymers.

6.3.2 Wear mechanisms

A coating is usually made up of the matrix and, in some cases, with particulate fillers. The matrix is the main constituent of the coating making up to about 70 – 98 % by volume of the coating depending on the manufacturing specification, thus the volume content of the fillers could vary from as low as 2 % to 30 %. Sometimes the coating is not filled with particulates and the matrix makes up the whole of the coating, such as the TP-9 (because it was difficult to fill PA11) and PVDF coatings. Usually, when considering the tribological applications of filled coatings, they are treated as a homogenous material i.e. the coating is considered to have an intrinsic property. However, for an in-depth performance characterisation of the coatings, it is necessary to consider the various constituents of the coating separately as the mechanical properties of the fillers and matrix usually differ. In addition, an understanding of the interactions between the two is important; for example, the bonding between the fillers and the matrix and how these two elements complement each other during wear.

6.3.2.1 Wear mechanisms of coating matrix

Figure 6.4 is an SEM image of the worn sample of TP-9 showing the edge of the wear track. The edge is characterised by plastically deformed coating material, which results from abrasion (ploughing) by the wireline asperities through the coating. This can be seen in the tiny grooves observed in the bottom of the wear track, see Figure 6.5. The grooves

found in Figure 6.5 are smooth and shallow, a feature that suggests a reasonably good resistance to the wireline abrasion because a deep groove would suggest that coating is easily abraded. The presence of carbon black in the coating may have aided the wear resistance of TP-9 by lowering the friction at the contact, ultimately reducing frictional heating; carbon black is a good frictional material. Thermoplastics have been found to produce tendrils during wear^[6.2]. However, in this work, tendrils have not been a feature of the wear mechanism. The pile of thick film of coating at the edge of the wear track, see Figure 6.4, is a result of plastic deformation after repeated sliding, which is due to the ductile nature of coating TP-9.

TS-5, TS-7 and TSX-4 are thermoset-based coatings, which suggests that their matrices are hard compared with TP-9, F-4001 and PVDF. The matrix of TS-5, a modified novolac powder, does not show any distinctive wear mechanism except for some microscopic grooves found on the fillers, see Figure 6.6. It has been discussed in section 2.2.2 that most thermoset-based coatings wear by fatigue process because of the cross-link nature of the matrix^[6.3 – 6.5]. TS-5 does not show any evidence of wear by fatigue, which may be due to the mode of manufacturing and/or the nature of matrix material.

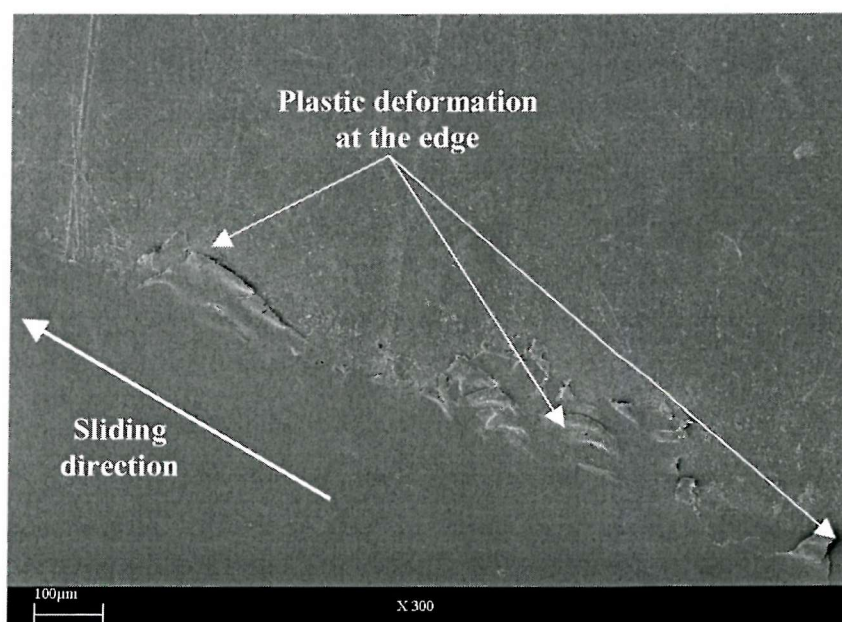


Figure 6.4: SEM of the worn surface of TP-9 showing plastic deformation around the edge of the wear track.

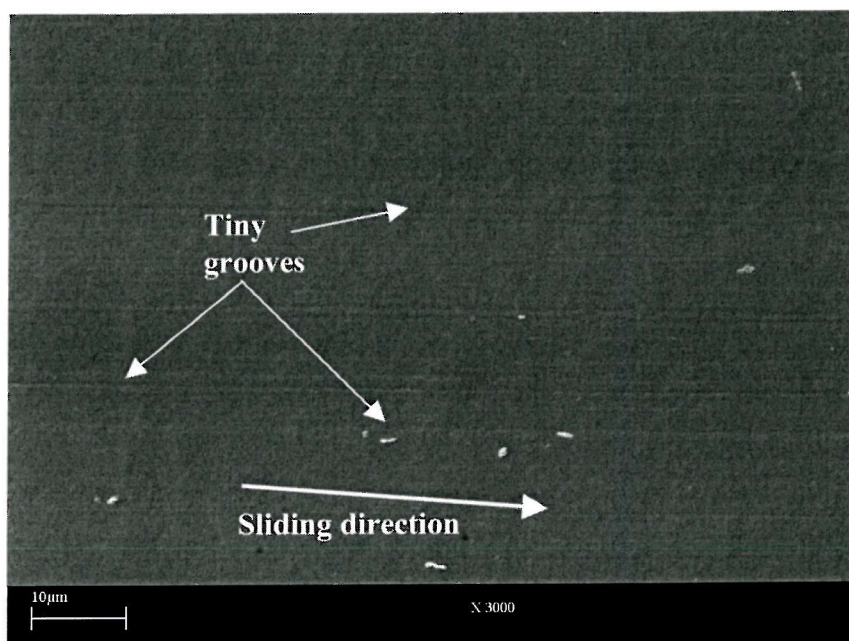


Figure 6.5: SEM of the centre of the wear scar. Note the tiny grooves and deposit of minute wear debris.

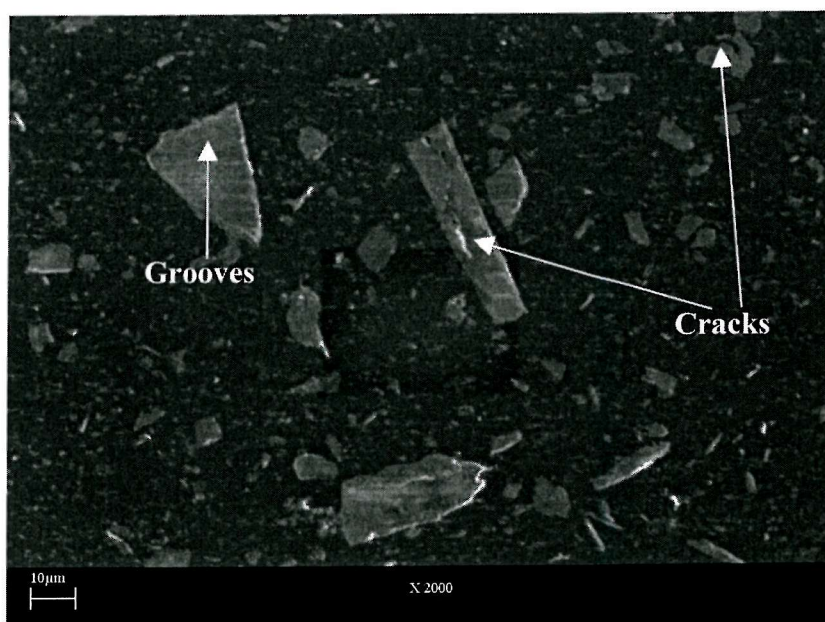


Figure 6.6: SEM of the worn surface of TS-5. Note the tiny grooves across the $\text{CaCO}_3/\text{SiO}_2$ Fillers and matrix as well as the cracks on the fillers.

Unlike TS-5, the matrix of TS-7 appears to be characterised by fatigue wear, see Figure 6.7. Usually, fatigue wear results from stress induced by the counterface asperities on the coating. The stress often gives rise to tiny cracks within the matrix due to the hardness, which results in wear after repeated sliding. Thus, the wear mechanism of a typical thermoset coating is usually not smooth and characterised by leaf-like features as seen in Figure 6.7.

The worst wear rate among the thermoset coatings was for TSX-4, see Figure 6.8. As explained earlier, fatigue initiates wear in most thermoset-based coatings due to induced stresses caused by repeated/cyclic loading by multiple asperities. The effect of fatigue in TSX-4 appears to have induced cracks in the coating, causing the matrix to “chip-off” easily. This explains the rough surface appearance of the matrix and the cracks found on the worn surface.

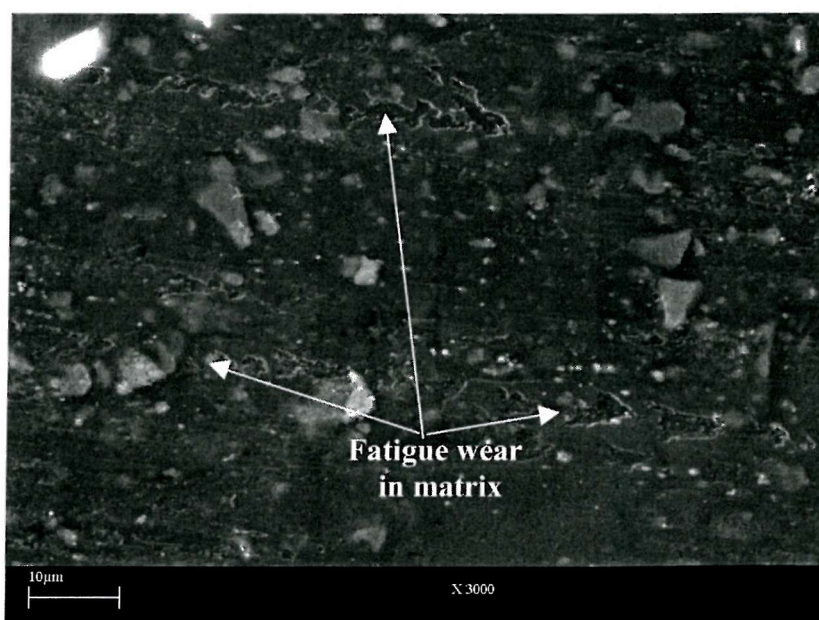


Figure 6.7: SEM of TS-7. Note the fatigue wear mechanism found in the matrix.

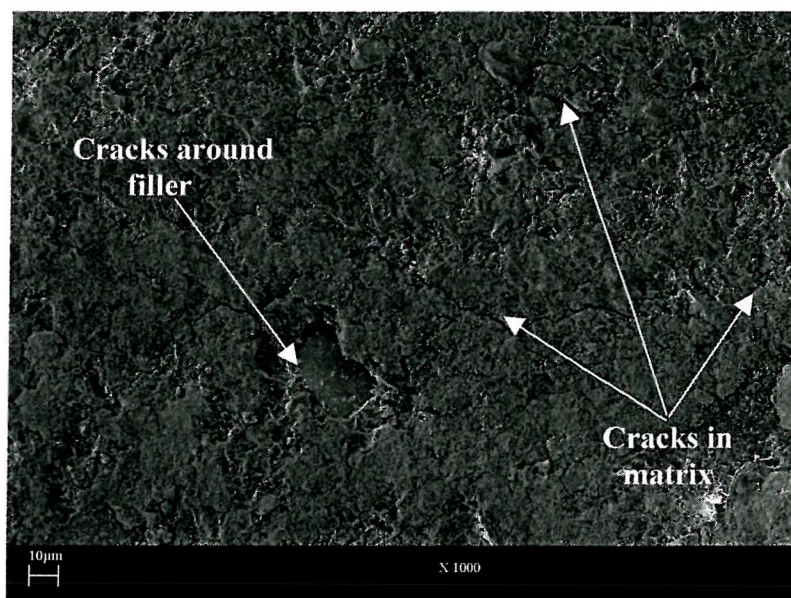


Figure 6.8: SEM image of TSX-4 showing the cracks all over the matrix and around the Al_2O_3 fillers.

Figures 6.9 and 6.10 are the SEM micrographs of the worn surface of coating F-4001. It can be seen that the coating matrix suffers material removal by micro-ploughing, which is evident in the grooves found in the centre of the wear track and the resulting tendrils produced at the edge of the wear track, see Figure 6.9. Similar to the wear behaviour of TP-9, the grooves shown in Figure 6.10, less than $1\text{ }\mu\text{m}$ in depth, are shallow but rough. The micro-ploughing of the coating, which resulted in the grooves and tendrils, is thought to be due to abrasion from the wireline asperities. Figure 6.11 is a 3-D profile of the wireline. The asperities on the wireline have average dimensions of $5\text{ }\mu\text{m}$ height, $12\text{ }\mu\text{m}$ base radius and $20\text{ }\mu\text{m}$ peak to peak asperity spacing and are hemi-spherical in shape are believed to cause abrasion of the coating when sliding occur.

A further examination of the bottom of the wear track at higher magnification showed that there are numerous cavities measuring approximately $20\text{--}30\text{ }\mu\text{m}$ in size, corresponding with the filler sizes. This might be due to two reasons: (1) the fillers, which make up 3 % of the total coating volume are not supporting the load well enough and thus are easily removed during wear. The behaviour of the fillers can also be explained by a model proposed by Axen and Jacobson ^[6.6] for the abrasive wear resistance of multiphase materials. Hence, the

microscopic cavities left behind becomes larger as wear progresses due to the ductile nature of the matrix. (2) Some microscopic voids induced during coating deposition are exposed and enlarged by progressive wearing of the coating from wireline.

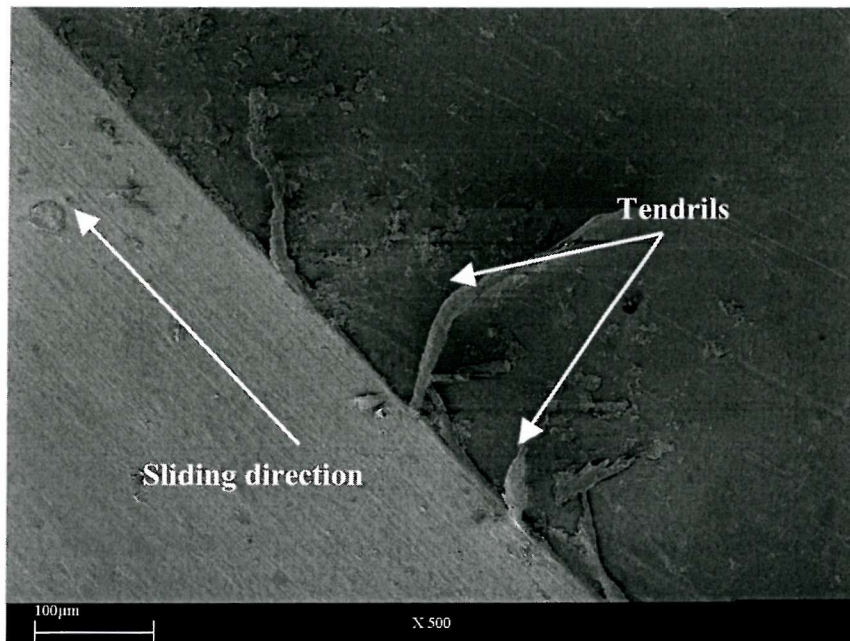


Figure 6.9: SEM image of F-4001 coating showing tendrils at the edge of the wear track.

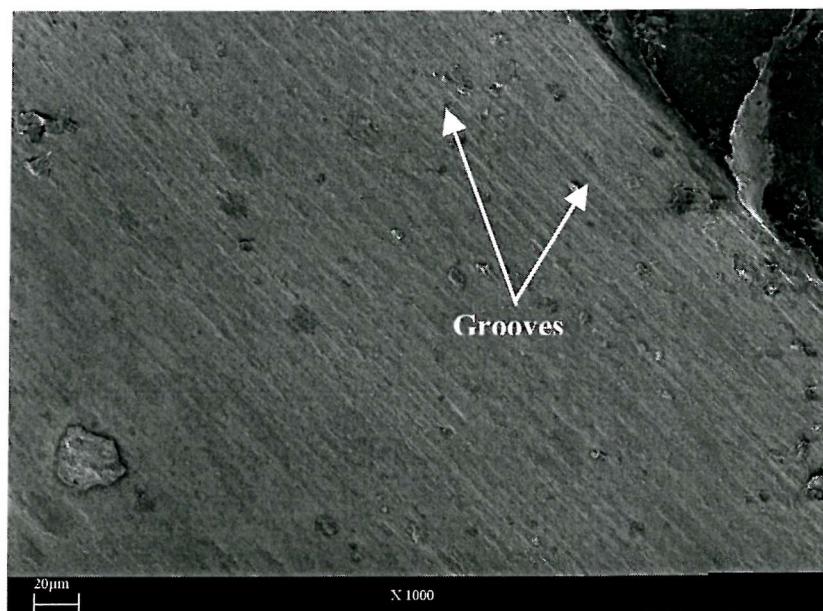


Figure 6.10: SEM image of F-4001 coating showing grooves on the wear scar.

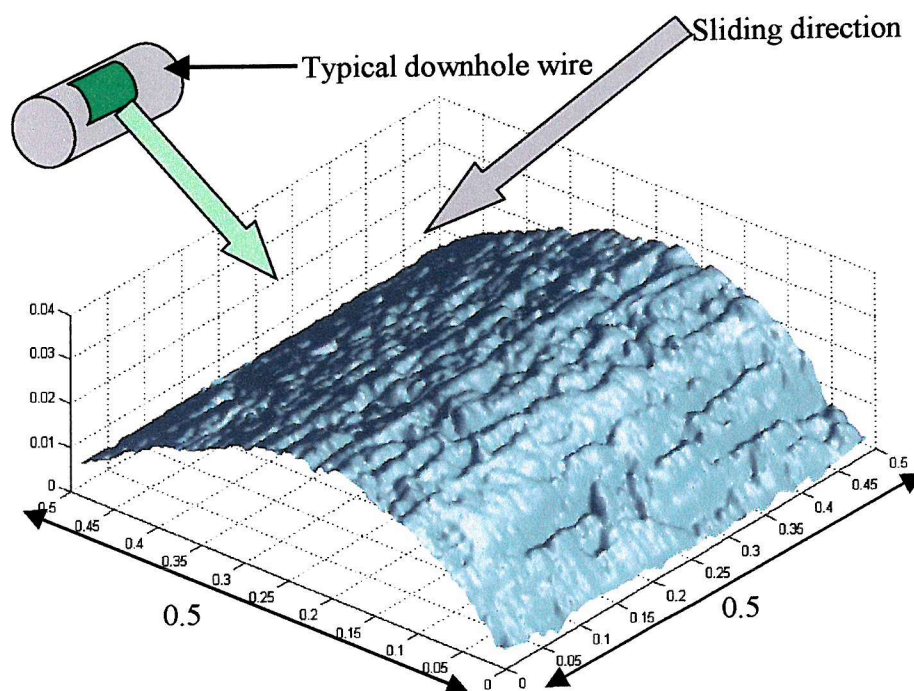


Figure 6.11: Surface profile of a wireline used to lower tools into the tubulars downhole. The asperities were found to have an average of $5\mu\text{m}$ height and $12\mu\text{m}$ base width and approximately $20\mu\text{m}$ peak-to-peak asperity spacing.

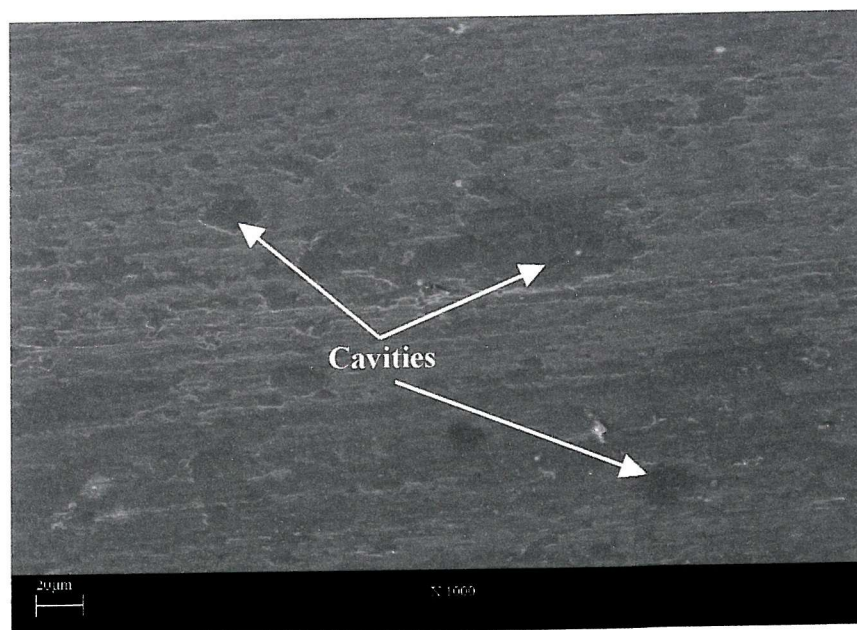


Figure 6.12: SEM image of F-4001 coating at a higher magnification showing cavities within the coating matrix.

The wear of PVDF, like F-4001, is characterised by the formation of short fragile tendrils at the edge of the wear track, Figure 6.13, which are believed to have resulted from micro ploughing by the wireline asperities. However, unlike F-4001, a significant amount of approximately 5 μm sized wear debris was found at the centre of the wear track. This suggests that some of the tendrils break off during ploughing and remain within the sliding contact leading to formation of debris. The debris can subsequently act as an abrasive material within the sliding contact therefore causing accelerated wear. This phenomenon was not observed for TP-9 because of the difference in the molecular structure of the two polymer matrices.



Figure 6.13: SEM image of the PVDF coating showing the edge of the wear track.



Figure 6.14: SEM image of the PVDF coating showing the centre of the wear scar.

6.3.2.2 Function of fillers in coating during wear

Among the six coatings studied, only TP-9 and PVDF are unfilled. TS-5, TS-7, TSX-4 and the Fluorocarbon coatings are filled with $\text{CaCO}_3/\text{SiO}_2$, Glass, Al_2O_3 and CaF_2 respectively. Figure 6.15 is a SEM micrograph of TS-5 coating showing cracks in some of the fillers; also, some of the fillers appear to be “crushed”. Figure 6.16 shows the initiation of filler pullout. Initiation of cracks at the edge of the fillers are thought to eventually lead to fillers being detached from the matrix, an indication of weak bonding between fillers and matrix, which is clearly seen for the TSX-4 coating in Figure 6.17. The detachment of fillers from matrix was found to be only associated with the TS-5 and TSX-4 coatings. The fillers in TS-7 do not show any evidence of cracks; however, some cracks are seen on the fillers in coating TSX-4, see Figure 6.18. The cracks in the fillers of TSX-4 appear to have originated from the cracks in the matrix because of the nature of the coating matrix. It is thought that the shear forces generated at the filler/matrix interface may be responsible for the cracks. However, the cracked fillers could result from the inability of the fillers themselves to support the normal load.

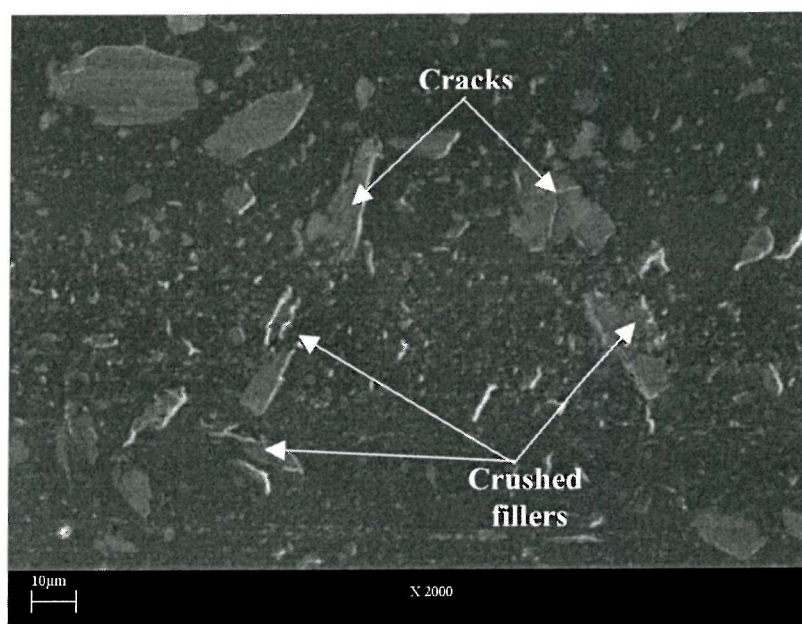


Figure 6.15: SEM of TS-5 showing the compression and cracking of the $\text{CaCO}_3/\text{SiO}_2$ fillers.

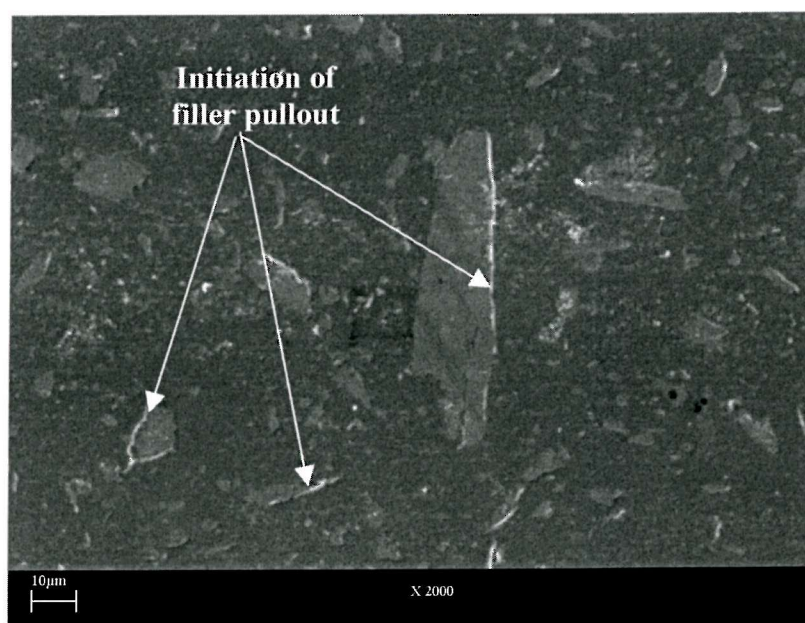


Figure 6.16: SEM of TS-5 showing possible initiation of the $\text{CaCO}_3/\text{SiO}_2$ filler pullout.

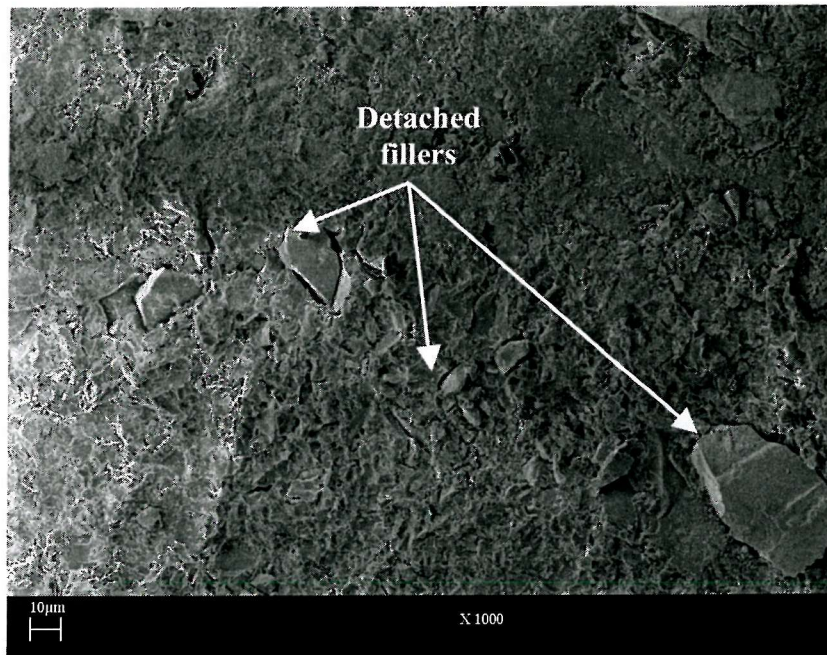


Figure 6.17: SEM micrograph of TSX-4. Note the fillers being pulled out

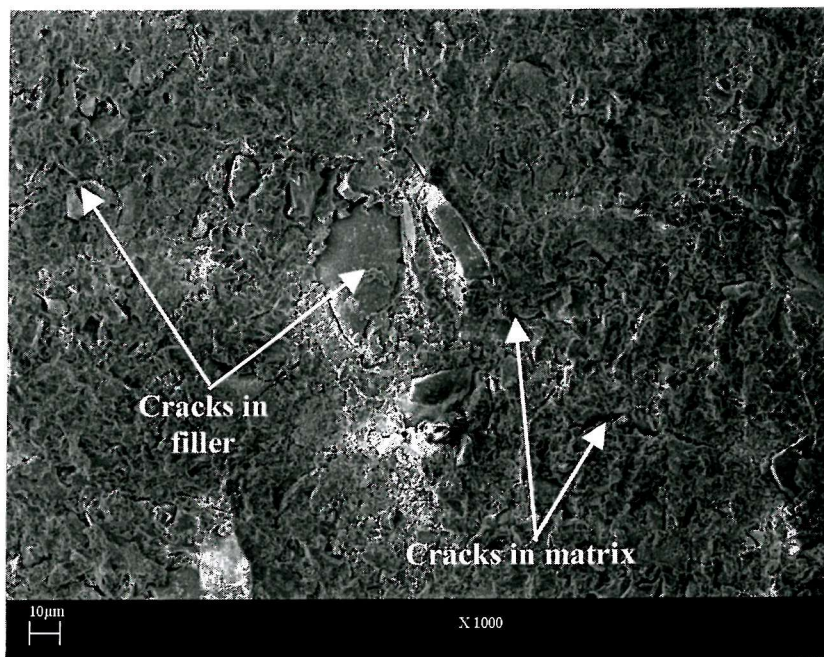


Figure 6.18: SEM of TSX-4. Note the cracks in the Al_2O_3 filler and the matrix.

Generally, the fillers tend to reduce the wear of the coating by preventing the abrasion of the matrix by wireline asperities. For example, in Figure 6.19, the highlighted filler seems to interrupt the groove preceding it, thus preventing a long filament of the matrix from being drawn. This is schematically shown in Figure 6.20. The Fluorocarbon coating did not show any unusual behaviour.

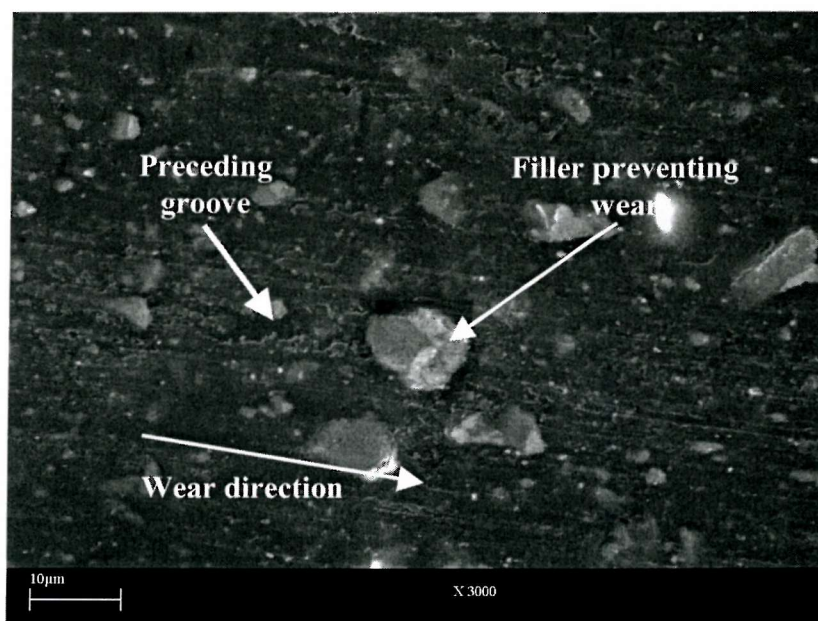


Figure 6.19: SEM of the worn surface of TS-7. Note the filler preventing wear of the matrix as indicated by the arrow.

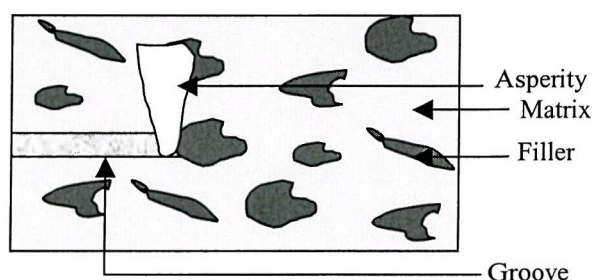


Figure 6.20: Schematic showing how the fillers prevent abrasion in coatings during wear.

In addition to the crushing and cracking of fillers, abrasion of fillers was also observed for some coatings. Except for TSX-4 fillers Al_2O_3 , abrasion of fillers was seen for TS-5 and TS-7 as is evident in the grooves across the fillers in TS-5, see Figure 6.6 and 6.21. This is an indication of low strength and low toughness. The Al_2O_3 filler in coating TSX-4 appear

to have better strength and hardness compared with $\text{CaCO}_3/\text{SiO}_2$ and glass fillers. Comparison between the performance of the fillers and their bulk mechanical properties has been hampered by the lack of enough data for the mechanical properties of the fillers. However, Table 2.5 {section 2.7.2}, details the mechanical properties of the Al_2O_3 and other ceramic filler materials.



Figure 6.21: SEM image of the worn surface of TS-7. Note the wear of fillers

The overall performance of the coating can also be linked to the interactions among the wear parameters such as: mean free path of fillers, filler sizes, relative spacing between wireline asperities, and asperities' sizes. The measured mean free path (MFP) of the fillers within the thermoset coatings was $\sim 14 \mu\text{m}$, relative spacing between wireline asperity peaks is $25 \mu\text{m}$, the average size of the fillers is $10 - 40 \mu\text{m}$ and relative size of the asperities is $12 \mu\text{m}$ base radius. Comparing the MFP and the asperity size suggests that the MFP is below the value for the optimal coating performance because if the wireline is loaded against the coating, asperities are able to penetrate between fillers. Any sliding initiated under this condition could lead to the fillers being pulled or gouged out.

However, filler pull out was not observed for most of the coatings except for fluorocarbon coatings. The reason for fillers not being pulled out despite the large MFP may be due to the large filler sizes. Assuming a total penetration of the asperities occurs (average height of asperities is 5 μm), the pull out of a filler cannot be initiated as the asperity height is much less than the size of the fillers ($\sim 40 \mu\text{m}$). In the worst case, the fillers will either be compressed leading to fracture and/or abraded, which is the case for the thermoset coatings studied. The effect of filler MFP was more prevalent in the fluorocarbon coating because it contains only 3 % of fillers of the total coating volume. Hence, the MFP in the coating is large since the fillers are well interspaced in the coating. The fillers were easily pulled out, which is an indication of the large wear rate observed for this coating. The fillers could not function to prevent the cutting action of the wireline asperities due to the large MFP, hence the tendrils produced. In addition, the fillers may remain within the sliding contact and act as further abrasant causing the wear rate of the fluorocarbon coating to increase. The issue of weak adhesion/bond strength between filler and matrix cannot be ruled out as another possibility for the behaviour of the fluorocarbon coatings.

6.3.3 Modelling the POW wear rate

The understanding of the tribo-contact process is essential to the prediction of wear rate and wear mechanism in any sliding contact. Sections 2.2.1 and 2.2.2 have established that wear often results from the interpenetration of asperities during sliding wear. Hence, making simple assumptions, a model will be developed in an attempt to predict the wear rate from a POW test. This model has been based on the geometry of the wireline asperities and the wear mechanism, using the Hertz contact mechanics theory. It must be emphasized that the model applies mostly to a situation where grooving abrasion, from micro-ploughing, is the predominant wear mechanism such as for TP-9. This model assumes elastic contact which clearly is not the case in tests here but will give estimates of contact conditions.

The Hertz line contact theory for an elastic contact, Figure 6.22, suggests that the initial elastic width (δ) in any macro contact can be calculated using Equation 6.2. The following conditions were used for the calculation of the width: a line load of 15 N/mm, Poisson's ratio of 0.33 for PA11 and 0.27 for steel. The radius of the steel wire was 1.6 mm while the PA11 sample has an infinite radius because it is flat.

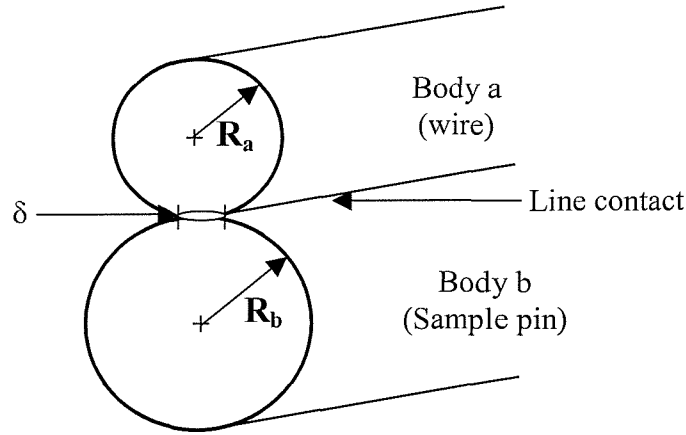


Figure 6.22: Schematic of an elastic line contact between two bodies.

$$\delta = \frac{2F_n'}{\pi} \left[\frac{1-\nu_a^2}{E_a} \left(\ln \frac{8R_a}{w} + \frac{1}{2} \right) + \frac{1-\nu_b^2}{E_b} \left(\ln \frac{8R_b}{w} + \frac{1}{2} \right) \right] \quad \dots\dots\dots 6.2$$

And

$$P_{\max} = \left(\frac{F_n' R}{\pi E'} \right)^{\frac{1}{2}} \quad \dots\dots\dots 6.3$$

$$\tau_{\max} = 0.3P_{\max} \quad \dots\dots\dots 6.4$$

Where

$$\frac{1}{R} = \frac{1}{R_a} + \frac{1}{R_b} \quad \dots\dots\dots 6.5$$

$$E' = \frac{1}{\left(\frac{1-\nu_a^2}{E_a} + \frac{1-\nu_b^2}{E_b} \right)} \quad \dots\dots\dots 6.6$$

$$w = 4 \left(\frac{F_n' R}{\pi E'} \right)^{\frac{1}{2}} \quad \dots\dots\dots 6.7$$

Where F_n is the normal force or load, ν is the poisson ratio, E is the elastic modulus, R is the radius of the contacting bodies, w is the depth of maximum shear stress, P_{\max} is the maximum pressure, τ_{\max} is the maximum shear stress. The subscripts a and b denotes parameters for body A and B respectively.

Using Equation 6.2 the contact conditions δ was estimated to be 0.180 mm. The value δ will allow the number of asperities within the contact, which are involved in the wear process to be estimated. Figure 6.23 is a schematic showing the contact width, δ as suggested by Hertz calculation.

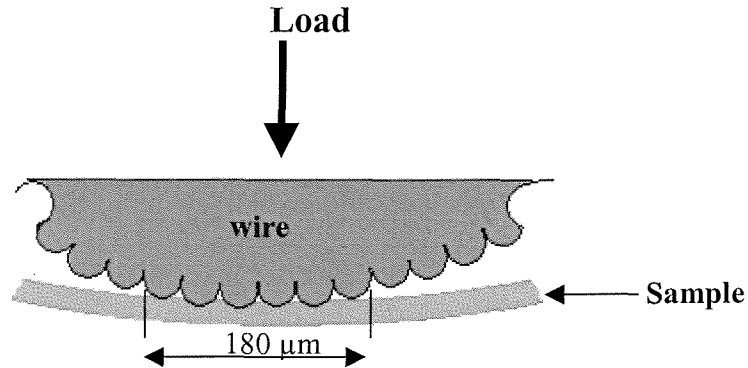


Figure 6.23: Schematic of tribo-contact pair of wire and PA11 sample.

The 2-D talysurf trace across the wireline, Figure 6.24, show that each asperity is approximately $9\ \mu\text{m}$ wide which is similar to the width of the grooves, $8\ \mu\text{m}$, found in the worn sample of TP-9, see Figure 6.25. Hence, assuming the load is uniformly distributed over the wireline asperities within the contact, this suggests that each asperity is ploughing $\sim 8\ \mu\text{m}$ groove width as shown by the SEM of the worn sample in Figure 6.25.

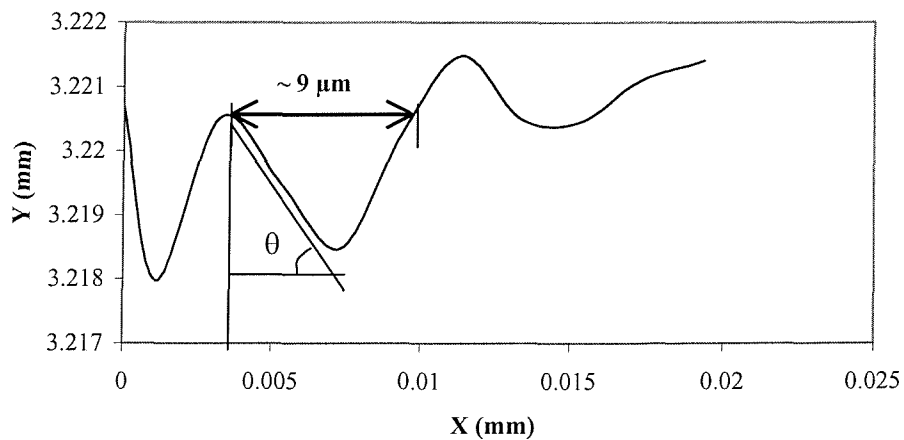


Figure 6.24: Talysurf trace across a wireline showing the size of an asperity.

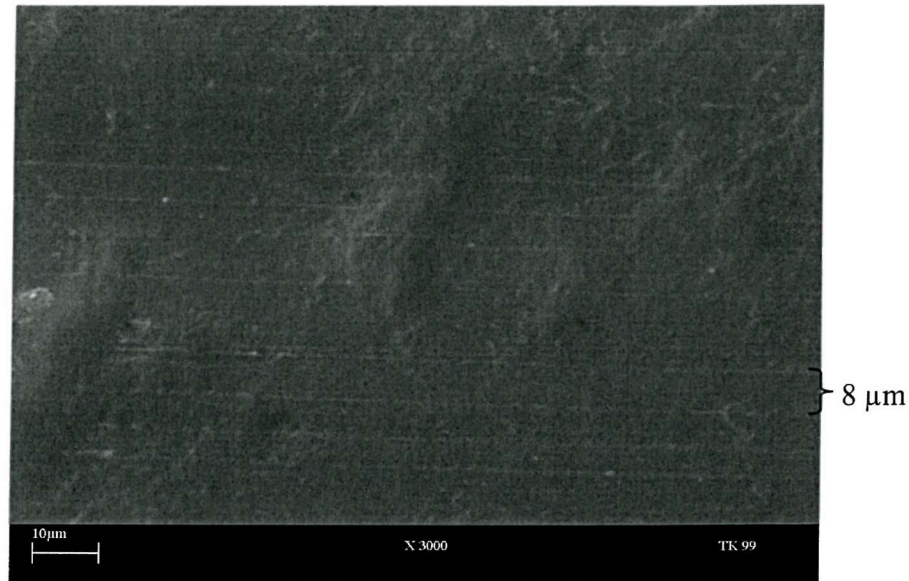


Figure 6.25: SEM of the wear scar of PA11 coating. Note the highlighted groove width.

Figure 6.26 further confirms the similarity between the width of the wireline asperities, Figure 6.24, and the grooves.

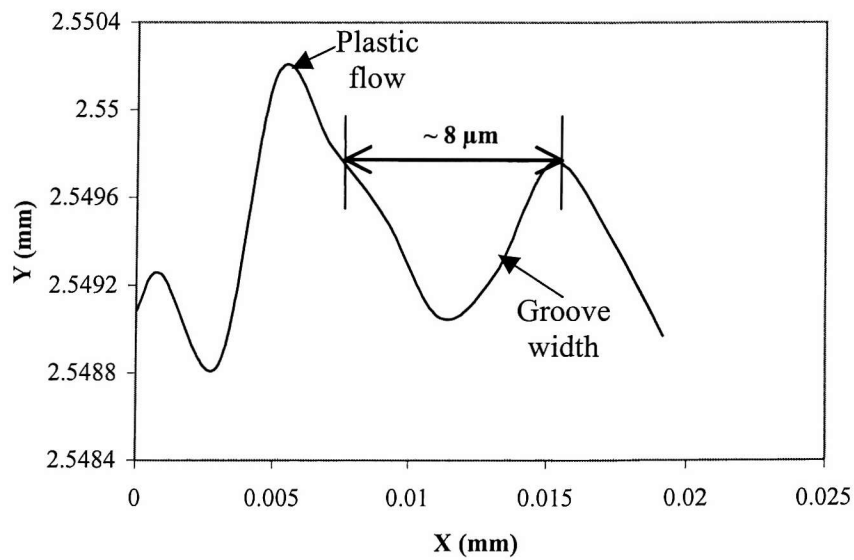


Figure 6.26: Talysurf trace of individual groove width on PA11 TP-9 at 150 N and 1000m sliding distance.

Treating an asperity contact individually, and assuming it has a spherical cap, and using Hertz point contact theory, Figure 6.27 and Equation 6.8 with the contact conditions stated earlier, but R_a of $9\text{ }\mu\text{m}$ predicts a contact diameter, δ of $4.6\text{ }\mu\text{m}$ approximately twice the width of the grooves. However, the yield stress of the coating, 27 MPa is orders of magnitudes lower than the maximum pressure of 1.1 GPa , suggesting plastic flow at the contact. Hence, the width of the groove, $8\text{ }\mu\text{m}$, after wear is reasonable.

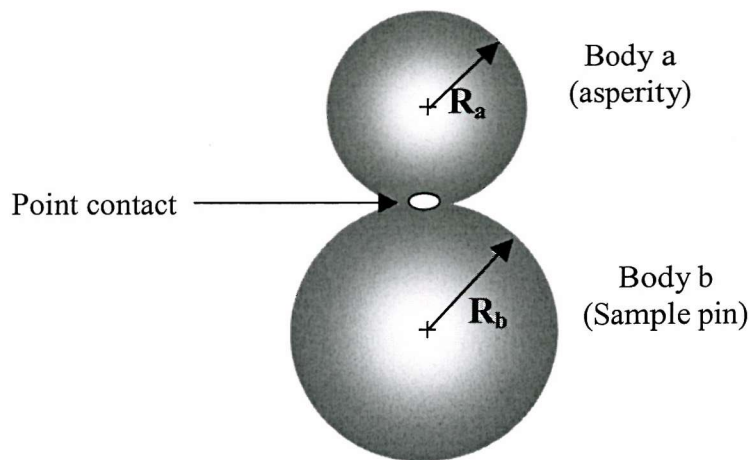


Figure 6.27: Schematic of an elastic point contact between two bodies.

$$\text{Contact diameter, } \delta = \frac{1}{2} \left(\frac{9}{2} \frac{F_n'}{E'^2 R} \right)^{\frac{1}{2}} \dots\dots\dots 6.8$$

If 18 asperities are assumed to be in contact across the wear scar width, Figure 6.28, and that for 1 m of sliding, the asperities removes 0.1 nm thick of coating, see Figure 6.29.

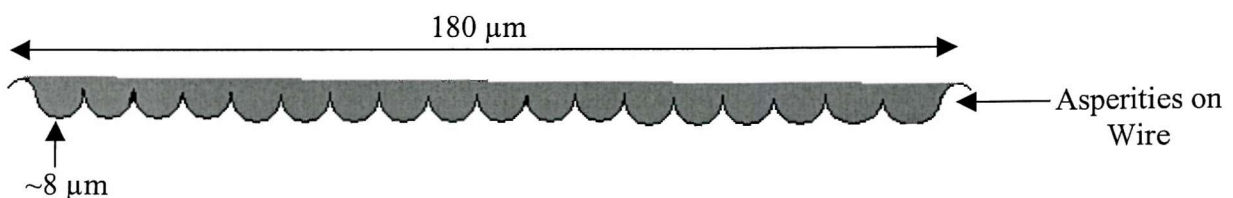


Figure 6.28: Schematic showing the total number of asperities in contact during wear.

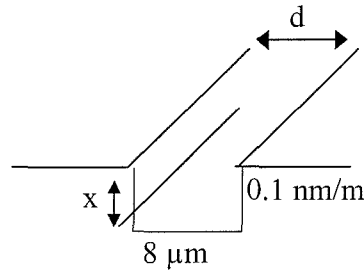


Figure 6.29: Schematic showing the depth of material removed by an asperity.

The specific wear rate, k , per asperity can be expressed by the following equation:

$$\frac{k}{\text{asperity}} = \frac{d \times x \times b \times n}{L \times S} \quad \dots\dots\dots 6.9$$

Where k = specific wear rate, d = size width of a groove ($8 \mu\text{m}$), x = depth of material removed by an asperity per metre of sliding (0.1 nm), b = the length of sample pin (10 mm), n = number of revolution (1000), L = normal load (150 N) and S = unit sliding distance (1 m)

$$\begin{aligned} \frac{k}{\text{asperity}} &= \frac{8 \times 10^{-6} \times 0.1 \times 10^{-9} \times 10 \times 10^{-3} \times 1000}{150 \times 1} \\ &= 5.33 \times 10^{-17} \text{ m}^3/\text{Nm} \end{aligned}$$

Thus, for 18 asperities,

$$\begin{aligned} k &= 5.33 \times 10^{-17} \times 18 \\ &= 9.6 \times 10^{-16} \text{ m}^3/\text{Nm} \end{aligned}$$

The value compares with the typical wear rate, $9.0 \times 10^{-16} \text{ m}^3/\text{Nm}$, obtained in this study.

Evans and Lancaster ^[6.7] have also proposed a model to predict the cutting action of asperities during sliding wear, {section 2.2.3}, using conical indenters of various angles

sliding over smooth, softer surface. It was suggested that for polymers, a linear relationship between volume and $\tan \theta$ only occurs when θ , the base angle of the cone, exceeds about 30° , see Figure 6.30.

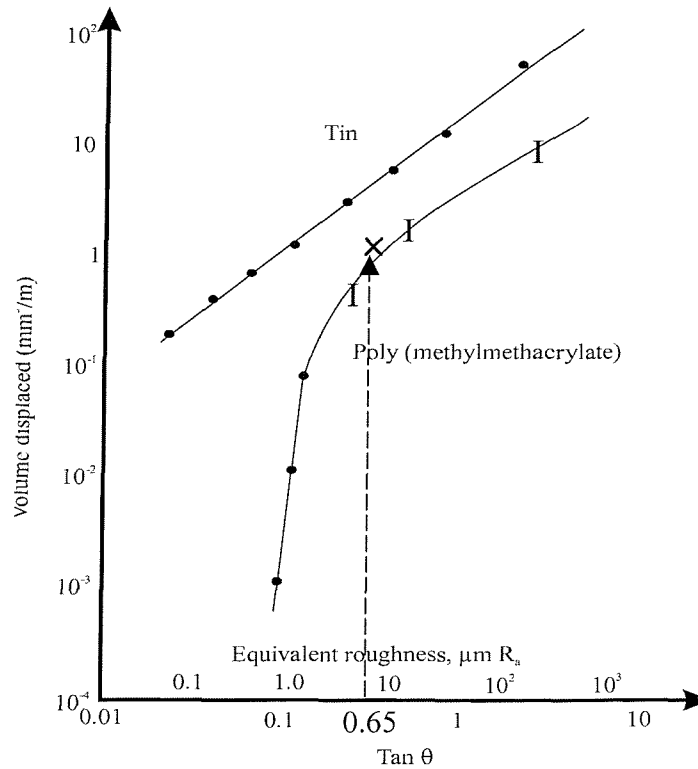


Figure 6.30: Relationship between the volumes of material displaced and the base angle of a conical indenter^[6,7].

The surface profilometry of the wireline, Figure 6.26, shows that the base angle for the asperities is about 33° . The dashed arrow in Figure 6.30 shows that a $\tan \theta$ of 0.65 falls within the direct proportionality range, suggesting that the asperities are responsible for the removal of material during the wear process.

6.3.4 Summary

Overall, the wear performance of a coating will depend on its micro-structural properties. For example, different fillers have different wear resistance.. Al_2O_3 appears to be the best filler, the $\text{CaCO}_3/\text{SiO}_2$ fillers are easily compressed suggesting low fracture toughness, CaF_2 fillers fall out of the matrix easily, while the glass fillers appear to be the worst as

they are easily worn. In terms of size and shape, bulk shaped fillers with a rough surface and between 20 to 30 μm would be preferable. However, the parameter of shapes and sizes will largely depend on the application of the coating and suitability of the filler with the matrix.

Compared to the work of Symonds ^[6.2], fewer tendrils have been observed in this work, in particular for TP-9; all other coatings studied in this programme are new. This suggests that tendrils observed by Symonds are because of vertical pin motion and wire end joining problem. In addition, no transfer film and less edge loading were observed. This show that the redesigned rig is more effective in evaluating and characterising the wear performance of polymeric coatings than the old pin-on-disc rig due to increased stiffness of the pin loading mechanism.

The proposed simple wear model suggests that wireline asperities are responsible for material removal during wear of the order 1 nm per meter slid, which show reasonable agreement with the model proposed by Evans and Lancaster ^[6.7].

Table 6.2 is a summary of the ranking of the coatings. The terms: good, fair and bad are used generally to rank the behaviour of these coatings for selection purposes. However, based on the performance of TP-9 in the POW test, further work will be carried out in order to fully characterise the tribological properties of the coating. A new test method, the micro-abrasive wear test, which allows a better control of the test conditions, will be used. In particular, effort will be made to use the micro-abrasive wear test to reproduce the type of wear mechanism, grooving abrasion, found in the POW test.

Coatings	Wear rate ranking	Matrix Wear ranking	Filler Wear ranking	Generic Name	Filler Type
TP-9	1	1	NA	Thermoplastic	NA
TS-5	2	2	4	Thermoset	CaCO ₃ /SiO ₂
TS-7	3	3	2	Thermoset	Glass
TSX-4	4	5	1	Thermoset	Al ₂ O ₃
F-4001	5	4	3	Thermoplastic	CaF ₂
PVDF	6	6	NA	Thermoplastic	NA

Table 6.2: Summary of the coating rankings in terms of wear rate and mechanism with the best performance assigned 1 and the least performance assigned 6.

6.4 Conclusions

1. The performance of the six coatings studied can be ranked, in ascending wear rate, such that TP-9 > TS-5 > TS-7 > TSX-4 > F-4001 > PVDF.
2. TP-9, F-4001 and PVDF wear by micro ploughing resulting in the formation of shallow grooves.
3. The three thermoset coatings, TS-5, TS-7 and TSX-4 wear by fatigue, initiated by cracks induced by the cyclic loading from wireline asperities during sliding contacts. The wear mechanism in TS-5 and TS-7 is characterised by irregular, “*leaf-shaped*” grooves.
4. The glass fillers in TS-7 help to reduce wear and thus improve the resistance of the coating but seem to be easily abraded.
5. The $\text{CaCO}_3/\text{SiO}_2$ and Al_2O_3 fillers in TS-5 and TSX-4 fail by micro cracking. Similar to the glass fillers in TS-7, the $\text{CaCO}_3/\text{SiO}_2$ in TS-5 show poor resistance to abrasion and do not seem to support load well, indicative of low strength and low fracture toughness.
6. Poor bonding between fillers and matrix in coatings TS-5, TSX-4 and F4001 resulted in micro cracks between fillers and matrix allowing the fillers to be detached easily from the matrix.
7. The fillers can be ordered according to their performance such that $\text{Al}_2\text{O}_3 > \text{CaCO}_3/\text{SiO}_2 > \text{CaF}_2 > \text{Glass}$.
8. A wear model has been proposed which shows that wireline asperities are responsible for wear of material in a POW test.

References

- 6.1 Schweitzer, P. A; Mechanical and corrosion Resistant Properties of Plastics and Elastomers, Mercel Dekker Publisher, (2000).
- 6.2 Symonds, N. Wear and Impact of Polymeric Coatings, PhD thesis, School of Engineering Sciences, University of Southampton, (2000).
- 6.3 Hutchings, I. M. Tribology- Friction and wear of engineering of materials, Arnold Publisher, 2nd (ed.), (1992).
- 6.4 Sarkar, A. D. Friction and Wear, Academy press, 1st (ed.) (1980).
- 6.5 Lu, Z. P and Friedrich, K; On the Sliding Friction and Wear of PEEK and its Composites, *Wear*, 181-183 (1995) 624-631.
- 6.6 Axen, N and Jacobson, S. A model for the abrasive wear resistance of multiphase materials, *Wear*, 174 (1 - 2) (1994) 1+87 – 199.
- 6.7 Evans, D. C. and Lancaster. J. K. The Wear of Polymers. Treatise on Materials Science and Technology, Ministry of Defence, Procurement Executive Materials Department, Royal Aircraft Establishment, Hants, England. Academy Press (1979)

7.0 Micro-abrasion performance of PA11 coating

7.1 Introduction

Based on the performance of TP-9 in Chapter 6 the coating was selected for a further, more detailed; study using a micro-scale abrasive wear test. The objectives are to (1) reproduce the grooving abrasion wear mechanism found in the pin-on-wire test as a result of wireline asperities; (2) improve the current understanding of the tribological properties of thermoplastic PA11 coatings, used for downhole protection of water injector tubulars; and (3) to advance the possible replacement of the pin-on-wire and the reciprocating wireline wear test with the micro-scale abrasive wear test for evaluating the tribological performance of the PA11 coatings. With the micro-abrasion test, it is also possible to monitor the wear rate of the coating, primer and substrate. In addition, the method offers a high degree of experimental repeatability ^[7.1, 7.2].

7.2 Experimental details

The experimental study consists of four tests using two different slurry abrasive particles: silicon carbide (SiC) grit and spherical glass (SG) beads. Silicon carbide abrasives have been used previously to investigate the abrasive wear performance of coatings ^[7.1 - 7.6]. However, the spherical glass beads were used in order to simulate the predominantly spherical asperities found on the wireline.

7.2.1 Preparation of test materials

The semi-crystalline unfilled PA11 coatings (TP-9) were applied up to a thickness of approximately 270 μm , onto a carbon steel plate of about $300 \times 150 \times 5$ mm and cut into test samples of 20×10 mm. According to the coating manufacturer, carbon black was used as the colouring pigment in the coating. The samples were cleaned using a degreasing agent to remove contamination and then air-dried. The slurry used was prepared by mixing 375 g of dry abrasive in 1 dm^3 of tap water (0.375 g/cm^3). The abrasive material used for the slurry was either F1200 silicon carbide particles ($\sim 5 \mu\text{m}$) or soda glass beads ($2\text{-}10 \mu\text{m}$). Figures 7.1 and 7.2 show the silicon carbide and glass beads abrasives respectively. The SiC abrasives are angular, which allows easy entrainment of the abrasive between the ball

and the test piece during an experiment. The hardness of the SiC particles, as supplied by the manufacturer, was 2500 Hv. The slurry concentration used was similar to other workers and allows two-body wear to be imposed on the test piece. The same procedure was adopted for preparing the slurry from glass bead abrasives, which have a hardness of 500 Hv. The hardness of the coatings was measured to be between 9-12 Hv.

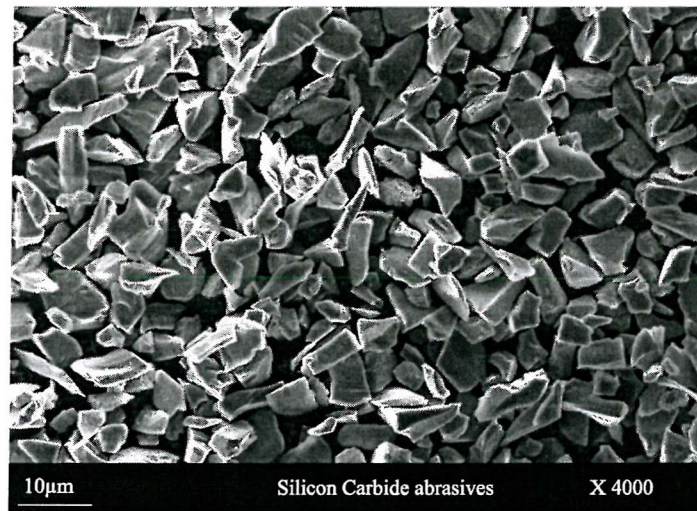


Figure 7.1: SEM of the silicon carbide (SiC) abrasives. Note the angular nature and sharp edges of the abrasives.

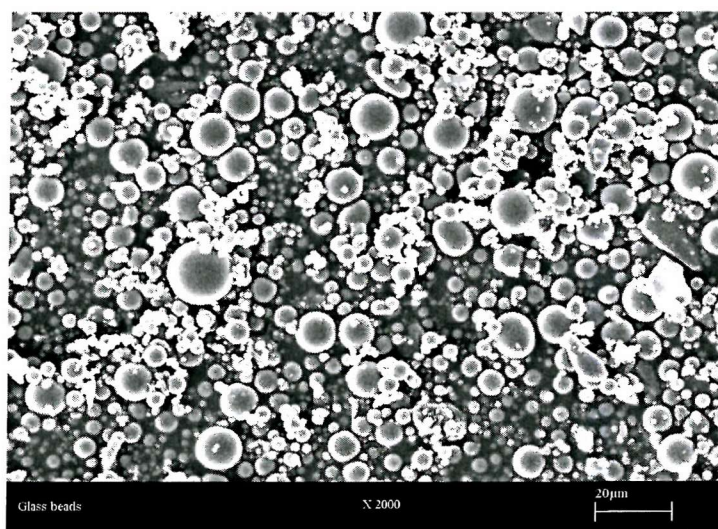


Figure 7.2: SEM of the glass beads abrasives. Note the spherical nature of the abrasives and the size range.

7.2.2 Methodology

The experiments were performed using a commercially available micro-abrasion test apparatus, the Phoenix Tribology TE66 Micro-Scale Abrasion Tester. A schematic diagram of the apparatus is shown in Figure 7.3 ^[7.1].

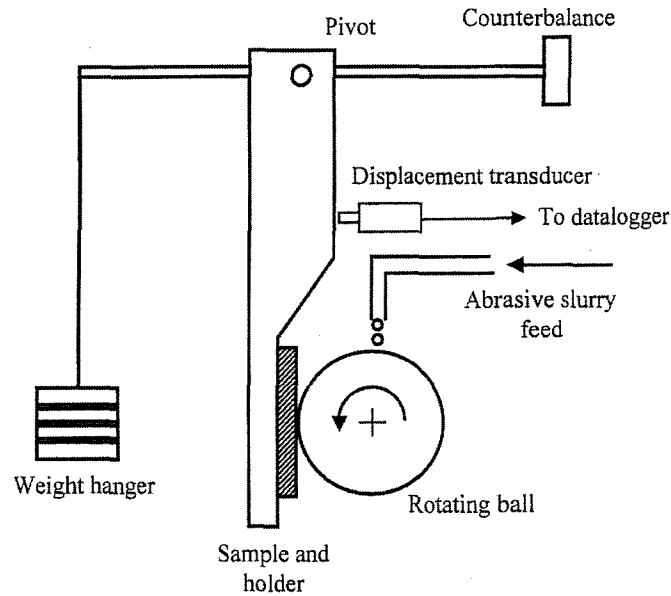


Figure 7.3: Schematic of the micro-scale abrasive wear-testing machine ^[7.1].

The sample is secured in the holder and loaded against the ball, which is held by friction and able to rotate parallel to the plane of the sample, while the slurry is drip-fed onto the ball at the rate of 10 drops/min. The geometry of the imposed wear scar is spherical. Pitted balls, supplied by Phoenix Tribology, which have been chemically roughened on its surface to about 3 μm , were used in place of the usual polished balls as they allow better entrainment of the abrasives and maintain two-body conditions. Figure 7.4 is a 3-D surface profile of the ball.

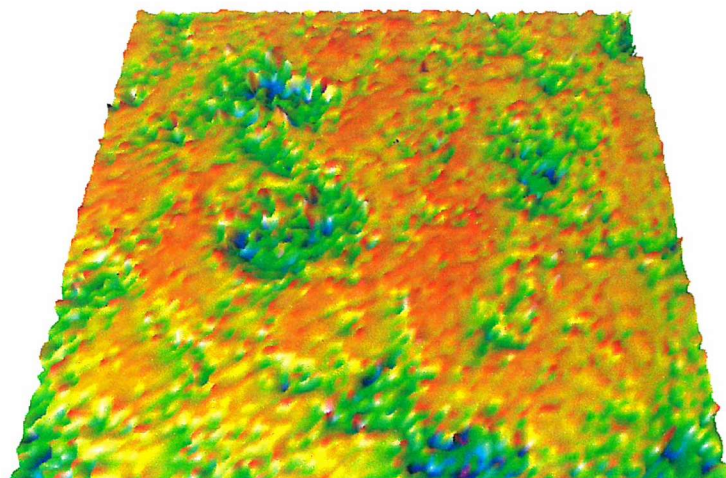


Figure 7.4: 3-D surface profile of the pitted ball used for the micro-abrasion tests. The pits on the ball surface were $\sim 3 \mu\text{m}$ size. Dimensions of the image are $500 \mu\text{m}$ by $500 \mu\text{m}$.

The diameter of the ball is 25 mm and is made of high-speed steel with hardness of 650-700 Hv. To prevent the abrasives in the slurry from settling out, the slurry was constantly agitated in a drip feed container to suspend the abrasives in the slurry. The test conditions are detailed in Tables 7.1 and 7.2. For each of the experiments, three measurements were made to ascertain the repeatability of the tests. The experimental study had two stages. First, the effect of varying the load and sliding distance on the wear rate was investigated using SiC abrasives. High loads were selected in order to get a measurable wear and produce a well form crater. In addition, to simulate aggressive conditions which the coatings are normally exposed to downhole. Using spherical glass abrasives, the effect of varying the sliding distance and the sliding speed on the wear rate of the coating was investigated. Post-test analysis of the samples was conducted by a field emission gun scanning electron microscope (FEG-SEM). The samples were gold coated and air blown prior to analysis.

Conditions/Experiments	First	Second
Applied Load (N)	2,4,6,8,10	6
Speed (rev/min)	75	75
Ball radius (mm)	25	25
Test times (min)	~27	~11,14,17,21,24
Temperature (°C)	25	25
Slurry concentration (g/dm ³ of H ₂ O)	375	375
Slurry feed rate (drops/min)	10	10
Slurry type	SiC	SiC

Table 7.1: The experimental conditions employed for the three SiC experiments.

Conditions/Experiments	Third	Fourth
Applied Load (N)	6	6
Speed (rev/min)	75	50 - 140
Ball radius (mm)	25	25
Sliding distance (m)	20 - 140	100
Temperature (°C)	25	25
Slurry concentration (g/dm ³ of H ₂ O)	375	375
Slurry feed rate (drops/mins)	4	4
Slurry type	SG	SG

Table 7.2: The experimental conditions employed for the SG abrasive experiments.

7.3.1 Wear measurements

Usually, for micro-abrasion tests, wear is measured in two ways: either by measuring the displacement or depth of wear scar with respect to the machine frame using a transducer or alternatively the wear crater dimension (diameter) can be measured using a calibrated eyepiece. In this work the latter method was used. The wear volume was calculated using an approximate formula, assuming the spherical cap geometry of the ball, see Equation 7.1.

$$V \approx \frac{\pi b^4}{64R} \quad \text{for } b \ll R \quad 7.1$$

where V , b and R are volume of wear, diameter of crater and radius of the ball respectively. In addition to the method described above, and to confirm the spherical sphere of the crater diameter, the measured crater was further analysed. The imposed spherical crater was first scanned using a 3-dimensional surface profilometer (Rank Taylor Hobson Form Talysurf 120L). The resulting image was then analysed using Computer Aided Surface Analysis

(CASA) software, developed at Southampton University. This provides information on the crater including the scar diameter and wear volume, which was useful where the generated crater was too large to be measured via the calibrated eyepiece on the rig. Figure 7.5 is a typical example of an image produced by CASA. The specific wear rate, k , was estimated by dividing the wear volume from Equation 7.1 by the applied load, N and total sliding distance, S , see Equation 6.1.

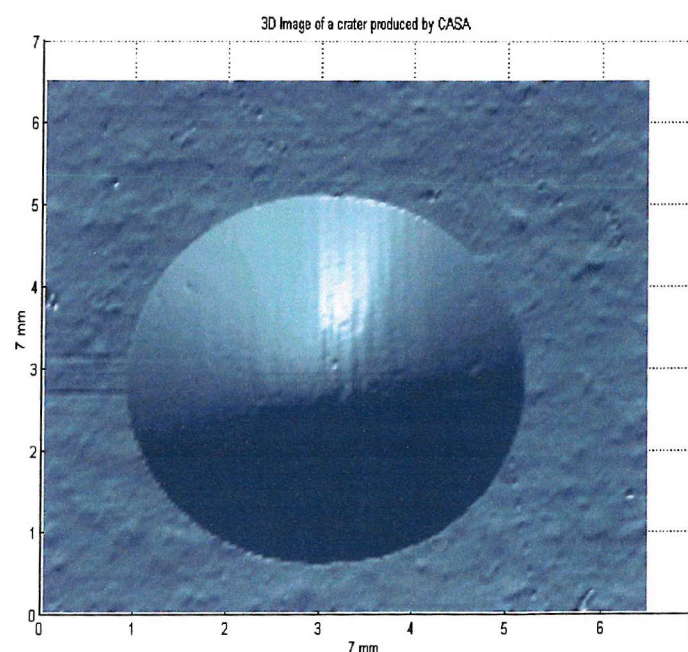


Figure 7.5: Typical image of a crater produced by CASA.

7.3 Results and discussion

7.3.1 Wear rates

An overview of the test results are given in Table 7.3, which also includes data from the reciprocating wire-on-tubular and pin-on-wire^[7.7] for comparison. When the average wear rate from the SiC micro-abrasion test was compared with the pin-on-wire and wire-on-tubular, it was found to be approximately 400 and 140 times higher, respectively.

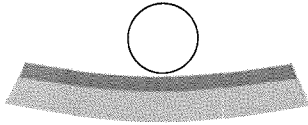
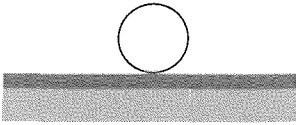
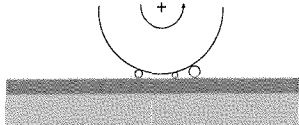
	Reciprocating Wire-on-tubular	Pin-on-wire	Micro-abrasion	
				
Coating	Polyamide 11	Polyamide 11	Polyamide 11	
Abrasive type	Slickline wire	Slickline wire	SiC	GB
\overline{SWR}	7.5×10^{-15}	$2.5 - 3.3 \times 10^{-15}$	1.0×10^{-12}	2.0×10^{-13}
Standard deviation (σ)	3.8×10^{-15}	$0.24 - 1.6 \times 10^{-15}$	2.0×10^{-14}	2.3×10^{-14}
Standard error $\left(\frac{\sigma}{\overline{SWR}}\right)$	50%	16 to 50%	2.9%	13.4%
$\frac{\overline{SWR}_{micro-abrasion_{SiC}}}{\overline{SWR}}$	~140	400	1	5
Reference	† [7.7]	* [7.7]	This work	

Table 7.3: Comparison of the wear rates from pin-on-wire and reciprocating rig tests with the micro-abrasion test.

† Load (20 to 410 N), velocity (0.5 m/s), room temperature, and water lubricated.

* Load (220 N), velocity (0.8 m/s), room temperature water lubricated.

Optical examination of the SiC micro-abrasion wear scar showed a similar appearance to both the wireline tests, suggesting the wear mechanism was consistent between the tests. The difference in wear rate was attributed to the difference in the nature of the abrasive particles used for the slurry and the asperities on the wireline. Although surface profilometry showed that the size of the asperities on the wireline and SiC abrasives are similar, with a mean value of $\sim 5 \mu\text{m}$, the shapes differ considerably. The asperity caps on the wireline were found to be spherical in nature, Figure 7.6, with an average base radius and height of 12 and $5 \mu\text{m}$ respectively, while the SiC abrasives are angular, see Figure 7.1.

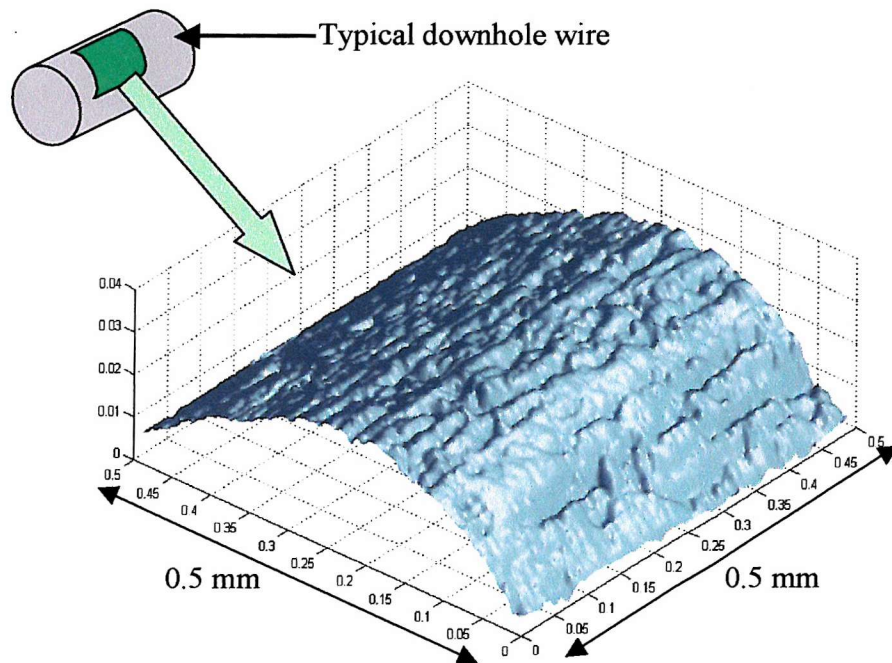


Figure 7.6: Talysurf trace showing the abrasive nature of the surface of the wireline. The asperities were found to have an average dimension of $5\ \mu\text{m}$ heights and $12\ \mu\text{m}$ base width.

Furthermore, the large difference between the specific wear rates in both tests may be linked to the concentration of the abrasives in the slurry, which is higher than the density of the asperities on the wireline, estimated to be approximately $1000\ \text{per mm}^2$.

It is not uncommon, however, for micro-abrasion studies to produce high wear rates. Table 7.4 compares the current work with studies by Rutherford ^[7.8] and Mergler ^[7.5]. The wear rates for the current study can be seen to be consistent with these other investigations.

Micro-abrasion	Material tested	Thickness μm	SWR m^3/Nm	Load (N)	Speed m/s	Slurry g/cm^3	Slurry type
Rutherford [7.8]	Polymeric clear-coat paint film	36	4×10^{-11}	0.18	0.05	0.75	SiC
Bello [this work]	Polyamide 11 coating	270	1×10^{-12}	6	0.1	0.375	SiC
Bello [this work]	Polyamide 11 coating	270	2×10^{-13}	6	0.1	0.375	GB
Mergler [7.5]	Polyamide 66	Bulk	1×10^{-12}	2 – 4	0.1	0.350	SiC

Table 7.4: Comparison of wear rates found in the literature with this work.

Elsewhere [7.4], it has been observed from studies into the effect of slurry concentration on wear rate that results using different concentrations are not always comparable due to a large and non-linear variation usually associated with such test results. This probably explains the differences between the results obtained in this study and that obtained by Rutherford [7.8]. In order to better simulate the spherical asperities on the wireline, tests were performed using spherical glass beads as abrasives. It was observed that the wear rates exhibited by the SiC abrasive wear tests is about 5 times higher than that of the spherical glass bead tests. Embedment of the glass beads within the coating was observed, which may have aided abrasion resistance.

From the current results it can be asserted that the abrasive concentration and the nature (shapes and sizes) of the abrasives can have a considerable effect on the wear rate produced by micro-abrasion tests. The difference between the wear rate shown by the wireline and the glass beads suggests that the concentration of the abrasives in the slurry and the density of the asperities on the wireline also affect the wear rate.

To establish the repeatability of the micro-abrasion test method the percentage standard error of the wear rate was estimated for both wireline tests and the micro-abrasion tests, see Table 7.3. Micro-abrasion tests show better repeatability compared to other wireline tests. A summary of the advantages and disadvantages of these tests are given in Table 7.5.

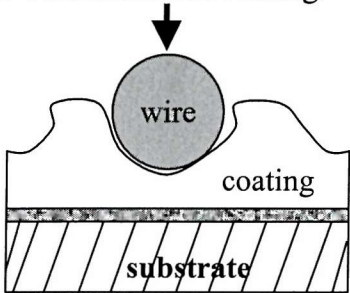
Pin-on-wire test	Micro-abrasion test
<p>Advantages</p> <ul style="list-style-type: none"> • Coating to wireline contact (i.e. consistent to true field conditions). • Application of realistic wireline loads and lubrication. 	<p>Advantages</p> <ul style="list-style-type: none"> • Accelerated test (up to 200 times). • Two-body wear mechanism similar to pin-on-wire. • Repeatability. • Fresh abrasives – no material transfer. • Extensive take-up and use as test method.
<p>Disadvantages</p> <ul style="list-style-type: none"> • Difficult to achieve a circular wire loop without welds or joints. • Material transfer alters contact conditions. • Not repeatable due to edge loading • Plastic deformation on loading.  <ul style="list-style-type: none"> • Low contact stiffness, leading to dynamic contact conditions. 	<p>Disadvantages</p> <ul style="list-style-type: none"> • High wear rate – diminishes sensitivity to polymer composition. • Spherical abrasives are embedded in coating reducing wear rate. • High abrasive concentrations in contact.

Table 7.5: Comparison between the pin-on-wire test and the micro-abrasion test.

7.3.2 Effect of load on wear rate

Figure 7.7 presents the results of the experimental study with SiC grit. It can be seen that any increase in the load causes a proportionate increase in the volume loss per unit sliding distance.

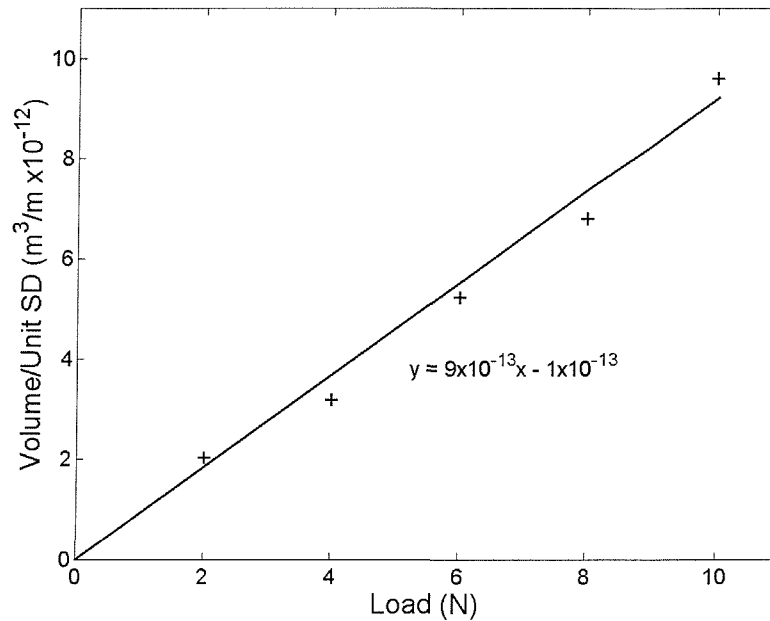


Figure 7.7: Micro-abrasion of the SiC test showing the behaviour of the volume loss per sliding distance against load at a sliding speed and distance of 0.1 m/s and 157 m respectively.

This behaviour shows a reasonable agreement with the Archard wear law (see Equation 7.2) with a slight zero offset which is thought to be due to balancing issues. The SEM micrographs of the worn surfaces at 4 N and 10 N, Figure 7.8 (a and b), suggest that micro-ploughing is the dominant wear mechanism. This is characterised by the formation of grooves, typical of two-body grooving abrasion, with short tendrils (extruded filaments of polyamide 11) at the edges of some grooves. It is worth mentioning here that the two-body grooving wear observed in this study is not surprising as the test condition was deliberately chosen to reproduce this type of wear since two-body wear mechanism dominates the wireline wear in chapter 6. The test conditions used in this study show a reasonable agreement with the model proposed by Adachi and Hutchings ^[7.9]. A critical condition for transition from grooving to rolling abrasive, which have been termed “severity of contact”, Sc , was suggested, see Figure 7.9. The Sc obtained in this study, ~ 3 , falls well within the two-body region. Although this value is high due to extreme test conditions adopted, it however, confirms that the wear mechanism observed in this study is two-body grooving abrasion. In addition, pitted balls were used in this study, whereas, Adachi and Hutchings used smooth balls. This may be another reason for the large discrepancies in results.

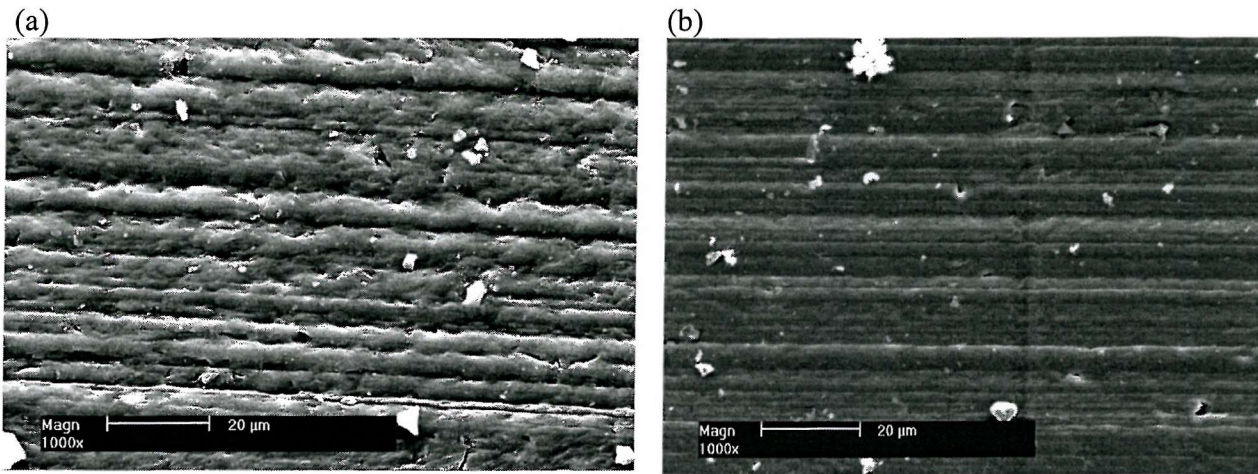


Figure 7.8: SEM images of the polyamide 11 coating at (a) at 4 N normal load and (b) at 10 N normal load (SiC).

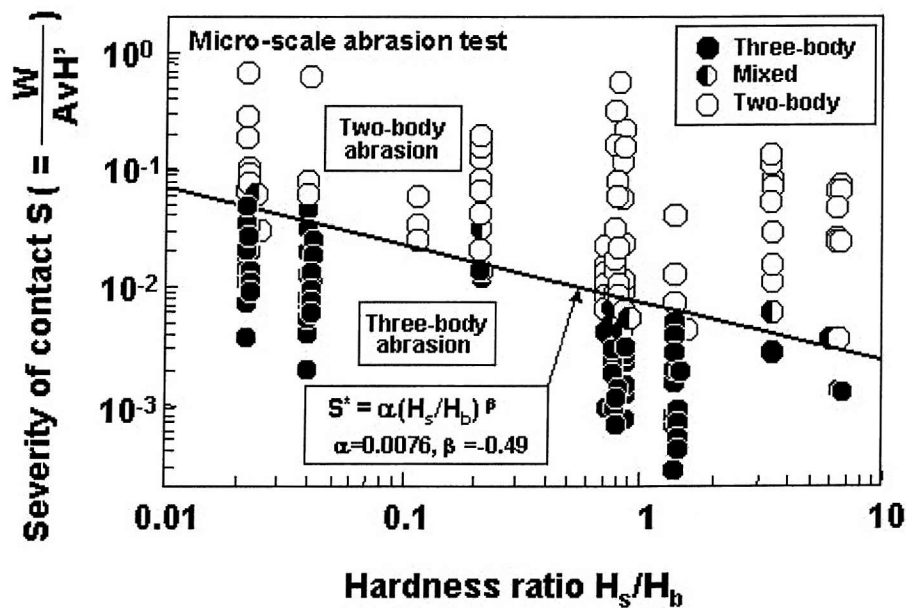


Figure 7.9: Wear mode map as a function of severity of contact and hardness ratio between ball and specimen^[7,9].

Close observation of Figure 7.8 (a and b) shows that the grooves found on both test samples differ in nature. For example, Figure 7.8 (a) is characterised by shallow grooves with rough peaks, while Figure 7.8 (b) is distinguished by smooth deep grooves with sharp peaks. The features observed at 10 N is possibly due to increased plastic deformation as evident by the smoother wear scar. Figure 7.10 is the SEM micrograph of the worn samples from a pin-on-wire test. The surface features, which are two-body grooves, are similar to those found on the micro-abrasion tests. Contrary to suggestions^[7,10] that the grooves produced by the

pin-on-wire are usually accompanied by large tendril formation, the results in this study suggest that few tendrils are produced. Tendril generation is thought to be linked to the dynamics or movement associated with pin-on-wire tests owing to inadequate stiffness of the rig, see chapter 6.



Figure 7.10: SEM of the bottom of the wear scar on the tested sample for the pin-on wire.

7.4.3 Effect of sliding distance on wear rate

The second experiment assessed the effect of sliding distance on the wear rate of the TP-9 polyamide 11 coating using two different abrasive slurries, SiC and spherical glass beads. Figure 7.11 presents the SiC results showing possibly two linear regions, 0-40 m and 60-140 m.

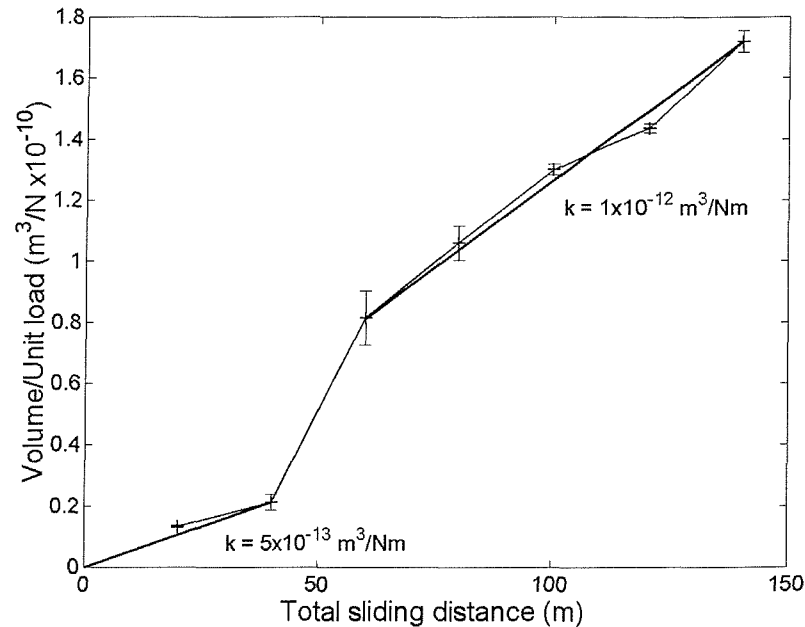


Figure 7.11: Results of the SiC test showing the behaviour of the volume loss per unit normal load at a sliding speed and load of 0.1 m/s and 6 N respectively. Note the two regions of wear rate.

Simple abrasion models predict that wear volume should be directly proportional to the sliding distance ^[7.11]. However, in the micro-abrasion test the contact area increases with sliding distance and therefore it is not obvious that a direct proportionality should hold.

This means that if the entrainment of abrasives into the contact is unaffected, the load per particle will decrease with increasing sliding distance and with wear volume. A change in the load per particle has been shown to have a slight influence on wear rates in micro-abrasion tests ^[7.4] and may explain the deviations from the linear trend seen for both regions in Figure 7.11. Generally, the wear volume per unit sliding distance remains constant for the two regions and this agrees well with other workers ^[7.4]. However, a possible error in the calculation of wear volume could arise from non-spherical wear scars. Hence, the spherical nature of the craters was confirmed by plotting the diameter and the depth obtained from CASA and compared with the geometrical relationship for spherical scars; good agreement was found, see Figure 7.12. In addition, sphere fitting performed on the craters confirmed a well-formed scar, see Figure 7.13. Figure 7.13 (a) is the mapped surface, (b) is the CASA derived best-fit sphere while (c) is the residual achieved by subtracting (b) from (a). When (a) is equal to (b), then (c) is flat. In Figure 7.11, it is thought that a mechanistic change could be responsible for the sudden change between 40

and 60 m as the coating investigated is about 270 μm thick. From Figure 7.13 the wear occurring between 0 and 40 m is a mild wear while that occurring between 60 m and 140 m is a severe wear, and this assumption agrees with the wear rate shown by the two regions.

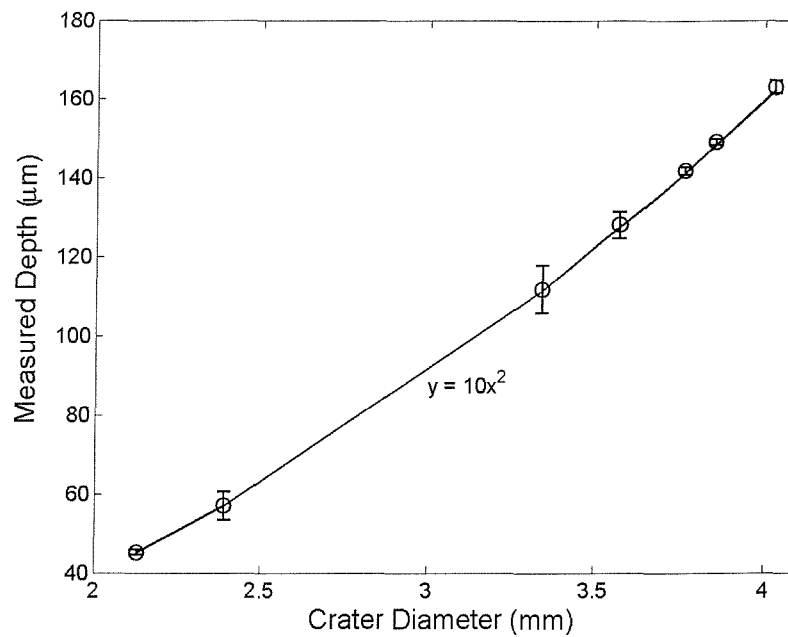


Figure 7.12: Comparison between experimental (O) and theoretical data (continuous line) for the craters at a sliding speed and load of 0.1 m/s and 6 N respectively.

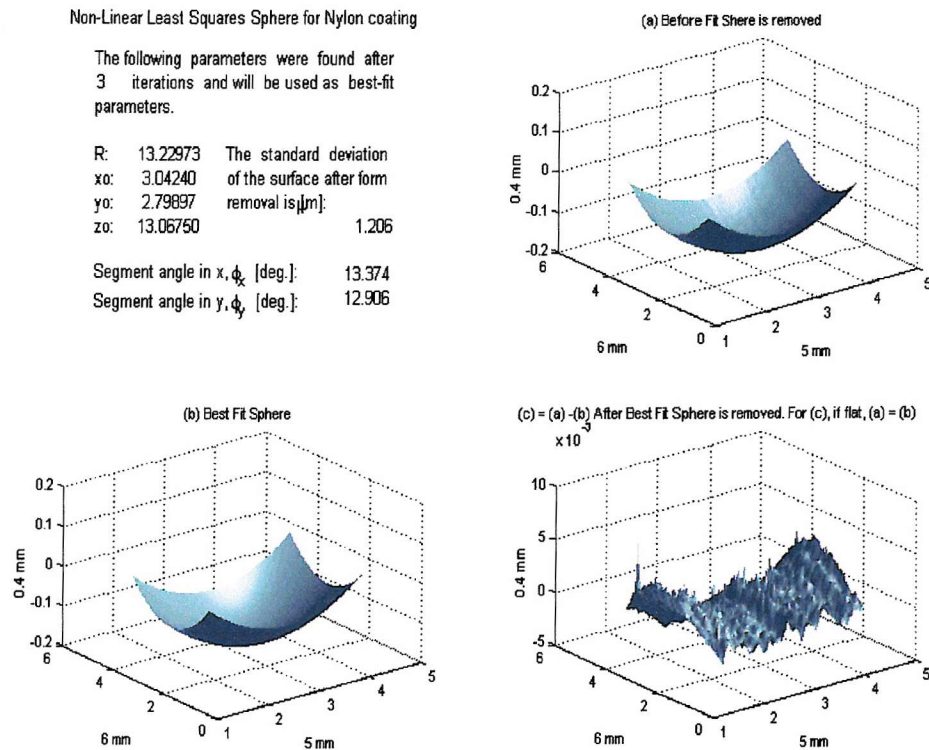


Figure 7.13: Sphere fit analysis of a typical crater, 40 m sliding distance and 6 N load (SiC).

The reason for the mechanistic change may be linked with activities occurring during the process of coating application. It is thought that different layers of the coating may have cooled at different rates, leading to anisotropic distribution of mechanical properties (such as hardness, toughness) with depth. Furthermore, exposure of the coating to the atmosphere may have caused an ultraviolet induced “*skin effect*” on the coating surface.

Initial wear mechanisms were examined in the scanning electron microscope and from Figure 7.14 (a), at a sliding distance of 20 m and (b) at a sliding distance of 40 m, it can be seen that the worn samples are characterised by two-body grooving wear, an indication of micro-ploughing.

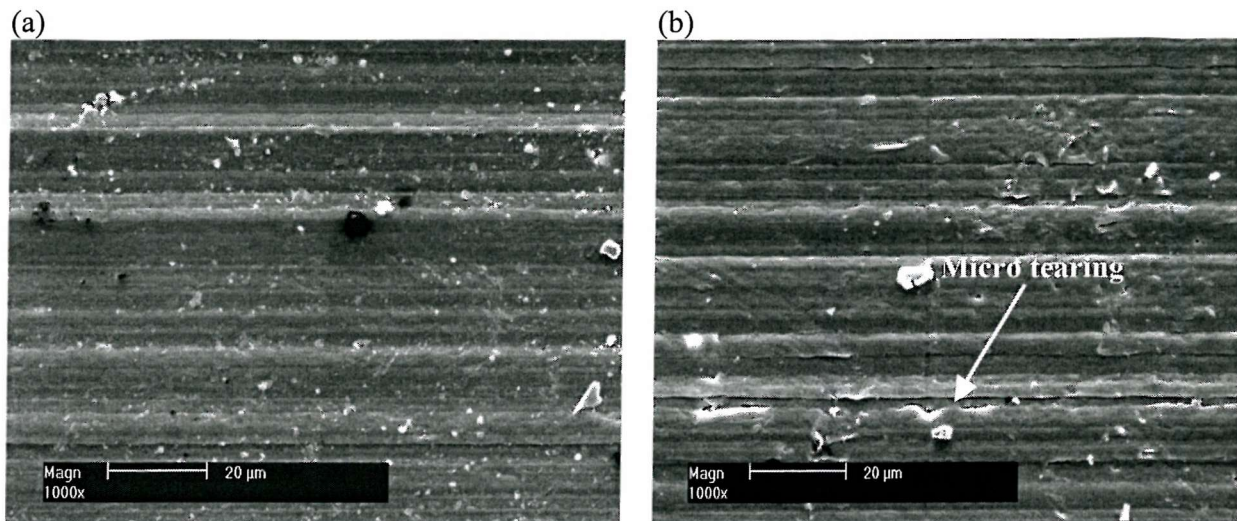


Figure 7.14: SEM images of the worn sample (a) at 20 m sliding distance and 6 N load (SiC) and (b) at 40 m sliding distance and 6 N load (SiC).

However, some significant differences can be seen between 20 and 40 m. The grooves found in Figure 7.14 (a) have shallow troughs while those in Figure 7.14 (b) have deep troughs; this probably explains the higher wear rate exhibited by the coating at 40 m. In addition to micro-ploughing, the features found on the worn sample at 40 m sliding distance show some evidence of micro-tearing, which suggests a mechanistic change with depth. At 20 m sliding distance, the depth of penetration of coating is about 42 μm , while at 40 m sliding distance it is about 58 μm from the coating surface, suggesting the skin effect is less than 50 μm deep. SEM images of the worn samples at higher sliding distance do not show any major difference from that at 40 m.

7.3.4 Comparing SiC and GB abrasives tests

The results of the glass bead abrasive tests are presented in Figure 7.15. Contrary to the results obtained with the SiC abrasive, the glass bead abrasive tests show good agreement with the Archard abrasive wear law, Equation 7.2, i.e. no skin effect.

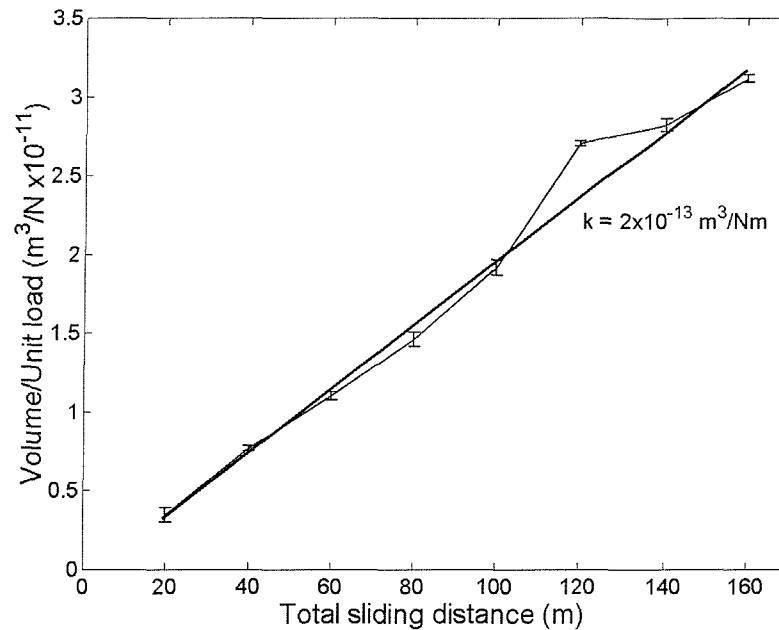


Figure 7.15: Result of the glass bead abrasive tests at 6 N load and sliding speed of 0.1 m/s.

However, the influence of the abrasive morphology (shape and size distribution) cannot be ruled out as a factor and could be responsible for the differences in the level of specific wear rate found with SiC. For instance, the SiC abrasive particles have a size range between 4 and 5 μm while the glass beads have a range of between 2 and 10 μm . Figure 7.16 is a schematic of the ball-on-coating contact for the cases where SiC and glass beads were used as abrasives. Assuming the applied load, abrasive volume fraction entrained into the contact and the rotation speeds are similar in both cases, the effect of a narrow SiC particle size distribution is to minimise the load per particle. However, the sharpness of the particle will increase the fraction of polymer removed as debris from the contact. For the glass beads with a wider size range, it could be argued that the small numbers of larger particles are likely to distribute the applied load in the contact increasing the load per particle and, thus, increasing the volume of polymer displaced per particle. Unlike SiC abrasives, the spherical geometry of the GB particles is likely to reduce the contact stress and the fraction of polymer removed as debris, resulting in a lower wear rate than experienced using SiC abrasives.

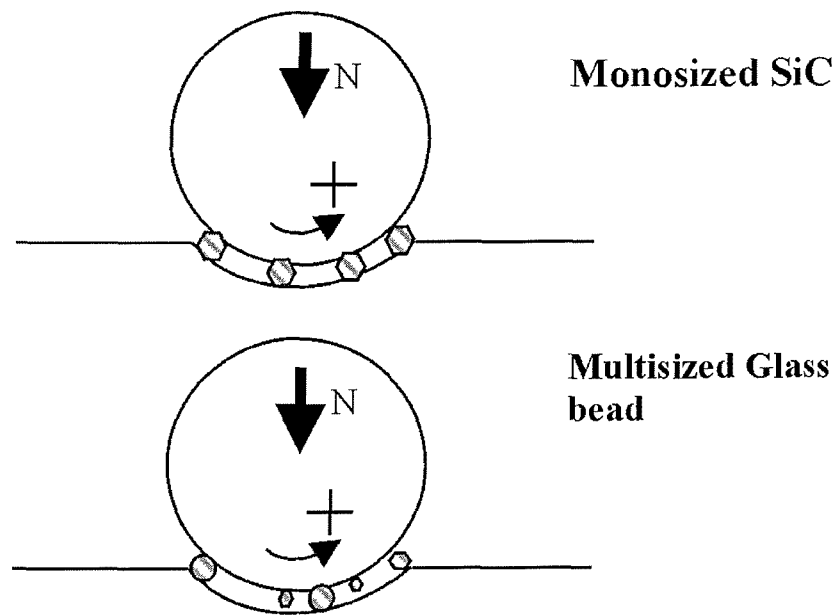


Figure 7.16: Schematic of the ball-on-coating contact for the cases where SiC and glass beads were used as abrasives

The smaller glass beads which pass through the contact, with lower loads per particle, either contact elastically and cause no wear, or abrade by rolling abrasion mechanisms. This is supported by SEM images of the glass beads tests, Figure 7.17 (a and b), which shows a marked difference in mechanism from those of the SiC abrasive tests. The worn surface of Figure 7.17 is characterised by irregular, rough grooves filled with spherical abrasive particles. The nature of the rough grooves suggests that plucking (adhesive) type mechanisms are present and probably explains why the skin effect was not observed in Figure 7.15.

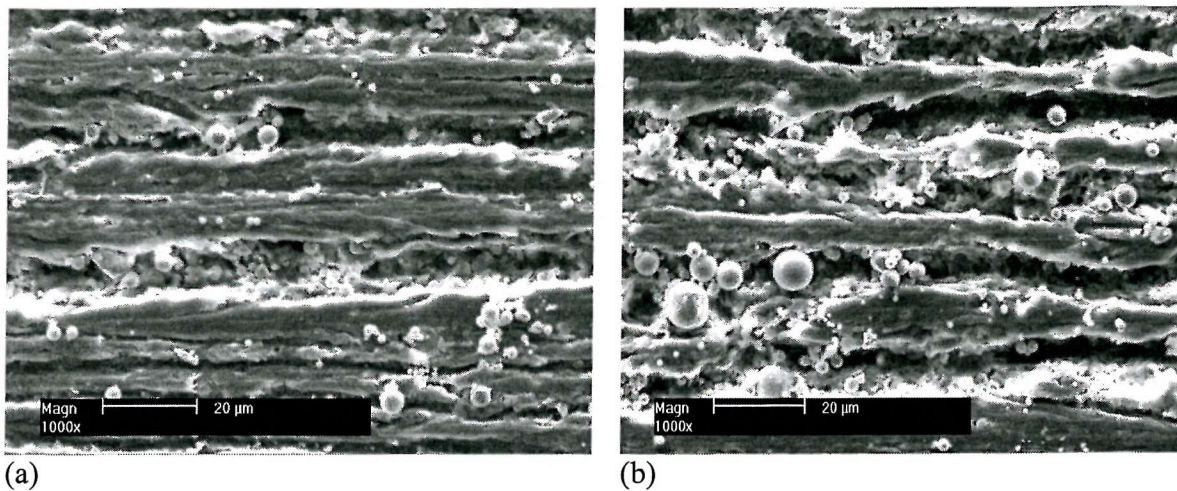


Figure 7.17: SEM images of the worn samples for the GB abrasive tests (a) at 120 m SD, 6 N load and, 0.1 m/s (b) at 140 m sliding distance 6 N load and 0.1 m/s.

7.3.5 Effect of speed on wear rate

The effect of speed on the wear rate of the polyamide 11 TP-9 coating was investigated using glass bead abrasives. The results are presented in Figure 7.18 and show a complex relationship between the wear rate and sliding speed.

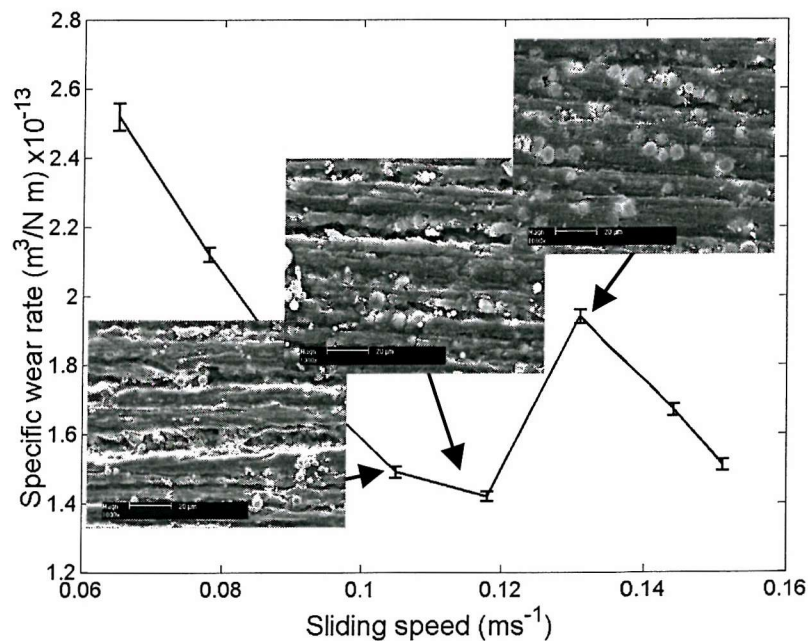
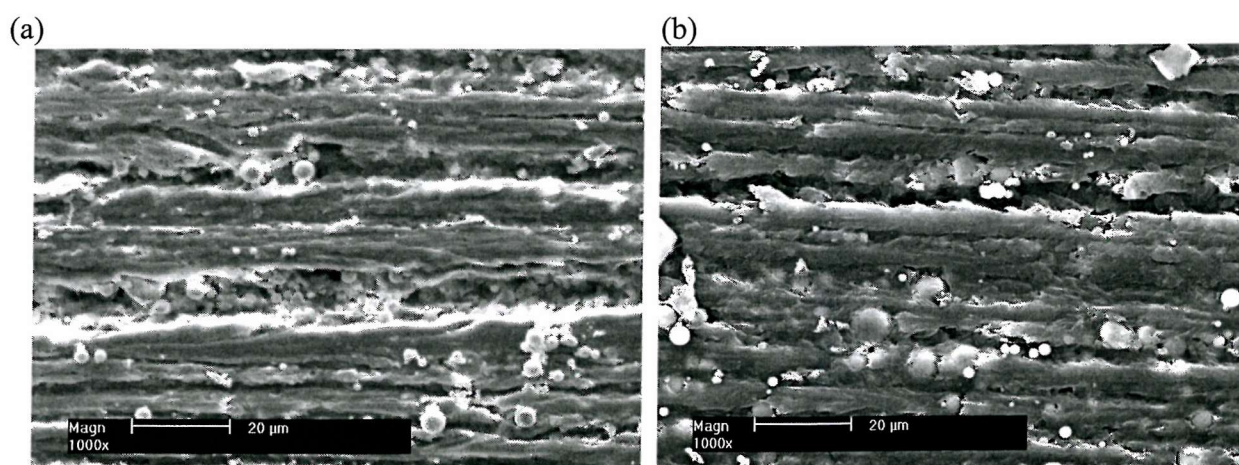


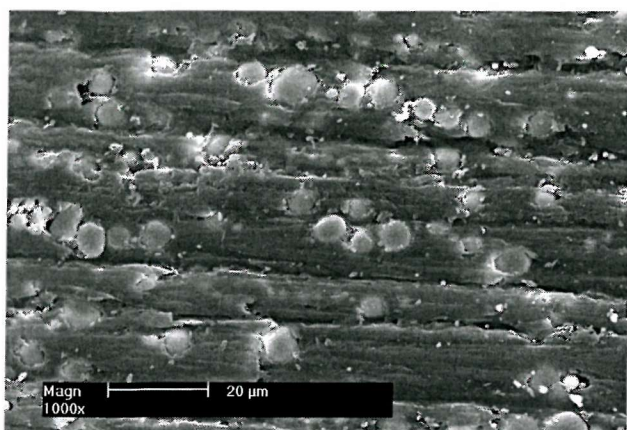
Figure 7.18: Result of the wear rate plotted against the sliding speed. The load was 6 N and sliding distance was 100 m using GB abrasives.

For a dry abrasive condition, frictional heating generated at the sliding contact between the polymer coatings and the counterface is known to be responsible for thermal softening leading to increased wear rates as the sliding speed is increased [7.12].

This result is contrary to the present work. This suggests that either the coating is not very sensitive to the frictional heating because of the carbon black present in the coating (carbon black helps to reduce friction) or there are other factors such as the influence of the hydrodynamic film between the ball and coating, which may be responsible for this behaviour. Lancaster [7.13], in his earlier work has reported a similar trend to that observed in Figure 7.18. It was suggested that temperature generation at the dry sliding contact often results in a mechanistic change in the wear mode, which usually occurs at a critical speed. This may be the case in Figure 7.18 where the wear rate suddenly increases at a speed of 0.13 m/s and then decreased again. However, there is no conclusive evidence to suggest a mechanistic change in the wear mode in this study. In addition, it is difficult to draw a direct comparison between the result in this study and that observed by Lancaster [7.13] because the sample studied in that work relates to dry sliding of leaded brass on hardened steel. However, this study relates to two-body abrasion of a polymer-based coating.

The SEM of the worn samples, Figures 7.19 (a-c) shows increasing embedment of the abrasive particles within the coating with increasing sliding speed.





(c)

Figure 7.19: SEM images of the worn samples for the GB tests, sliding distance of 100 m at (a) at 0.12 m/s sliding speed and load of 6 N, (b) at 0.13 m/s sliding speed and load of 6N, (c) at 0.15 m/s sliding speed and load of 6N.

This behaviour is a result of thermal softening induced by frictional heating in the coating during sliding contacts. This embedment probably is a better explanation of the decrease in wear rate with increasing sliding speed. Other investigations have identified that a combination of low slurry concentration and high applied load may cause total embedment of abrasive particles in a coating during sliding contacts in micro-scale abrasive wear tests [7.4]. The load (6 N) and slurry (0.375 g/cm^3) used in this study are considered to be high and low respectively.

7.3.6 Control test

For comparison purposes, a control test was performed on monolithic polyamide 11 samples using the test conditions for the SiC abrasive, see Table 7.1 with variable test time. The results of the test, shown in Figure 7.20, show good agreement between the coating and monolithic sample over a sliding distance of 40 m. However, the monolithic sample showed a sudden increase in wear rate at 100 m compared with 40 m observed for the coating. Both tests did not strictly obey the Archard wear law, which predicts a linear relationship. It is worth noting that the wear volume per unit load at a sliding distance of 140 m for the monolithic sample is 1.4 times higher than that of the coating. Overall, this shows that the coating performed better over a longer sliding distance than the monolithic polyamide 11, probably due to improved properties induced by the manufacturing process.

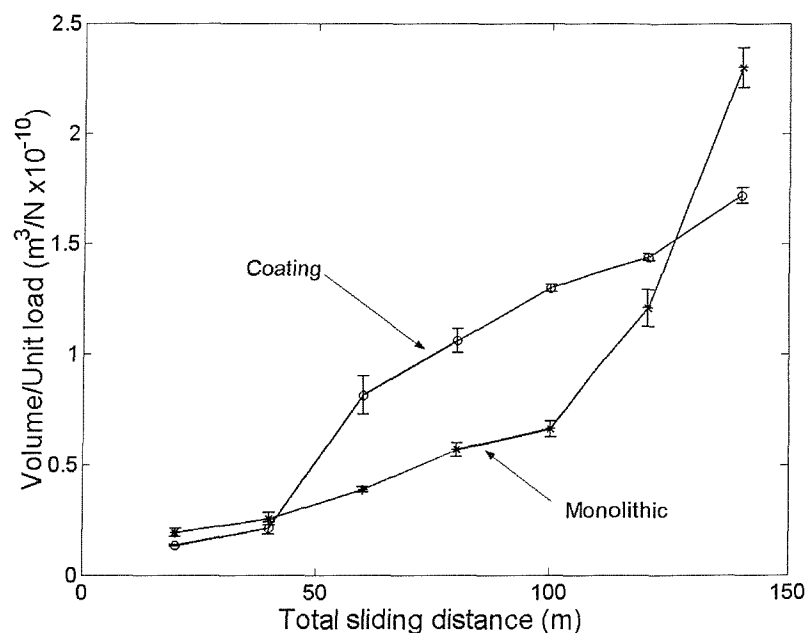


Figure 7.20: Comparison between the results of the coating and monolithic tests at 0.1 m/s and 6 N normal load (SiC).

7.3.7 Summary

Overall, the experiments have repeated well, which is evident by the small error bars on figures. Micro scale abrasion wear test have shown a more severe wear than the wireline using SiC and spherical glass bead abrasives. Several factors have been identified to be responsible for the wear performance of the micro scale abrasion wear test of the coating studied, among which are: the morphology of the abrasives used in slurry (shapes and size range), slurry concentration, applied normal load (load per abrasive particle), sliding distance, sliding speed (frictional heating generated at sliding contact). The wear mechanism is predominantly micro ploughing, which is characterised by grooves of differing peaks and troughs. Total embedment of the abrasive particles were observed for the spherical glass bead abrasive tests, which are thought to offer some resistance to wear of the coating. The intrinsic properties of the coating such as: hardness and toughness are thought to have a considerable impact on the wear performance of the coating, although this investigation is not conclusive as at the time of this report. In all, the micro scale abrasive wear test method has shown to be a more reliable wear test method compared with the pin-on-wire. This is because the method offers a better control of the test parameters

and allows a micro-scale wear test to be performed on the coating. With this method, it was possible to measure the crater depth as wear progresses, consequently, the primer and substrate wear (not reported) can be measured. However, the pin-on-wire wear test method allows a true tribo-couple to be performed on the coating.

7.3.8 Other abrasives

Abrasive morphology was identified as a major cause of discrepancies in wear rates produced by the micro-abrasion and the pin-on-wire tests. To further establish this fact, the effect of a less angular, cuboid-shaped natural diamond abrasive on wear rate of TP-9, TS-5 and TS-7 was studied. Preliminary indications suggest that diamond abrasive produced a wear rate about 62.5 times lower than the silicon carbide abrasives, see Figure 7.21. For instance, typical values for diamond abrasive micro abrasion tests are $2.0 \times 10^{-14} \text{ m}^3/\text{Nm}$, compared to that of silicon carbide abrasive, $1.3 \times 10^{-12} \text{ m}^3/\text{Nm}$. The difference observed is thought to be due to difference in the morphology of the two abrasives. In addition, it appears that the thermoset coatings are generally less wear resistant than the thermoplastic coating, TP-9, which is consistent with the pin-on-wire test.

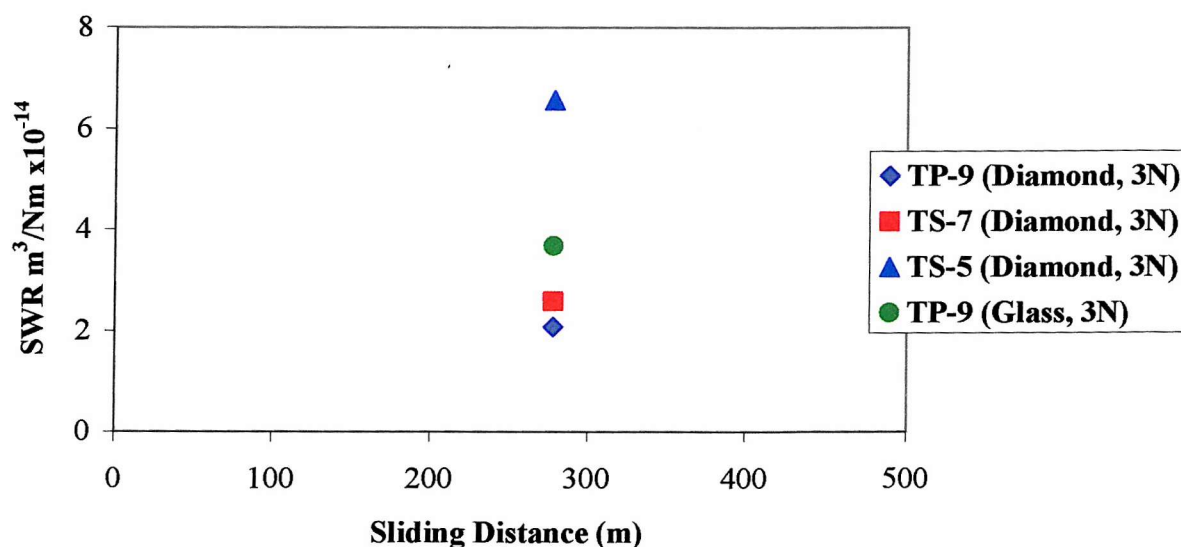


Figure 7.21: Graph comparing wear rate of TP-9 and other thermosets using glass abrasives (2-10 μm), or natural diamond (4-8 μm) sizes.

7.4 Conclusions

1. The study of polyamide 11 coatings using the relatively new micro-abrasion approach was found to have superior repeatability when compared to wireline test methods.
2. The micro-abrasion test using SiC produced an identical wear mechanism to that produced in wireline tests but was found to generate wear rates between 140 and 400 times greater. Therefore the micro-abrasion test is proposed as a candidate for '*accelerated*' testing of these coatings.
3. Experiments using glass beads aimed at better simulation of the wireline contact resulted in lower (5 times) wear rates compared to the SiC abrasive tests. However, this reduction can be partly explained by abrasive embedment in the coating, as a result of frictional heating, which altered the contact. The abrasive shape change from angular to round also explains the wear rate reduction.
4. Experiments show that the wear rate generally follows the Archard wear law but a significant change in wear rate was observed at a crater depth of 50 μm , indicating the presence of a more wear resistant surface layer (termed '*skin effect*') approximately 50 μm in depth. Comparisons with monolithic polyamide 11 show no such feature indicating that the skin effect is probably related to the coating deposition process.
5. The wear rate of the polyamide 11 coating out-performed the monolithic polyamide 11.

References

- 7.1 Shipway, P. H., The Role of Test Conditions on the Micro-Abrasive Wear behaviour of Soda-lime Glass, *Wear*, 233-235 (1999) 191-199.
- 7.2 Allsopp, D. N. Trezona, R. I., Hutchings, I. M. The Effect of Ball Surface condition in the Micro-Scale Abrasive Wear Test, *Tribology Letters*, 5 (1998) 259-264.
- 7.3 Rutherford, K. L. and Hutchings I. M., Theory and Application of a Micro-Scale Abrasive Wear Test, *JTEVA*, 25 (2) (1997) 250-260.
- 7.4 Trezona, R. I., Allsopp, D. N., Hutchings, I. M., Transitions between Two-Body and Three-Body Abrasive Wear: Influence of TEST conditions in the Micro-Scale Abrasive Wear Test, *Wear*, 225-229 (1999) 205-214.
- 7.5 Mergler. Y. J and Huis. A. J., Micro-abrasive wear of semi-crystalline Polymers. *Tribological Series*, 4 (2003) 165 - 173.
- 7.6 Stack M and Mathew, M., Micro-Abrasion Transitions of Metallic Materials, *Wear*, 255 (2003) 14 – 22.
- 7.7 Bello, J. O., Evaluation and Characterisation of the Tribological Properties of Polymeric Coatings for Downhole Application. MPhil/PhD Transfer thesis, School of Engineering Sciences, University of Southampton (2002).
- 7.8 Rutherford, K. L., Trezona, R. I., Ramamurthy, A. C., Hutchings, I. M., The Abrasive and Erosive Wear of Polymeric Paint Films, *Wear*, 203-204 (1997) 325-334.
- 7.9 Adachi, K and Hutchings, I. M., Wear-Mode Mapping for the Micro-Scale Abrasion Test, *Wear*, 255 (2003) 23 – 29.
- 7.10 Symonds, N., Wear and Impact of Polymeric Coatings. PhD thesis, School of Engineering Sciences, University of Southampton (2000).
- 7.11 Williams, J. A., Wear Model: Analytical, Computational and Mapping: a continuum mechanics approach, *Wear*, 225 (1999) 1-17.
- 7.12 Evans, D. C and Lancaster, J. K. *Wear*, 13 (1979) 85-139.
- 7.13 Lancaster, J. K. The formation of surface films at the transition between mild and severe metallic wear, *Proc. Roy. Soc. A* 273 (1963) 466 – 483.

8.0 Micro-abrasion performance of filled and unfilled PA11 coatings: Influence of fillers and coating properties on wear rates and wear mechanism

8.1 Introduction

In Chapter 7, the possible replacement of the wireline wear test methods with the relatively new micro-abrasion approach to study the abrasion resistance of PA11 coatings was advanced. It was concluded that, although the micro-abrasion test method will be broadly suitable for accelerated wear tests, its overall superiority over the wireline wear test methods lies in the repeatability and the ability to have a better control of the test conditions.

However, two important observations were made on the behaviour of PA11 coating (TP-9), which have led to this study of filled and unfilled PA11 coatings. First, a significant change was observed in the wear rate of TP-9 with depth, and has been attributed to the presence of a more resistant layer termed “skin effect”. Secondly, total embedment of the glass abrasive particles was observed to aid abrasion resistance in TP-9 coating. There were questions about the manufacturing process/method adopted for depositing the coating, as there appears to be some manufacturing induced defects. In addition, considering the behaviour of the embedded glass abrasives, it was thought, after due consultation with another coating manufacturer, that inclusion of suitable filler particles could further enhance the properties of the coating.

Hence, new coatings were formulated with filler reinforcement whilst keeping the same matrix. The ‘skin effect’ observed in TP-9 raised the question of whether different layers of the coating may have cooled at different rates during coating deposition. It has been established in section 2.1.1 that PA11 have the ability to form different structures when a different mode of cooling is used to cool the polymer from the melt. In line with this, coatings were deposited and cooled by different modes: water-cooled and air-cooled, in order to investigate the effect of cooling on wear rate and wear mechanism of the coatings; all other coatings were air-cooled. In all, four different experimental coatings supplied by Atofina designated coating A to D, were investigated in this study

and compared with commercially available coating E and monolithic PA11. Two variants of coating A were produced: one was air-cooled and the other water-cooled. Details of the coatings are shown in Table 8.1 and have been characterised previously in chapter 3.

8.2 Experimental details

The experimental details employed in this study are similar to that described for the SiC abrasive test in section 7.1.1.

8.2.1 Tensile test method

The test procedure used for investigating the mechanical properties of the Atofina coatings is described in the ASTM standard D638 “Standard Tensile test Methods for plastics”. Tests were conducted at 22°C using an Instron 1197 tester with a 1 mm/minute extension rate. The stress-strain curves for all the coatings (A-D) are detailed in Appendix 3.

Designation	A	B	C	D	E (TP-9)	Bulk
Resin type	PA11 (powder)	PA11 (powder)	PA11 (powder)	PA11 (powder)	PA11 (powder)	PA11
Filler type	None	None	TiO ₂	TiO ₂ and Dolomite	None	None
Colour	Colourless	Black (contains 2 % carbon black)	Blue (contains blue pigment and carbon black)	Blue (contains blue pigment and carbon black)	Black (contains 2 % carbon black)	White
Filler percentage	NA	N/A	14 %	16.5 %	N/A	N/A
Filler size (µm)	NA	N/A	1-2	1-5	N/A	N/A
Filler shape	NA	N/A	Cuboids	Cuboids	N/A	N/A
Matrix thickness (µm)	350 – 400	350- 400	350- 400	350- 400	270	8000
Primer type	Phenolic	Phenolic	Phenolic	Phenolic	Phenolic	N/A
Primer thickness (µm)	10 – 15	10 - 15	10 - 15	10 - 15	10 - 15	N/A
Surface roughness (Ra, µm)	0.60 ± 0.01	0.40 ± 0.03	0.20 ± 0.06	0.30 ± 0.07	11.00 ± 0.20	0.70 ± 0.05

Table 8.1: Details of the coatings studied. The bulk sample is included for comparison purpose. Note the inclusion of Coating E (TP-9) is for comparison.

Conditions/Experiments	Variable Load	Variable sliding distance
Applied load (N)	2 - 10	6
Speed (m/s)	0.1	0.1
Ball radius (mm)	25	25
Sliding distance (m)	154	20 - 140
Temperature (°C)	25	25
Slurry concentration (g/dm ³ of H ₂ O)	375	375
Slurry feed rate (drops/min)	10	10
Slurry type	SiC	SiC

Table 8.2: Details of the test conditions employed in this study.

8.2.2 Methodology

The methodology used in this study has been previously described in section 7.2. Thus direct comparisons between the TP-9 and the new coatings can be made. The experimental conditions used in this study are similar to that used for the SiC abrasive test in section 7.2, and are detailed in Table 8.2.

8.3 Results an discussion

One of the reasons for opting for the micro-abrasion test method is because of its repeatability. Bello and Wood ^[8.1] have quantitatively established the repeatability of this test method over other methods such the wireline test methods, in terms of the percentage standard error.

8.3.1 Effect of load on wear rates

Plots of volume loss per unit sliding distance (mm³/m) versus load (N) show a linear relationship for all the samples. The slopes or specific wear rates, k , (with units m³/Nm) for the coatings and monolithic sample are tabulated in Table 8.3 along with the values of the correlation coefficient R^2 as a measure of the goodness-of-fit.

Figure 8.1 is the plot of k values of all the coatings, which also include the data for coating E (TP-9), for variable load. It can be seen that coating E (TP-9) produced the highest value of k while the water-cooled coating A has the least specific wear rate.

Comparing the water-cooled coating A (WC) and the air-cooled coating A (AC) would suggest an early indication of the influence of the cooling mode. For example, the k value for AC coating A is approximately 1.5 times higher than the k value for WC coating A, suggesting a better abrasion resistance by WC coating A.

The significance of the application technique can also be seen from Figure 8.1 by comparing the value of k for coating B and coating E (TP-9) with nominally the same composition. Coating B, which was deposited by a hot-dip process show a wear rate that is 1.4 times lower than coating E which was applied by a hot spray process using a spray gun.

However, among all the four new coatings (A – D), coating C is the least abrasion resistant. Figure 8.2 shows the results for coating B, which has the least best fit to a linear trend of all the samples tested, see Table 8.3. However, the data shows reasonable agreement to that expected by the Archard wear law, see Equation 6.1.

	Air cooled (m ³ /Nm)	R ²	Water cooled (m ³ /Nm)	R ²
Coating A	6.94×10 ⁻¹³	0.995	4.75×10 ⁻¹³	0.977
Coating B	6.63×10 ⁻¹³	0.973		
Coating C	8.38×10 ⁻¹³	0.988		
Coating D	7.37×10 ⁻¹³	0.978		
Coating E	9.40×10 ⁻¹³	0.980		
Monolithic PA11	5.89×10 ⁻¹³	0.999		

Table 8.3: Specific wear rates ($SWR_{(load)}$) from variable loading (2 – 10 N) and correlation coefficients (R^2) for 154 m sliding distance.

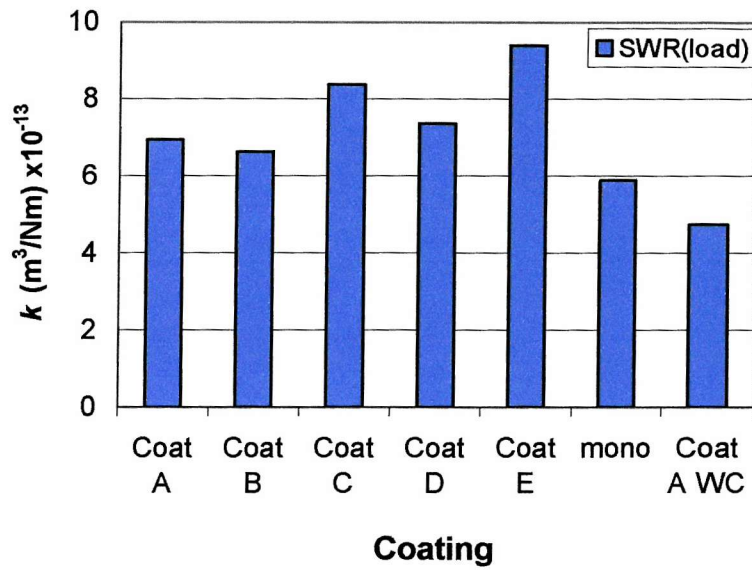


Figure 8.1: Graph showing the SWR of all the coatings for variable loading.

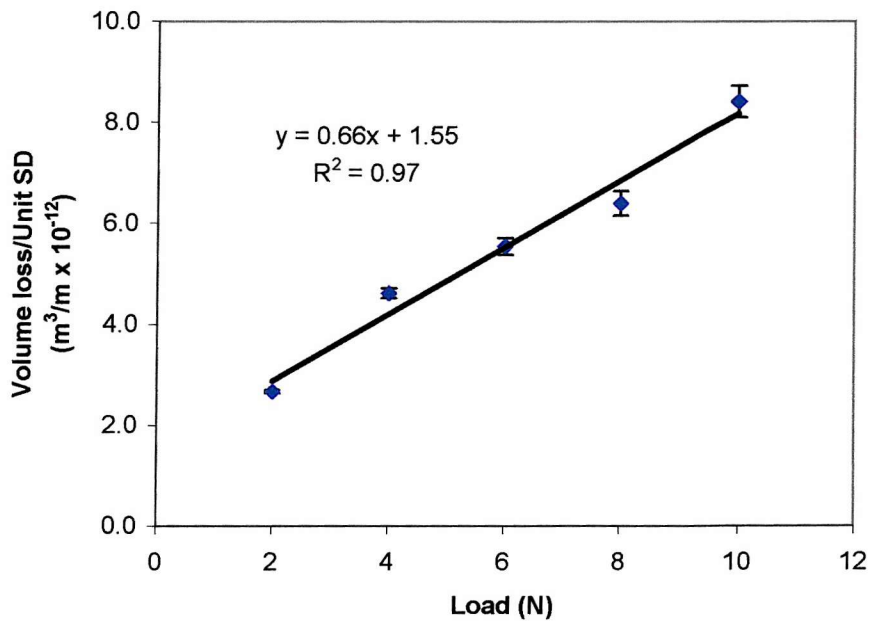


Figure 8.2: Volume loss per sliding distance (V/D) versus load (L), at a sliding speed of 0.1 m/s and sliding distance of 154 m for coating B.

Figure 8.3 plots the SWRs of all the samples as a function of load. The wear rates gradually decrease with increasing load, Coating D appears to be the most sensitive to load since the wear rate at 10 N is half that at 2 N. Coating C is the least abrasion resistant coating over this load range while no coating matches the performance of the monolithic polyamide 11.

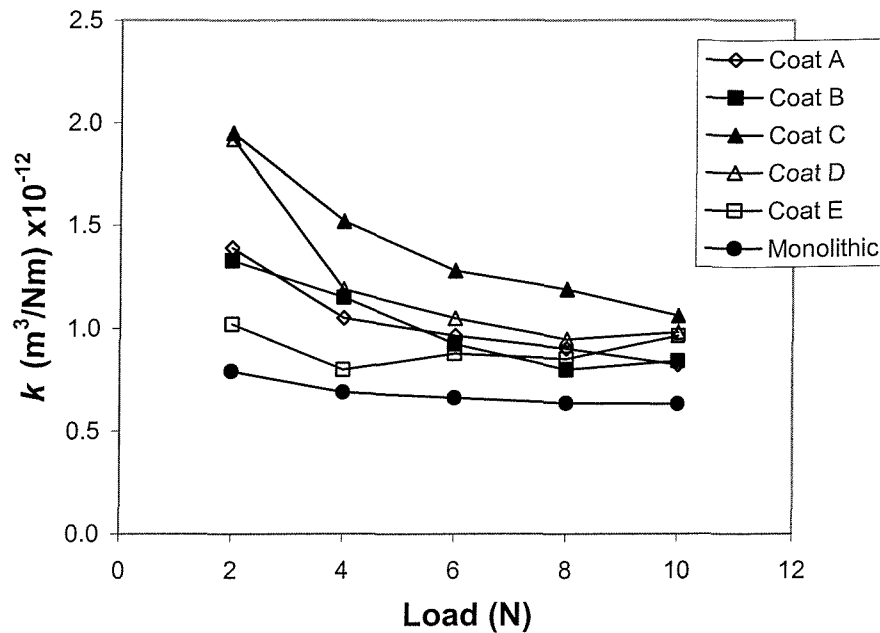


Figure 8.3: *SWR (m^3/Nm) of the coatings versus load (L), at a sliding speed of 0.1 m/s and sliding distance of 154 m.*

Figure 8.4 illustrates the wear rate as a function of load for the air and water-cooled samples along with the results for the commercial Coating E and monolithic sample. The relative performance of the two coatings is dependent on the load, with the WC Coating A being superior at loads above 4 N whereas the AC is superior at lower loads (2 N). SEM examination of the two coatings at 2 and 6 N are shown in Figure 8.5. At low load, the wear mechanisms appear slightly different between the WC and AC samples. The WC sample has the smoother wear surface but suffered a greater wear rate compared to the more grooved surface of the air-cooled sample. The lack of extruded lips, Figure 8.5 (a), on either side of the grooves on the water-cooled sample may indicate more efficient material removal by plastic extrusion processes.

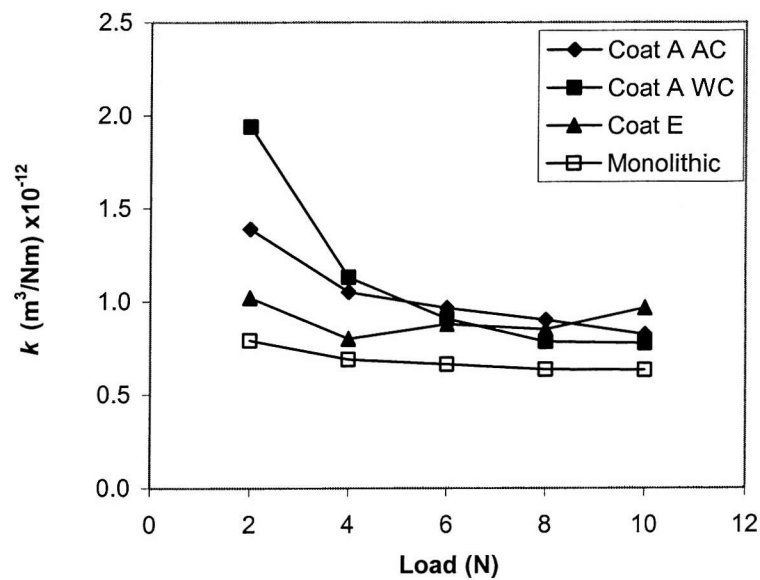
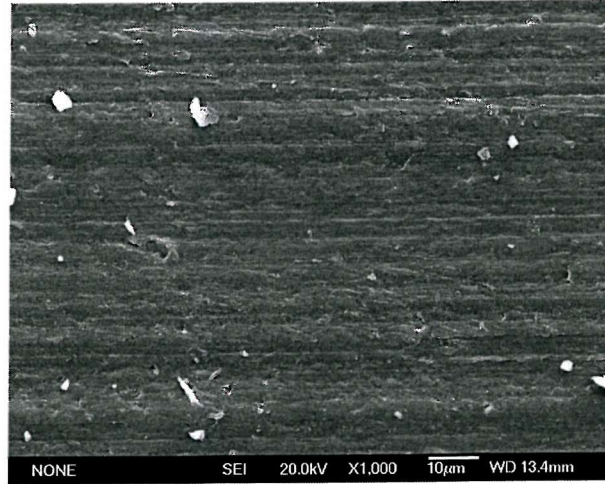


Figure 8.4: SWR (m^3/Nm) versus load (L), at a sliding speed of 0.1 m/s and sliding distance of 154 m for air and water-cooled sample compared with Coating E and the monolithic PA11.



(a)



(b)

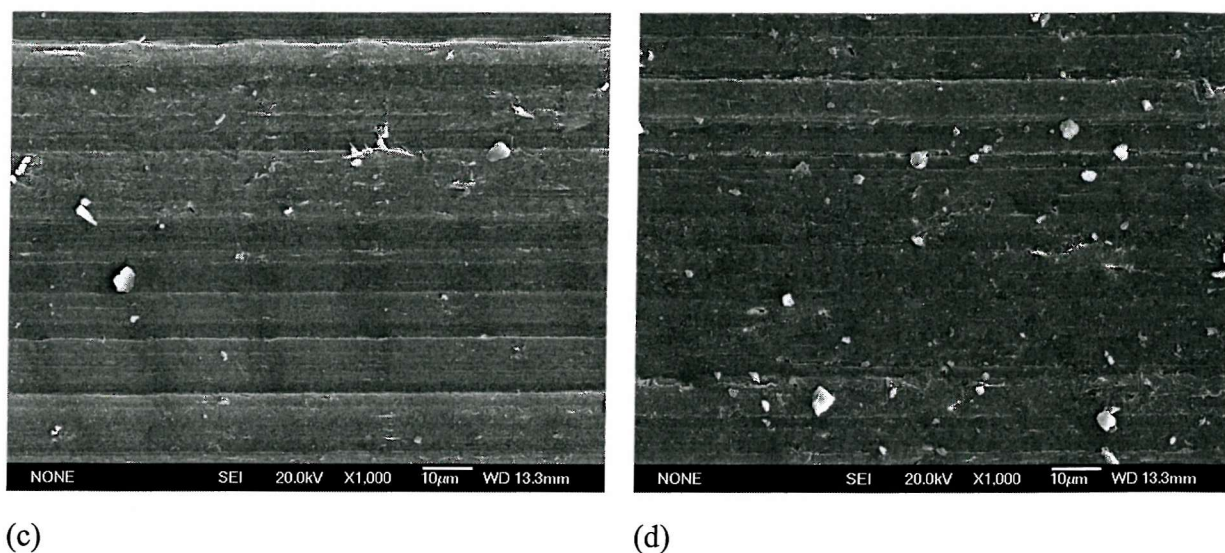


Figure 8.5: SEM of worn surface of (a) water-cooled and (b) air-cooled both at 154 m and 2N respectively, (c) water-cooled and (d) air-cooled both at 20 m and 6 N respectively.

The rate of cooling is likely to affect the degree of crystallisation and entanglement density at the near surface of the coating. In polyamide 11, $[(CH_2)_{10}-CO-NH]_n$, the polarity of the amide group induces hydrogen bonds between chains that are crucial to the crystalline structure. During the forming from the melt, the polyamides are sheared, which leads to persistent chain alignments due to hydrogen bonds. The crystalline structure at room temperature depends on the cooling rate. A quench leads to the smectic delta' structure, whereas a slow cooling favours the formation of the triclinic alpha phase in addition to the smectic delta' phase {see section 2.1.1}, ^[8.2]. Thus, the superior wear resistance shown by coating A WC over coating A AC at high loads suggests that the formation of the smectic delta structure is beneficial to wear resistance at high loads but not at low loads.

Lancaster ^[8.3] suggested that large spherulites produced by slow cooling are detrimental to wear resistance, as they tend to reduce elongation to break and the toughness of polymers. Similarly, Fedorchuk ^[8.4] observed that the optimum wear resistance of a particular polyamide (polycaprolactum B) was obtained when a heat treatment produced spherulites of 3-4 μm in diameter.

The wear mechanisms for Coatings A (AC), B, C and D at 10 N after 154 m sliding are shown in Figure 8.6. Comparative observations of Coating A and B does not reveal any obvious difference between the two micrographs. Micro-ploughing is the dominant wear mechanism, characterised by the formation of grooves, typical of 2-body abrasion, with extruded filaments of polyamide at the edges of the grooves.

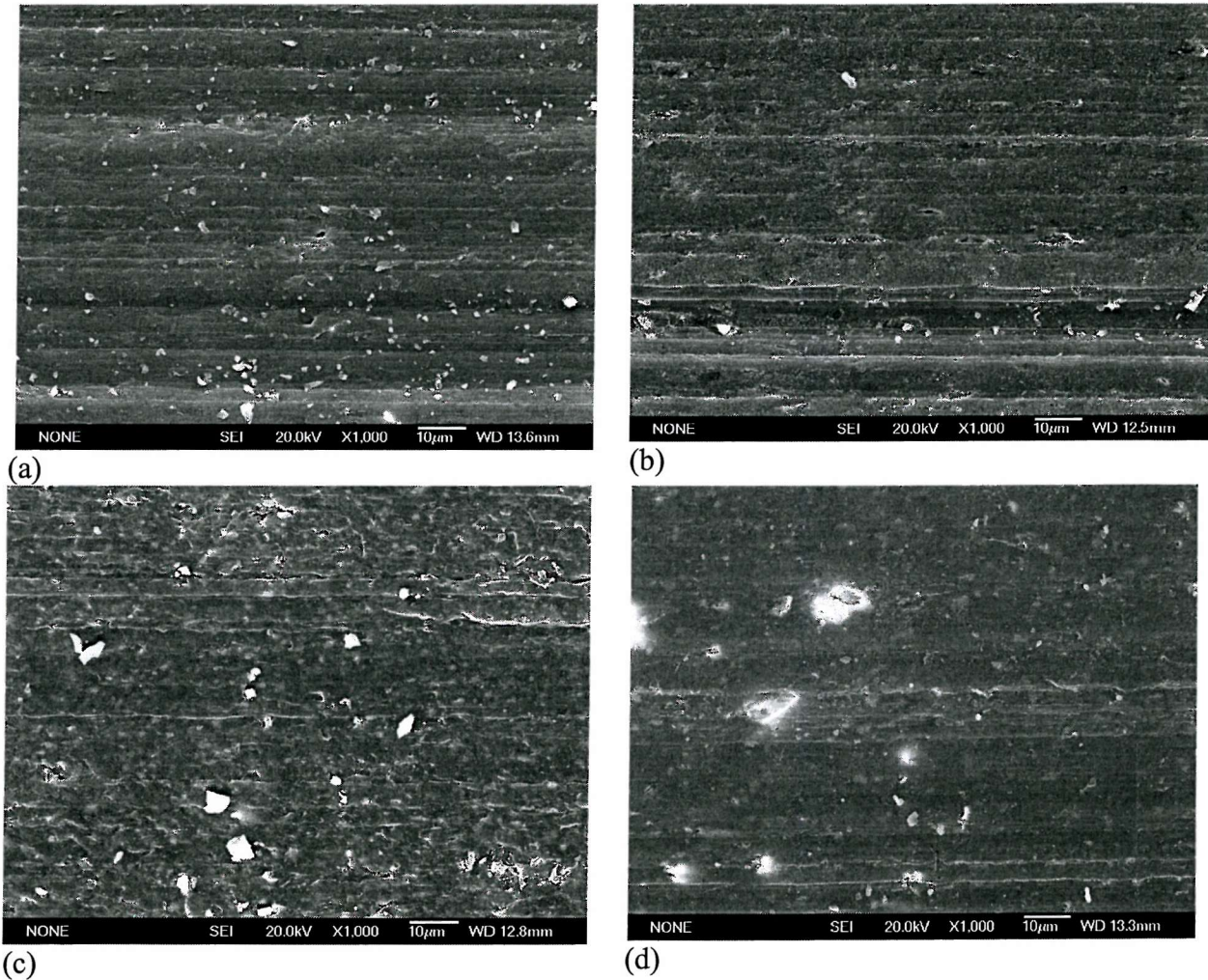


Figure 8.6: SEM of worn surface of (a) Coating A, (b) Coating B, (c) Coating C and (d) Coating D all at 10 N and sliding speed of 0.1 m/s.

The grooves in Figure 8.6 (a and b) are smooth with no obvious surface defect such as cracks. However, differences between these coatings and coatings C and D are noticeable. The wear scars of the filled coatings show more delamination and 'pitting' type damage to Coating C, which has the highest wear rate, while filler disbondment from the polymer matrix is seen on Coating D. The 'pitting' type of damage found in

Coating C would suggest a fatigue process during wear. While not ruling out this possibility, no evidence was found to suggest that wear involves fatigue process. The presence of dolomite second filler in Coating D may be the reason for superior wear rate shown over Coating D. The wear rates obtained in this study compare with values around $6.5 \times 10^{-11} \text{ m}^3/\text{Nm}$ for monolithic polyamide 11 obtained by Rajesh et. al. [8.5], tested under dry abrasion conditions using 80 grade ($175 \mu\text{m}$) SiC at 0.05 m/s sliding speed and loads between 4-10 N. The difference between the value of wear rate obtained in this study and that observed by Rajesh et. al. [8.5] can be attributed to the size of the abrasive ($175 \mu\text{m}$) used by the authors, and the fact that the test was performed under dry conditions compared to slurry abrasion adopted for this study.

8.3.2 Effect of sliding distance on wear rates

Figure 8.7 is the volume loss per unit load (V/L) versus sliding distance (D) for coating B, showing a good agreement with the Archard wear law, see Equation 6.1. Table 8.4 shows the specific wear rates and correlation coefficient obtained from the slope of such plots for all the samples.

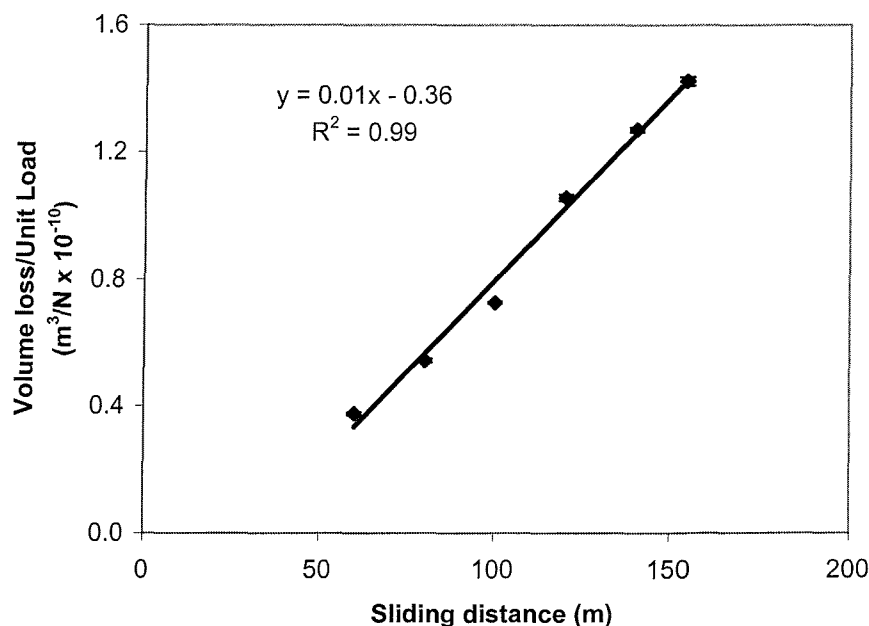


Figure 8.7: Plot of the wear volume per unit load (V/L) against sliding distance (m) for Coating B.

	Air cooled (m ³ /Nm)	R ²	Water cooled (m ³ /Nm)	R ²
Coating A	1.16×10 ⁻¹²	0.991	7.84×10 ⁻¹³	0.955
Coating B	1.16×10 ⁻¹²	0.991		
Coating C	1.70×10 ⁻¹²	0.991		
Coating D	1.31×10 ⁻¹²	0.987		
Coating E	1.09×10 ⁻¹²	0.991		
Monolithic PA11	0.63×10 ⁻¹²	0.978		

Table 8.4: Specific wear rates ($SWR_{(SD)}$) from variable sliding distance (20 – 140 m) and correlation coefficients (R^2) from volume loss at 6 N.

Table 8.4 thus confirms that all coatings appear to obey the Archard wear law. These results are also plotted on Figure 8.8 and show more sensitivity between the different coatings than the results obtained for the variable loads, see section 8.3.1.

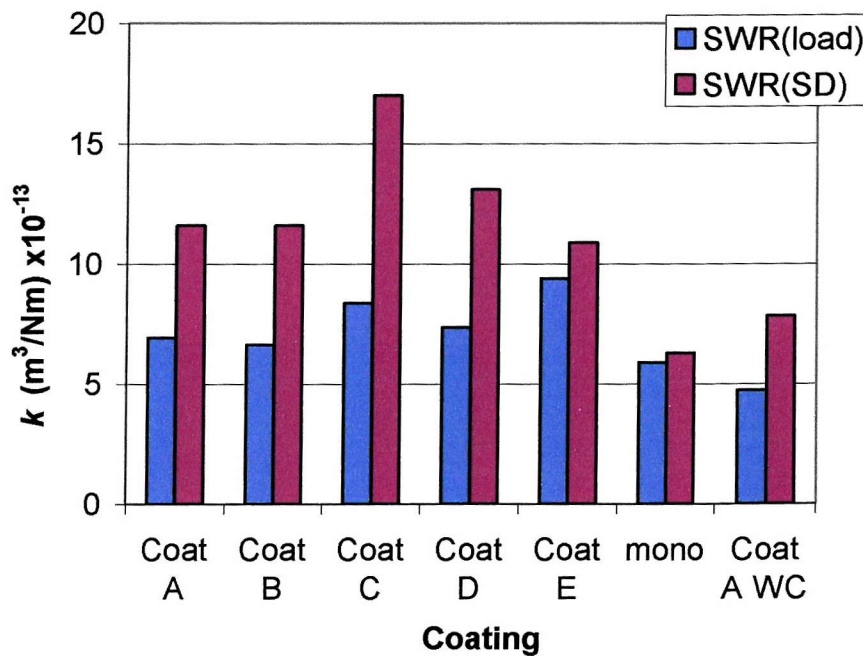


Figure 8.8: Comparison between the $SWR_{(load)}$ for the variable load and the variable sliding distance.

A complex relationship between the specific wear rate and sliding distance for coatings E and C as well for the monolithic sample are seen in Figure 8.9. The

coatings E and C suffer significant increases in wear rate after 40 m and 80 m of sliding, respectively. The reasons for this behaviour in the commercial unfilled PA11 coating E has been discussed in detail elsewhere ^[8.1] and suggests a skin effect or inhomogeneous coating structure with depth. The wear rate of the monolithic sample, after 120 m of sliding, appeared to increase but after 150 m returns to a similar level to that seen between 0-120 m. The effect of the expected reduction of load per particle as the wear scar develops (increases in diameter) over the test duration, see Trezona ^[8.6], could also explain these changes in wear rate with sliding distance but not in a consistent way, as the other coatings appear to have constant wear rates as a function of sliding distance. The general increase in wear rate seen for coatings (A – D) and the monolithic sample after about 60 m sliding could be also be associated with fatigue issues.

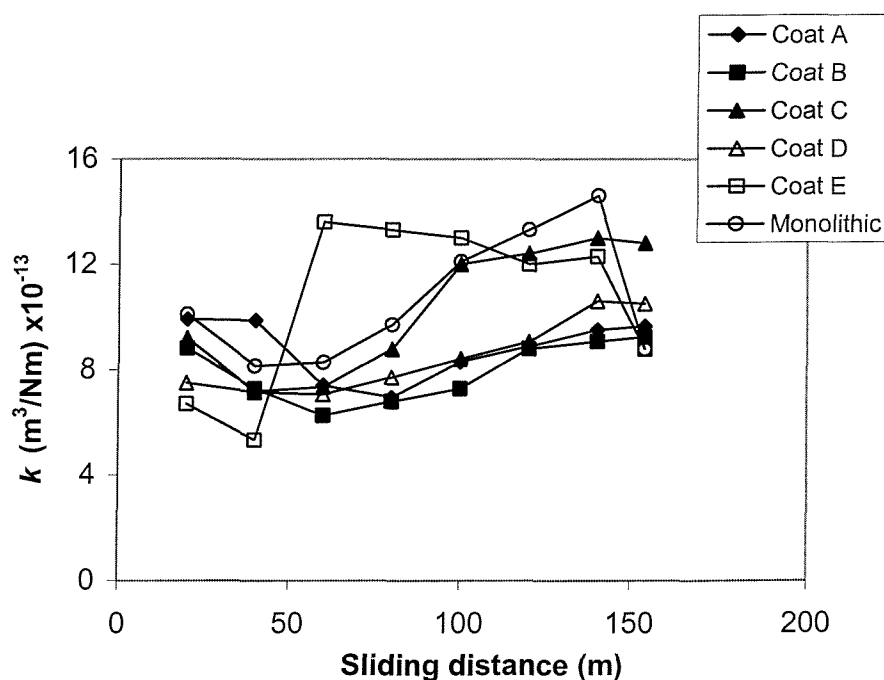


Figure 8.9: SWR (m^3/Nm) of the coatings versus sliding distance (m), at a sliding speed of 0.1 m/s and normal load of 6 N.

As with the results based on varying loads (SWR_{load}), the influence of coating cooling mode is also seen when comparing wear rates based on sliding distance (SWR_{SD}) of AC and WC coatings, with a 32% increase in resistance offered by the WC coating.

8.3.3 Effect of fillers on wear resistance of coatings

By comparing Coating A with B, the addition of 2% carbon black can be seen from Figure 8.8 to have little influence on the abrasion of these coatings. However, the addition of brittle fillers to polymer coatings is known to influence their wear performance. The addition of 14% TiO₂ into Coating C and 16.5% TiO₂ and Dolomite (typically contains 40 to 45% MgCO₃ and 54 to 58% CaCO₃) into Coating D have detrimental effects on wear resistance as shown on Figure 8.8. The addition of 14% TiO₂ appears to be worst than adding 16.5% TiO₂ and Dolomite. The presence of Dolomite offers approx. 20% better wear resistance compared to the TiO₂ filled coating C.

There are several mechanisms that could explain an increase in wear rate for filled coatings. As Table 8.5 shows, the SiC abrasive is harder than both the filler materials and thus is likely to abrade the fillers or induce stresses beyond the crush strength of the filler to cause filler fragmentation.

	SiC	TiO ₂	Dolomite
Mohs' Hardness	9.0-10.0	6.5 – 7.0	3.5 – 5.0
Specific Gravity	3.2	4.26	2.80 - 2.95

Table 8.5: Hardness and density details for the filler particulates and abrasive used.

This process would seriously undermine any reinforcement of the wearing surface and enhance wear rates. Secondly, the additions of angular fillers can act as stress raisers and promote tensile rupture of the polymer matrix and thus increase polymer wear rates. A third issue with filled coatings, is that of filler/matrix adhesion which controls the ability of SiC abrasives to pull-out filler particles by their micro-cutting action or through traction (the drawing or pulling action of the abrasives over the coating surface). A fourth issue arises from filler fracture or detachment from the polymer matrix. Due to the filler size range (2-5 µm) and some being slightly larger than that of the SiC abrasives (4.3 µm), they act as abrasives themselves until they are ejected

from the contact. Thus, a simple model of the total abrasion rate, A_T , for filled coatings can be postulated as:

$$A_T = A_M + A_F + \phi_F + \eta_F + \Delta A_M \quad \dots\dots\dots 8.1$$

Where

A_T is the total abrasion rate of coating/composite

A_M is the abrasion rate of matrix

A_F is the abrasion rate of fillers

ϕ_F is the rate of filler pull-out

η_F is the rate of filler fracture

ΔA_M is the additional abrasion rate caused by filler material from pull-out or fracture

8.3.4 Correlation between wear rate and mechanical properties

The mechanical properties such as UTS, σ_y , σ_b , ϵ_b and E of the coatings were investigated in order to understand any trend between mechanical properties and wear resistance of the coatings, see Table 8.6. The results show that addition of fillers is detrimental to the mechanical properties and appear to be governed by the product of stress at break (σ_b) and the strain at break (ϵ_b). For example, $\sigma_b \epsilon_b$ for coatings B, C and D are 1041, 629 and 260 N/m² respectively. This suggests the higher the percentage filler content the lesser the value of $\sigma_b \epsilon_b$ for the coatings. This is also evident in the superior wear rate shown by coating B over coatings C and D.

Thus, the results suggest that the wear rate should follow the Ratner-Lancaster model, see Equation 8.2.

$$W = \frac{C\mu}{H\sigma_b\epsilon_b} \quad \dots\dots\dots 8.2$$

where: W is the wear rate, C is a constant, μ is the coefficient of friction, H is the hardness and σ_b and ϵ_b are the stress and strain at tensile break respectively.

Air cooled	UTS (MPa)	Yield stress (MPa)	σ_b (MPa)	ϵ_b (%)	E (GPa)	SWR (m^3/Nm)
Coating A	28.3	13.1	25.9	55.8	0.34	6.94×10^{-13}
Coating B	32.0	15.9	27.4	38.0	0.45	6.63×10^{-13}
Coating C	35.1	23.6	30.7	20.5	0.48	8.38×10^{-13}
Coating D	20	13.3	18.6	14.0	0.47	7.37×10^{-13}
Monolithic PA11	56-66		44.0	320.0	1.28	5.89×10^{-13}

Table 8.6: Ultimate tensile stress (UTS) and Young's modulus (E) values for coatings from this study compared with the wear rates.

Figure 8.10 plots k (SWR) based on sliding distance and load as a function of $1/(\sigma_u \epsilon_u)$. Both k values show a linear relationship over the narrow range of $1/(\sigma_u \epsilon_u)$.

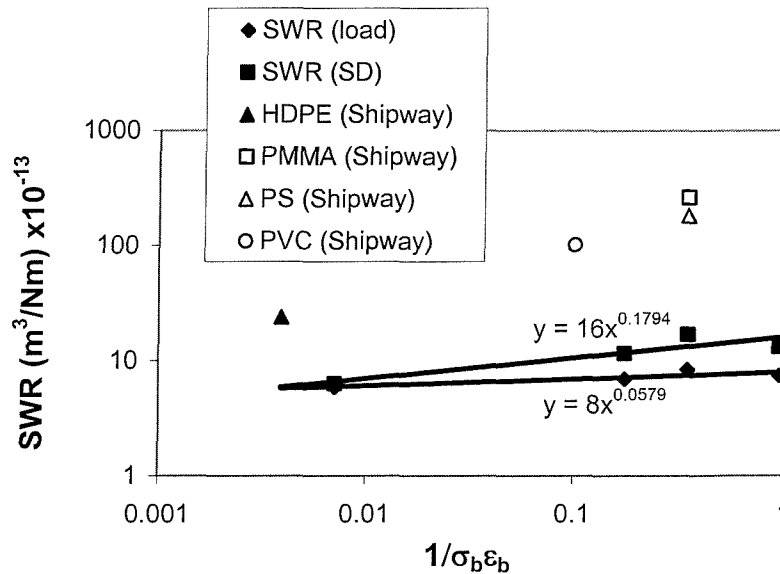


Figure 8.10: Comparing trends found between mechanical properties and SWR in this study with those of other authors.

This correlation shows that the predominant wear mechanism may possibly be related to tensile fracture and influenced by the work done given by the product of failure stress (after chain disentanglement) and strain (elongation) at failure. The processes of chain scission and increased crystallisation both weaken the material and lead to

embrittlement i.e. when the process of long chain formation in polymers ceases, the tendency is for the structure of the polymer to approach that of a crystal, causing embrittlement in the polymer. Figure 8.10 also includes data from the results of Shipway and Ngao ^[8.8], for a number of bulk polymers from micro-abrasion tests at 0.5N, 17.2% SiC slurry, and 0.112 m/s ball speed. Comparison between the results in this study and that of Shipway and Ngao would suggest that abrasion of the matrix, A_M is a function of $1/(\sigma_b \varepsilon_b)$.

8.4 Conclusions

1. Under extreme abrasive conditions some differentiation between tribological behaviour of PA11 based coatings was seen under the micro abrasion test method.
2. Fillers generally did not enhance wear resistance of the PA11 coatings. The addition of TiO_2 has a modest effect while the addition of TiO_2 and Dolomite reduces the values σ_b and ε_b . However, the presence of secondary dolomite filler was found to offer approximately 20% more wear resistance compared to the TiO_2 filled coating.
3. The unfilled coating exhibited a superior wear resistance compared with the filled counterpart, with ~30% higher abrasion resistance.
4. A model equation has been postulated for the overall abrasion rate of coatings during wear:

$$A_T = A_M + A_F + \phi_F + \eta_F + \Delta A_M$$

5. It has been shown that the abrasion of the matrix A_M is inversely proportional to $(\sigma_b \varepsilon_b)$
6. Correlation with Ratner-Lancaster shows that $k \propto \frac{1}{\sigma_b \varepsilon_b}$
7. The cooling mode was found to affect wear resistance of coatings at high load i.e. water-cooled coatings would be advantageous for high load applications compared to the air cooled coatings. This has been attributed to the possible formation of a smectic delta structure within the structure of the polymer.
8. Micro-ploughing is the dominant wear mechanism characterised by the formation of grooves, typical of 2-body abrasion, with extruded filaments of polyamide at the edges of the grooves.

References

- 8.1 Bello, J. O and Wood, R. J. K. Grooving Micro-Abrasion of Polyamide 11 Coated Carbon Steel Tubulars for Downhole Application, *Wear*, 255 (2003) 1157-1167.
- 8.2 Chocinski-Arnault L, Gaudefroy V, Gacougnolle JL, Riviere A, Memory effect and crystalline structure in polyamide 11, *Journal of Macromolecular Science-Physics*, B41 (4-6): (2002) 777-785.
- 8.3 Lancaster, J. K. Abrasive wear of polymers, *Wear*, 14 (1969) 223-239.
- 8.4 Fedorchuk, E. A. Effect of structure of a polyamide on its abrasion resistance, *Soviet Plastics*, 14 (2) (1966) 38.
- 8.5 Rajesh, J. J. Bijwe, J. and Tewari, U. S. Abrasive wear performance of various polyamides, *Wear*, 252 (2002) 769-776.
- 8.6 Trezona, R. I. Allsopp, D. N. and Hutchings, I. M. Transitions between two-body and three-body abrasive wear: influence of test conditions in the micro-scale abrasive wear test, *Wear*, 255-229, (1999) 205-214.
- 8.7 Lancaster, J. K. Basic mechanisms of friction and wear of polymers. *Plast. Poly.* 41 (1973) 297-306.
- 8.8 Shipway, P. H and Ngao, N. K, Micro-scale abrasive wear of polymeric materials, *Wear*, 255 (2003) 742-750.

9.0 Summary and Future work

9.1 Summary

This work has been conducted to evaluate and characterise the tribological properties of commercial and experimental polymeric coatings. The focus of this study was on the microstructure property interaction of the matrix and fillers as it relates to wear resistance optimisation of the coatings. Detailed conclusions have been provided at the end of every chapter; however, this chapter intends to provide a general summary of those conclusions and a number of suggestions for future work.

Literature review

The use of pin-on-disc and the micro-abrasion test method to investigate the tribological performance of polymeric materials were comprehensively reviewed. Several mechanisms were suggested for material removal, one of which is the shearing of material due to *adhesion* processes occurring during asperities interaction. It was also established that a number of thermosetting coatings wear by fatigue processes leading to failure by micro-cracking. Likewise, wear by micro-ploughing was reported for some thermoplastic coatings. This was attributed to deformation from inter-penetration of asperities.

Evidence was found that inclusion of fillers in the matrix of polymers reduced the wear rate of coatings considerably. The wear reducing mechanisms of these fillers have been discussed and the optimum filler content was suggested to be between 20-30% of the total coating volume. The addition of solid lubricants (friction modifiers) such as PTFE and graphite was observed to encourage material transfer as this helps to substantially lower the wear rate. The cause and the consequence of corrosion, which compromises the protection offered by the coatings to the tubulars, were elucidated. The conclusion from this review was that current coating options lack the necessary robustness to resist damage found downhole.

Material Characterisation

Detailed characterisation of the materials used in this study has been carried out. In all eleven coatings, supplied by two coating manufacturers were investigated, which can be categorised into two groups: thermoplastic and thermoset, based on the matrix type. The filled coatings were observed to contain fillers of differing shapes, sizes and chemical composition; properties that influenced their wear resistance and wear mechanisms. Some manufacturing defects were seen for several coatings, in particular the dual layer coating. Overall, agreement was seen between the results of the characterisation and the information provided by the coating manufacturers.

Overview of previous and initial wear tests

The preliminary investigation led to the development of a basic level of understanding of the wear behaviour of the commercial polymeric coatings. Particularly, how the fillers influence the wear performance of the coatings. Substantial improvement was achieved in the pin-on-wire rig due to modification of the loading system and improved stiffness of the frame; however, edge loading was still prevalent. Thus, it was concluded that further modification of the pin holder assembly to improve its rigidity was necessary to optimise the pin-on-wire rig. The reciprocating wireline wear test was found to be more aggressive than the pin-on-wire wear test method. Preliminary results showed that inclusion of fillers influenced the wear rate beneficially, particularly TS-5, which was found to wear by a micro-cracking mechanism. In addition, thermoplastic coatings exhibited a better wear resistance than the thermoset coatings. The knowledge gained and the overall performance of the coatings was used for the selection of experimental conditions for the further studies in chapters 6-8.

Evaluation of the adhesion of coatings

The truncated version of the ASTM G8 – 98 has been shown, using the cathodic disbondment (CD) method, to be effective for the evaluation of the adhesive properties of thermoplastic and thermoset polymeric coatings. In addition, the interfacial indentation test (IIT) was also used to study the adhesive properties of these coatings. The coatings have been ranked based on their resistance to delamination. A combination

of chemical and mechanical mode of delamination has been identified as the governing mechanism for the CD test. Inadequate control of the shot blasting applied to the substrate was found to influence the adhesion of coating. Also, increasing the thickness of coating unnecessarily has been shown to detrimentally affect coating adhesion. Under the IIT delamination predominantly occurred at the coating/primer interface for all the coatings and at the coating/substrate for coating A without primer. Generally, the thermoplastic coatings out-performed the thermosets in the cathodic disbondment test due to their superior resistance to chemical attack at both coating/primer and primer/substrate interfaces. The IIT and CD methods clearly showed that coatings responded to mechanical delamination (IIT) and chemical/electrochemical delamination mechanisms differently.

Wireline wear of polymeric coatings

The micro-structural properties of filled and unfilled polymeric coatings have been shown to influence the overall wear performance. The Al_2O_3 performed best in preventing wear among all the fillers. Poor bonding between fillers and matrix was observed to initiate cracks at the filler/matrix interface, which leads ultimately to total detachment of fillers from matrix. Two distinct wear mechanisms were identified to govern material removal: micro-ploughing associated with thermoplastic coatings and fatigue associated with thermoset coatings. A simple model has been proposed to explain the process of material removal by wireline asperities.

Micro-abrasion of PA11 (TP-9) coating

The micro-abrasion test using SiC abrasives has been used to reproduce a similar wear mechanism (2-body abrasion from micro-ploughing of abrasives) to that observed in the wireline tests (POW and RWL). However, the micro-abrasion test produced wear rates between 140 and 400 times greater, thus it was proposed as a candidate test method for 'accelerated' testing of these coatings. Experiments using glass beads aimed at better simulation of the wireline asperity contact resulted in lower (5 times) wear rates compared to the SiC abrasive tests, which can be partly explained by abrasive embedment in the coating, as a result of frictional heating, which had the effect of altering the contact. The morphology of the abrasives was found to greatly influence the

wear rate and mechanism of a coating. Hence, the reduction in the wear rate of the glass beads abrasive tests was attributed to abrasive shape change from angular (silicon carbide) to round (glass bead). Although, experiments have shown that the wear rate generally follows the Archard wear law a significant change in wear rate was observed at a crater depth of 50 μm , indicating the presence of a more wear resistant surface layer, termed 'skin effect'.

Micro-abrasion of filled and unfilled PA11 coatings

The inclusion of fillers has been shown not to enhance wear resistance of the filled experimental PA11 coatings. The addition of TiO_2 had a detrimental effect on wear resistance of coating, while the presence of secondary dolomite filler was found to offer approximately 20% more wear resistance compared to the TiO_2 filled coating. Nevertheless, the unfilled coating exhibited a superior wear resistance compared with the filled coatings, with ~30% higher abrasion resistance. Addition of TiO_2 and Dolomite was seen to reduce the values of stress at break (σ_b) and strain at break (ϵ_b) of the coatings, whereas, the abrasion of the matrix was shown to be governed by coatings property $1/(\sigma_b \epsilon_b)$. The mode of cooling applied after coating deposition was found to affect the wear resistance at high load i.e. water-cooled coatings would offer superior wear resistance for high load applications compared to the air cooled ones. This has been attributed to the possible formation of a smectic delta structure within the structure of the polymer when quenched from melt. As with the abrasion test of TP-9, micro-ploughing was the dominant wear mechanism characterised by the formation of grooves, typical of 2-body abrasion, with extruded filaments of polyamide at the edges of the grooves. Overall, a postulated model, expressed by the following equation, will govern the abrasion rate of the coatings:

$$A_T = A_M + A_F + \phi_F + \eta_F + \Delta A_M$$

Concluding remarks

The highpoints of this research work that has strengthened the current understanding of the tribology of polymeric coatings used downhole are outlined below:

- A *novel approach* using a truncated ASTM G8-98 method has been used to study the adhesion of coatings to their substrates, with the aim of providing information on the design of coatings for impact resistance. To optimise the adhesion of polymeric coatings to their substrate, the surface preparation (shot blasting) applied to the substrate prior to coating deposition has to be adequately controlled, and a binder (primer) between coating and substrate is essential for a good adhesion.
- Modification of the pin-on-wire wear test rig led to a substantial improvement in the performance of the rig. Ranking of commercial polymeric coatings based on their microstructure property interaction was made possible using the modified pin-on-wire rig. The bonding between fillers and matrix has to be adequately strong for optimisation of the tribological properties of polymeric coatings for engineering applications.
- Contrary to the general view that the micro-abrasive wear test is typically only suitable for thin coatings, this study has shown that this test is also reliable for investigating the abrasion resistance of thick coatings. Although the micro-abrasion test method is suitable for accelerated tests, its superiority over other wear test methods, such as wireline wear tests, has been shown to be significantly high. Using the right test conditions, the micro-abrasion test method can be used to reproduce the type of wear mechanism found in the pin-on-wire wear test for thermoplastic coatings.
- When considering material options for downhole protection against ‘wear’, PA11 coatings are recommended.

9.2 Future work

Adhesion tests have shown that surface preparation applied to the steel substrate will significantly influence the adhesion of the coatings. Further work could be undertaken to characterise the effect of substrate roughness on adhesion of polymeric coatings. This could be achieved by shot blasting substrates to different roughness values and coatings applied onto them before testing. Quantification of the adhesion and mechanism of debonding of the coatings can then be related to known roughness values. This work has been undertaken at room temperature. However, the temperature of the well downhole

could be up to 55 °C minimum. Hence, further work at high temperatures is required to simulate similar downhole conditions.

A detailed knowledge of the tribo-contacts between the wireline asperities and the coating surface is crucial to the understanding of the material removal processes during wireline wear. Modelling the contact using a finite element model will be worth investigating. As stated earlier, downhole conditions operate at high temperatures, and since temperature is known to affect the structural and the visco-elastic properties of the polymers, wear tests at higher temperature, between 40 °C and 55 °C, using the pin-on-disc will further strengthened the current understanding of the wear behaviour of polymeric coatings.

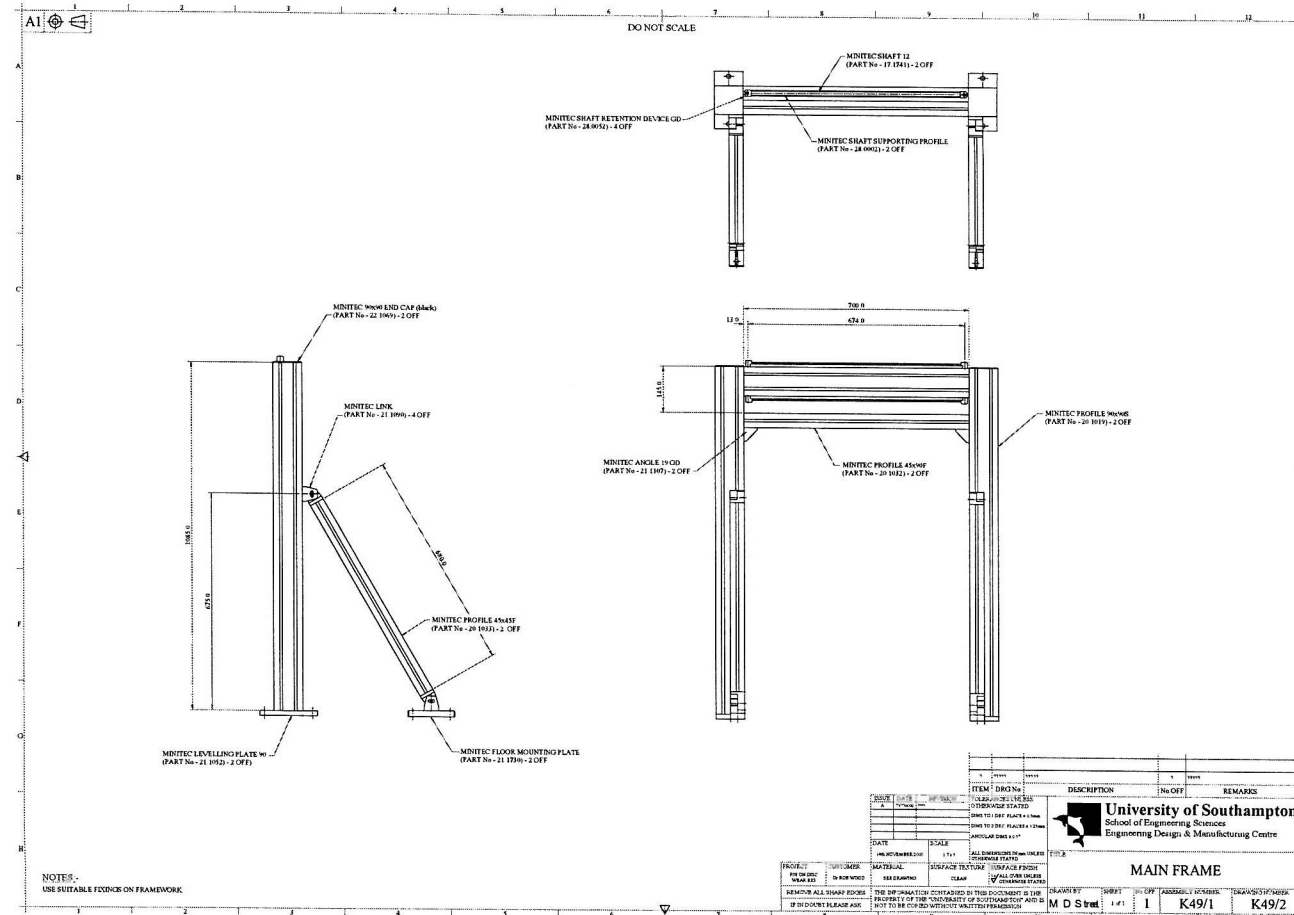
This study investigated using less angular abrasives such as synthetic or natural diamonds in slurry abrasive wear tests in order to improve the understanding of the effect of abrasive morphology on the wear rate and wear mechanism of polymeric coatings. The continuation of this investigation is recommended for detail understanding of the role of abrasive morphology in micro-abrasion tests. It has also been established that specific coating properties, such as $1/\sigma_b \epsilon_b$, appear to govern the wear of matrix. The design of experimental coatings to incorporate such properties within the matrix and subsequent investigation of the abrasion of such coatings can further establish the suitability and the applicability of polymeric coatings for downhole applications.

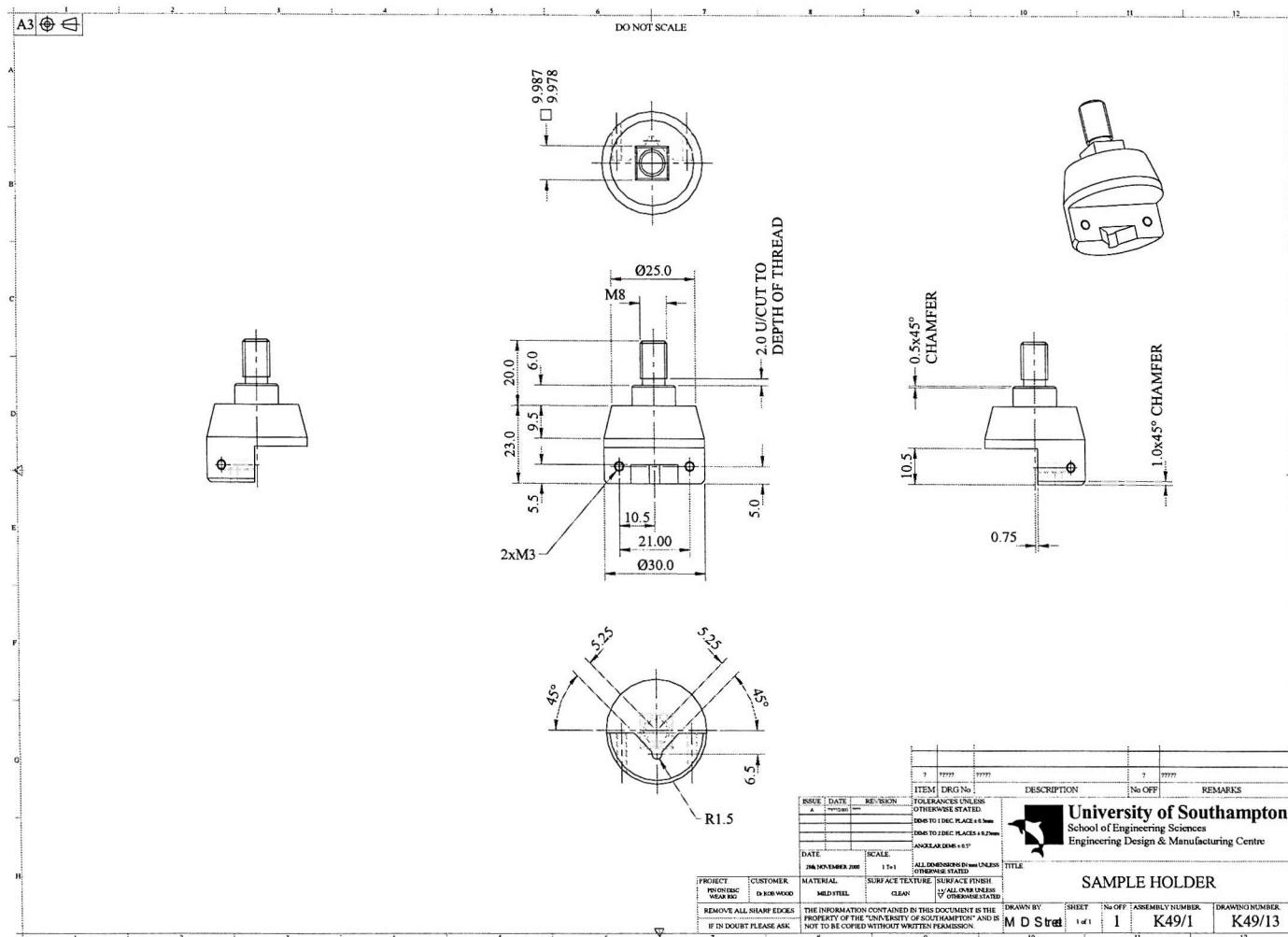
A coating with the following composition, deposited on a carbon steel substrate after a layer of phenolic primer has been applied, is proposed for future studies: PA11 matrix containing about 12 % by volume of cuboid-shaped Al_2O_3 fillers of 12 – 15 μm size, and 3 % by volume of carbon black and water cooled after coating deposition.

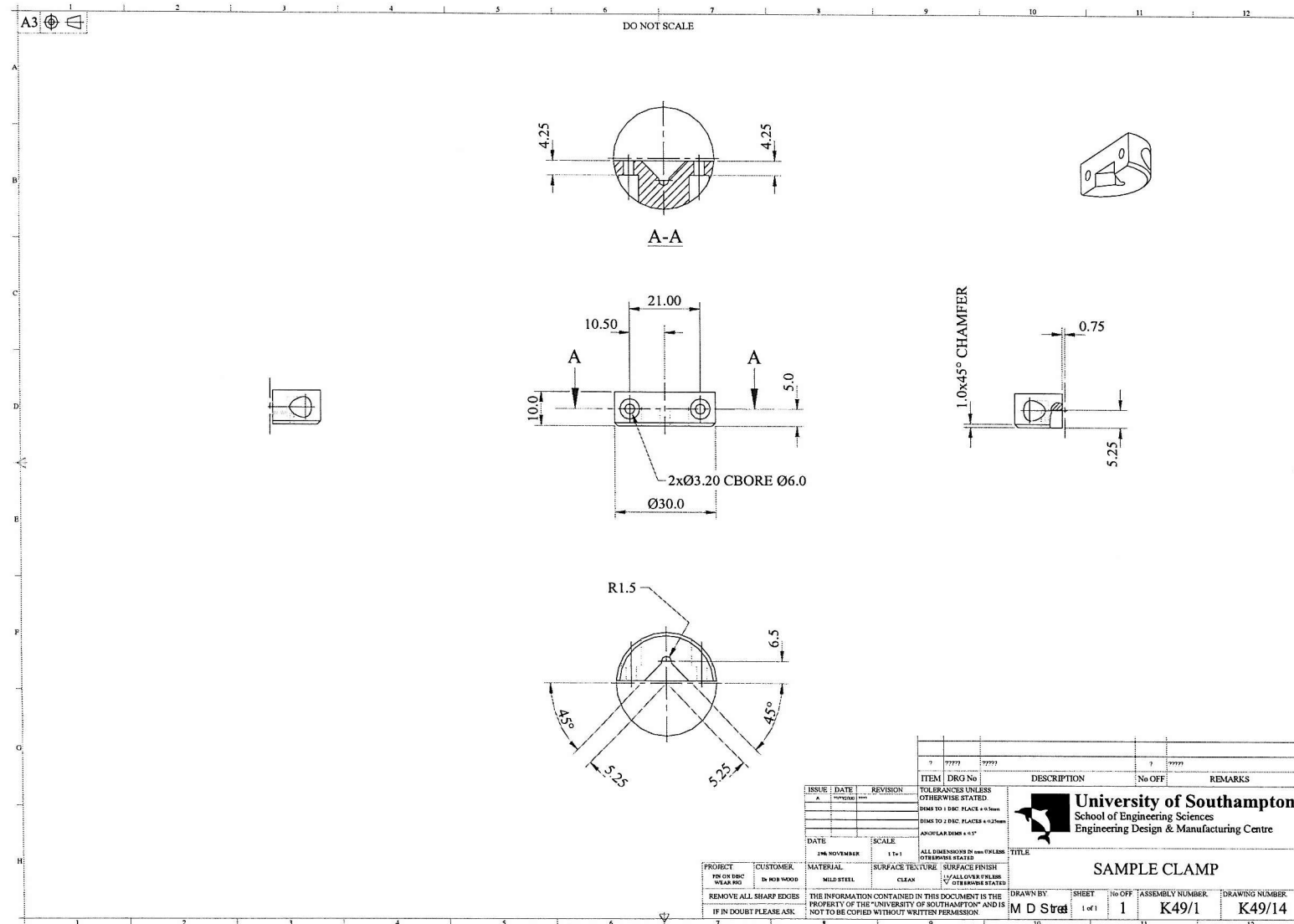
Appendix 1 – Glass transition temperatures (T_g) and melting temperatures (T_m) of common polymers

Polymers	T_g (°C)	T_m (°C)
Low density polyethylene (LDPE)	- 110	115
Polytetrafluoroethylene (PTFE)	-97	327
High density polyethylene (HDPE)	- 90	137
Polypropylene	- 18	175
Polyamide 66	57	265
Polyamide 6	52	225
Polyamide 11 (PA11)	47	191
Polyamide 12	45	180
Polyester (PET)	69	265
Polyvinyl chloride	87	212
Polystyrene	100	240
Polycarbonate	150	265

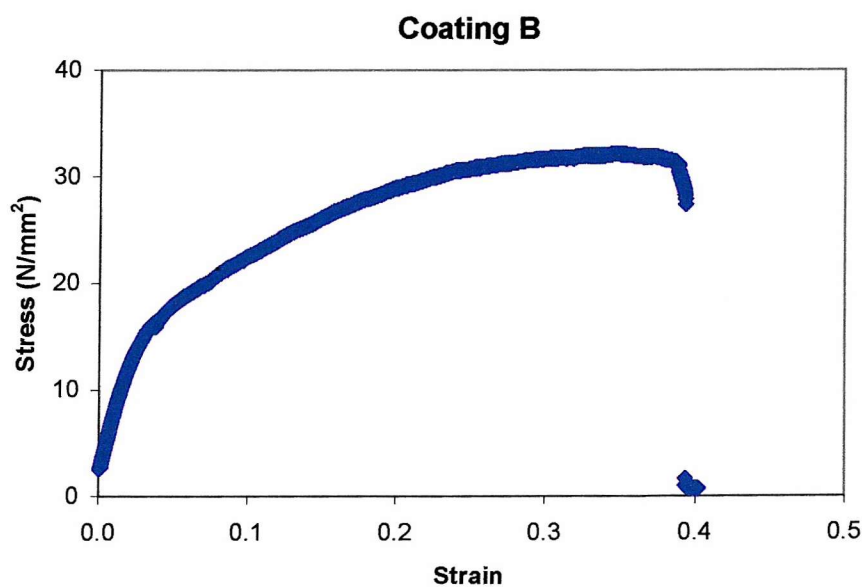
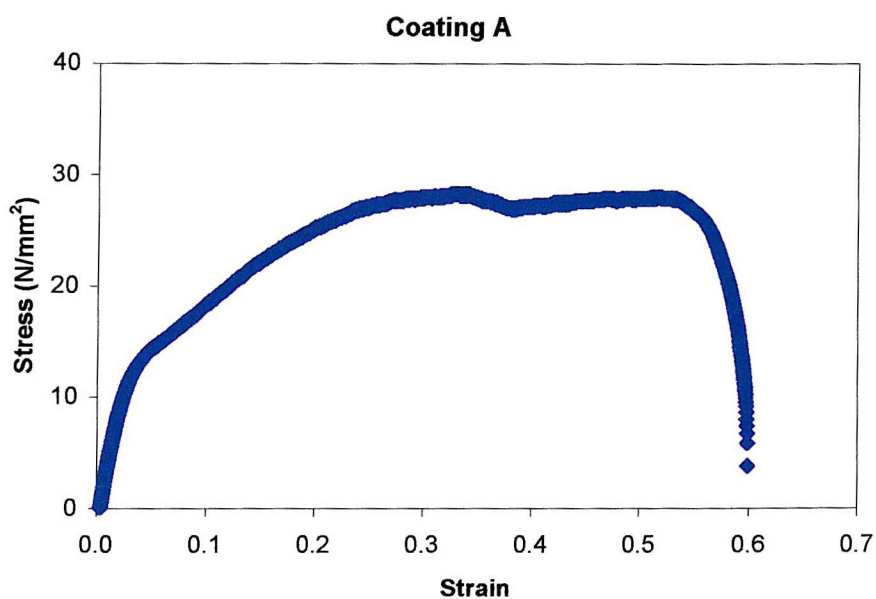
[illegible]

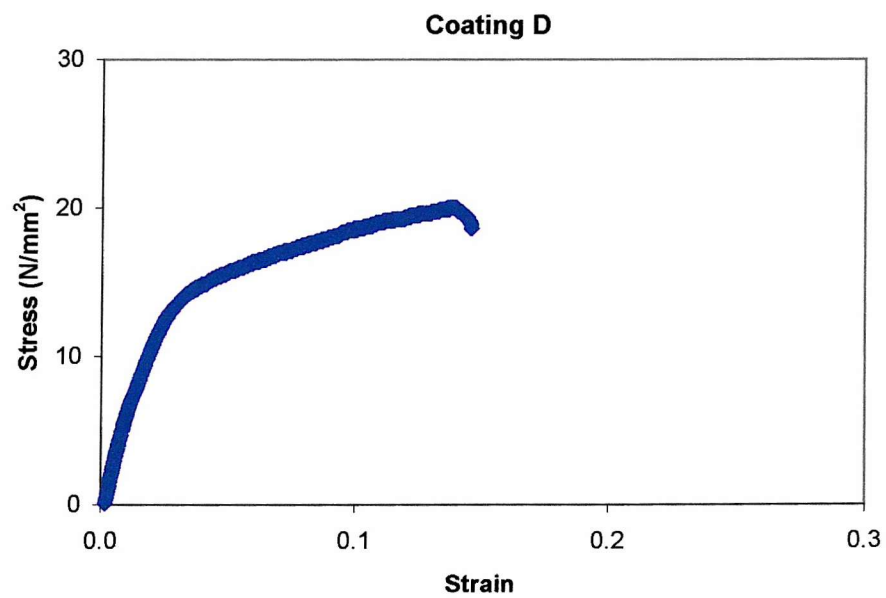
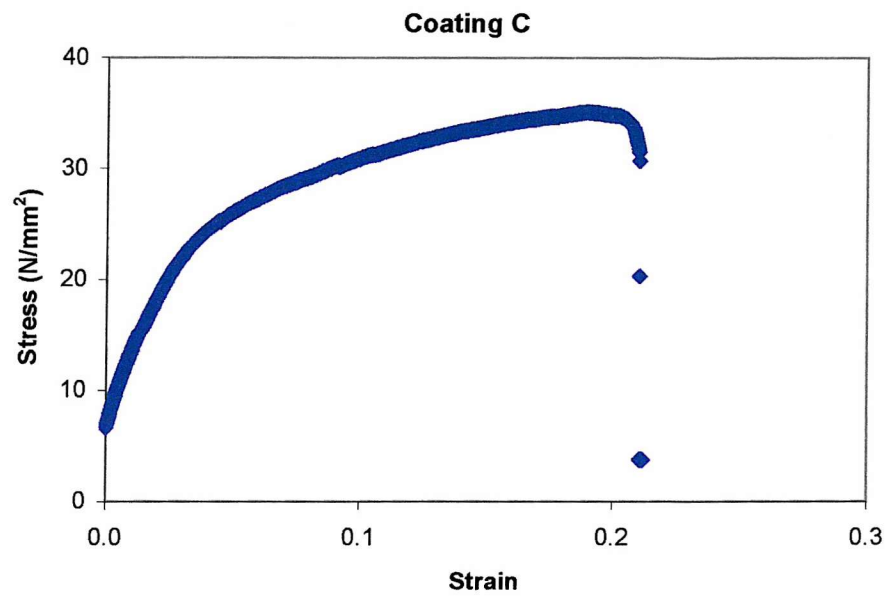






Appendix 3 – The stress-strain curves for coatings A – D investigated in the second study.





Appendix 4 – List of conference and journal publications

Conferences/symposiums attended

- Bello, J. O and Wood, R. J. K. Evaluation of the adhesive properties of downhole polymeric coatings determined by cathodic disbondment, The Mission of Tribology Research 10, December 2001, I mech E, London, UK.
- Bello, J. O and Wood, R. J. K. 2-body Micro-abrasion of Nylon Coated Carbon Steel. 23rd IRG-OECD meeting on Wear of Engineering Materials, May 2002, Coimbra, Portugal.
- Bello, J. O. Wharton, J. A and Wood, R. J. K. Evaluation of the Adhesive Properties of Polymeric Coatings for Downhole corrosion Protection. Paper Number 03607, NACE Corrosion 2003, San Diego, USA.

Journal publications

- Bello, J. O and Wood, R. J. K. Two Body Micro-Abrasion of PA11 coated steel Tubulars for Downhole Applications. *Wear*, 255 (7-12) (2003) 1157-1167.
- Bello, J. O and Wood, R. J. K. Micro Abrasion of Filled and Unfilled Polyamide 11. International conference on Erosive and abrasive wear. September 2003, Churchill College, Cambridge, UK. Manuscript under review for publication in the Special issue of Wear of Material Journal.